




## Analyses

The Reaction Set, Rate Constants and g-Values for the Simulation of the Radiolysis of Light Water over the Range 20° to 350°C Based on Information Available in 2008

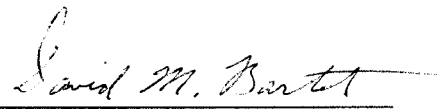
## Nuclear Platform Research and Development

153-127160-450-001  
Revision 0

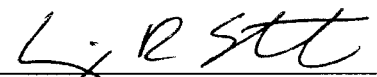
Prepared by  
Rédigé par

  
A.J. Elliot  
Reactor Chemistry & Corrosion  
Chalk River Laboratories


Prepared by  
Rédigé par

  
D.M. Bartels  
Notre Dame Radiation Laboratory  
Notre Dame, Indiana, 46556  
U.S.A.

Reviewed by  
Examiné par

  
C.R. Stuart  
Component Life Technology  
Chalk River Laboratories

Approved by  
Approuvé par

  
I.J. Muir, Manager  
Reactor Chemistry & Corrosion  
Chalk River Laboratories

2009 August

août 2009

UNRESTRICTED

ILLIMITÉ

© Atomic Energy of  
Canada Limited

© Énergie atomique du  
Canada limitée

2251 Speakman Drive  
Mississauga, Ontario  
Canada L5K 1B2

2251, rue Speakman  
Mississauga (Ontario)  
Canada L5K 1B2



## Analyses

The Reaction Set, Rate Constants and g-Values for the Simulation of the Radiolysis of Light Water over the Range 20° to 350°C Based on Information Available in 2008

### **Nuclear Platform Research and Development**

**153-127160-450-001  
Revision 0**

2009 August

août 2009

**UNRESTRICTED**

**ILLIMITÉ**

© Atomic Energy of  
Canada Limited

© Énergie atomique du  
Canada limitée

2251 Speakman Drive  
Mississauga, Ontario  
Canada L5K 1B2

2251, rue Speakman  
Mississauga (Ontario)  
Canada L5K 1B2



## Revision History

## Liste de révisions

**UNRESTRICTED**

**ILLIMITÉ**

Page 1 of /de 1

CW-511300-FM-168 Rev. 0

CW-511300-PRO-161

Document No. / Numéro de document:

153	127160	450	001
Doc. Collection ID ID de la collection de doc.	SI Répertoire du sujet	Section	Serial No. N° de série

### Document Details / Détails sur le document

Title

Titre

The Reaction Set, Rate Constants and g-Values for the Simulation of the Radiolysis of Light Water over the Range 20° to 350°C Based on Information Available in 2008

Total no. of pages

N<sup>bre</sup> total de pages

162

**For Release Information, refer to the Document Transmittal Sheet accompanying this document. / Pour des renseignements portant sur la diffusion, consultez la feuille de transmission de documents ci-jointe.**

### Revision History / Liste de révisions

Revision / Révision		Details of Rev. / Détails de la rév.	Prepared by Rédigé par	Reviewed by Examiné par	Approved by Approuvé par
No./N°	Date				
D1	2009-07-06	Issued for Review and Comments	A.J. Elliot D.M. Bartels	C.R. Stuart G.A. Glowa	
0	2009-08-04	Issued as Approved for Use	A.J. Elliot D.M. Bartels	C.R. Stuart	I.J. Muir

## TABLE OF CONTENTS

SECTION	PAGE
1.	INTRODUCTION .....1-1
2.	METHODOLOGY .....2-1
3.	LOW LINEAR ENERGY TRANSFER G-VALUES .....3-1
3.1	g-Value: Hydrated Electron.....3-3
3.2	g-Value: Hydroxyl Radical .....3-7
3.3	g-Value: Hydrogen Peroxide.....3-11
3.4	g-Value: Molecular Hydrogen.....3-13
3.5	g-Value: Hydrogen Atoms .....3-14
3.6	Material Balance for Low LET Water Radiolysis as a Function of Temperature.....3-17
4.	REACTION RATE CONSTANTS .....4-1
4.1	Reactions not involving Equilibria .....4-4
4.1.1	Reaction R2: $e_{aq}^- + e_{aq}^- + 2 H_2O \rightarrow H_2 + 2 OH^-$ .....4-4
4.1.2	Reaction R3: $H + H \rightarrow H_2$ .....4-7
4.1.3	Reaction R4: $OH + OH \rightarrow H_2O_2$ .....4-9
4.1.4	Reaction R5: $e_{aq}^- + H (+ H_2O) \rightarrow H_2 + OH^-$ .....4-12
4.1.5	Reaction R6: $e_{aq}^- + OH \rightarrow OH^-$ .....4-15
4.1.6	Reaction R7: $H + OH \rightarrow H_2O$ .....4-17
4.1.7	Reaction R8: $e_{aq}^- + H_2O_2 \rightarrow OH + OH^-$ .....4-19
4.1.8	Reaction R9: $e_{aq}^- + O_2 \rightarrow O_2^-$ .....4-21
4.1.9	Reaction R10: $e_{aq}^- + O_2^- + H_2O \rightarrow H_2O_2 + 2 OH^-$ .....4-23
4.1.10	Reaction R11: $e_{aq}^- + HO_2 \rightarrow HO_2^-$ .....4-23
4.1.11	Reaction R12: $H + H_2O_2 \rightarrow OH + H_2O$ .....4-24
4.1.12	Reaction R13: $H + O_2 \rightarrow HO_2$ .....4-26
4.1.13	Reaction R14: $H + HO_2 \rightarrow H_2O_2$ (or $2 OH$ ).....4-28
4.1.14	Reaction R15: $H + O_2^- \rightarrow HO_2^-$ .....4-31
4.1.15	Reaction R16: $OH + H_2O_2 \rightarrow HO_2 + H_2O$ .....4-31
4.1.16	Reaction R17: $OH + O_2^- \rightarrow (HO_3^-) \rightarrow O_2 + OH^-$ .....4-33
4.1.17	Reaction R18: $OH + HO_2 \rightarrow (H_2O_3) \rightarrow O_2 + H_2O$ .....4-35
4.1.18	Reactions R19, R20 and R21: $HO_2/O_2^- + HO_2/O_2^- \rightarrow H_2O_2 + O_2$ .....4-37
4.1.19	Reaction R22: $H_2O_2 \rightarrow \frac{1}{2}O_2 + H_2O$ .....4-42
4.2	Equilibria and Associated Rate Constants .....4-51
4.2.1	Acid/Base Equilibrium Constants.....4-51
4.2.2	Rate Constants Associated with Acid/Base Equilibria (Table 4-2) .....4-54
4.2.2.1	Equilibrium R23: $H_2O \rightleftharpoons H^+ + OH^-$ .....4-56

4.2.2.2	Rate Constants for Acid-Base Equilibria R24 through R29 .....	4-58
4.2.3	Rate constants associated with equilibria involving the hydrogen atom (Table 4-3) .....	4-61
4.2.3.1	Equilibrium R30: $H \rightleftharpoons H^+ + e_{aq}^-$ .....	4-61
4.2.3.2	Equilibrium R31: $H + OH^- \rightleftharpoons e_{aq}^- + H_2O$ .....	4-63
4.2.3.3	Equilibrium R32: $H + H_2O \rightleftharpoons H_2 + OH^-$ .....	4-65
4.3	Reactions of Oxide Radical Anion Relevant to High Temperature Reactor Coolant Radiolysis .....	4-68
4.3.1	Reactions R16, R33, R34, R35: $OH/O^- + H_2O_2 \rightarrow H_2O/OH^- + HO_2/O_2^-$ .....	4-68
4.3.2	Reaction R36: $O^- + H_2 \rightarrow H + OH^-$ .....	4-72
4.3.3	Equilibrium R37: $O^- + O_2 \rightleftharpoons O_3^-$ .....	4-72
5.	HIGH LET G-VALUES .....	5-1
5.1	g-Value: Hydrated Electron .....	5-4
5.2	g-Value: Molecular Hydrogen .....	5-8
5.3	g-Value: Hydrogen Atom .....	5-12
5.4	g-Value: $HO_2/O_2^-$ .....	5-16
5.5	g-Value: Hydrogen Peroxide .....	5-18
5.6	g-Value: Hydroxyl Radical .....	5-21
6.	ESTIMATION OF FAST NEUTRON G-VALUES AS A FUNCTION OF TEMPERATURE .....	6-1
6.1	Determination of the recoil proton spectrum .....	6-2
6.2	Estimation of the g-values for fast neutron at room temperature .....	6-2
6.3	Estimation of the g-values for fast neutron at reactor operating temperatures .....	6-3
7.	CONCLUSIONS .....	7-1
8.	ACKNOWLEDGEMENTS .....	8-1
9.	REFERENCES .....	9-1

## TABLES

Table 3-1	g-Values for water at near neutral pH at room temperature for low LET radiation .....	3-3
Table 3-2	The extinction coefficient at 600 nm for the $\bullet CO_3^-$ as a function of temperature .....	3-8

Table 3-3	Polynomials that describe the temperature dependence of the g-values for the primary species formed in the radiolysis of light water by low LET radiation in the temperature range 20°-350°C.....	3-19
Table 3-4	The g-values for low LET radiation deposited in light water at temperatures between 25° and 350°C based on the polynomials in Table 3-3. <sup>14</sup> .....	3-19
Table 4-1	Water Radiolysis Reaction Set .....	4-2
Table 4-2	Equilibrium Reactions not involving the Hydrogen Atom .....	4-3
Table 4-3	Equilibrium Reactions involving the Hydrogen Atom.....	4-3
Table 4-4	The extinction coefficient of the hydroxyl radical at 250°C as a function of temperature .....	4-10
Table 4-5	Polynomials describing the pKs (in ‘Molar’ units) of H <sub>2</sub> O, H <sub>2</sub> O <sub>2</sub> , OH, HO <sub>2</sub> and H* .....	4-52
Table 4-6	Polynomials describing the diffusion coefficients for H <sup>+</sup> , OH <sup>-</sup> and H <sub>2</sub> O .....	4-54
Table 6-1	Polynomial functions describing track-averaged LET as function of proton energy and g-values as a function of LET at room temperature .....	6-5
Table 6-2	The g-Values for the different energy recoil protons and for fast neutrons at room temperature.....	6-6
Table 6-3	Polynomial functions describing the rate of change of d(g-value)/d(temperature) with track-averaged LET.....	6-7
Table 6-4	The g-Values for fast neutrons deposited in light water at temperatures between 25° and 350°C for natural uranium.....	6-7

## FIGURES

Figure 1-1	Results of preliminary radiolysis modelling of the data that shows agreement between the hydrogen and oxygen profiles around the time of hydrogen addition. To obtain the fit, the radiolysis model had an unreasonably low value for the OH + H <sub>2</sub> → H + H <sub>2</sub> O rate constant. (Simulations performed by G. Glowa, AECL-CRL).....	1-4
Figure 3-1	The g-value for the hydrated electron as a function of temperature as measured from experiments where a stable product was analyzed by Jha et al. [37], by Elliot et al. [38], by Kent and Sims [40] and by Janik et al. [26]. The dash-dot-dot line is the recommended temperature dependence for g(e <sub>aq</sub> <sup>-</sup> ) based on nitrogen yields from N <sub>2</sub> O containing solutions – see text for more information. The ‘accepted’ room temperature value for g(e <sub>aq</sub> <sup>-</sup> ) given by Spinks and Woods [34] in Table 3-1 is also plotted.....	3-5
Figure 3-2	The measured g(e <sub>aq</sub> <sup>-</sup> ) and {g(e <sub>aq</sub> <sup>-</sup> ) + g(OH) + g(H)} using the transient MV <sup>+</sup> absorption as a function of temperature by Elliot et al. [38], by Shiraishi et al. [39] by Lin et al. [28], and by Buxton and Wood [43]. The recommended temperature dependence for g(e <sub>aq</sub> <sup>-</sup> ) from Figure 3-1 and the value for {g(e <sub>aq</sub> <sup>-</sup> ) + g(OH) + g(H)} calculated from the material balance equations in Section 3.5 are also given.....	3-6

Figure 3-3	The g-value for the hydroxyl radical measured as a function of temperature by Elliot et al. [38]. The black dash-dot-dot line is the recommended temperature dependence for g(OH) based on a temperature dependent extinction coefficient for the $\bullet\text{CO}_3^-$ . The red dash line is the recommended temperature dependence for g(OH) based on a temperature independent extinction coefficient for the $\bullet\text{CO}_3^-$ . The ‘accepted’ room temperature value for g(OH) given by Spinks and Woods [34] in Table 3-1 is also plotted. ....	3-9
Figure 3-4	The normalized absorption spectra for the carbonate radical anion as a function of temperature [38]. ....	3-10
Figure 3-5	The relative extinction coefficient of the carbonate radical anion based on the area under the absorption curve and on the width of the absorption peak at half height, based on the spectra shown in Figure 3-4 . ....	3-10
Figure 3-6	The g-value for $\text{H}_2\text{O}_2$ measured as a function of temperature by Elliot et al. [38], Elliot (unpublished), Kent and Sims [40] and Stefanic and LaVerne [47]. The dash-dot line is the recommended temperature dependence for g( $\text{H}_2\text{O}_2$ ). The ‘accepted’ room temperature value for g( $\text{H}_2\text{O}_2$ ) given by Spinks and Woods [34] in Table 3-1 is also plotted. ....	3-12
Figure 3-7	The g-value for $\text{H}_2$ measured as a function of temperature by Janik et al. [26], Elliot et al. [38] and Kent and Sims [40]. The dash-dot line is the recommended temperature dependence for g( $\text{H}_2$ ). The ‘accepted’ room temperature value for g( $\text{H}_2$ ) given by Spinks and Woods [34] in Table 3-1 is also plotted. ....	3-13
Figure 3-8	The G-values measured for hydrogen as a function of temperature by Janik et al. [26], Elliot et al. [38] and Kent and Sims [40]. The solid black stars are g(H) as calculated from the difference between G( $\text{H}_2 + \text{H}$ ) as measured by Elliot et al. [38] and g( $\text{H}_2$ ) (red dash-dot-dot line) taken from Figure 3-7. Also shown are the estimates for g(H) based on the g(H)/g( $e_{\text{aq}}^-$ ) given in Figure 3-9 – see text. The recommended functional dependence for g(H) determined by a material balance fit in Section 3.5 is also shown. The ‘accepted’ room temperature values for g(H) and g(H) + g( $\text{H}_2$ ) as given by Spinks and Woods [34] in Table 3-1 are also plotted. ....	3-15
Figure 3-9	The ratio of g(H)/g( $e_{\text{aq}}^-$ ) measured from archived time profiles where the hydrogen atom was converted to the hydrated electron after the end of the pulse. Unpublished data from archived absorbance-time profiles by Bartels and co-workers. ....	3-16
Figure 3-10	The g-values for the primary species formed in Reaction (R1) for low LET radiation as a function of temperature. The lines are the fit to primary yields given in Sections 3.1 through 3.3. In the case of g(H), the temperature dependence shown has been fitted to the data using the adjustment of g(OH) above 250°C as described in the text. The data points on the plot provide a sense of the experimental uncertainty. ....	3-20

Figure 4-1	The extinction coefficient for the hydrated electron as a function of temperature by Bartels and co-workers (data to be published) and Elliot et al. [50].	4-5
Figure 4-2	The temperature dependence of the rate constant for the bimolecular decay of the hydrated electron as measured by Christensen and Sehested [49], Marin et al. [27] and Stuart and Ouellette in Elliot et al. [50].	4-6
Figure 4-3	The rate constants for the bimolecular reaction of hydrogen atoms as measured by Sehested and Christensen [52].	4-8
Figure 4-4	The temperature dependence of the bimolecular rate constant for the self-reaction of hydroxyl radicals by Elliot et al. [54] and by Janik et al. [25]. All data has been corrected to the revised extinction coefficients for the hydroxyl radical – see text. Also shown is the rate constant, $k_{diff}$ , for encounters between hydroxyl radicals.	4-11
Figure 4-5	The rate constants for the reaction of the hydrated electron reacting with hydrogen atom as measured by Marin et al. [27], Christensen et al. [55], Stuart and Ouellette (unpublished results), Schwarz [56], and Janek and Bartels (unpublished – see text).	4-14
Figure 4-6	The temperature dependence of the reaction of the hydrated electron with the hydroxyl radical as reported by Stuart et al. [57], by Christensen et al. [55] and by Janik and Bartels (to be published). All data have been adjusted for the revised hydrated electron extinction coefficient – see text.	4-16
Figure 4-7	The rate constant for the reaction of hydrogen atoms with hydroxyl radicals as measured by Buxton and Elliot [59] and by Lundström et al. [30].	4-18
Figure 4-8	The rate constants for the reaction of the hydrated electron reacting with hydrogen peroxide as measured by Elliot et al. [50], [57] and by Christensen et al. [55].	4-20
Figure 4-9	The rate constants for the reaction of the hydrated electron with oxygen as measured by Stuart et al. [57] and by Cline et al. [21].	4-22
Figure 4-10	The temperature dependence for the reaction of hydrogen atoms with hydrogen peroxide as reported by Elliot [61], Mezyk and Bartels [62], and by Lundström et al. [29]. The regression line is through the data of Mezyk and Bartels [62].	4-25
Figure 4-11	The temperature dependence for the reaction of hydrogen atoms with oxygen as reported by Janik et al. [24] and by Elliot et al. [54].	4-27
Figure 4-12	The temperature dependence for the rate constant for the reaction of hydrogen atoms with the perhydroxyl radical as reported by Lundström et al. [31] and by Janik et al. [24].	4-30
Figure 4-13	The temperature dependence for the reaction of hydroxyl radicals with hydrogen peroxide as reported by Christensen et al. [63] and by Stuart and co-workers [50], [57].	4-32



Figure 4-14	The temperature dependence of the rate constant for the reaction of the hydroxyl radical with the superoxide radical as reported by Christensen et al. [64] and by Elliot and Buxton [65].	4-34
Figure 4-15	The temperature dependence of the rate constant for the reaction of the hydroxyl radical with the perhydroxyl radical as reported by Lundström et al. [31] and by Elliot and Buxton [65].	4-36
Figure 4-16	The rate constant for the decay of $\text{HO}_2/\text{O}_2^-$ as a function of pH at room temperature Bielski et al. [67].	4-38
Figure 4-17	The temperature dependence of the rate constant for the dismutation Reaction R19 of the perhydroxyl radical as calculated from the data of Christensen and Sehested [68].	4-39
Figure 4-18	The rate constant for Reaction R20 between $\text{O}_2^-$ and $\text{HO}_2$ as a function of temperature [68] showing the two distinct temperature dependencies above and below $100^\circ\text{C}$ .	4-40
Figure 4-19	The observed bimolecular decay constant, expressed as $2k_{\text{obs}}/\epsilon$ , for the reactions of $\text{O}_2^-$ and $\text{DO}_2$ in heavy water at different pD values. Unpublished work by Stuart and Chenier (AECL-CRL).	4-41
Figure 4-20	Arrhenius plot of the thermal decomposition of hydrogen peroxide in ~4-5 mm tubing [70], [72], [74] showing a possible activation energies.	4-45
Figure 4-21	Arrhenius plot of the thermal decomposition of hydrogen peroxide in neutral water showing the effect of tube diameter and of stainless steel and PTFE tube material [70].	4-46
Figure 4-22	Arrhenius plot of the thermal decomposition of hydrogen peroxide in neutral water showing the effect of tube material (PTFE, stainless steel and titanium) and of hydrogen [72], [73].	4-47
Figure 4-23	Arrhenius plot of the thermal decomposition of hydrogen peroxide in an SS 316 lined autoclave showing the effect of pH as reported by Haines et al. [71].	4-48
Figure 4-24	The thermal decomposition of hydrogen peroxide in Pyrex glass ampoules at $110^\circ\text{C}$ , with and without $2 \times 10^{-4}$ mol/kg hydrogen (Chenier and Elliot - unpublished data).	4-49
Figure 4-25	The effect of temperature on the yield of $\text{CO}_2$ from the reaction of hydrogen peroxide and sodium formate in a solution containing $5 \times 10^{-3}$ mol/kg $\text{HCOONa}$ , $2 \times 10^{-4}$ mol/kg methyl viologen and $1.2 \times 10^{-5}$ mol/kg $\text{H}_2\text{O}_2$ . Figure copied from Reference [76]. 500 $\mu\text{g}/\text{kg}$ carbon dioxide in water is equivalent $\sim 1.1 \times 10^{-5}$ mol/kg.	4-50
Figure 4-26	The measured and extrapolated values for the pK (in 'Molar' units) of $\text{H}_2\text{O}$ as $\text{pK}_w$ [77], $\text{H}_2\text{O}_2$ [78], $\text{OH}$ [79], [80], [81], $\text{HO}_2$ [79], [82], [68] and $\text{H}$ [83] as a function of temperature. The pK (in 'Molar' units) of $\text{H}_2\text{O}$ as $\text{pK}_{\text{H}_2\text{O}}$ (see text) is also shown.	4-53

Figure 4-27	The temperature dependence of the self-diffusion coefficient for water (Yosida et al. [86], Harris and Woolf [87] and by Krynicki et al. [88] and the diffusion coefficient for the proton and the hydroxide ion (Quist and Marshall [89] and Robinson and Stokes [90]).....	4-55
Figure 4-28	The rate constants for the recombination of $H^+$ and $OH^-$ (Natzle and Moore [91], Knight et al. [92], Ertl and Gerischer [93] and Bannister et al. [94]) and the Smoluchowski extrapolation to 350°C.....	4-57
Figure 4-29	The rate constants for the recombination of $H^+$ and $O_2^-$ (Ilan and Rabani [97]) and reaction $OH$ with $OH^-$ (Buxton [95]; Zahavi and Rabani [96]) and the Smoluchowski extrapolations to 350°C.....	4-60
Figure 4-30	The temperature dependence of the reaction on the hydrated electron with the proton as measured by Elliot [18], Shiraishi et al. [83] and Stanisky, Bartels and Takahashi [98].....	4-62
Figure 4-31	The temperature dependence of the rate constant for the reaction of hydrogen atoms with the hydroxide ion as measured by Bartels and co-workers [21], [23], [99], [100].....	4-64
Figure 4-32	The calculated rate constant, $k_{R32f}$ , as a function of temperature for the reaction of the hydrogen atom with water as calculated by Bartels [101]. Also shown is the value reported by Shiraishi et al. [83] estimated from experimental data at 25°C.....	4-66
Figure 4-33	The temperature dependence for the reaction of hydroxyl radicals with hydrogen as reported by Christensen and Sehested [102], by Stuart and co-workers [50], [57] and by Marin et al. [16]. The temperature dependence for the reaction of the oxide radical anion with hydrogen is also shown [103]. .....	4-67
Figure 4-34	The observed rate constant for the reaction of $OH/O^-$ with $H_2O_2/HO_2^-$ as a function of pH at the measurement temperature in $N_2O$ -saturated solutions [57]. The coloured symbols are data from AECL-CRL with lines joining experimental sets. Some experiments used buffer solutions while others set the pH by adding LiOH. The grey circles are data of Christensen et al. [63] measured at room temperature. The simulation for $k_{obs}$ as a function of pH at 300°C is shown (see text). Also shown is the simulation of $k_{obs}$ at 20°, 50°, 75°, 100° and 300°C for an unbuffered solution that had a pH of 10.3 at 20°C (red x and red dotted line).....	4-70
Figure 4-35	The temperature dependence for the rate constants $k_{R16}$ , ( $k_{R33} + k_{R34}$ ) and $k_{R35}$ based on the fits in Figure 4-34.....	4-71
Figure 4-36	The temperature dependence for the reaction involved with Equilibrium R37 as reported by Elliot and McCracken [80]. .....	4-73
Figure 5-1	Illustration of the effect of LET on distribution of chemical events initiated by the passage of ionizing radiation. ....	5-2

Figure 5-2	The electronic stopping power [111] and the calculated track-averaged LET for protons as a function of incident proton energy. Also shown is the relative energy deposited by the recoil protons, in binned energy ranges, that were formed by a fast neutron flux from natural uranium fuel in light water.....	5-3
Figure 5-3	The g-value of the hydrated electron as a function of track-averaged LET at room temperature as measured by Appleby and Schwarz [112], LaVerne and Yoshida [113], Elliot et al. [110], LaVerne et al. [114] and Ashmore et al. [76]. The line is the fit to the data given by the polynomial equation in Table 6-1.....	5-5
Figure 5-4	The g-value for the hydrated electron at different temperatures as a function of room temperature track-averaged LET [110].....	5-6
Figure 5-5	The temperature dependence of the g-value for the hydrated electron for gamma-radiation, 26 MeV <sup>2</sup> H and 157 MeV <sup>7</sup> Li ion beams measured by Elliot and co-workers [38], [110]. The results reported by Ashmore et al. [76] are for solutions at pH 8.1 (room temperature). Also shown is g-value for the hydrated electron recommended in Section 3.1 for gamma-radiation. ....	5-7
Figure 5-6	The g-value of molecular hydrogen as a function of track-averaged LET at room temperature as measured by Appleby and Schwarz [112], Burns and Sims [115], Anderson and Hart [116], Elliot et al. [110], LaVerne [117] and Ashmore et al. [76]. The line is the fit to the data given by the polynomial equation in Table 6-1.....	5-9
Figure 5-7	The g-value for molecular hydrogen at different temperatures as a function of room temperature track-averaged LET [110].....	5-10
Figure 5-8	The temperature dependence of the g-value for molecular hydrogen for gamma-radiation, 26 MeV <sup>2</sup> H and 157 MeV <sup>7</sup> Li ion beams measured by Elliot and co-workers using material balance [38], [110]. The results reported by Ashmore et al. [76] for a 2.6 and 5.9 MeV <sup>1</sup> H ion beam are shown. Also shown is g-value for molecular hydrogen recommended in Section 3.3 for gamma-radiation.....	5-11
Figure 5-9	The g-value of atomic hydrogen as a function of track-averaged LET at room temperature as measured by Appleby and Schwarz [112], Elliot et al. [38], [110] and Parajon et al. [118]. The line is the fit to the data given by the polynomial equation in Table 6-1.....	5-13
Figure 5-10	The g-value for atomic hydrogen at different temperatures as a function of room temperature track-averaged LET [38], [110]. ....	5-14
Figure 5-11	The temperature dependence of the g-value for atomic hydrogen for gamma-radiation, 26 MeV <sup>2</sup> H and 157 MeV <sup>7</sup> Li ion beams measured by Elliot and co-workers [38], [110]. Also shown is g-value for atomic hydrogen derived in Section 3.5 for gamma-radiation. ....	5-15

Figure 5-12	The g-value for the yield of HO <sub>2</sub> /O <sub>2</sub> <sup>-</sup> (and possibly O <sub>2</sub> ) as a function of track-averaged LET at room temperature as measured by Appleby and Schwarz [112], LaVerne [109] and Burns and Sims [115]. The line is the fit to the data given by the polynomial equation in Table 6-1.....	5-17
Figure 5-13	The g-value of hydrogen peroxide as a function of track-averaged LET at room temperature as measured by Appleby and Schwarz [112], Burns and Sims [115], Anderson and Hart [116], Elliot et al. [110] and Pastina and LaVerne [120]. The line is the fit to the data given by the polynomial equation in Table 6-1. ....	5-19
Figure 5-14	The temperature dependence of the g-value for hydrogen peroxide for gamma-radiation, 26 MeV <sup>2</sup> H and 157 MeV <sup>7</sup> Li ion beams measured by Elliot and co-workers [38], [110]. The results reported by Ashmore et al. [76] for a 5.9 MeV <sup>1</sup> H ion beam are shown. Also shown is g-value for hydrogen peroxide recommended in Section 0 for gamma-radiation. ....	5-20
Figure 5-15	The g-value of the hydroxyl radical as a function of track-averaged LET at room temperature as measured by Appleby and Schwarz [112] (material balance), LaVerne [109], Elliot et al. [110] (material balance), Burns and Sims [115], Anderson and Hart [116]. The line is the fit to the data given by the polynomial equation in Table 6-1.....	5-22
Figure 5-16	The g-value for the hydroxyl radical at different temperatures as a function of room temperature track-averaged LET [110].....	5-23
Figure 5-17	The temperature dependence of the g-value for the hydroxyl radical for gamma-radiation, 26 MeV <sup>2</sup> H and 157 MeV <sup>7</sup> Li ion beams measured by Elliot and co-workers [38], [110] using material balance with the revised g(H <sub>2</sub> O <sub>2</sub> ) in Section 5.2. Also shown is g-value for the hydroxyl radical recommended in Section 3.2 for gamma-radiation. ....	5-24
Figure 6-1	The relative 'energy binned' fast neutron group-fluxes and proton recoil spectrum for the light water-cooled, high temperature U-2 loop, NRU reactor. The fuel was natural uranium after 250 MWh/kg uranium burn-up. Also shown are the percent of the total energy deposited by protons within each energy bin. ....	6-8
Figure 6-2	The rate of change of the g-values with temperature as a function of track-averaged LET. The solid lines are dependences used to calculate the fast neutron g-values at reactor operating temperatures.....	6-9
Figure 6-3	The g-values for fast neutrons as a function of temperature for natural uranium fuel.....	6-10

## APPENDICES

Appendix A	Tabulations of Rate Constants and pKs at Different Temperatures based on Mathematical Functions provided in this Report.....	A-1
------------	--	-----

**APPENDIX TABLES**

Table A-1	Rate Constants Associated with Reactions in Table 4-1.....	A-2
Table A-2	Rate Constants Associated with the Equilibrium Reactions in Table 4-2 and Table 4-3 .....	A-3
Table A-3	pK Values for Equilibria in Table 4-2 and Table 4-3 .....	A-4
Table A-4	Rate Constants Associated with the Alkaline Reactions in Discussed in Section 4.3 .....	A-5

## 1. INTRODUCTION

An understanding of the aqueous radiolysis-induced chemistry in nuclear reactors is an important key to the understanding of materials integrity issues in reactor systems. Significant materials and chemistry issues have emerged in Pressurized Water Reactors (PWR), Boiling Water Reactors (BWR) and CANDU<sup>®</sup> reactors that have required a detailed understanding of the radiation chemistry of the coolant. For each reactor type, specific computer radiolysis models have been developed to gain insight into radiolysis processes and to make chemistry control adjustments to address the particular issues (References [1] through [11]).<sup>1</sup>

There are a number of groups around the world that model the high temperature radiolysis of coolant water in reactor circuits. These groups all use slightly different radiolysis chemical yields, chemical reactions and rate constants for their modelling calculations [13].

Over the last three decades, there has been a concerted effort in various research laboratories in different countries (Reference [13] and references therein) to establish the dependence on temperature of:

1. The g-values<sup>2</sup> of the primary species for ionizing radiation with different linear energy transfer (LET) characteristics; and
2. The rate constants of the chemical and acid/base equilibria reactions involved in water radiolysis.

Until recently, there were no well-defined experimental high temperature water radiolysis results available for 'benchmarking' the models. For a reactor coolant radiolysis model to be successful, it must meet a number of criteria. The criteria include being able to predict:

1. The concentrations of hydrogen, oxygen and hydrogen peroxide under normal steady-state radiolysis conditions when no additional hydrogen or oxygen has been added to the coolant.
2. The critical hydrogen concentration (CHC)<sup>3</sup> required to suppress the net radiolytic production of oxygen and hydrogen peroxide; and
3. The time profiles of the chemical species as operational conditions change.

In 1995, a series of tests were undertaken in the high temperature, light water cooled, fuelled U-2 loop in the National Research Universal (NRU) reactor at the Chalk River Laboratories (CRL) of Atomic Energy of Canada Limited [14]. These tests were performed under controlled chemical

---

<sup>®</sup> CANada Deuterium Uranium, registered trademark of Atomic Energy of Canada Limited (AECL)

<sup>1</sup> While not the focus of this report, an understanding of the aqueous radiolysis-induced chemistry at temperatures below 100°C is also required for reactor safety cases in predicting the fission product chemistry/transport and hydrogen production after postulated Loss-of-Coolant accidents, e.g. see Reference [12].

<sup>2</sup> The term g-value is reserved for the homogeneous yield of the primary species after they have escaped the spur. The term G-value will refer to the measured yield of an experiment.

<sup>3</sup> The Critical Hydrogen Concentration is the minimum concentration of dissolved hydrogen required to prevent the net radiolytic breakdown of the water. Radiolysis is said to be in suppression when there is no net decomposition of the water due to the addition of excess hydrogen. This is when the concentration of oxygen and hydrogen peroxide are much lower than 1 µg/kg, i.e.,  $<10^{-8}$  mol/kg.

and physical conditions similar to those found in the coolant circuits in nuclear power reactors. The concentrations of hydrogen and oxygen in the circulating coolant were monitored continuously at three points around the loop as the coolant chemistry was changed by additions of either hydrogen or oxygen over a range of loop powers and temperatures. In some tests, the coolant was permitted to boil with steam qualities up to 9 wt% at the core outlet. A description of these tests can be found in Reference [14].

Within Reference [14], more detailed experimental information was provided for one well-defined non-boiling test that is sufficient to compare the radiolysis simulations with the experimentally observed time profile of the hydrogen and oxygen concentrations. From earlier benchmarking attempts, it was recognised that radiolysis simulations using the then-current AECL radiolysis model gave poor fits to the U-2 loop experimental data [15]. Several options were explored to achieve a satisfactory simulation of the experiment results, which included the operating conditions of dose rates and thermal-hydraulics. Finally, Glowa (published in internal AECL reports) was able to simulate the radiolysis water chemistry in the U-2 loop well as shown in Figure 1-1. However, this fit required that the rate constant for reaction:<sup>4</sup>



be reduced to ~15% of the measured value of  $8 \times 10^8$  L/mol/s at 300°C [16]. The modification of this single rate constant provided an acceptable fit to the experimental results (CHC, oxygen and hydrogen concentration time profiles including their steady-state concentrations) as shown in Figure 1-1, whereas other approaches such as including impurities failed to simulate all the qualitative features of the data. This unrealistically lowering of a measured rate constant indicated that a re-evaluation was required of the radiolysis database used, including the rate constants, the reaction mechanisms and the g-values.

Henshaw and Sims [17] have attempted to model just the CHC observed in the U-2 loop test [14], but they did not attempt to model the temporal concentration profiles of the measured hydrogen and oxygen. The coolant radiolysis data set that they used underestimated the CHC by about a factor of three.

Most of the published high temperature water radiation chemistry models are largely based on data available up to the mid 1990's [13], [18]. Since about 2000, there has been a revival in the study of the high temperature radiolysis of water driven, in part, by the need for information on water in the super-critical regime ([16], [19] through [31]). These studies have re-measured g-values for the primary radiolysis species for low Linear Energy Transfer (LET) radiation and have re-measured many of the reaction rate constants. Generally, these studies have been able to extend the measurements to higher temperatures than the original investigations, thereby reducing or eliminating the need to extrapolate the data to the temperatures of interest.

More recently, it has been recognised that many of the published pulse radiolysis studies are subject to systematic errors as result of an incorrect value of  $G \times \epsilon$  value<sup>5</sup> being used for dosimetry and/or the incorrect extinction coefficient used for species such as the hydrated electron, hydroxyl radical and  $\text{HO}_2/\text{O}_2^-$ .

---

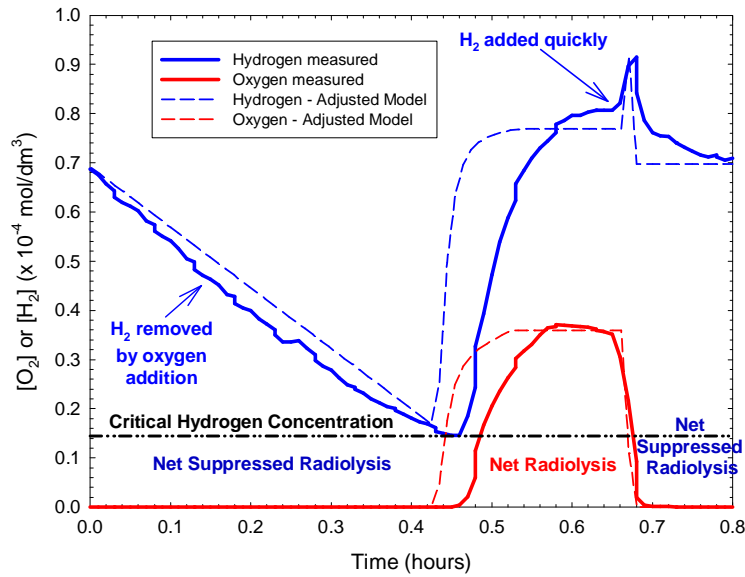
<sup>4</sup> The letter 'f' and 'b' after reaction numbers indicates whether it is a forward or back reaction of equilibrium.

<sup>5</sup> G is the yield of the absorbing species and  $\epsilon$  is its extinction coefficient at a given wavelength.

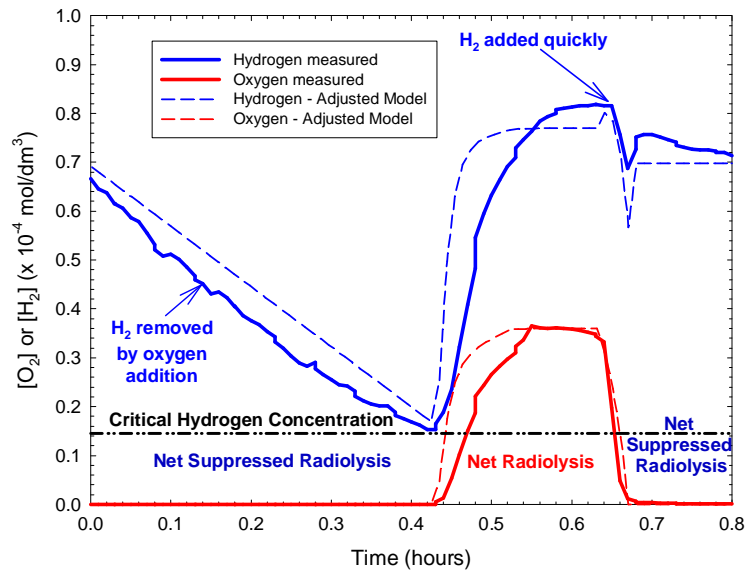
The objective of this report is to compile and review the radiolysis data now available and, where possible, correct the reported g-values and rate constants to provide a recommendation for the best values to use in high temperature modelling of light water radiolysis up to 350°C.

With a few exceptions, the review has been limited to those reactions that occur in slightly acid and slightly alkaline solutions, e.g., it does not address reactions involving the oxide radical anion,  $O^-$ , or ionized forms of hydrogen peroxide,  $HO_2^-$ , beyond their acid-base equilibria reactions. However, a few reactions have been included where the rate constant for a reaction involving  $O^-$  is significantly larger than the corresponding hydroxyl radical reaction rate constant and thus can influence the chemistry below the  $pK_A$  of the hydroxyl radical.





### O-17 Inlet Sampling Location



### O-17 Outlet Sampling Location

**Figure 1-1 Results of preliminary radiolysis modelling of the data that shows agreement between the hydrogen and oxygen profiles around the time of hydrogen addition. To obtain the fit, the radiolysis model had an unreasonably low value for the  $\text{OH} + \text{H}_2 \rightarrow \text{H} + \text{H}_2\text{O}$  rate constant. (Simulations performed by G. Glowa, AECL-CRL)**

## 2. METHODOLOGY

The data reviewed for this report have been measured in a number of laboratories around the world and over about a 50-year time span. Over this time period, the understanding of aqueous radiolysis has continually improved and new information has been continually accumulated. In doing any review of radiolysis data, one has to be cognisant of the state of knowledge when the research was performed. This has an impact on the reliability or accuracy of some of the data published. Corrections to published data can sometimes be undertaken. Some general examples are given below to illustrate the issues.

### 1. Three simple cases are:

- The simplest case is when no correction is necessary such as the measurement of a pseudo-first order rate constant from a time dependence of the transient absorption in a pulse radiolysis experiment.
- If an incorrect extinction coefficient is used for extracting the second order rate constant from the time dependence of an absorption in a pulse radiolysis experiment, it is a straightforward correction to the rate constant provided the original and the correct extinction coefficient are known.
- If an outdated  $G \times \epsilon$  value was used for a dosimeter in pulse radiolysis for a yield measurement, a simple correction to the results can generally be undertaken using the revised  $G \times \epsilon$  value [32].

### 2. Cases which are complex or un-resolvable:

- Situations where a rate constant for a particular reaction has required computer modelling of the time profile of an absorbance where a number of competing or parallel reactions are involved. If incorrect dosimetry, extinction coefficients and/or rate constants were used, it is generally not possible to correct the derived rate constant accurately as it requires remodelling the data.

In this report, where possible, corrections have been made to the published results. These corrections will be noted in the text.

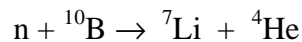
In a number of cases, especially where modelling has been used to fit rate constants, it is impossible to rework the data. In this case, the results will be presented as reported, or with minor corrections, but it will be noted that the rate constants are possibly in error. It should be noted that a large uncertainty in the value of many of the rate constants does not have a significant impact on the results of the radiolysis simulations. In general, there are only a small number of critically important reactions involved in the simulations. Sensitivity studies where the effect of varying the value of a rate constant on the simulated result can provide insight as to the acceptable uncertainty in a reaction rate constant. This sensitivity check should be done for the modelling conditions where net radiolysis is suppressed and is not suppressed. This is

necessary as different reactions can be important under the two conditions. It is recommended for those critical reactions which do impact on the simulated results that, if the experimental determination of the rate constant as a function of temperature is questionable, the determination should be repeated to establish the correct result.

As will be discussed in Section 3, the measurement of G-values by pulse radiolysis techniques requires a knowledge of the extinction coefficient of the absorbing, often transient, species as a function of temperature. The 'choice' of this extinction coefficient can be a subjective exercise and can lead to uncertainties in the measured yields and rate constants. Where possible, extinction coefficients have been 'chosen' which provided the most consistent g-values that were in material balance with the decomposition of water.

The approach used in this report is to establish the g-values for the primary species formed in the decomposition of water by low LET radiation, i.e., fast electron and gamma-radiation, as a function of temperature. These established g-values are then used to correct the measured rate constants where applicable. Finally, the g-values for higher LET radiation as a function of temperature will be presented as these form the basis of the calculation of the g-values associated with the fast neutron radiolysis. The estimation of the g-values for fast neutron irradiation requires the energy spectrum of the neutrons specific to the reactor being modelled. An example is provided on how to estimate the g-values for fast neutrons.

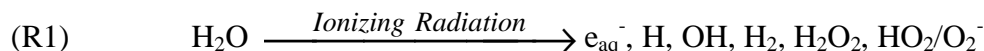
The same high LET g-value information can be used to estimate the g-values associated with the recoil of lithium ions and  $\alpha$ -particles from the nuclear reaction:



where boron-10, as boric acid, is used as a reactivity control chemical to limit the flux of thermal neutrons in a PWR core.

### 3. LOW LINEAR ENERGY TRANSFER G-VALUES

In this section, the temperature dependence for the g-values for the primary radiolysis species formed in Reaction (R1) will be assessed:



The yields will be reported in 'old' units for g-value of number formed per 100 eV of energy absorbed.<sup>6</sup>

Only the g-values for low LET radiation will be considered in this section. The principal reason for establishing these yields at this point in the report is that these yields are required for re-evaluation of some of the rate constants. Low LET radiation is typical of the gamma-radiation and high-energy electrons used in laboratory studies as well as the gamma-radiation found in the core of a water-cooled reactor from fission and activation processes. For this type of radiation, energy deposition tends to occur in well-separated locations giving rise to small clusters of excited and ionized molecules, called spurs. In the spurs, for primary species created close together, there is a competition between their reaction and their diffusion out of the spur. Thus the yields and spatial distribution of the primary species are, in general, a function of time after the ionization/excitation event, and trend towards a limiting 'escape' yield. The g-values given here will ideally be close to the 'escape' yields from the spur, i.e., effectively the 'homogeneously distributed' yields reached by about 1  $\mu$ s after the ionizing event for most applications.

The g-values for the fast neutrons, which deposit most of their energy by ion recoils following inelastic collisions, depends on the energy spectrum of the fast neutrons entering the water. These g-values will be discussed later in the report in Section 6.

The data for high temperature g-values can be broken down into two classes:

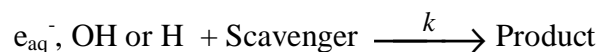
1. Yields available from steady-state radiolysis experiments where products are measured after irradiation and the radiation field intensity has been determined by reliable, well-established dosimetry methods. The analytical chemistry measurements are all made at room temperature.
2. Yields from pulse radiolysis experiments where the yield is determined from the transient absorption after a short pulse of radiation at the temperature of interest. These require knowledge of the extinction coefficient of the absorbing species as a function of temperature. As noted above in Section 2, sometimes there are issues associated with the dosimetry choice used in the pulse radiolysis experiments, requiring correction of the reported data.

In general, the reported yields from steady-state experiments, provided that the solutes and the products are thermally stable over the temperature range used, are considered to be the more reliable and will be used preferentially in this report.

The major issue with either method of yield measurement is the concentration of solutes present to scavenge the primary species.

---

<sup>6</sup> To convert yields in 'old' units of #/100 eV to S.I. units of mol/J multiply by  $1.036 \times 10^{-7}$ .



The scavenger acts in competition with recombination reactions, which would otherwise occur, including the intra-spur recombinations. One can easily measure a g-value significantly larger than the ideal 'escape yield' by adding too much scavenger. As the scavenger concentration is typically two or more orders of magnitude greater than that of the primary specie formed, the 'scavenging power' is defined as the pseudo-first order rate constant:  $k[\text{Scavenger}]$ . At room temperature, to ensure minimal scavenging in the spur, it has been generally agreed that the value of  $k[\text{Scavenger}]$  should be  $10^7 \text{ s}^{-1}$  or lower [33]. In actual fact, this scavenging power can still give a g-value on the order of 5% larger than the true escape yield, and lower scavenging powers are preferred. At too low a scavenger concentration, experiments may become limited by the presence of impurities or other signal/noise issues, and the homogeneous reactions between primary species. An unresolved question is how low the scavenging power must be at high temperature (e.g., 300°C) in order to give a good representation of the escape yield.

The room temperature g-values for water under low LET radiation conditions ( $10^7 \text{ s}^{-1}$  scavenging power) are well established (Table 3-1) [34], [35]. For the purpose of this section, as the g-value for  $\text{HO}_2/\text{O}_2^-$  under low LET radiation is so small, the g-value for  $\text{HO}_2/\text{O}_2^-$  will be assumed to be zero. It should be remembered that the yields of the primary species are measured using various scavenging systems and that there is some scatter in the reported yields [36]. Any measurement of the temperature dependence of a g-value should start, within experimental uncertainty, with the room temperature values given in (Table 3-1). For the purpose of this report, the g-values listed by Spinks and Woods [34] have been used as the reference room temperature values.

As noted above, there are a number of issues associated with some of the high temperature experiments used to measure yields. In some cases, the solutions used have solute concentrations that have lead to some scavenging in the spur. In other cases, there has been some uncertainty about the dosimetry used in the pulse radiolysis investigations. In both these cases, provided that there is no other issue, such as temperature dependence of an extinction coefficient, the *relative* change of yield with temperature can be useful to corroborate a temperature dependence observed in other experiments.

In this section, the temperature dependent yield for each primary specie will be assessed separately and then the information will be collected to produce a set of polynomials, which describe the g-values over the temperature range 20° to 350°C.

**Table 3-1**  
**g-Values for water at near neutral pH at room temperature for low LET radiation**

Primary Species	$e_{aq}^-$	H	OH	H <sub>2</sub>	H <sub>2</sub> O <sub>2</sub>	HO <sub>2</sub> /O <sub>2</sub> <sup>-</sup>	Reference
<b>g-Value</b> (#/100 eV)	2.63	0.55	2.72	0.45	0.68	0.008	[34]
<b>g-Value</b> (#/100 eV)	2.70	0.61	2.87	0.43	0.61	0.026	[35]

### 3.1 g-Value: Hydrated Electron

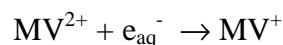
The temperature dependence for the g-value of the hydrated electron has been reported by a number of laboratories [26], [28], [37], [38], [39], [40]. To determine the temperature dependence for the g-value, the product analysis studies have been used as the dosimetry is less prone to error and there are no issues with the value of extinction coefficients as found with the pulse radiolysis studies. In Figure 3-1, the results of those studies are shown [26], [37], [38], [40]. This data indicates that the g-value for the hydrated electron increases above room temperature reaching a maximum near 250°C and then slightly decreases. In Figure 3-1, the dash-dot line indicates the recommended temperature dependence for the g-value. The basis for this line up to 250°C is the G(N<sub>2</sub>) measured from 2.5×10<sup>-3</sup> mol/kg N<sub>2</sub>O/0.02 mol/kg perdeutero-ethanol solution as this solution provides the lowest scavenging powers [26]. Above 250°C, a chain reaction producing excess nitrogen was suspected which involved the reducing radical derived from ethanol [26]. Above 250°C, the g(e<sub>aq</sub><sup>-</sup>) yield was approximated as being parallel to that from the 2.5×10<sup>-3</sup> mol/kg N<sub>2</sub>O/0.01 mol/kg phenol solution where the hydroxyl radical scavenging power was slightly higher and will have slightly increased the measured G(N<sub>2</sub>).

The temperature dependence for the g-value for the hydrated electron is given by:

$$g(e_{aq}^-) = 2.641 + 4.162 \times 10^{-3} t + 9.093 \times 10^{-6} t^2 - 4.717 \times 10^{-8} t^3$$

where t is the temperature in °C. The reader is reminded that scavenged yields asymptotically approach the true escape yield from higher values. Even though the lowest available scavenging power was used for the g-value estimate, it may be still be high by several percent.

In Figure 3-2, the hydrated electron yields as measured in pulse radiolysis experiments using methyl viologen (MV<sup>2+</sup>) as an electron scavenger and t-butanol as a hydroxyl scavenger are shown [28], [38], [39].



These results have all been corrected/normalized to the dosimetry value of G×ε of 2.51×10<sup>4</sup> (G in #/100 eV and ε in L/mol/cm) recommended by Buxton and Stuart [32] for the oxygen saturated 10<sup>-2</sup> mol/L thiocyanate dosimeter at 475 nm. Where required, the data for the methyl

viologen cation radical ( $MV^+$ ) was corrected using the room temperature extinction coefficient at 605 nm of 13,700 L/mol/cm [41] and the temperature dependence of this absorption as measured by Shiraishi et al. [39].

As can be seen in Figure 3-2, the estimated  $g(e_{aq}^-)$  from  $G(MV^+)$  tended to parallel the 'recommended' fit line for  $g(e_{aq}^-)$  from the product analyses and, with the exception of the data from Lin et al. [28], all tended to be slightly higher. The slight elevation above the fit line for the solutions containing  $\sim 2.6 \times 10^{-4}$  mol/kg  $MV^{2+}$  and 0.01-0.02 mol/kg t-butanol [38] can probably be assigned to the small extra formation of  $MV^+$  from the scavenging of the hydrogen atoms by methyl viologen [42].<sup>7</sup> The reason the results of Shiraishi et al. [39], who used  $\sim 10^{-3}$  mol/kg  $MV^{2+}$ , lie further above the recommended line is that scavenging of the hydrated electron in the spur has occurred to increase the yield [33]. No explanation can be suggested as to why the results of Lin et al. [28], who used  $5 \times 10^{-4}$  mol/kg  $MV^{2+}$  and 0.02 mol/kg t-butanol, lie noticeably below the recommended line.

Above 150°C there is a definite increase of the  $G(MV^+)$  above the recommended  $g(e_{aq}^-)$  line (Figure 3-2) for the results of Elliot et al. [38] and Shiraishi et al. [39]. One likely reason for this deviation could be the inaccuracies in the estimation of the temperature dependence for the extinction of the  $MV^+$  cation at 605 nm at these elevated temperatures [39].

---

<sup>7</sup> The high rate of reaction of hydrogen atoms with  $MV^{2+}$  of  $6.4 \times 10^8$  L/mol/s (25°C) [42] ensures essentially complete scavenging of the hydrogen atoms in competition with the t-butanol present. It is reported that ~15% of the hydrogen atoms are converted to  $MV^+$ , i.e., an increase in  $G(MV^+)$  of ~0.1.

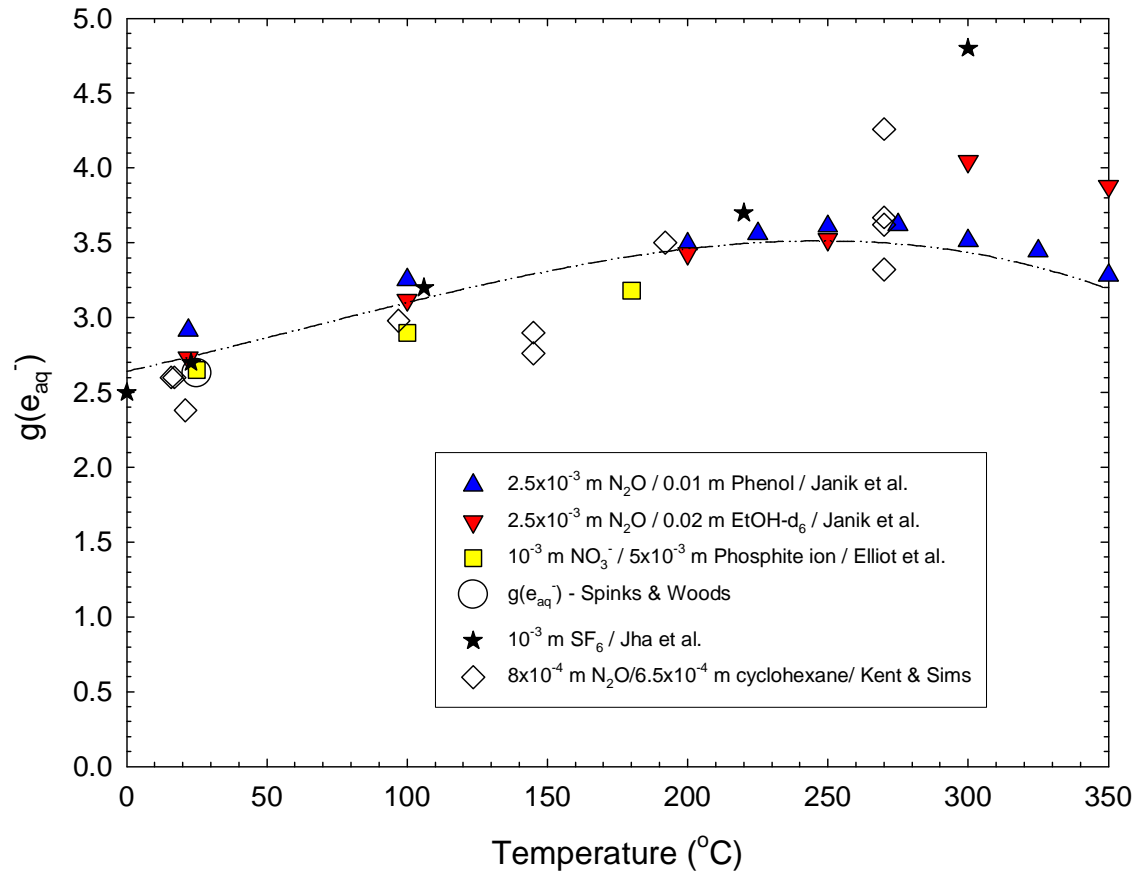


**Figure 3-1** The g-value for the hydrated electron as a function of temperature as measured from experiments where a stable product was analyzed by Jha et al. [37], by Elliot et al. [38], by Kent and Sims [40] and by Janik et al. [26]. The dash-dot-dot line is the recommended temperature dependence for  $g(e_{aq}^-)$  based on nitrogen yields from  $\text{N}_2\text{O}$  containing solutions – see text for more information. The ‘accepted’ room temperature value for  $g(e_{aq}^-)$  given by Spinks and Woods [34] in Table 3-1 is also plotted.



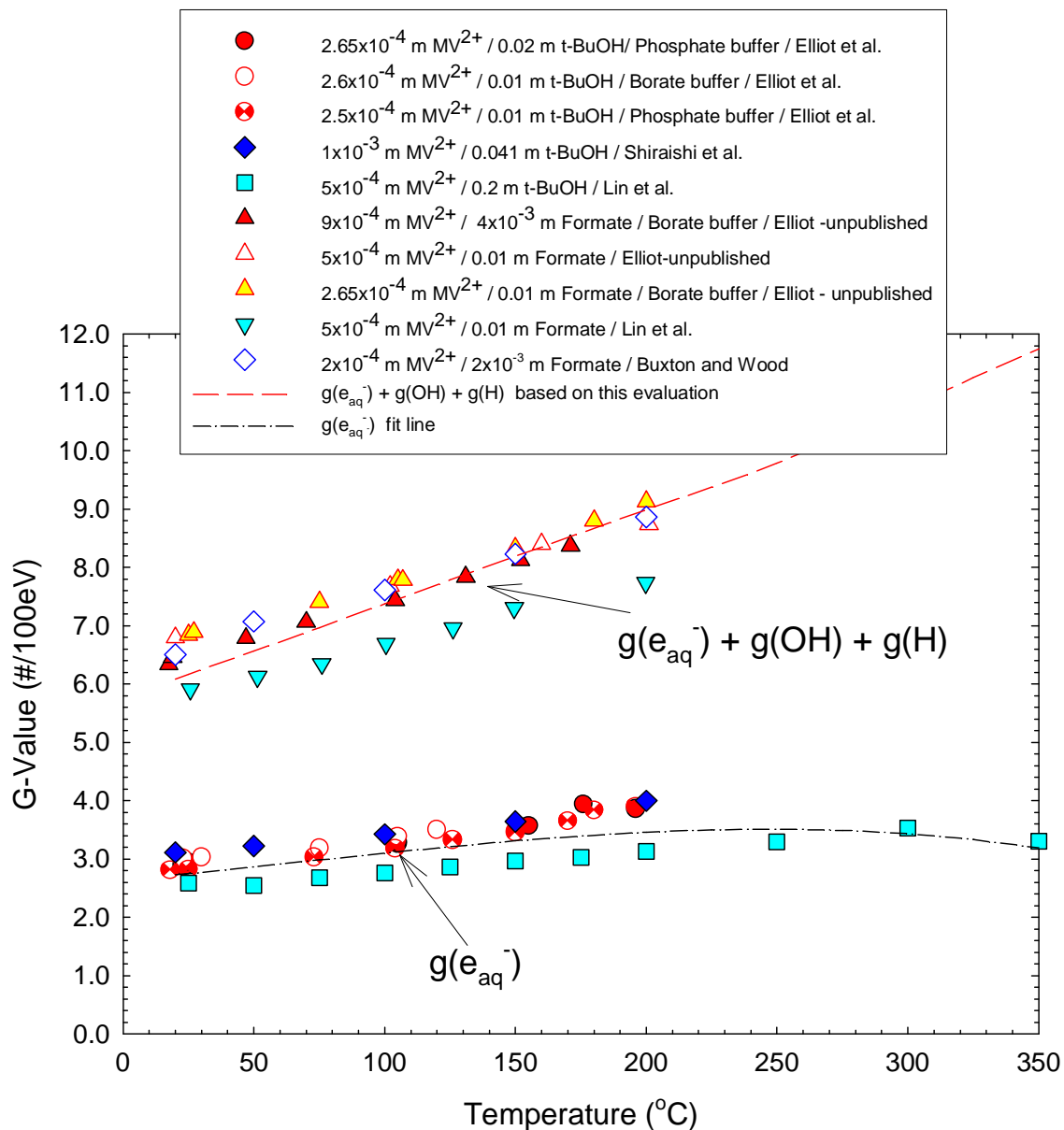


**Figure 3-2 The measured  $g(e_{aq}^-)$  and  $\{g(e_{aq}^-) + g(OH) + g(H)\}$  using the transient  $MV^+$  absorption as a function of temperature by Elliot et al. [38], by Shiraishi et al. [39] by Lin et al. [28], and by Buxton and Wood [43]. The recommended temperature dependence for  $g(e_{aq}^-)$  from Figure 3-1 and the value for  $\{g(e_{aq}^-) + g(OH) + g(H)\}$  calculated from the material balance equations in Section 3.6 are also given.**

### 3.2 g-Value: Hydroxyl Radical

A chemical system has yet to be found where a stable end product can be measured with confidence after the irradiation to determine the dependence of  $g(\text{OH})$  with temperature up to 350°C. All reports on hydroxyl radical yields as a function of temperature have involved pulse radiolysis experiments where the OH radical is converted into a longer-lived product. The results from these experiments are subject to the  $G \times \epsilon$  used for the dosimeter and the value of the extinction coefficient used for the long-lived absorption.

Elliot et al. [38] have measured the  $g(\text{OH})$  using aerated  $10^{-3}$  mol/kg ferrocyanide ion solution between 20° and 105°C and using aerated 0.025-0.1 mol/kg bicarbonate ion solutions. These  $g$ -values are shown in Figure 3-3. The  $g$ -values in Figure 3-3 have all been normalized to the value of  $G \times \epsilon$  of  $2.51 \times 10^4$  ( $G$  in #/100 eV and  $\epsilon$  in L/mol/cm) at 475 nm for the oxygen saturated  $10^{-2}$  mol/L thiocyanate dosimetry as recommended by Buxton and Stuart [32]. In the case of the ferrocyanide ion solution, the temperature dependence of the extinction coefficient of the product ferricyanide ion has been measured up to 90°C in a spectrophotometer and extrapolated to 105°C [38].

The temperature dependence of the extinction coefficient for the  $\bullet\text{CO}_3^-$  radical formed by the reaction of hydroxyl radicals with bicarbonate ions has not been established.<sup>8</sup> The optical spectrum of  $\bullet\text{CO}_3^-$  broadens slightly on the high-energy side as the temperature increases as shown in Figure 3-4 [38] and as confirmed in Reference [44]. This suggests that the extinction coefficient at a given wavelength is temperature dependent. If it is assumed that the integrated absorption coefficient for this absorption is constant over the 20°-300°C range of interest, then the relative extinction coefficient at the peak maximum as a function of temperature can be estimated in two ways. The relative extinction coefficient should decrease as the inverse of the spectral bandwidth at half-height as a function of temperature or as the ratio of the area under the normalized absorption curves. Both methods give the same temperature dependence as shown in Figure 3-5. This is summarised in Table 3-2.

In calculating the  $g$ -value for the hydroxyl radical, an estimate for the extinction coefficient at room temperature for the carbonate radical anion at 600 nm of 2,000 L/mol/cm was selected based on the reported values of 1,934 L/mol/cm [38], 2,000 L/mol/cm [45], and 2,062 L/mol/cm [46].<sup>9</sup> Using 2,000 L/mol/cm gives a value for  $g(\text{OH})$  of 2.7 at room temperature in agreement with the value in Table 3-1 thus effectively normalizing the results to the accepted value for  $g(\text{OH})$ .

Figure 3-3 shows the estimates of  $g(\text{OH})$  both assuming the temperature dependence for the extinction coefficient as shown in Table 3-2 and also assuming a temperature invariant extinction coefficient. As can be seen in Figure 3-3, the temperature dependence for  $g(\text{OH})$  assuming a

<sup>8</sup> It should be noted that Wu et al. [44] have postulated that the  $\bullet\text{CO}_3^-$  radical is actually a 'dimer' radical of the acid-base form  $\text{H}(\text{CO}_3)_2 \bullet^{2-} / (\text{CO}_3)_2 \bullet^{3-}$ .

<sup>9</sup> These values have been corrected to  $G \times \epsilon$  for  $\text{N}_2\text{O}$  or air saturated /0.01 mol/L  $\text{SCN}^-$  dosimetry as recommended by Buxton and Stuart [32].

temperature independent or dependent extinction coefficient are both in agreement within experimental uncertainty with the  $g(\text{OH})$  estimated from the yield of ferricyanide ions from pulse irradiated aerated  $10^{-3}$  mol/kg ferrocyanide ion solutions.

The temperature dependence up to  $300^\circ\text{C}$  for  $g(\text{OH})$ , assuming a temperature dependence as given in Table 3-2 for the extinction coefficient of  $\bullet\text{CO}_3^-$ , is given by:

$$g(\text{OH}) = 2.557 + 1.012 \times 10^{-2} t$$

and for the  $g(\text{OH})$  assuming temperature independent extinction coefficient for  $\bullet\text{CO}_3^-$ :

$$g(\text{OH}) = 2.535 + 9.554 \times 10^{-3} t - 7.966 \times 10^{-6} t^2$$

where  $t$  is the temperature in  $^\circ\text{C}$ .

As will be discussed below in Section 3.6, based on material balance considerations it appears that the most appropriate function for  $g(\text{OH})$  up to  $\sim 250^\circ\text{C}$  is the one derived from the temperature dependent extinction coefficient. Above  $250^\circ\text{C}$ , material balance consideration suggests that this equation may slightly under predict  $g(\text{OH})$ .

**Table 3-2**  
**The extinction coefficient at 600 nm for the  $\bullet\text{CO}_3^-$  as a function of temperature**

Temperature ( $^\circ\text{C}$ )	Relative Intensity	Extinction Coefficient (L/mol/cm)
30	1.00	2000
75	0.96	1918
150	0.93	1853
193	0.89	1773
273	0.86	1730
295	0.85	1706

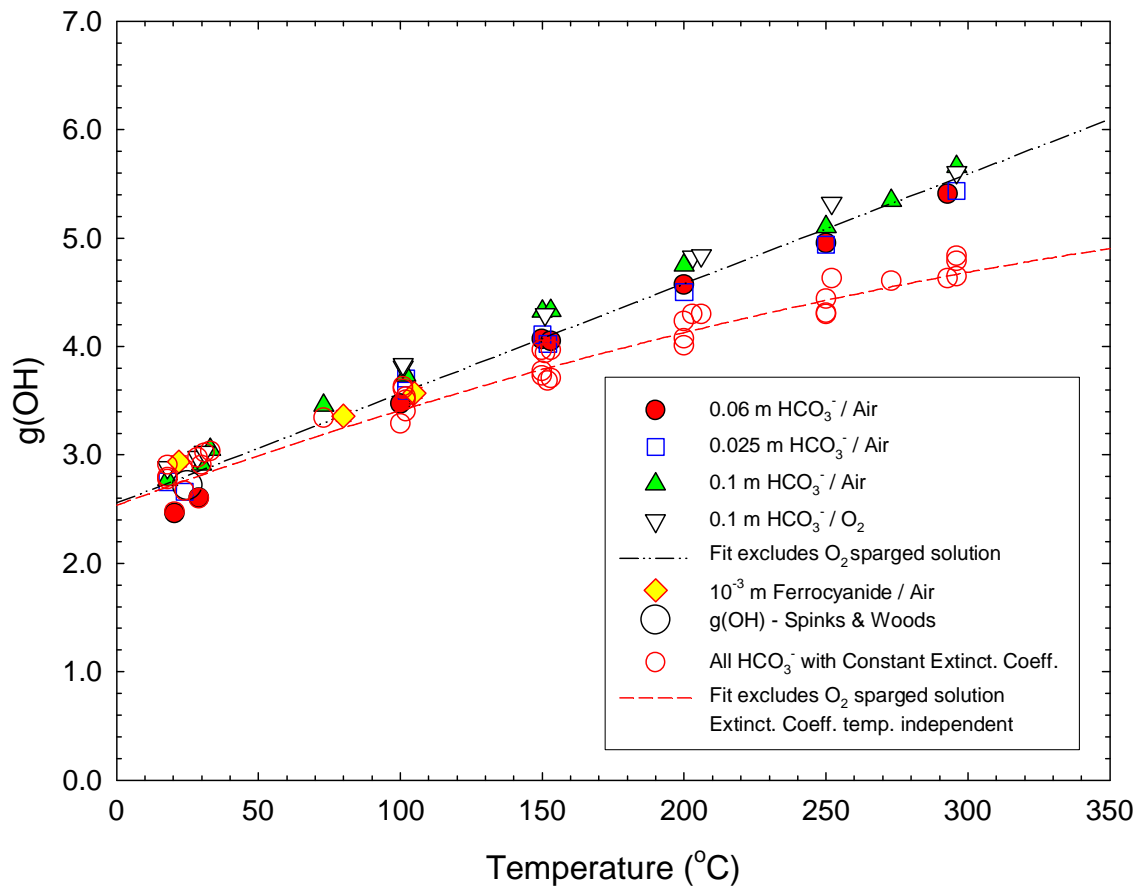


**Figure 3-3 The g-value for the hydroxyl radical measured as a function of temperature by Elliot et al. [38]. The black dash-dot-dot line is the recommended temperature dependence for  $g(\text{OH})$  based on a temperature dependent extinction coefficient for the  $\bullet\text{CO}_3^-$ . The red dash line is the recommended temperature dependence for  $g(\text{OH})$  based on a temperature independent extinction coefficient for the  $\bullet\text{CO}_3^-$ . The ‘accepted’ room temperature value for  $g(\text{OH})$  given by Spinks and Woods [34] in Table 3-1 is also plotted.**

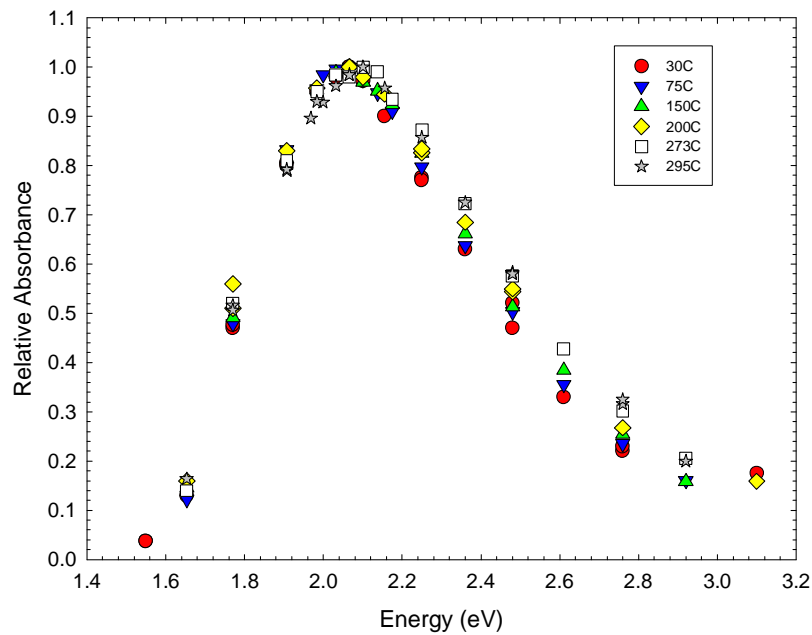


**Figure 3-4 The normalized absorption spectra for the carbonate radical anion as a function of temperature [38].**

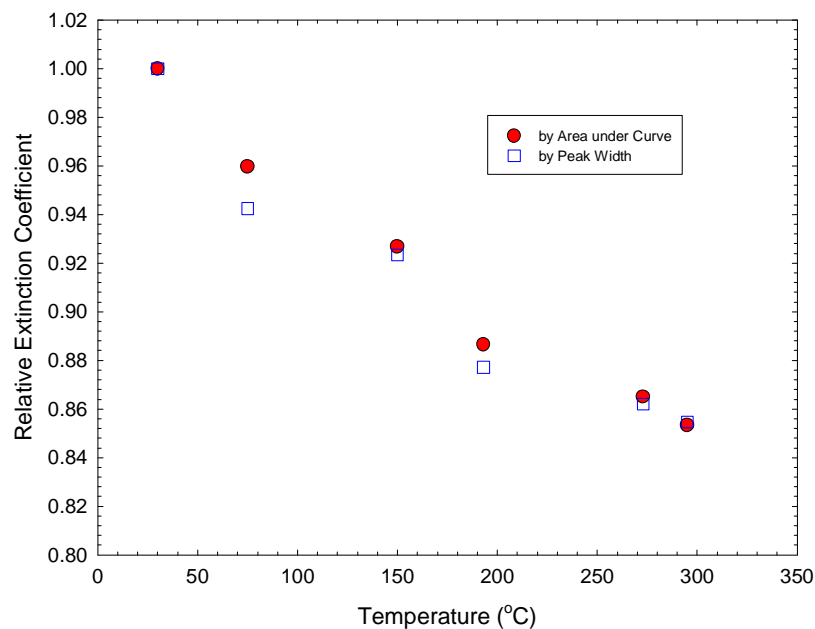


**Figure 3-5 The relative extinction coefficient of the carbonate radical anion based on the area under the absorption curve and on the width of the absorption peak at half height, based on the spectra shown in Figure 3-4 .**

### 3.3 g-Value: Hydrogen Peroxide

The temperature dependence of the hydrogen peroxide yield as estimated by Elliot et al. [38], by Kent and Sims [40] and by Stefanic and LaVerne [47] are shown in Figure 3-6.

Elliot et al. measured hydrogen peroxide directly from a degassed  $5 \times 10^{-4}$  mol/kg acrylamide solution [38] up to 100°C. The  $g(\text{H}_2\text{O}_2)$  reported in these acrylamide experiments have been corroborated in unpublished results (at AECL-CRL) using degassed solutions containing  $10^{-3}$  mol/kg  $\text{NO}_3^-$  /  $10^{-4}$  mol/kg  $\text{NO}_2^-$  as shown in Figure 3-6.

Kent and Sims [40] estimated  $g(\text{H}_2\text{O}_2)$  assuming that it was equivalent to  $G(\text{O}_2)$  from a slightly alkaline solution containing  $\text{N}_2\text{O}$  and  $10^{-3}$  or  $10^{-4}$  mol/kg iodide ions.

Stefanic and LaVerne [47] measured  $g(\text{H}_2\text{O}_2)$  directly in irradiated de-aerated  $2.5 \times 10^{-2}$  mol/kg  $\text{NO}_3^-$  containing methanol over the temperature range 25° to 150°C. The yields shown in Figure 3-6 are the limiting yields at low methanol concentrations.<sup>10</sup>

There is reasonable agreement between the three independent sets of results. From a fit of the data, the temperature dependence of  $g(\text{H}_2\text{O}_2)$  is given by the linear equation:

$$g(\text{H}_2\text{O}_2) = 0.752 - 1.620 \times 10^{-3} t$$

where t is the temperature in °C.

---

<sup>10</sup> Stefanic and LaVerne [47] also measured the limiting hydrogen peroxide yield from de-aerated  $2.5 \times 10^{-2}$  mol/kg  $\text{NO}_3^-$  containing bromide ions. This data was not used in the current assessment as it is believed the measured hydrogen peroxide yields are low as a consequence of transient  $\text{HOBr}^-$  reacting with peroxide.

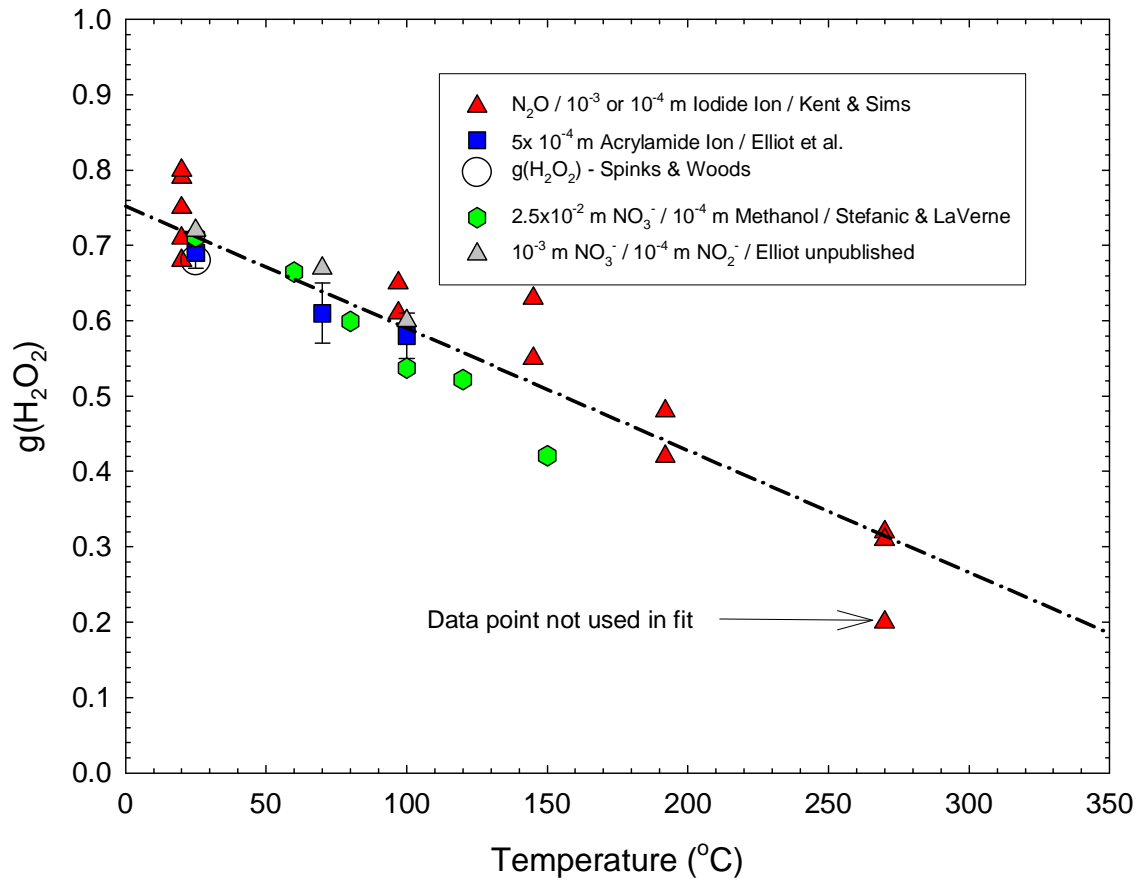


**Figure 3-6** The g-value for H<sub>2</sub>O<sub>2</sub> measured as a function of temperature by Elliot et al. [38], Elliot (unpublished), Kent and Sims [40] and Stefanic and LaVerne [47]. The dash-dot line is the recommended temperature dependence for g(H<sub>2</sub>O<sub>2</sub>). The 'accepted' room temperature value for g(H<sub>2</sub>O<sub>2</sub>) given by Spinks and Woods [34] in Table 3-1 is also plotted.

### 3.4 g-Value: Molecular Hydrogen

The molecular hydrogen yield,  $g(\text{H}_2)$ , as a function of temperature for water irradiated with low LET radiation has been measured by three laboratories [26], [38], [40]. The measured  $g$ -values are shown in Figure 3-7. There is good agreement between the measurements by Elliot et al. [38] who used the hydrogen yield from degassed nitrite ion containing solutions to the results from Janik et al. [26] who used a flowing  $2.5 \times 10^{-3}$  mol/kg  $\text{N}_2\text{O}$  solution containing either phenol or perdeutero-ethanol. The data from References [26] and [38] was used to define the temperature dependence for  $g(\text{H}_2)$ .

$$g(\text{H}_2) = 0.419 + 8.721 \times 10^{-4} t - 4.971 \times 10^{-6} t^2 + 1.503 \times 10^{-8} t^3$$

where  $t$  is the temperature in  $^{\circ}\text{C}$ .

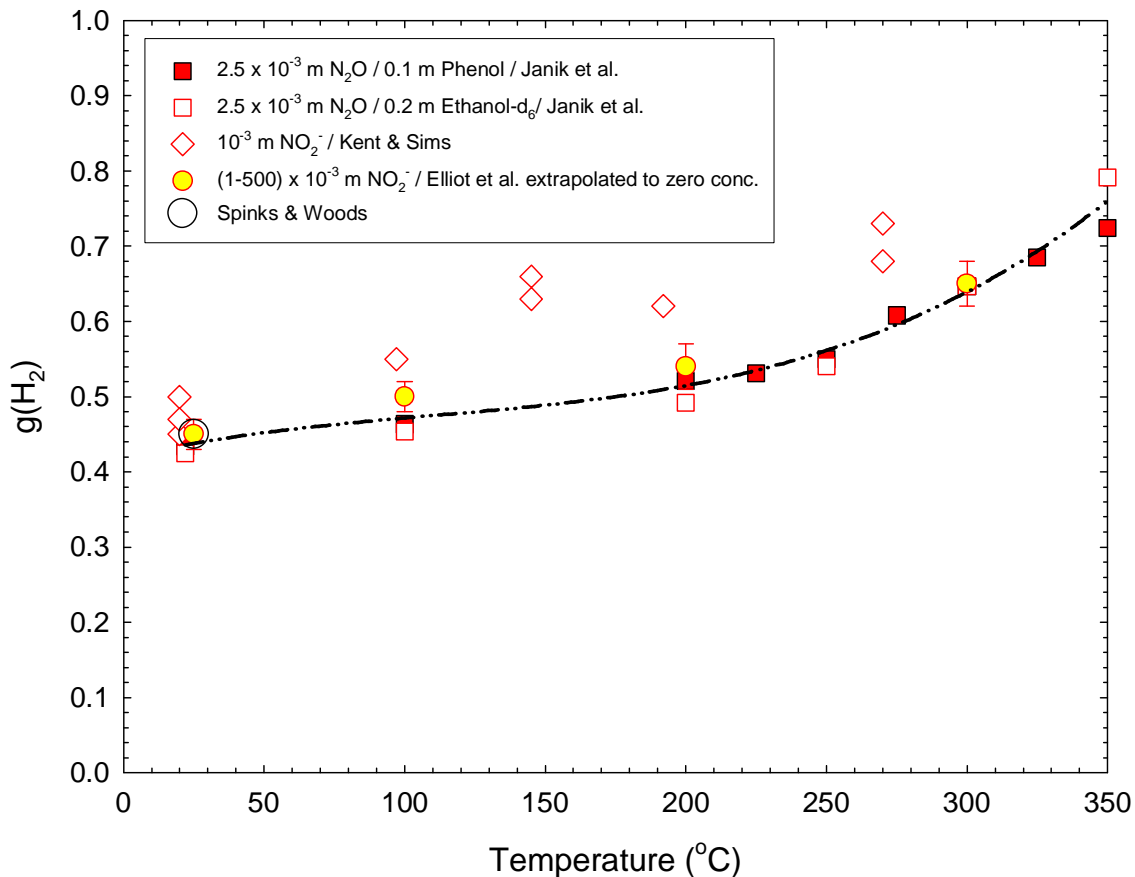


**Figure 3-7** The  $g$ -value for  $\text{H}_2$  measured as a function of temperature by Janik et al. [26], Elliot et al. [38] and Kent and Sims [40]. The dash-dot line is the recommended temperature dependence for  $g(\text{H}_2)$ . The ‘accepted’ room temperature value for  $g(\text{H}_2)$  given by Spinks and Woods [34] in Table 3-1 is also plotted.



### 3.5 g-Value: Hydrogen Atoms

Elliot et al. [38] have estimated the g-value for hydrogen atoms,  $g(\text{H})$ , up to 200°C by subtracting the g-value for molecular hydrogen  $g(\text{H}_2)$  from the total  $G(\text{H}_2)$  measured in degassed solutions containing  $10^{-3}$  mol/kg nitrate ion and  $5 \times 10^{-3}$  mol/kg phosphite ion. The latter yield was assumed to be the total of  $g(\text{H}) + g(\text{H}_2)$ .<sup>11</sup> The  $g(\text{H})$  measured by this difference method is shown by the black stars in Figure 3-8. The room temperature value is in agreement with the accepted values reported in Table 3-1.

Janek et al. [26] have attempted to measure  $g(\text{H})$  directly by measuring the yield of HD from a solution containing  $2.5 \times 10^{-3}$  mol/kg  $\text{N}_2\text{O}$ / 0.2 mol/kg perdeutero-ethanol. These results are shown as the open stars in Figure 3-8. Some caution has to be placed on these results on two counts. Firstly the room temperature value is significantly below the accepted value, as already noted in Reference [26], probably because the scavenging efficiency was too low. Secondly, the rapidly increasing g-values above 250°C are occurring in a temperature range where an increase in  $G(\text{N}_2)$  was attributed to a short chain reaction occurring [26] and where Elliot et al. [48] had also observed increased hydrogen yields in alcohol containing solutions.

To clarify this situation, an estimate of the ratio of  $g(\text{H})/G(e_{\text{aq}}^-)$  has been made by analysing absorption of the hydrated electron in alkaline solutions where H atoms react with hydroxide ions to form the hydrated electron following the pulse.



The analysis was carried out on absorption time profiles from experiments performed by Bartels and co-workers previously. Experiments in de-oxygenated alkaline solutions (designed to measure the reaction of hydrated electron with hydroxyl radical (see Section 4.1.5 below)) were analysed by correcting the initial growth for the simultaneous decay of the reacting species. A second set of profiles was from the experiments studying the bimolecular decay of the hydrated electron in alkaline solutions containing an over-pressure of hydrogen (see Section 4.1.1). In this case, as the hydroxyl radicals are also converted to hydrogen atoms, the ratio that is estimated is  $(g(\text{H}) + g(\text{OH}))/g(e_{\text{aq}}^-)$ . As  $g(\text{OH})$  and  $g(e_{\text{aq}}^-)$  are known (Sections 3.1 and 3.2), the value for  $g(\text{H})/g(e_{\text{aq}}^-)$  can be determined. The values for  $g(\text{H})/g(e_{\text{aq}}^-)$  from both experiments are shown in Figure 3-9.<sup>12</sup>

From the g-value of the hydrated electron given in Section 3.1, an estimate of the g-value for hydrogen atoms can be made. This estimate is shown by the '✕' symbols in Figure 3-8. At 200°C, there is acceptable agreement with  $g(\text{H})$  as measured by Elliot et al. [38] using product analysis. Above 200°C, these  $g(\text{H})$  values support the increase in  $g(\text{H})$  above 200°C as measured using the HD yield by Janik et al. [26]. Indeed, the HD yield measurements gave a value that was too low, probably because of insufficient scavenging power.

<sup>11</sup> The temperature dependence of the value of  $G(\text{H}_2)$  ( $= g(\text{H}) + g(\text{H}_2)$ ) has been confirmed using three different solutions – see Figure 7 in Reference [48].

<sup>12</sup> It should be noted that these numbers represent a minimum value of the ratio. The experiments need to be repeated by obtaining data at the lowest dose per pulse compatible with good signal-to-noise, to minimize the second order decay of the radical species.

As will be described in the next Section 3.6, a recommended equation for the dependence of the  $g(H)$  with temperature is given by:

$$g(H) = 0.556 + 2.198 \times 10^{-3} t - 1.184 \times 10^{-5} t^2 + 5.223 \times 10^{-8} t^3$$

where  $t$  is the temperature in  $^{\circ}C$ . This equation has been developed from material balance considerations.

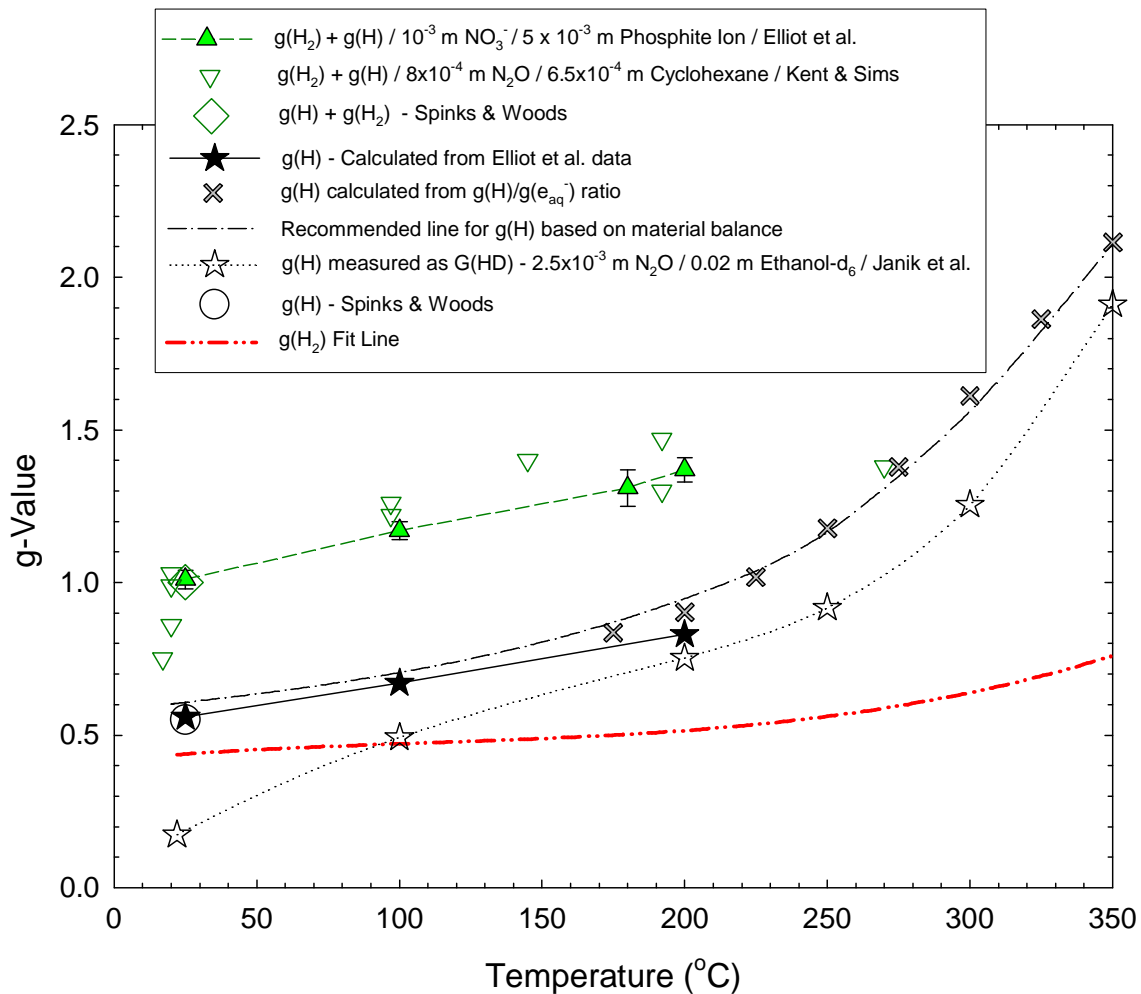


**Figure 3-8** The G-values measured for hydrogen as a function of temperature by Janik et al. [26], Elliot et al. [38] and Kent and Sims [40]. The solid black stars are  $g(H)$  as calculated from the difference between  $G(H_2 + H)$  as measured by Elliot et al. [38] and  $g(H_2)$  (red dash-dot-dot line) taken from Figure 3-7. Also shown are the estimates for  $g(H)$  based on the  $g(H)/g(e_{aq^-})$  given in Figure 3-9 – see text. The recommended functional dependence for  $g(H)$  determined by a material balance fit in Section 3.6 is also shown. The ‘accepted’ room temperature values for  $g(H)$  and  $g(H) + g(H_2)$  as given by Spinks and Woods [34] in Table 3-1 are also plotted.

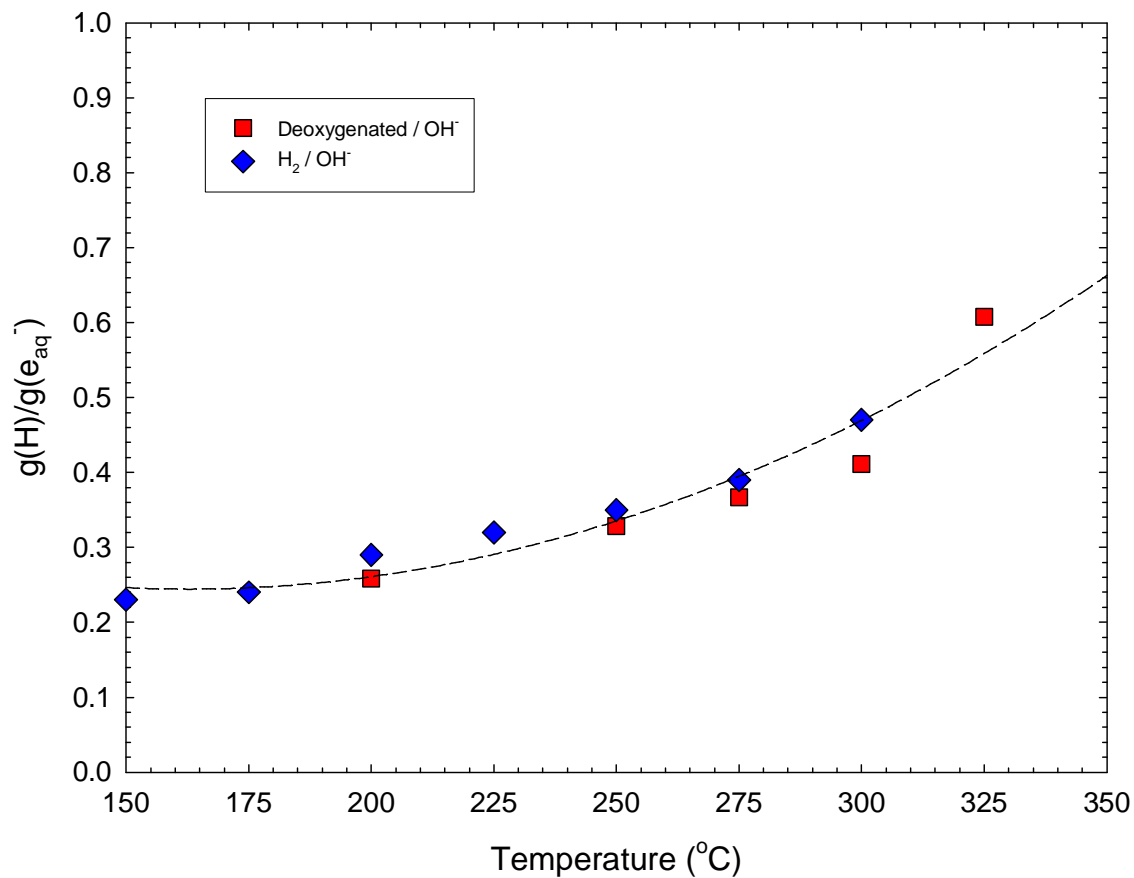


**Figure 3-9** The ratio of  $g(H)/g(e_{aq}^-)$  measured from archived time profiles where the hydrogen atom was converted to the hydrated electron after the end of the pulse. Unpublished data from archived absorbance-time profiles by Bartels and co-workers.

### 3.6 Material Balance for Low LET Water Radiolysis as a Function of Temperature

The g-values for the hydrated electron (Section 3.1), hydrogen peroxide (Section 3.3) and molecular hydrogen (Section 3.4) are given by the three equations below, where t is the temperature in °C:

$$g(e_{aq}^-) = 2.641 + 4.162 \times 10^{-3} t + 9.093 \times 10^{-6} t^2 - 4.717 \times 10^{-8} t^3$$

$$g(H_2O_2) = 0.752 - 1.620 \times 10^{-3} t$$

$$g(H_2) = 0.419 + 8.721 \times 10^{-4} t - 4.971 \times 10^{-6} t^2 + 1.503 \times 10^{-8} t^3$$

The g-values for the hydrated electron, hydrogen peroxide and molecular hydrogen were all based on measured stable products, not by pulse radiolysis. Their temperature dependence has been confirmed using different chemical systems, often in different laboratories. The g-value for H atom has been reliably measured by product analysis up to 200°C. At higher temperatures, the transient absorption from the hydrated electron in alkaline solutions provides a reliable ratio of  $g(H)/g(e_{aq}^-)$ , which does not depend on dosimetry or extinction coefficient. From the temperature dependence of  $g(e_{aq}^-)$ , values of  $g(H)$  have been estimated.

In the radiolysis of water there must be a material balance between the primary species as given in the equation below:

$$g(OH) + 2 g(H_2O_2) - g(e_{aq}^-) - 2 g(H_2) - g(H) = 0$$

The one specie for which only pulse radiolysis yield data is available is the hydroxyl radical. As described in Section 3.2, the temperature dependence for  $g(OH)$  up to 300°C was based on absorbance of the  $\bullet CO_3^-$  radical ion where the temperature dependence of the extinction coefficient is not well established. The temperature dependence of  $g(OH)$  was calculated using an extinction coefficient for  $\bullet CO_3^-$  at 600 nm that was temperature dependent (Table 3-2) and one that was temperature independent at 2,000 L/mol/cm. A comparison of the  $g(OH)$  calculated from the material balance equation indicates that the temperature-dependent extinction coefficient for the  $\bullet CO_3^-$  radical ion best represents  $g(OH)$  up to ~250°C.<sup>13</sup>

$$g(OH) = 2.557 + 1.012 \times 10^{-2} t$$

Above 250°C, the use of the above  $g(OH)$  equation slightly under-predicts the value of  $g(OH)$  required to achieve a material balance. A pragmatic approach has been taken to accommodate this observation. The approach chosen was to slightly increase  $g(OH)$  above 250°C to the values shown in Figure 3-10 in order to fit the observations of  $g(H)$ , assumed that the temperature dependence for  $g(e_{aq}^-)$ ,  $g(H_2O_2)$  and  $g(H_2)$  is correct. The temperature dependence for  $g(OH)$  that achieves this fit is given by the polynomial:

$$g(OH) = 2.531 + 1.134 \times 10^{-2} t - 1.269 \times 10^{-5} t^2 + 3.513 \times 10^{-8} t^3$$

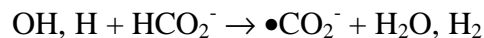
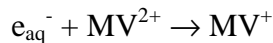
The temperature dependence for  $g(H)$  derived from this fitting is shown in Figure 3-8 and Figure 3-10 and is given by the polynomial:

<sup>13</sup> For the temperature independent  $g(OH)$  given in Section 3.2 to be correct, the value of  $g(H)$  would remain near ~0.5 over the temperature range 20-300°C. Clearly this is not the case as can be seen in Figure 3-8.

$$g(\text{H}) = 0.556 + 2.198 \times 10^{-3} t - 1.184 \times 10^{-5} t^2 + 5.223 \times 10^{-8} t^3$$

In summary, the recommended temperature dependences for the g-value of the primary species formed in the low LET radiolysis of water in the temperature range 20° to 350°C are given in Table 3-3.<sup>14</sup> The g-values for the primary species are given in Table 3-4 for a number of temperatures up to 350°C. It should be remembered that while these g-values are satisfactory for radiolysis modelling purposes, they are probably higher than the true 'escape' yield as a consequence of the slightly high scavenging powers used in many of the experiments.

An estimate of the total free radical yield  $\{g(e_{\text{aq}}^-) + G(\text{OH}) + g(\text{H})\}$  as a function of temperature has been made in a number of laboratories ([28], [43], Elliot and Ouellette – unpublished). These were all pulse radiolysis experiments using methyl viologen as an electron scavenger and formate as a hydroxyl radical and hydrogen atom scavenger to form the reducing  $\bullet\text{CO}_2^-$  radical. The  $\bullet\text{CO}_2^-$  radical reduces methyl viologen to the  $\text{MV}^+$  that is monitored in the experiments.



These results, shown in Figure 3-2, indicate acceptable agreement between the estimated and measured values of  $\{g(e_{\text{aq}}^-) + G(\text{OH}) + g(\text{H})\}$ , although the results of Lin et al. [28] tended to be lower than the results from the other two laboratories. The results have all been corrected/normalized to the values of  $G \times \epsilon$  recommended by Buxton and Stuart [32] for the thiocyanate dosimeter at 475 nm. Where required, the data for the methyl viologen cation radical was corrected using the room temperature extinction coefficient at 605 nm of 13,700 L/mol/cm [41] and the temperature dependence of this absorption as measured by Shiraishi et al.[39].

<sup>14</sup> The equations in Table 3-3 do not constitute a precise material balance as required in computer simulations of steady-state radiolysis. To achieve this one of the g-values should be calculated through the material balance equation. In computer simulations, a charge balance must also be maintained so yield of protons equal to the hydrated electron yield has to be included also.

**Table 3-3**

**Polynomials that describe the temperature dependence of the g-values for the primary species formed in the radiolysis of light water by low LET radiation in the temperature range 20°-350°C.**

<b>g-Value</b>	<b>Polynomial</b>
$g(e_{aq}^-)$	$2.641 + 4.162 \times 10^{-3} t + 9.093 \times 10^{-6} t^2 - 4.717 \times 10^{-8} t^3$
$g(H_2O_2)$	$0.752 - 1.620 \times 10^{-3} t$
$g(H_2)$	$0.419 + 8.721 \times 10^{-4} t - 4.971 \times 10^{-6} t^2 + 1.503 \times 10^{-8} t^3$
$g(OH)$	$2.531 + 1.134 \times 10^{-2} t - 1.269 \times 10^{-5} t^2 + 3.513 \times 10^{-8} t^3$
$g(H)$	$0.556 + 2.198 \times 10^{-3} t - 1.184 \times 10^{-5} t^2 + 5.223 \times 10^{-8} t^3$

Temperature, t, in °C.

**Table 3-4**

**The g-values for low LET radiation deposited in light water at temperatures between 25° and 350°C based on the polynomials in Table 3-3.<sup>14</sup>**

<b>Temperature (°C)</b>	<b>g(e)</b>	<b>g(H<sub>2</sub>)</b>	<b>g(H)</b>	<b>g(OH)</b>	<b>g(H<sub>2</sub>O<sub>2</sub>)</b>
25	2.75	0.44	0.60	2.81	0.71
50	2.87	0.45	0.64	3.07	0.67
100	3.10	0.47	0.71	3.57	0.59
150	3.31	0.49	0.80	4.07	0.51
200	3.46	0.51	0.94	4.57	0.43
250	3.51	0.56	1.18	5.12	0.35
300	3.43	0.64	1.56	5.74	0.27
350	3.19	0.76	2.11	6.45	0.19

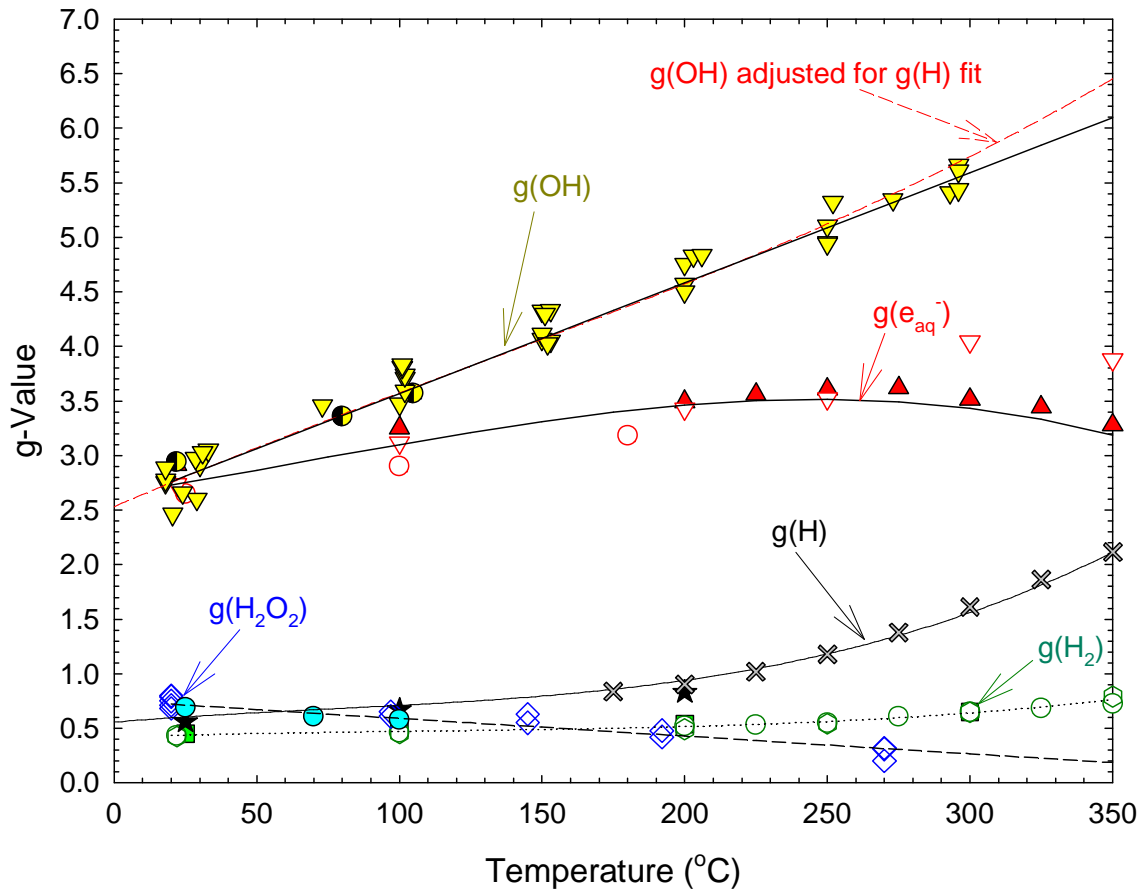
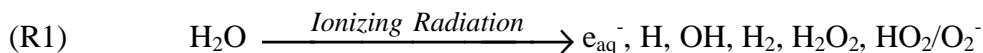


**Figure 3-10** The g-values for the primary species formed in Reaction (R1) for low LET radiation as a function of temperature. The lines are the fit to primary yields given in Sections 3.1 through 3.4. In the case of g(H), the temperature dependence shown has been fitted to the data using the adjustment of g(OH) above 250°C as described in the text. The data points on the plot provide a sense of the experimental uncertainty.

#### 4. REACTION RATE CONSTANTS

In this section, the temperature dependence of the rate constants for reactions involving the primary radiolysis species formed in Reaction (R1) will be assessed. The reactions are summarised in Table 4-1, Table 4-2, and Table 4-3.



Recommendations for the temperature dependence of the individual rate constants are given in the sections below. In Section 4.1, the ‘irreversible’ reactions are discussed and in Section 4.2, those reactions involving equilibria are considered.

To assist the reader, the  $pK_A$ 's of the primary species, as a function of temperature, can be found in Figure 4-26 and are discussed in Section 4.2. In this report, one of the most important reactions in the suppression of net water radiolysis, Reaction R32b



is considered to be the back reaction of Equilibrium R32



and is discussed in the equilibrium reaction Section 4.2, and not in the ‘irreversible’ reaction Section 4.1.

As noted in the Introduction, this review has primarily been limited to those reactions that occur in acid and slightly alkaline solutions. It does not address reactions involving the oxide radical anion,  $O^-$ , or ionized forms of hydrogen peroxide,  $HO_2^-$ , beyond their acid-base equilibria reactions and a few reactions where the rate constant for a reaction involving  $O^-$  is significantly larger than the corresponding hydroxyl radical reaction rate constant. These few reactions involving the oxide radical anion,  $O^-$ , or ionized forms of hydrogen peroxide,  $HO_2^-$ , are discussed in Section 4.3.



**Table 4-1**  
**Water Radiolysis Reaction Set**

Number	Reaction
R2	$e_{aq}^- + e_{aq}^- + (2 H_2O) \rightarrow H_2 + 2 OH^-$
R3	$H + H \rightarrow H_2$
R4	$OH + OH \rightarrow H_2O_2$
R5	$e_{aq}^- + H (+ H_2O) \rightarrow H_2 + OH^-$
R6	$e_{aq}^- + OH \rightarrow OH^-$
R7	$H + OH \rightarrow H_2O$
R8	$e_{aq}^- + H_2O_2 \rightarrow OH + OH^-$
R9	$e_{aq}^- + O_2 \rightarrow O_2^-$
R10	$e_{aq}^- + O_2^- (+ H_2O) \rightarrow H_2O_2 + 2 OH^-$
R11	$e_{aq}^- + HO_2 \rightarrow HO_2^-$
R12	$H + H_2O_2 \rightarrow OH + H_2O$
R13	$H + O_2 \rightarrow HO_2$
R14	$H + HO_2 \rightarrow H_2O_2$
R14a	$H + HO_2 \rightarrow 2 OH$
R15	$H + O_2^- \rightarrow HO_2^-$
R16	$OH + H_2O_2 \rightarrow HO_2 + H_2O$
R17	$OH + O_2^- \rightarrow (HO_3^-) \rightarrow O_2 + OH^-$
R18	$OH + HO_2 \rightarrow (H_2O_3) \rightarrow O_2 + H_2O$
R19	$HO_2 + HO_2 \rightarrow H_2O_2 + O_2$
R20	$O_2^- + HO_2 (+ H_2O) \rightarrow H_2O_2 + O_2 + OH^-$
R21	$O_2^- + O_2^- (+ 2 H_2O) \rightarrow H_2O_2 + O_2 + 2 OH^-$
R22	$H_2O_2 \rightarrow \frac{1}{2} O_2 + H_2O$
R22a	$H_2O_2 \rightarrow 2 OH$

**Table 4-2**  
**Equilibrium Reactions not involving the Hydrogen Atom**

#	Equilibria	Comments
R23	$\text{H}_2\text{O} \rightleftharpoons \text{H}^+ + \text{OH}^-$	$K_w = [\text{H}^+] \times [\text{OH}^-]$ $K_{\text{H}_2\text{O}} = [\text{H}^+] \times [\text{OH}^-] / [\text{H}_2\text{O}]$ $= K_w / [\text{H}_2\text{O}]$
R24	$\text{H}_2\text{O}_2 \rightleftharpoons \text{H}^+ + \text{HO}_2^-$	$K_{\text{H}_2\text{O}_2}$
R25	$\text{H}_2\text{O}_2 + \text{OH}^- \rightleftharpoons \text{HO}_2^- + \text{H}_2\text{O}$	$K_{\text{H}_2\text{O}_2}^{\text{B}}$
R26	$\text{OH} \rightleftharpoons \text{H}^+ + \text{O}^-$	$K_{\text{OH}}$
R27	$\text{OH} + \text{OH}^- \rightleftharpoons \text{O}^- + \text{H}_2\text{O}$	$K_{\text{OH}}^{\text{B}}$
R28	$\text{HO}_2 \rightleftharpoons \text{H}^+ + \text{O}_2^-$	$K_{\text{HO}_2}$
R29	$\text{HO}_2 + \text{OH}^- \rightleftharpoons \text{O}_2^- + \text{H}_2\text{O}$	$K_{\text{HO}_2}^{\text{B}}$

**Table 4-3**  
**Equilibrium Reactions involving the Hydrogen Atom**

#	Equilibria	Comments
R30	$\text{H} \rightleftharpoons \text{H}^+ + \text{e}_{\text{aq}}^-$	$K_{\text{H}}$
R31	$\text{H} + \text{OH}^- \rightleftharpoons \text{e}_{\text{aq}}^- + \text{H}_2\text{O}$	$K_{\text{H}}^{\text{B}}$
R32	$\text{H} + \text{H}_2\text{O} \rightleftharpoons \text{H}_2 + \text{OH}$	$K_{32}$

## 4.1 Reactions not involving Equilibria

### 4.1.1 Reaction R2: $e_{aq}^- + e_{aq}^- + 2 H_2O \rightarrow H_2 + 2 OH^-$

The temperature dependence for the rate constant,  $k_{R2}$ , of the second order bimolecular decay of the hydrated electron has been studied up to and above 200°C by Christensen and Sehested [49], by Stuart and Ouellette as reported in Elliot et al. [50] and by Marin et al. [27]. The reported bimolecular rate constants from all these studies have to be corrected to a revised extinction coefficient for the hydrated electron.

In the original work by Christensen and Sehested [49], it was assumed that the extinction coefficient of the hydrated electron was 18,600 L/mol/cm over the whole temperature range at the wavelength of maximum absorption. Marin et al. [27] assumed a room temperature extinction coefficient of 18,400 L/mol/cm and then estimated the temperature dependence for the extinction coefficient based on conservation of the oscillator strength, i.e. the area under the absorption curve. Stuart and Ouellette used the extinction coefficients shown in Figure 4-1 [50]. In a recent publication [51], Hare et al. have revisited the extinction coefficient of the hydrated electron at room temperature and report a value of 22,700 L/mol/cm based on the methyl viologen radical cation extinction coefficient of 13,700 L/mol/cm at 605 nm. In more recent unpublished work, Bartels and co-workers have estimated the hydrated electron extinction coefficient at its maximum absorbance up to 350°C as shown in Figure 4-1. This work was performed in two parts: the first involved the extension of the use of methyl viologen cation radical absorbance as a reference up to 200°C, and assumed the temperature dependence of  $MV^+$  extinction coefficient given in Reference [39]; the second part involved measuring simultaneously the hydrated electron transient absorption and the yield of fluoride ions from scavenging of the hydrated electron with sulphur hexafluoride. The results of this unpublished work are shown in Figure 4-1. The relatively large error bars are a realistic attempt to estimate 95% confidence intervals from both random and systematic sources of error.

For this review, the extinction coefficient of the hydrated electron at its absorption maximum, as a function of temperature, as shown by the dashed line in Figure 4-1 has been used. The extinction coefficient,  $\epsilon$ , in units of L/mol/cm is given by the polynomial expression below:

$$\epsilon = 22,775 - 8.777 t - 4.691 \times 10^{-2} t^2 + 2.090 \times 10^{-4} t^3$$

where  $t$  is the temperature in °C.

The rate constants for the bimolecular decay of the hydrated electron, normalized to the extinction coefficients given by the polynomial above, are given in Figure 4-2. These rate constants were measured as  $k_{R2}/\epsilon$  and should be dose independent. Hence, the correction applied was a multiplication of the reported rate constant by the ratio of the revised extinction coefficient to the one used in the original report.

There is reasonable agreement between all three studies with an apparent Arrhenius dependence shown up to 150°C followed by an abrupt decrease in the rate constants

above 150°C. For modelling calculations, the revised rate constant,  $k_{R2}$ , are given for temperatures up to 150°C by:

$$\text{Log } k_{R2} = 12.281 - 3.768 \times 10^2/T - 6.673 \times 10^4/T^2 - 1.075 \times 10^7/T^3$$

and for temperatures above 150°C by:<sup>15</sup>

$$\text{Log } k_{R2} = -47.532 + 4.920 \times 10^4/T - 1.036 \times 10^7/T^2$$

T is in Kelvin units and  $k_{R2}$  has units of L/mol/s. Above 150°C, the data of Christensen and Sehested [49] were not used in the fits as Marin et al. [27] have indicated that even the low values for  $k_{R2}$  they had reported above 250°C were only upper bound values, set by the impurity levels in their system.

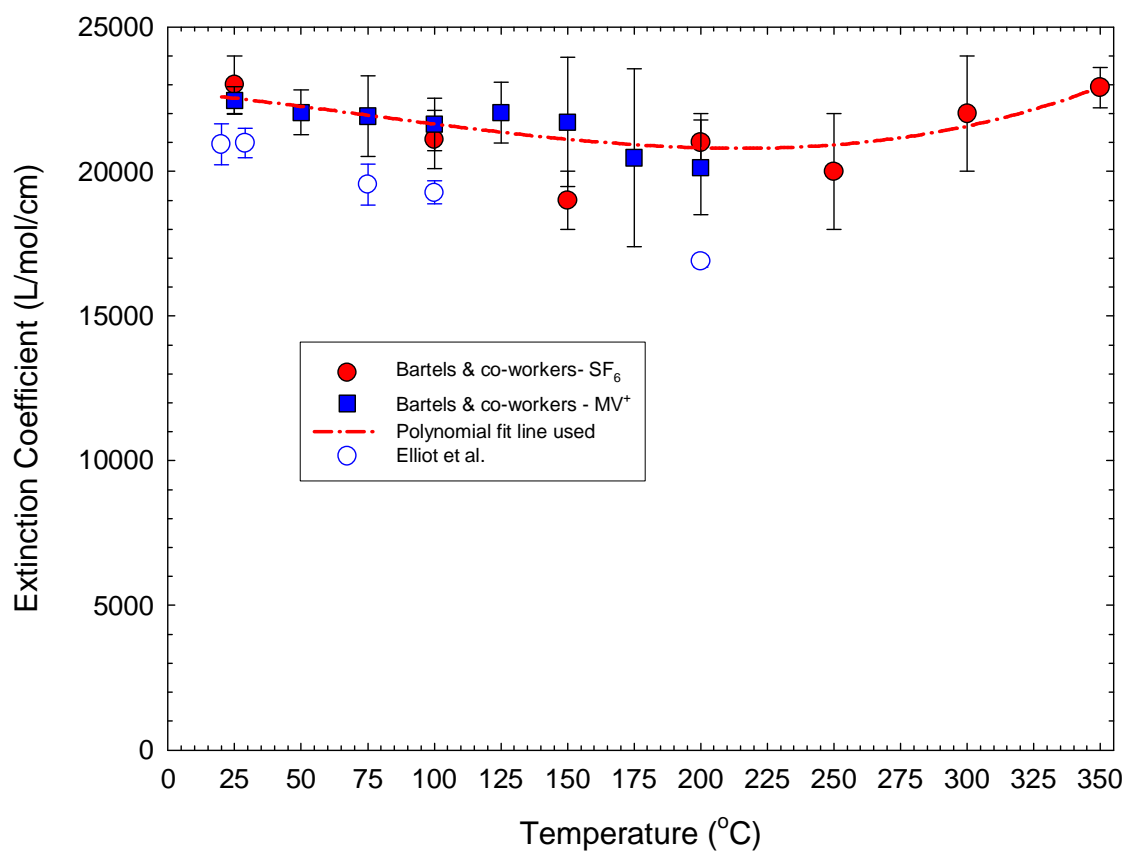


**Figure 4-1 The extinction coefficient for the hydrated electron as a function of temperature by Bartels and co-workers (data to be published) and Elliot et al. [50].**

<sup>15</sup> A simple quadric fit was used for temperatures above 150°C as higher order polynomial fits, above the upper limit of 275°C for the fit, tended to give rate constants above  $10^{11}$  L/mol/s. The quadratic fit just tended to lower value rate constants.

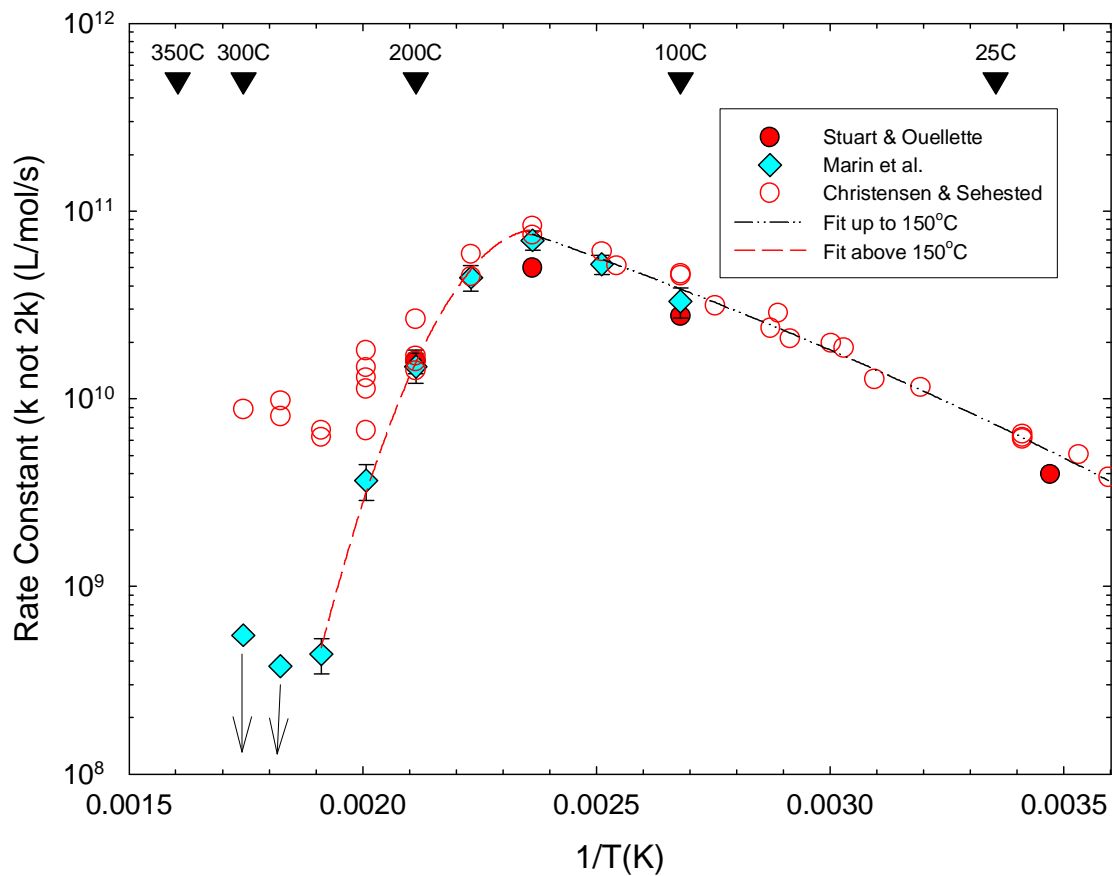


**Figure 4-2 The temperature dependence of the rate constant for the bimolecular decay of the hydrated electron as measured by Christensen and Sehested [49], Marin et al. [27] and Stuart and Ouellette in Elliot et al. [50].**

#### 4.1.2 Reaction R3: $\text{H} + \text{H} \rightarrow \text{H}_2$

The bimolecular recombination reaction of the hydrogen atom has been studied up to 250°C by Sehested and Christensen [52] by monitoring the decay of the far UV hydrogen atom absorption. The spectrum shape (roughly an exponential decay toward increasing wavelength) between 195 and 220 nm was found not to change with temperature in this range. The rate constants shown in Figure 4-3 were calculated from the  $2k/\epsilon I$  results shown in Figure 2 of Reference [52]. It was assumed that the extinction coefficient of the hydrogen atom at 200 nm was 950 L/mol/cm and did not vary with temperature. (It is assumed that the cell length was 2.5 cm based on information in Reference [53]). This cell length is supported by the fact that the rate constant of  $5.0 \times 10^9$  L/mol/s at 20°C agreed with the value reported in Reference [52].<sup>16)</sup> The authors caution that the extinction coefficient for the hydrogen atom may be increasing slightly (perhaps 10% up to 200°C) with temperature, so the rate constants and activation energy represent a lower limit. Above 200°C, Janik et al. [24] found it necessary to postulate a larger increase in the extinction coefficient (i.e., a red shift in the spectrum) to fit their 230 nm kinetics for the  $\text{H} + \text{O}_2$  reaction. Further study of the reaction at higher temperature is warranted.

The bimolecular recombination reaction of hydrogen atoms follows an Arrhenius temperature dependence over the 18°-250°C studied with an activation energy of 15.5 kJ/mole (Figure 4-3). The value of the rate constant,  $k_{R3}$ , at 25°C is estimated to be  $5.1 \times 10^9$  L/mol/s. The temperature dependence for the rate constant,  $k_{R3}$ , for Reaction R3 is:

$$k_{R3} = 2.70 \times 10^{12} e^{-1867.5/T} \text{ L/mol/s}$$

where T is the temperature in Kelvin.

---

<sup>16)</sup> It appears that the y-axis label in Figure 2 of Reference [52] should read  $(2 k/\epsilon I \times 10^{-6})$  not  $(2 k/\epsilon I \times 10^{-7})$ .

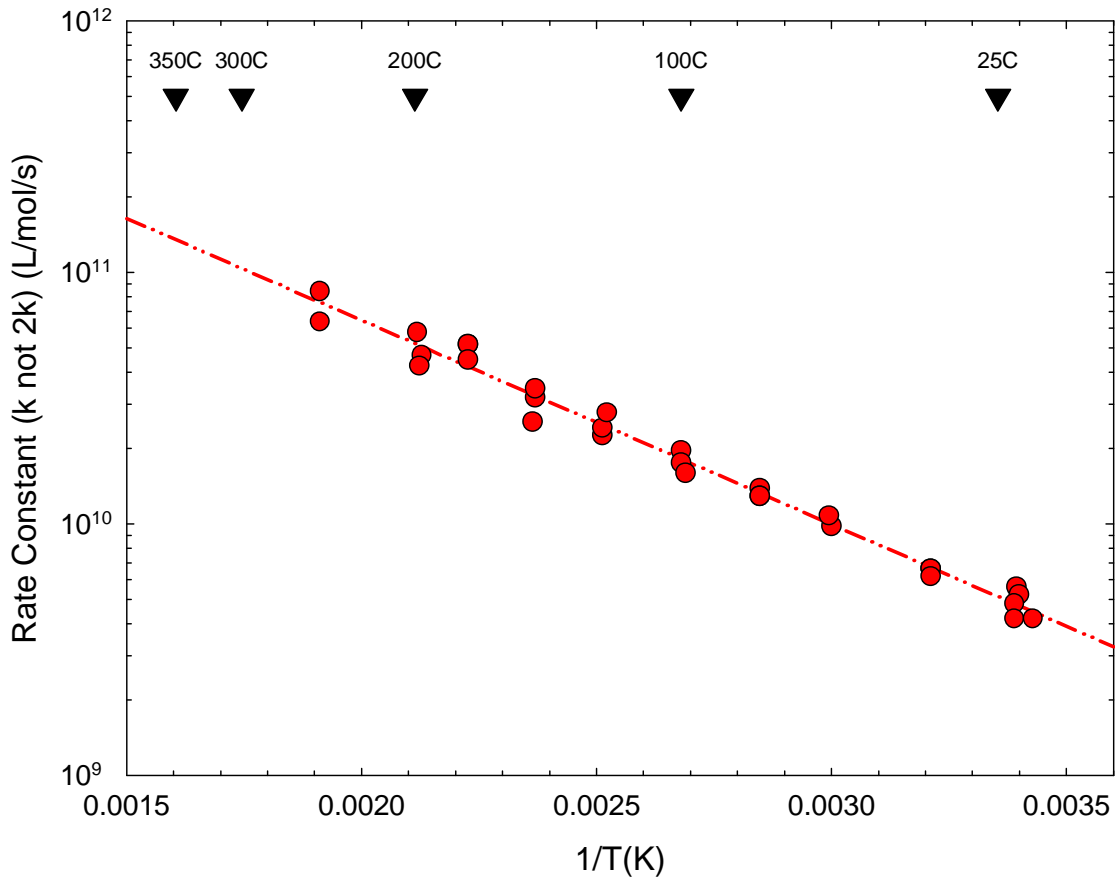


Figure 4-3 The rate constants for the bimolecular reaction of hydrogen atoms as measured by Sehested and Christensen [52].

### 4.1.3 Reaction R4: $\text{OH} + \text{OH} \rightarrow \text{H}_2\text{O}_2$

The temperature dependence for the bimolecular rate constant,  $k_{R4}$ , for the self-reaction of the hydroxyl radical has been reported by Elliot et al. [54] and by Janik et al. [25]. The rate constants reported in both of these papers need to be corrected to a revised extinction coefficient for the hydroxyl radical. In Reference [54], a temperature independent extinction coefficient of 510 L/mol/cm at 250 nm was assumed. In Reference [25], the extinction coefficient for the hydroxyl radical needs to be slightly revised to reflect the updated evaluation of g-values given in Section 3.6.

While a full retrofit correction to both the reported results [25], [54] is not possible, it has been assumed that the absorbance at 250 nm is dominated by the hydroxyl radical absorption and that the adjustment can be made through recreating ' $k_{R4}/\epsilon$ '. The extinction coefficient for the hydroxyl radical at 250 nm reported in Table 1 in Reference [25] has been revised based on the yields reported in Section 3.6. The  $G(\text{OH})$  for the  $\text{N}_2\text{O}$  saturated solution has been approximated as the sum of  $g(e_{aq}^-)$  and  $g(\text{OH})$ . The G-values used and the revised extinction coefficient as a function of temperature is given in Table 4-4.

The revised rate constants,  $k_{R4}$ , as a function of temperature is shown in Figure 4-4. Where there is overlap in the temperature range of the data, there is good agreement between the two published results [25], [54].

$$\text{Log } k_{R4} = 8.054 + 2.193 \times 10^3/T - 7.395 \times 10^5/T^2 + 6.870 \times 10^7/T^3$$

where T is in Kelvin and where  $k_{R4}$  has units of L/mol/s. The value of  $k_{R4}$  at 25°C is estimated to be  $4.8 \times 10^9$  L/mol/s.

The Reaction R4 is not a diffusion-controlled reaction [25], [54]. This can be seen in Figure 4-4 where the diffusion controlled encounter rate constant,  $k_{\text{diff}}$ , has been calculated from the Smoluchowski equation [85].

$$k_{\text{diff}} = 4 \pi D_{\text{OH}} \times d \times N \times 10^3 \text{ L/mol/s}$$

where  $D_{\text{OH}}$  is the diffusion coefficient for the hydroxyl radical and N is Avagadro's number. At room temperature, a value for  $D_{\text{OH}}$  of  $2.2 \times 10^{-9}$  m<sup>2</sup>/s was assumed. The temperature dependence for  $D_{\text{OH}}$  was assumed to be the same as for the self-diffusion of water [54] (see Table 4-6 in Section 4.2.2). The reaction distance, d, was assumed be constant at 0.44 nm over the temperature range [25], [54].

As can be seen in Figure 4-4, by 300°C, the rate constant,  $k_{R4}$ , is an order of magnitude lower than the encounter rate constant,  $k_{\text{diff}}$ . This information will be used in Section 4.1.13 when Reactions R14 and R14a are discussed.



**Table 4-4**  
**The extinction coefficient of the hydroxyl radical at 250°C as a function of temperature**

<b>Temperature</b>	<b>G(OH)</b> <b>(= g(e<sub>aq</sub><sup>-</sup>) + g(OH))</b>	<b>ε<sub>250 nm</sub></b>
°C	#/100 eV	L/mol/cm
25	5.56	538
150	7.39	439
200	8.04	388
225	8.33	352
250	8.62	325
275	8.91	292
300	9.18	259
325	9.43	228
350	9.64	199

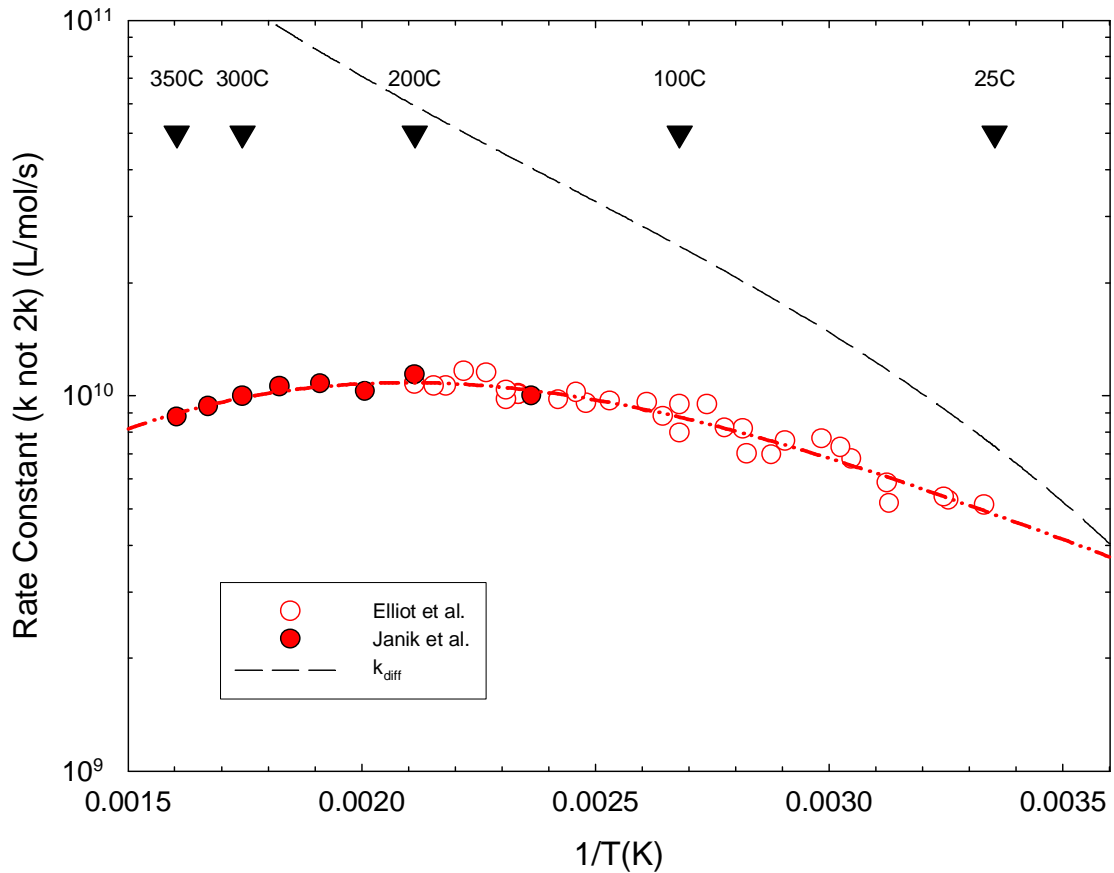


**Figure 4-4** The temperature dependence of the bimolecular rate constant for the self-reaction of hydroxyl radicals by Elliot et al. [54] and by Janik et al. [25]. All data has been corrected to the revised extinction coefficients for the hydroxyl radical – see text. Also shown is the rate constant,  $k_{diff}$ , for encounters between hydroxyl radicals.

**4.1.4 Reaction R5:  $e_{aq}^- + H (+ H_2O) \rightarrow H_2 + OH^-$** 

The temperature dependence for the reaction of the hydrated electron with the hydrogen atom has been reported from three laboratories [27], [55], [56]. The extinction coefficient for the hydrated electron used in all three publications was based on the room temperature value of 18,400 L/mol/cm at the maximum absorbance wavelength rather than the recently determined value of 22,700 L/mol/cm [51]. As the value for the rate constant,  $k_{R5}$ , was extracted by Marin et al. [27] from the same high dose experiments used to determine  $k_{R2}$ , their reported rate constants for  $k_{R5}$  were simply scaled by the ratio of the new to old extinction coefficients. The corrected data are shown in Figure 4-5. The rate constant appears to increase at high temperature above that predicted by an Arrhenius dependence. Theoretical analysis in Marin et al. [27], assuming diffusion limited electron transfer, was unable to explain this temperature dependence above 200°C. Recent work at the Notre Dame Radiation Laboratory (Janik and Bartels, unpublished) on alkaline solutions without added  $H_2$  indicates that the rate constant,  $k_{R5}$ , above 250°C reported by Marin et al. [27] must be high. An estimate from this unpublished work suggests that the rate constant,  $k_{R5}$ , at 350°C is of the order of  $5 \times 10^{11}$  L/mol/s.

Christensen et al. [55] extracted the value for the rate constant,  $k_{R5}$ , by fitting the decay of the hydrated electron absorption in water containing dissolved hydrogen to convert the hydroxyl radical to hydrogen atoms in near neutral pH solution. The principal competing reactions were the bimolecular decay of the hydrated electron (Reaction R2) and the bimolecular decay of the hydrogen atom (Reaction R3), the rate constants of which they had measured previously. The difficulty is that the  $G \times \epsilon$  at 420 nm of 5,900 ( $G$  in #/100 eV and  $\epsilon$  in L/mol/cm) for the  $N_2O$ -saturated  $10^{-3}$  mol/L ferrocyanide ion dosimeter they used is consistent with the recommended dosimetry of Stuart and Buxton [32], yet the extinction coefficient used for the hydrated electron was taken as 18,600 L/mol/cm from the literature and is not consistent with the dosimetry they used. Another complication is the computer simulations used to extract  $k_{R5}$  used the original reported values for the rate constants for Reaction R2 [49] and these have now been revised in the previous Section 4.1.1. It is not possible to correct for all these factors. However, for simplicity, a crude correction to the reported rate constants for  $k_{R5}$  was undertaken by scaling the reported  $k_{R5}$  by the ratio of the new to old extinction coefficient of the hydrated electron. The correction amounts to an increase in the rate constants by 21% to 12% as the temperature increases from 20° to 250°C. The corrected data are shown in Figure 4-5.

Schwarz [56] has studied Reaction R5 over the temperature range 4°-65°C as part of study of Reaction R39b, the reaction of the hydrated electron with water (see Section 4.2.3.2). Schwarz [56] reported a value of  $k_{R5}$  at 25°C of  $3.4 \times 10^{10}$  L/mol/s and an activation energy of 16.1 kJ/mol. The data of Schwarz is shown as a line in Figure 4-5.<sup>17</sup> As the study by Schwarz employed very low radiation doses, and involved the

---

<sup>17</sup> Schwarz (personal communication ~1994) had indicated that this rate constant as reported was possibly 20% high.

measurement/analysis of first order rate constants, no correction was done for the incorrect extinction coefficient.

Also shown in Figure 4-5 are the rate constants for Reaction R5 measured by Stuart and Ouellette (unpublished AECL-CRL from 1995). The method used was similar to that used by Christensen and Sehested [55]; the data were originally fitted using the AECL extinction coefficients for the hydrated electron as shown in Figure 4-1 and the originally published rate constants for Reaction R2 [50]. A small correction was applied by simple scaling of  $k_{R5}$  by the ratio of the new to old extinction coefficient of the hydrated electron. The corrected rate constants are shown in Figure 4-5.

As can be seen in Figure 4-5, there is reasonable agreement between the results from the four laboratories. An Arrhenius relationship has been fitted through the data for the temperature dependence, which ignores the high temperature results of Marin et al. [27] in favour of the more recent Notre Dame estimate for 350°C. The temperature dependence of the rate constant,  $k_{R5}$ , for Reaction R5 is given by the function:

$$k_{R5} = 1.14 \times 10^{13} e^{-1795.7/T} \text{ L/mol/s}$$

where T is the temperature in Kelvin. The value of the rate constant,  $k_{R7}$ , at 25°C is estimated to be  $2.76 \times 10^{10}$  L/mol/s and activation energy of 14.9 kJ/mol.

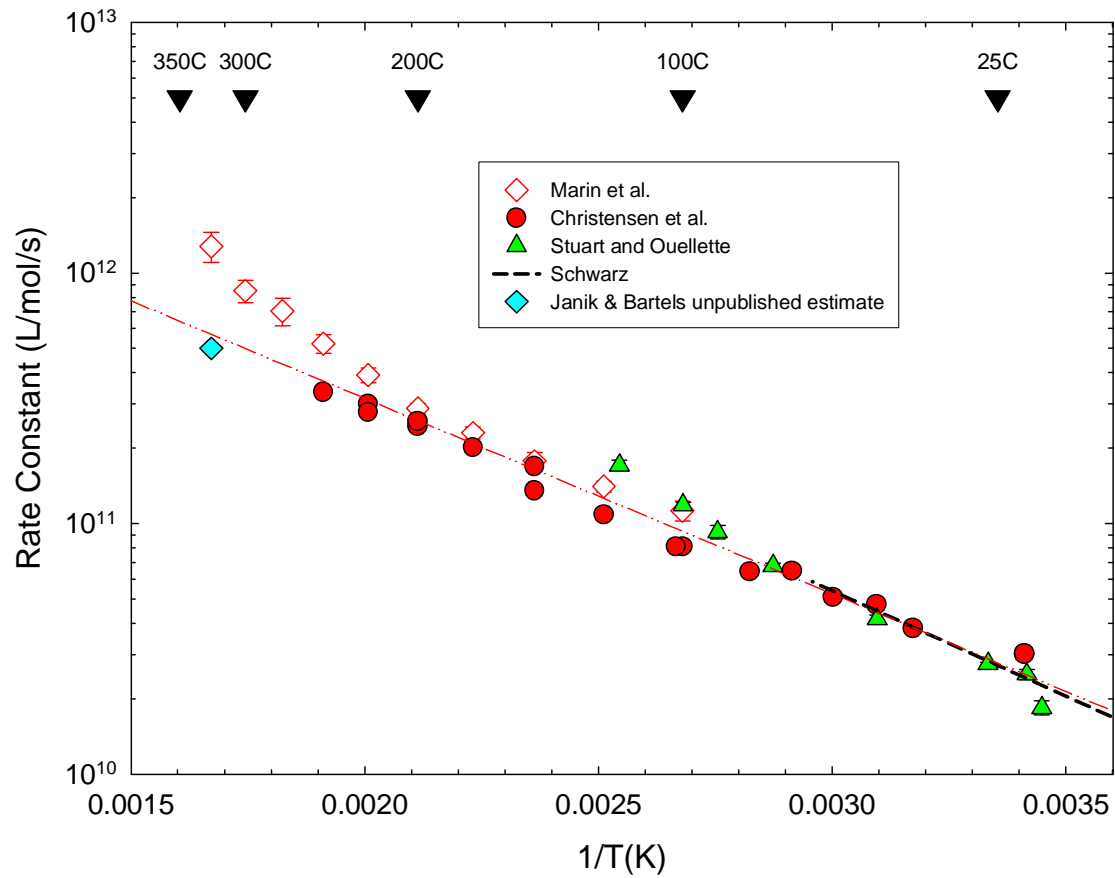


**Figure 4-5** The rate constants for the reaction of the hydrated electron reacting with hydrogen atom as measured by Marin et al. [27], Christensen et al. [55], Stuart and Ouellette (unpublished results), Schwarz [56], and Janek and Bartels (unpublished – see text).

#### 4.1.5 Reaction R6: $e_{aq}^- + OH \rightarrow OH^-$

Three laboratories have reported the temperature dependence for the rate constant,  $k_{R6}$ , for the reaction of the hydrated electron with the hydroxyl radical ([55], [57] and Janik and Bartels (to be published)). All studies monitored the decay of the hydrated electron in deoxygenated water that was either buffered or slightly alkaline. The value of  $k_{R6}$  was adjusted in computer simulations until a match was obtained with the absorption profile.

The original published results of Elliot and Ouellette [58], where a  $10^{-3}$  mol/kg borate buffer was used, were re-analysed by Stuart et al. [57] in 2002 incorporating updated extinction coefficients (Elliot et al. in Figure 4-1) and rate constants. The results of Christensen et al. [55] were measured in a  $10^{-2}$  mol/kg  $H_2SiO_3/HSiO_3^-$  buffer and were simulated using a constant extinction coefficient for the hydrated electron of 18,600 L/mol/cm up to 225°C, at the wavelength of maximum absorbance. Both laboratories reported [55], [57] that the decay above 150°C contained a large first order kinetic component. The rate constants reported by Janik and Bartels were obtained in alkaline solutions using either a borate buffer or potassium hydroxide.

The results are shown in Figure 4-6. The rate constants reported from the three laboratories have all been scaled for hydrated electron extinction coefficient shown in Figure 4-1.<sup>18</sup> The results of Janik and Bartels (to be published) have also been scaled to address the revised free radical yields given in this report.

There is reasonable agreement between the results of Stuart et al. [57] and of Janik and Bartels (to be published) whereas the results of Christensen et al. [55] trend above these results. Because of the uncertainty in the use of the  $10^{-2}$  mol/kg  $H_2SiO_3/HSiO_3^-$  buffer by Christensen et al. [55]<sup>19</sup> it is recommended that the results of Janik and Bartels be used for modelling.

$$\text{Log } k_{R6} = 13.123 - 1.023 \times 10^3/T + 7.634 \times 10^4/T^2$$

Where T is the temperature in Kelvin and where  $k_{R6}$  has units of L/mol/s. The value of  $k_{R6}$  at 25°C is estimated to be  $3.5 \times 10^{10}$ /mol/s.

The rate constants for this important water radiolysis reaction have all been corrected/scaled from the original reported numbers. It is recommended that these rate constants be re-evaluated/re-measured using updated extinction coefficients, yields and rate constants.

<sup>18</sup> A simple scaling of the results of Christensen et al. [55] by extinction coefficient increased the room temperature rate constants by ~20% and the rate constant at 200°C by ~11%.

<sup>19</sup> Christensen et al. [55] noted that their higher temperature results might have been compromised by the use of this  $H_2SiO_3/HSiO_3^-$  buffer.

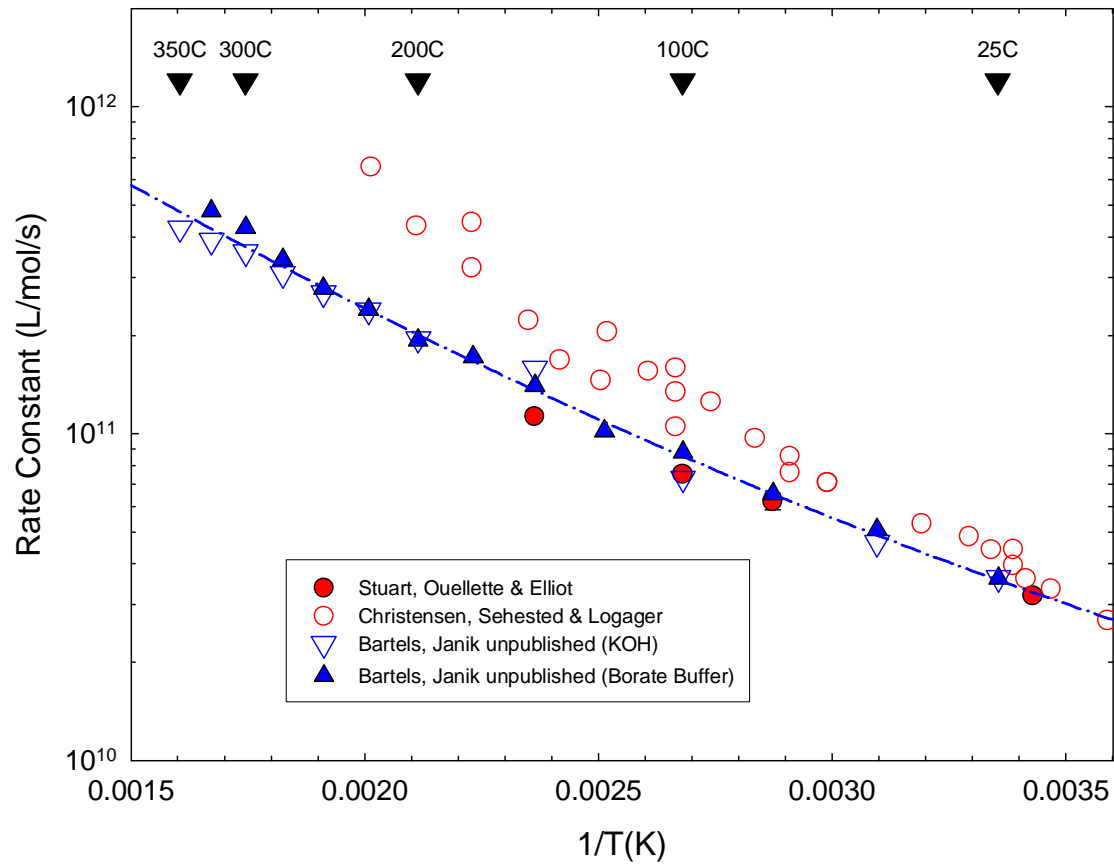


**Figure 4-6** The temperature dependence of the reaction of the hydrated electron with the hydroxyl radical as reported by Stuart et al. [57], by Christensen et al. [55] and by Janik and Bartels (to be published). All data have been adjusted for the revised hydrated electron extinction coefficient – see text.

#### 4.1.6 Reaction R7: $\text{H} + \text{OH} \rightarrow \text{H}_2\text{O}$

The rate constant for the reaction of hydrogen atoms with hydroxyl radicals has been studied by Buxton and Elliot [59] and by Lundström et al. [30]. The rate constant for Reaction R6 was obtained by modelling the decay of the hydroxyl radical absorption in degassed  $10^{-2}$  mol/kg perchloric acid solutions.



There is acceptable agreement between the two studies as can be seen in Figure 4-7. A shortfall in the analyses is that both studies assumed that the extinction coefficient of the hydroxyl radical did not change with temperature. It is now recognized that the extinction coefficient decreases with increasing temperature (see Section 4.1.3). Over the 25° to 220°C temperature range covered in these studies, the hydroxyl radical extinction coefficient decreased by about 30%. While it is not possible to retrofit a simple correction to the reported rate constants, it is recognised that the values plotted in Figure 4-7 are likely to be increasingly low as the temperature increases. Reaction R7 is not a diffusion-controlled reaction [59]; however, the data up to 220°C does follow a reasonable Arrhenius fit as can be seen in Figure 4-7 where the data from both studies have been used for the fit. The temperature dependence as given by the Arrhenius fit for the rate constant,  $k_{R7}$ , for Reaction R7 is:

$$k_{R7} = 4.26 \times 10^{11} e^{-1091.9/T} \text{ L/mol/s}$$

where T is the temperature in Kelvin. The value of the rate constant,  $k_{R7}$ , at 25°C is estimated to be  $1.1 \times 10^{10}$  L/mol/s and activation energy of 9.1 kJ/mol.<sup>20</sup>

It is recommended that these rate constants be re-evaluated/re-measured using updated extinction coefficients, yields and rate constants.

---

<sup>20</sup> It is expected that the increasing influence of activation control on the rate constant, as the temperature increases above 200°C, will decrease the rate of increase with temperature of the observed rate constant. The extrapolated Arrhenius fit will underestimate this decrease. However, this underestimation will help offset the errors due to the use of a constant extinction coefficient for the hydroxyl radical.



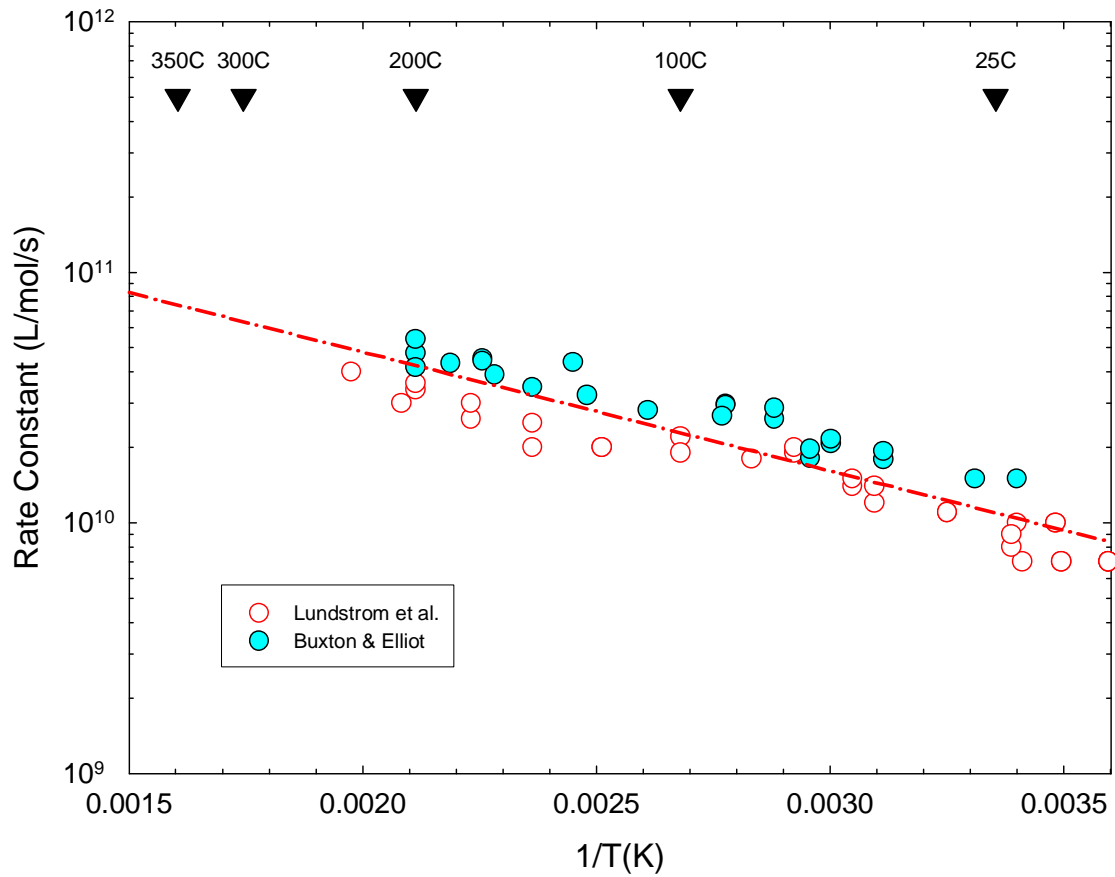


Figure 4-7 The rate constant for the reaction of hydrogen atoms with hydroxyl radicals as measured by Buxton and Elliot [59] and by Lundström et al. [30].

**4.1.7 Reaction R8:  $e_{aq}^- + H_2O_2 \rightarrow OH + OH^-$** 

The temperature dependence of the rate constant for the hydrated electron reacting with hydrogen peroxide is shown in Figure 4-8. The results reported by Elliot et al. [50], [57] and Christensen et al. [55] laboratories are in agreement over the temperature range studied.<sup>21</sup> As hydrogen peroxide thermally decomposes to form oxygen, this limited the temperature range that could be studied. In the absence of any other information, it has to be assumed that an Arrhenius temperature dependence is appropriate to estimate the rate constants up to 350°C.

The value of the rate constant,  $k_{R8}$ , at 25°C is  $1.4 \times 10^{10}$  L/mol/s and the activation energy is 15.7 kJ/mole. The temperature dependence of the rate constant,  $k_{R8}$ , for Reaction R8 is given by:

$$k_{R8} = 7.70 \times 10^{12} e^{-1889.6/T} \text{ L/mol/s}$$

where T is the temperature in Kelvin.

---

<sup>21</sup> The current AECL-CRL data, first reported in Reference [50], and shown in Figure 4-8 of this report supersedes the data shown in Figure 5 of Reference [54].

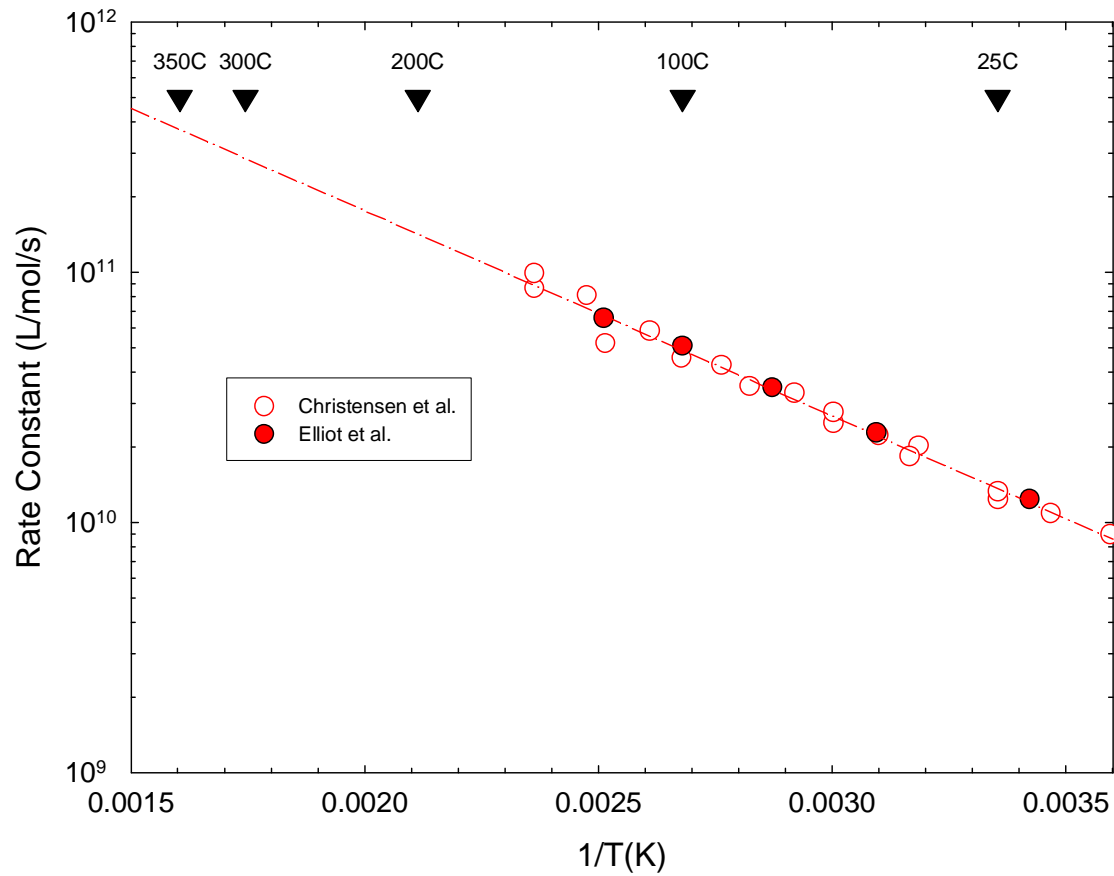


**Figure 4-8 The rate constants for the reaction of the hydrated electron reacting with hydrogen peroxide as measured by Elliot et al. [50], [57] and by Christensen et al. [55].**

**4.1.8 Reaction R9:  $e_{aq}^- + O_2 \rightarrow O_2^-$** 

The temperature dependence of the rate constant for reaction of the hydrated electron with oxygen is shown in Figure 4-9. The results reported by Stuart et al. [57] supersede previous rate constants reported earlier from this laboratory [18], [54]. Where overlap occurs, there is agreement with the results by Cline et al. [21] and the AECL-CRL data. While the room temperature reaction rate is consistent with a diffusion-limited reaction, the activation energy is lower than expected based on known diffusion coefficients. Thus, by 100°C, the reaction is clearly not limited by diffusion.

An Arrhenius temperature dependence for the rate constants is appropriate to estimate the rate constants up to 350°C. The value of the rate constant,  $k_{R9}$ , at 25°C is  $2.3 \times 10^{10}$  L/mol/s and the activation energy is 11.6 kJ/mole. The temperature dependence of the rate constant,  $k_{R9}$ , for Reaction R9 is given by:

$$k_{R9} = 2.52 \times 10^{12} e^{-1401.5/T} \text{ L/mol/s}$$

where T is the temperature in Kelvin.

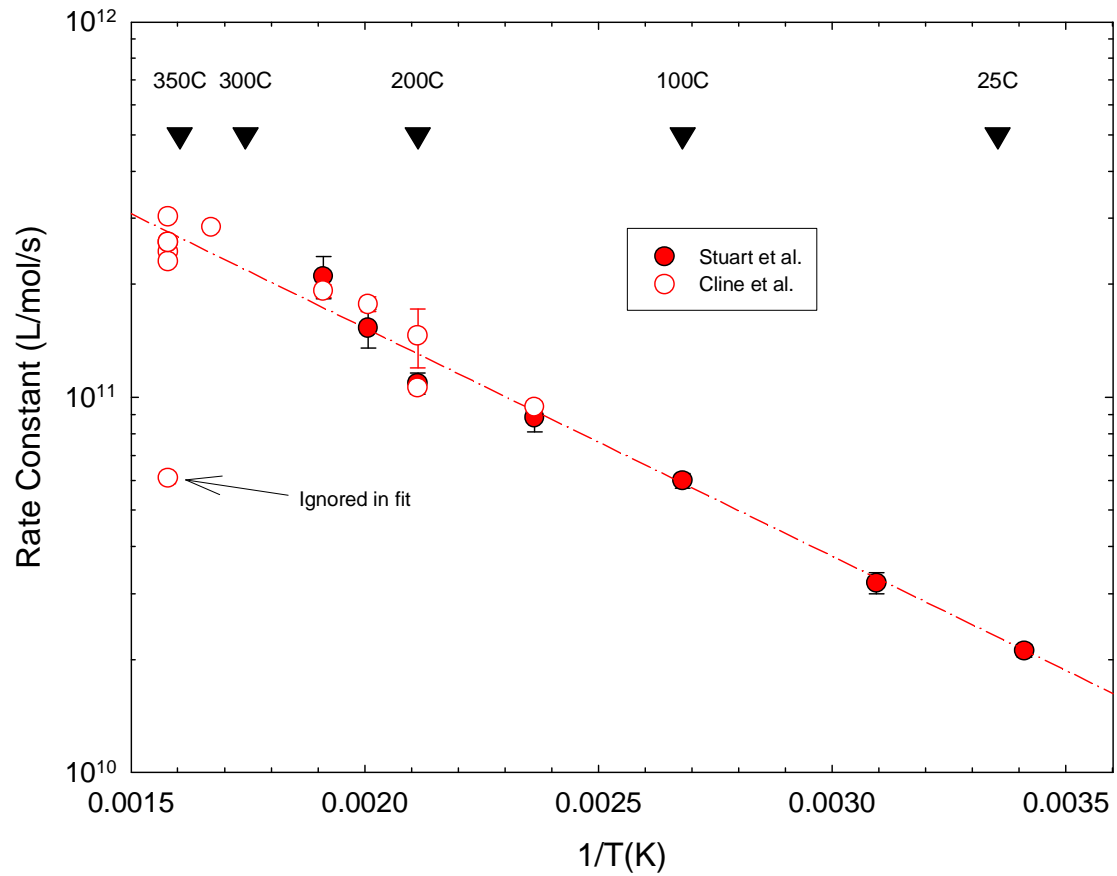


Figure 4-9 The rate constants for the reaction of the hydrated electron with oxygen as measured by Stuart et al. [57] and by Cline et al. [21].

**4.1.9 Reaction R10:  $e_{aq}^- + O_2^- + H_2O \rightarrow H_2O_2 + 2 OH^-$** 

The only report of the rate constant for Reaction R10 is a room temperature measurement by Gruenbein et al. for  $k_{R10}$  of  $1.3 \times 10^{10}$  L/mol/s [60]. Certainly this reaction should be investigated further. The pragmatic approach taken to estimate the temperature dependence of this rate constant is to assume it follows an Arrhenius dependence with an activation energy of 13 kJ/mole. The activation energy was taken as the average for the reaction of the hydrated electron with hydrogen peroxide (15.7 kJ/mole, Section 4.1.7) and with oxygen (11.6 kJ/mole, Section 4.1.8).

$$k_{R10} = 2.46 \times 10^{12} e^{-1563.6/T} \text{ L/mol/s}$$

**4.1.10 Reaction R11:  $e_{aq}^- + HO_2 \rightarrow HO_2^-$** 

There do not appear to be any measurements of the rate constant,  $k_{R11}$ , for Reaction R11. Certainly this reaction should be investigated. The pragmatic approach taken is to assume it has the same room temperature rate constant of  $1.3 \times 10^{10}$  L/mol/s and activation energy of 13 kJ/mole as assumed for Reaction R10 (Section 4.1.9).

$$k_{R11} = 2.46 \times 10^{12} e^{-1563.6/T} \text{ L/mol/s}$$

#### 4.1.11 Reaction R12: $\text{H} + \text{H}_2\text{O}_2 \rightarrow \text{OH} + \text{H}_2\text{O}$

The temperature dependence for the reaction of hydrogen atoms with hydrogen peroxide has been reported by three laboratories [29], [61], [62] as shown in Figure 4-10. Both Elliot [61] and Lundström et al. [29] used the optical pulse radiolytic technique utilizing the same chemical method (growth of the  $\text{Cl}_2^-$  optical absorption) to estimate the rate constants. Inspection of the data in Figure 4-10 indicates reasonable agreement up to about 60°C after which the results of Elliot are slightly higher. The rate constants measured by Mezyk and Bartels [62] used a pulse radiolysis/FID attenuation method where the pseudo-first order scavenging of hydrogen atoms was followed using the free induction decay of the electron paramagnetic resonance signal. Their reported rate constants tend to fall slightly below optical methods at lower temperatures.

Because of the thermally unstable nature of hydrogen peroxide, only a narrow temperature range could be studied. Lundström et al. [29] noted that any decomposition of hydrogen peroxide to form oxygen could compromise the results, because oxygen reacts about 200 times more rapidly with hydrogen atoms than does hydrogen peroxide.<sup>22</sup> The optical studies are susceptible to error if trace amounts of oxygen are present from thermal decomposition. The FID attenuation experiment used fast re-circulation of the solution and continuous sparging to avoid this problem.

On review, as the free induction decay method appears much less prone to analysis errors, this data has been used to extrapolate the temperature dependence of the rate constant up to 350°C assuming an Arrhenius dependence (Figure 4-10).

The value of the rate constant,  $k_{\text{R12}}$ , at 25°C is  $3.6 \times 10^7$  L/mol/s and the activation energy is 21.1 kJ/mole. The temperature dependence of the rate constant,  $k_{\text{R12}}$ , for Reaction R12 is given by:

$$k_{\text{R12}} = 1.79 \times 10^{11} e^{-2533.6/T} \text{ L/mol/s}$$

where T is the temperature in Kelvin.

---

<sup>22</sup> The experimental apparatus of Lundström et al. [29] did not allow for flushing of the solution in the radiation cell whereas in the experimental arrangement used by Elliot in 1989 [61], the solution could be replaced between each pulse.

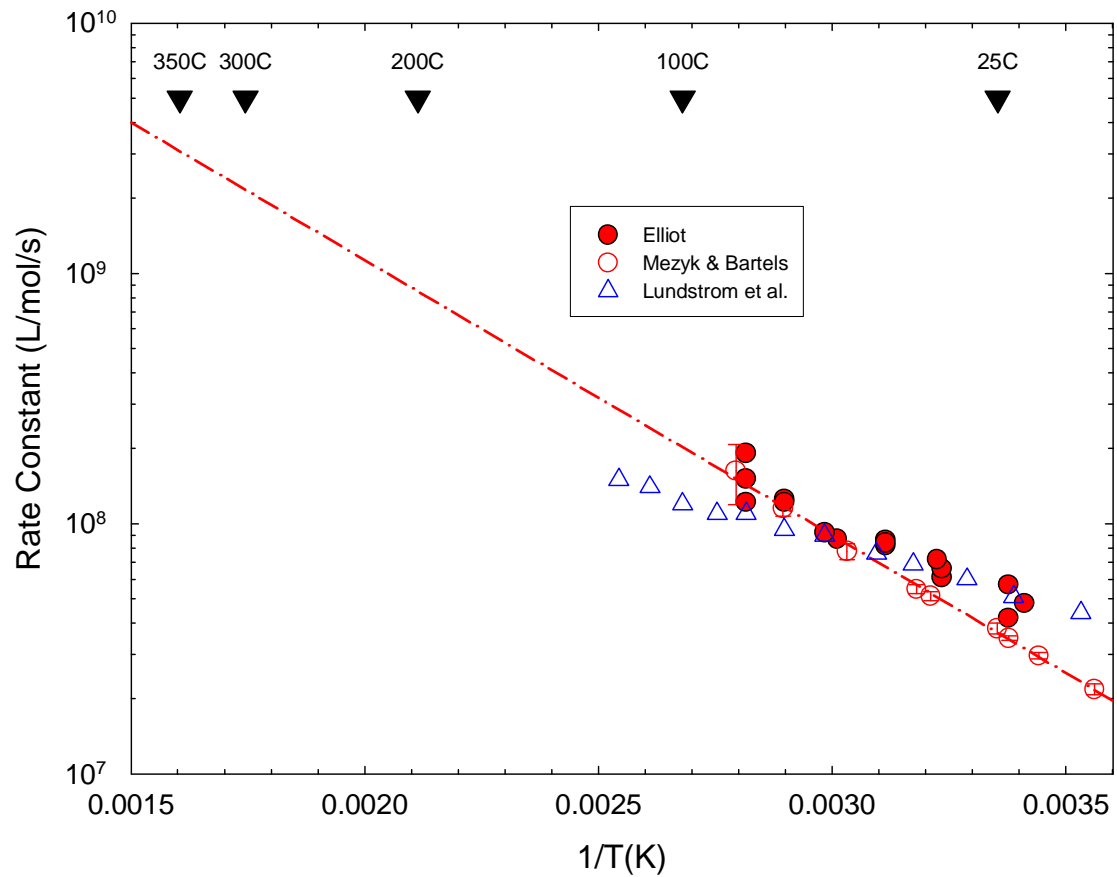


**Figure 4-10** The temperature dependence for the reaction of hydrogen atoms with hydrogen peroxide as reported by Elliot [61], Mezyk and Bartels [62], and by Lundström et al. [29]. The regression line is through the data of Mezyk and Bartels [62].



**4.1.12 Reaction R13: H + O<sub>2</sub> → HO<sub>2</sub>**

The temperature dependence for the reaction of the hydrogen atom with oxygen has been measured recently by Janik et al. [24] up to 350°C by monitoring the absorption of the reacting species and products at 230 and 250 nm, in pulse radiolysis experiments in near neutral pH water. The rate constant,  $k_{R13}$ , for Reaction R13 was extracted by extensive computer modelling of the absorptions at the different temperatures. Although the kinetics were dominated by Reaction R13, Janik et al. [24] included adjustments to the rate constant,  $k_{R14}$ , for Reaction R14 to get acceptable global fits to the optical data.

Initially, Janik et al. assumed that hydrogen atoms reacted with the perhydroxyl radical as shown in Reaction R14:



As will be discussed in the next Section 4.1.13, the estimated rate constant,  $k_{R14}$ , using the pathway shown in Reaction R14 decreased markedly above 200°C (Figure 4-12). When Janik et al. [24] changed the products in Reaction R14 to that which predominates in the gas phase:



and then refitted, the estimated values for the rate constant,  $k_{R13}$ , increased slightly as shown in Figure 4-11 above 250°C, but the fitted rate constant for Reaction R14a increased at temperatures above 200°C rather than decreased (Figure 4-12). Reaction R14 and R14a will be discussed in the next Section 4.1.13.

Elliot and co-workers [54] studied Reaction R13 using competition kinetics up to 200°C using pulse radiolysis. Both the data of Elliot and co-workers and the results of Janik et al. are shown in Figure 4-11. In general, within the experimental uncertainties, there is agreement between the two sets of results.

For the polynomial fit to the temperature dependence, the Janik et al. values for  $k_{R13}$  estimated when using Reaction R14a have been used along with the data from Reference [54]. This is shown in Figure 4-11 as a polynomial fit through the marked data. The temperature dependence of the rate constant,  $k_{R13}$ , for Reaction R13 is given by:

$$\text{Log } k_{R13} = 10.704 + 2.840 \times 10^2/T - 1.369 \times 10^5/T^2$$

where T is the temperature in Kelvin and where  $k_{R13}$  has units of L/mol/s. The value of  $k_{R13}$  at 25°C is estimated to be  $1.3 \times 10^{10}$  L/mol/s.

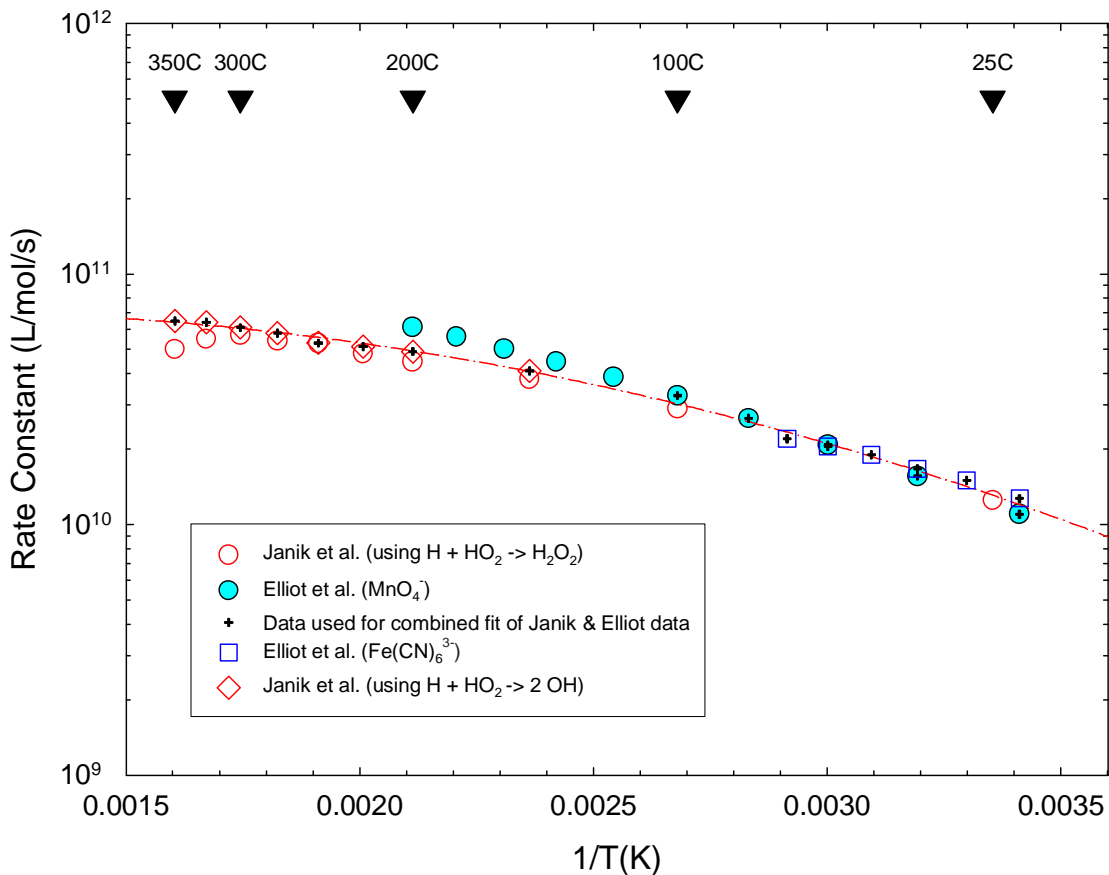


Figure 4-11 The temperature dependence for the reaction of hydrogen atoms with oxygen as reported by Janik et al. [24] and by Elliot et al. [54].

**4.1.13 Reaction R14:  $\text{H} + \text{HO}_2 \rightarrow \text{H}_2\text{O}_2$  (or 2 OH)**

The temperature dependence for the reaction of the hydrogen atom with the perhydroxyl radical has been reported by Lundström et al. [31] up to 150°C and by Janik et al. [24] up to 350°C. In the case of Lundström et al. [31], the rate constant,  $k_{\text{R14}}$ , was measured by the competition for the hydrogen atom between Reaction R13 and Reaction R14 in pH ~1 (25°C) water containing oxygen and hydrogen:



by monitoring the yield of the perhydroxyl radical immediately after a 1 microsecond radiolysis pulse. The results of Lundström et al. [31] are given in Figure 4-12. It should be noted that the value of the reference rate constant,  $k_{\text{R13}}$ , that Lundström et al. [31] used in their fitting of the data was about 50% higher than the values given in this report (Section 4.1.12). This would suggest that the values for  $k_{\text{R14}}$  reported by Lundström et al. [31] will be biased high.

As discussed in Section 4.1.12, the estimation of the rate constant,  $k_{\text{R14}}$ , by Janik et al. [24] was less direct in that  $k_{\text{R14}}$  was one of the variables used in the fitting of the optical data to measure the rate constant,  $k_{\text{R13}}$ , for Reaction R13. At lower temperatures the data analyses of Janik et al. [24] were not sensitive to values of  $k_{\text{R14}}$  for Reaction R14. At higher temperature, if the product of the reaction was assumed to be hydrogen peroxide, then  $k_{\text{R14}}$  must decrease significantly above 150°C (Figure 4-12) because the expected attenuation of the  $\text{HO}_2$  product absorption was not observed. However, if the product is assumed to be two hydroxyl radicals:



it is not necessary to postulate a strong decrease in the rate constant,  $k_{\text{R14}}$ , with temperature. The hydroxyl radicals would react with the hydrogen present to regenerate hydrogen atoms (Reaction R32b), which in turn will react with oxygen to reform the hydroperoxyl radical (Reaction R13). These higher temperature values for Reaction R14a appear to be consistent with the values for Reaction R14 measured by Lundström et al. [31] as can be seen in Figure 4-12, although it is recognised that the latter data may be biased high.

At the present time, because of the consistency between the measured values of  $k_{\text{R14}}$  by Lundström et al. [31] and the values estimated by Janik et al. [24] using the Reaction R14a mechanism, the data of Lundström et al. is recommended for the temperature dependence. The value of the rate constant,  $k_{\text{R14}}$ , at 25°C is  $1.13 \times 10^{10}$  L/mol/s and the activation energy is 15.2 kJ/mole.<sup>23</sup> The temperature dependence of the rate constant,  $k_{\text{R14}}$ , for Reaction R14a is given by:

$$k_{\text{R14}} = 5.17 \times 10^{12} e^{-1824.2/T} \text{ L/mol/s}$$

<sup>23</sup> It is noted that this calculated activation energy of 15.2 kJ/mole is lower than the 17.5 kJ/mole reported by Lundström et al. [31] using the same data.

where  $T$  is the temperature in Kelvin.

It is recommended that the rate constant for the overall Reaction R14 be re-measured using revised rate constants. One of the issues that should be addressed is the possible branching between Reactions R14 and R14a. At high temperature, we must assume that H and HO<sub>2</sub> react on one or more of the triplet electronic surfaces to give the hydroxyl radical products. These hydroxyl radicals are produced as a geminate pair in a solvent cage. It is expected that some fraction will escape the cage, given that for reaction between two hydroxyl radicals (Reaction R4), the reaction rate at high temperature is much lower than the diffusion-controlled limit (see Figure 4-4 in Section 4.1.3). If  $k_{\text{diff}}$  is the diffusion-limited encounter rate constant for Reaction R4, and  $k_{\text{R4}}$  is the actual rate constant for production of hydrogen peroxide, then the probability of reaction for caged hydroxyl radicals is given by  $k_{\text{R4}}/k_{\text{diff}}$ . If the net rate constant for Reactions R14 and R14a can be measured, an approach to estimating the branching ratio between Reactions R14 and R14a is to multiply the observed net rate constant by  $k_{\text{R4}}/k_{\text{diff}}$ . Likewise, if the rate constant for  $k_{\text{R14a}}$  is measured, as the method of Lundström et al. [31] does by monitoring the perhydroxyl radical absorption, the rate constant for Reaction R14a can then be calculated.

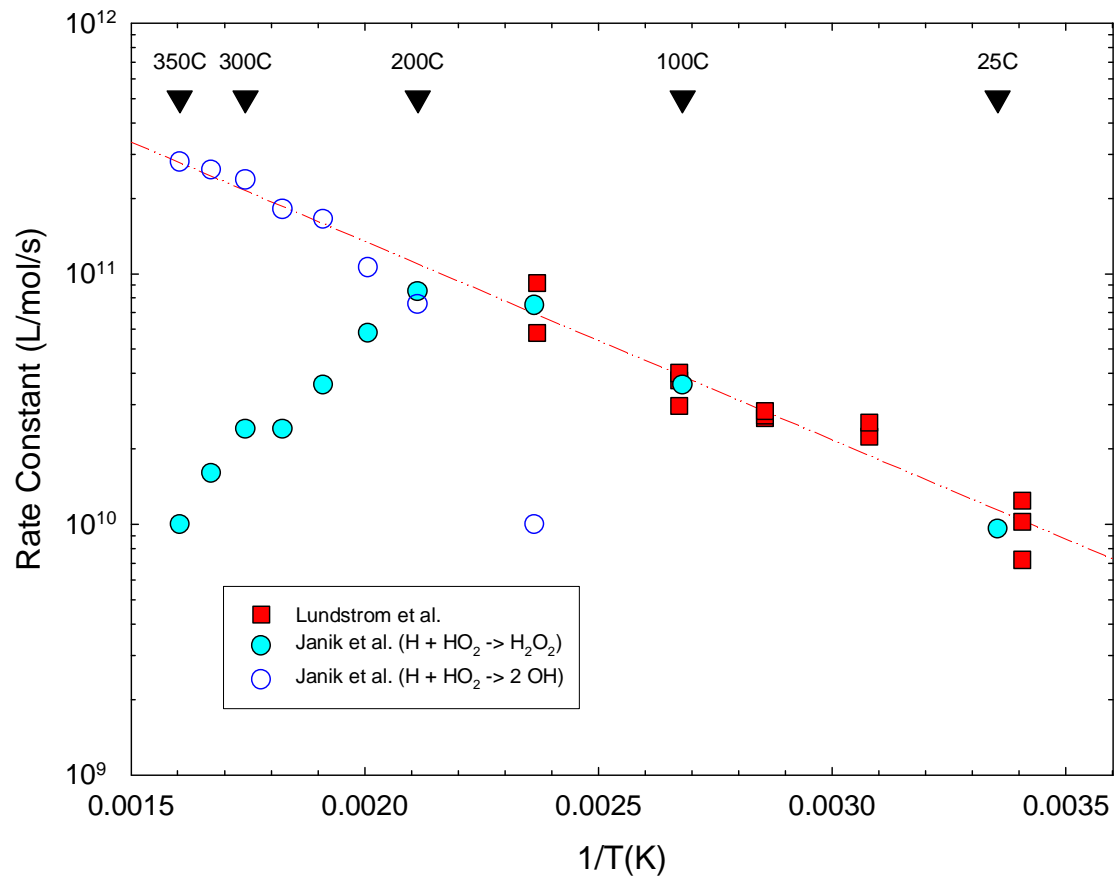


Figure 4-12 The temperature dependence for the rate constant for the reaction of hydrogen atoms with the perhydroxyl radical as reported by Lundström et al. [31] and by Janik et al. [24].

**4.1.14 Reaction R15:  $\text{H} + \text{O}_2^- \rightarrow \text{HO}_2^-$** 

There do not appear to be any measurements of the rate constant,  $k_{\text{R15}}$ , for Reaction R15. It is unlikely that this reaction would be very significant in any modelling of high temperature water. The pragmatic approach taken is to assume it has the same room temperature rate constant of  $1.13 \times 10^{10}$  L/mol/s and activation energy of 15.2 kJ/mole as assumed for Reaction R14 (Section 4.1.13).

$$k_{\text{R15}} = 5.17 \times 10^{12} e^{-1824.2/T} \text{ L/mol/s}$$

**4.1.15 Reaction R16:  $\text{OH} + \text{H}_2\text{O}_2 \rightarrow \text{HO}_2 + \text{H}_2\text{O}$** 

The temperature dependence of the rate constant for the reaction of the hydroxyl radical with hydrogen peroxide has been studied using the same pulse radiolysis method (growth of  $\text{O}_2^-$  in  $\text{N}_2\text{O}$  saturated aqueous solutions containing hydrogen peroxide<sup>24</sup>) in two laboratories [50], [57], [63]. There is agreement between the results (Figure 4-13). Recognising that only a limited temperature range could be studied due to the poor thermal stability of hydrogen peroxide, it is assumed that the reaction rate constant follows an Arrhenius temperature dependence. The value of the rate constant,  $k_{\text{R16}}$ , at 25°C is  $2.9 \times 10^7$  L/mol/s and the activation energy is 13.8 kJ/mole.

Based on the data in (Figure 4-13), the temperature dependence of the rate constant,  $k_{\text{R16}}$ , for Reaction R16 is given by:

$$k_{\text{R16}} = 7.68 \times 10^9 e^{-1661.4/T} \text{ L/mol/s}$$

where T is the temperature in Kelvin.

---

<sup>24</sup> The initially formed  $\text{HO}_2$  dissociates rapidly to  $\text{O}_2^-$  on the time scale of the experiment [50].

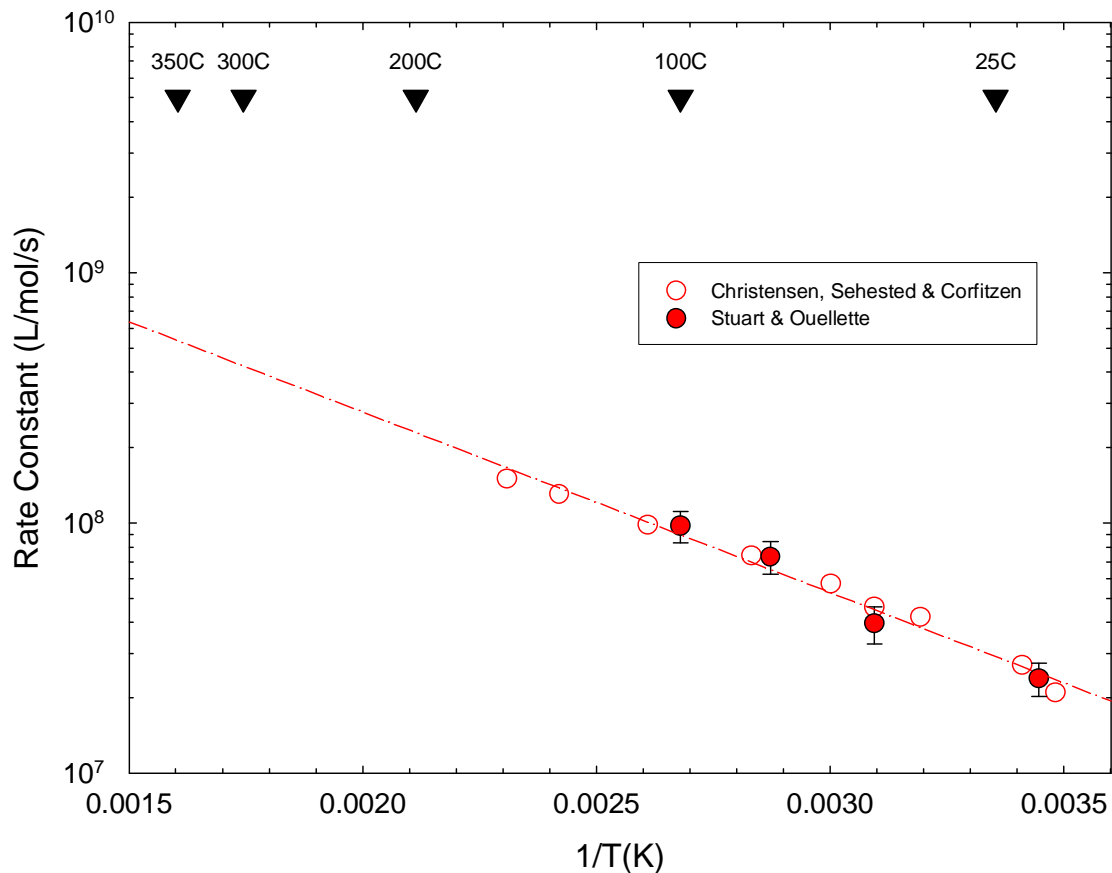


**Figure 4-13 The temperature dependence for the reaction of hydroxyl radicals with hydrogen peroxide as reported by Christensen et al. [63] and by Stuart and co-workers [50], [57].**

**4.1.16 Reaction R17:  $\text{OH} + \text{O}_2^- \rightarrow (\text{HO}_3^-) \rightarrow \text{O}_2 + \text{OH}^-$** 

The temperature dependence of the rate constant,  $k_{\text{R17}}$ , for the reaction of the hydroxyl radical with the superoxide radical has been measured by Christensen et al.[64] and by Elliot and Buxton [65] using the pulse radiolysis technique. Christensen et al. [64] used a competition method and measured the yield of the superoxide radical anion as function of the concentration of hydrogen, with an oxygen concentration set by a 0.3 MPa partial pressure. In a computer simulation of the final superoxide concentration, the rate constant,  $k_{\text{R17}}$ , was varied until a fit was achieved of the yield versus hydrogen concentration. Elliot and Buxton [65] determined the rate constant,  $k_{\text{R17}}$ , as a function of temperature by fitting the time dependence of the optical absorption at three wavelengths, 240, 250 and 260 nm, obtained when water containing oxygen was pulse irradiated. The results reported by Christensen et al. [64] and by Elliot and Buxton [65] are shown in Figure 4-14.

Both these studies were performed over 17 years ago, and used computer fitting to extract the results with radiation chemistry databases which are now out of date. A review of the different data sets used by both laboratories indicated that both analyses used high temperature g-values for the primary species that were significantly lower than the recommended values given in Section 3. The extinction coefficient for the superoxide radical anion used by Christensen et al. [64] at room temperature of 2110 L/mol/cm (at 243 nm) was 11% higher than the later re-evaluated values [65], [24] and then Christensen et al. assumed the extinction coefficient increased by 25% as the temperature increased to 300°C.<sup>25</sup> Janik et al. [24] has reported that the extinction coefficient decreased by ~12% over the temperature range.

Elliot and Buxton [65], in order to get a good fit to the optical traces, invoked the formation of a weakly absorbing long-lived intermediate  $\text{HO}_3^-$  as shown in Reaction R17.



Elliot and Buxton [65] cautioned that  $\text{HO}_3^-$ , if formed, would be involved in reactions with other species.

Obviously Reaction R17 should be re-investigated based on the current understanding of high temperature water radiolysis. The temperature dependence as measured by Elliot and Buxton [65] for Reaction R17 is recommended for use in modelling until improved values are available. The results of Elliot and Buxton [65] have been selected because the g-values used in their simulations were closer to the currently recommended values and the appropriate extinction coefficient was used for the superoxide radical anion at room temperature, although it was assumed to remain constant with temperature.

---

<sup>25</sup> The impact of the higher extinction coefficients for the superoxide radical anion and lower g-values may partially cancel out the impact on the estimation of  $k_{\text{R17}}$  for estimates above room temperature.



The value of the rate constant,  $k_{R17}$ , at 25°C is  $1.1 \times 10^{10}$  L/mol/s and the activation energy is 10.9 kJ/mole. Based on the Elliot and Buxton [65] data in (Figure 4-14), the temperature dependence of the rate constant,  $k_{R17}$ , for Reaction R17 is given by:

$$k_{R17} = 8.77 \times 10^{11} e^{-1306.2/T} \text{ L/mol/s}$$

where T is the temperature in Kelvin.

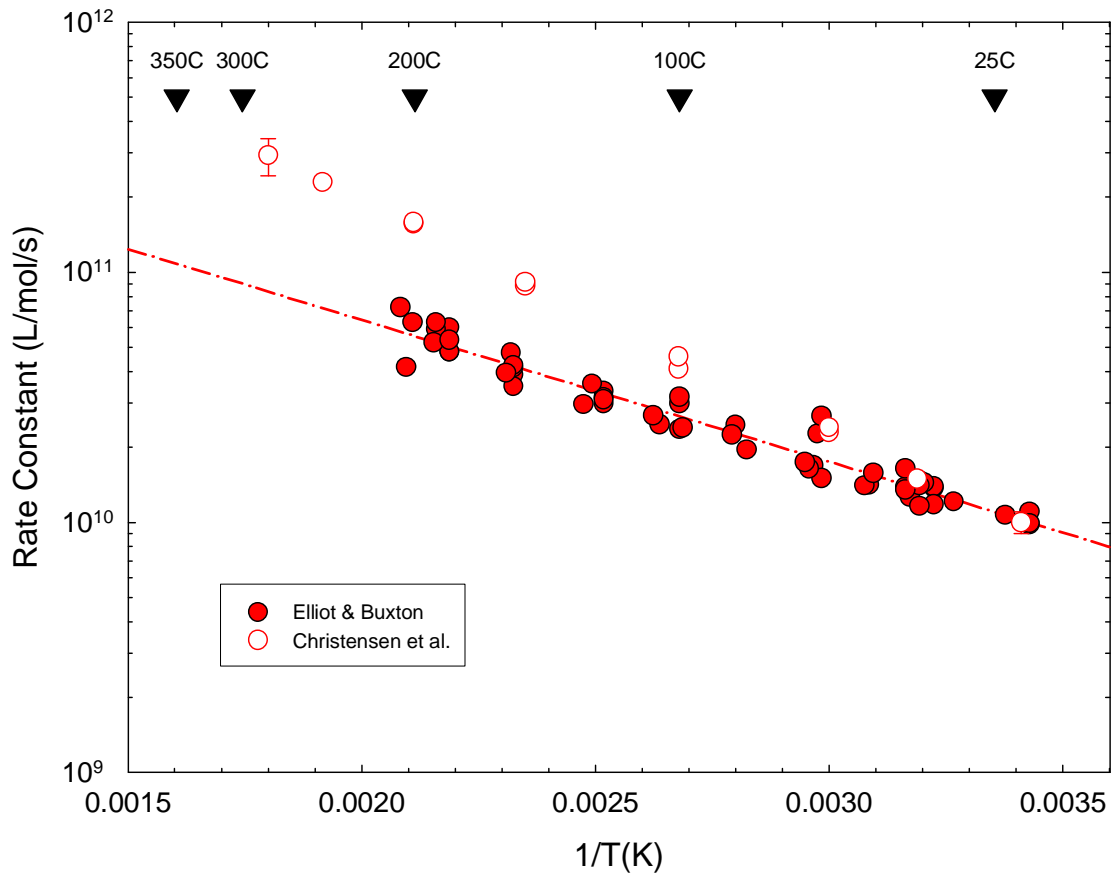


**Figure 4-14 The temperature dependence of the rate constant for the reaction of the hydroxyl radical with the superoxide radical as reported by Christensen et al. [64] and by Elliot and Buxton [65].**

**4.1.17 Reaction R18: OH + HO<sub>2</sub> → (H<sub>2</sub>O<sub>3</sub>) → O<sub>2</sub> + H<sub>2</sub>O**

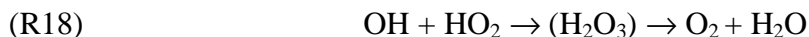
The temperature dependence of the rate constant,  $k_{R18}$ , for the reaction of the hydroxyl radical with the perhydroxyl radical has been measured by Elliot and Buxton [65] and by Lundström et al. [31] by using the pulse radiolysis technique in pH 2 water. Elliot and Buxton [65] determined the rate constant,  $k_{R18}$ , as a function of temperature by fitting the time dependence of the optical absorption of the reacting species at 252.5 nm in water containing oxygen. Lundström et al. [31] used a competition method and measured the yield of the perhydroxyl radical as a function of the concentration of hydrogen for a fixed oxygen concentration. In the computer simulations, the rate constant,  $k_{R18}$ , was varied until a fit was achieved of the yield versus hydrogen concentration.

The results reported by Elliot and Buxton [65] and by Lundström et al. [31] are shown in Figure 4-15. There is reasonable agreement between the results from the two laboratories. This agreement may be due, in part, to the radiolysis data set used by Lundström et al. [31] in 2004 was improved over the one used in 1989 by Christensen et al. [64] for the very similar Reaction R17 discussed in the previous Section 4.1.16. A simple Arrhenius temperature dependence through all the reported data has been assumed for the temperature dependence of  $k_{R18}$  as shown in Figure 4-15. The fitted Arrhenius equation is:

$$k_{R18} = 1.29 \times 10^{11} e^{-799.2/T} \text{ L/mol/s}$$

where T is the temperature in Kelvin. The value of the rate constant,  $k_{R18}$ , at 25°C is  $8.8 \times 10^9$  L/mol/s and the activation energy is 6.6 kJ/mole.

As with Reaction R17, Elliot and Buxton [65], in order to get a good fit to the optical traces, invoked the formation of a weakly absorbing long-lived intermediate H<sub>2</sub>O<sub>3</sub> as shown in Reaction R18.



H<sub>2</sub>O<sub>3</sub> is quite long-lived at room temperature; the first order decay rate of H<sub>2</sub>O<sub>3</sub> into oxygen and water has been measured as a function of pH. Information on H<sub>2</sub>O<sub>3</sub> has been summarised in Reference [66].

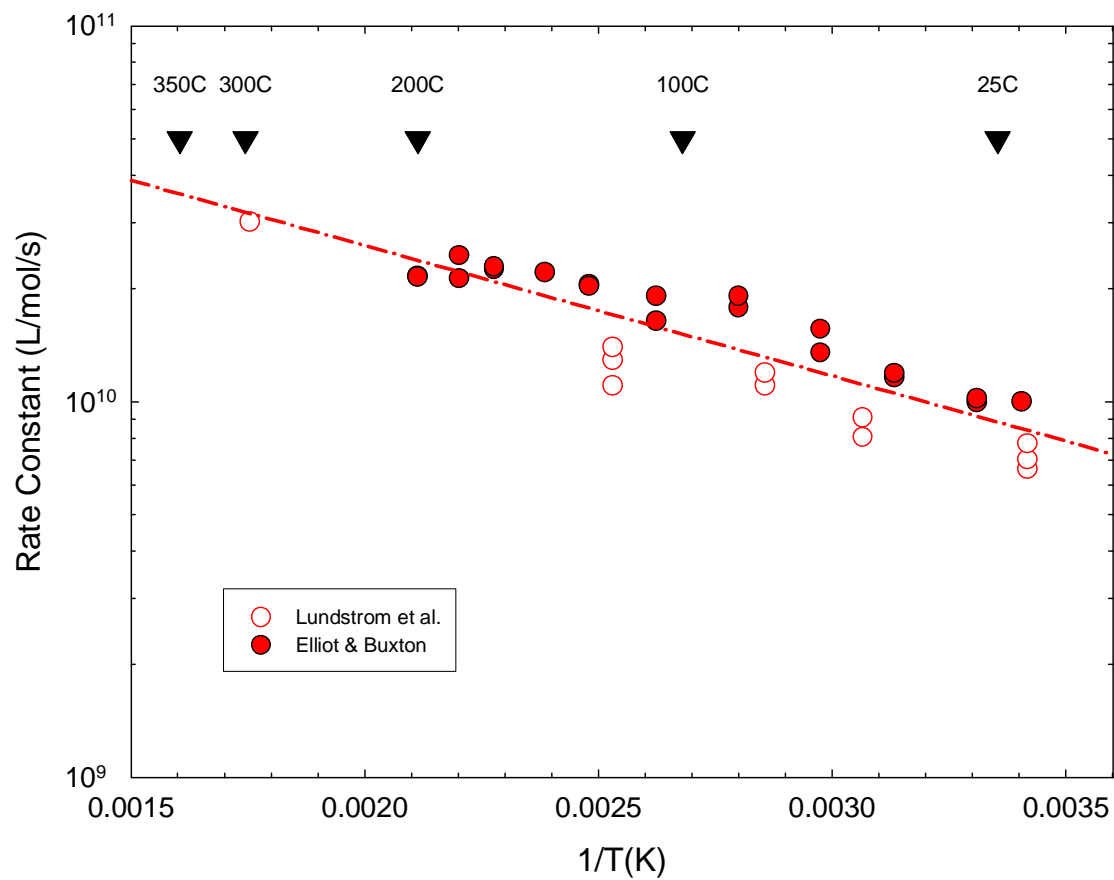
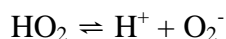


**Figure 4-15** The temperature dependence of the rate constant for the reaction of the hydroxyl radical with the perhydroxyl radical as reported by Lundström et al. [31] and by Elliot and Buxton [65].

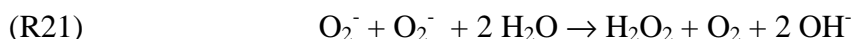
**4.1.18 Reactions R19, R20 and R21:  $\text{HO}_2/\text{O}_2^- + \text{HO}_2/\text{O}_2^- \rightarrow \text{H}_2\text{O}_2 + \text{O}_2$** 

At room temperature, the observed rate constant for the dismutation reaction involving  $\text{HO}_2/\text{O}_2^-$  as a function of pH is well established and is shown in Figure 4-16. At room temperature, the  $\text{pK}_A$  for the acid-base equilibrium:



is  $\text{pK}_{\text{HO}_2} = 4.8$  [67] and Figure 4-26.

The three reactions involved over the pH range are given below:<sup>26</sup>



The room temperature value for  $k_{\text{R19}}$  is  $\sim 8.4 \times 10^5$  L/mol/s, for  $k_{\text{R20}}$  is  $\sim 1 \times 10^8$  L/mol/s and for  $k_{\text{R21}}$  is  $< 0.3$  L/mol/s [67].

Below  $\text{pH} \sim 2$  (Figure 4-16), the decay is principally through Reaction R19. Christensen and Sehested have studied this reaction as a function of temperature up to  $285^\circ\text{C}$  [68] and report the rate constant as  $2k_{\text{R19}}/\epsilon l$  at 230 nm. Using the extinction coefficient reported by Janik et al. [24] and a path-length  $l$  of 2.5 cm, the values of  $k_{\text{R19}}$  have been calculated and plotted in Figure 4-17. The rate constant  $k_{\text{R19}}$  follows an Arrhenius temperature dependence over the range studied. The value of the rate constant,  $k_{\text{R19}}$ , at  $25^\circ\text{C}$  is  $8.4 \times 10^5$  L/mol/s and the activation energy is 6.6 kJ/mole. The temperature dependence of the rate constant,  $k_{\text{R19}}$ , for Reaction R19 is given by:

$$k_{\text{R19}} = 2.78 \times 10^9 e^{-2416.4/T} \text{ L/mol/s}$$

where  $T$  is the temperature in Kelvin.

Below  $100^\circ\text{C}$ , activation energies of 8.6 and 7.6 kJ/mole have been reported for the rate constant of Reaction R20 [67], [68]. The results reported by Christensen and Sehested [68] are shown by the red line in Figure 4-18. As the rate constant,  $k_{\text{R20}}$ , at room temperature is  $\sim 1 \times 10^8$  L/mol/s and assuming an activation energy of 8.1 kJ/mole, the temperature dependence of the rate constant,  $k_{\text{R20}}$ , below  $100^\circ\text{C}$ , is given by:

$$k_{\text{R20}} = 2.63 \times 10^9 e^{-974.3/T} \text{ L/mol/s}$$

where  $T$  is the temperature in Kelvin.

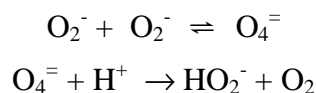
Above  $100^\circ\text{C}$ , the rate of Reaction R20 increases significantly as can be seen by the blue line in Figure 4-18 for data measured by Christensen and Sehested [68]. Stuart and Chenier (unpublished AECL-CRL) have seen similar behaviour in the decay of  $\text{O}_2^-/\text{DO}_2$  in heavy water as can be seen in the Arrhenius type plots in Figure 4-19.<sup>27</sup> As the solution

<sup>26</sup> For simplicity, hydrogen peroxide is written in its undissociated state,  $\text{H}_2\text{O}_2$ , in these reactions. As the  $\text{pK}_A$  for  $\text{H}_2\text{O}_2$  is 11.8 at  $25^\circ\text{C}$ , the base form,  $\text{HO}_2^-$ , will be present at higher pH values.

<sup>27</sup> The use of  $2k_{\text{obs}}/\epsilon$  is necessary as the  $\text{pK}$  of  $\text{DO}_2$  and the temperature dependent extinction coefficients of  $\text{O}_2^-$  and  $\text{DO}_2$  in heavy water have not been established yet.

becomes more alkaline, the two distinct kinetic regimes become more apparent.

Christensen and Sehested [68] have postulated that as the temperature increases, the rate of Reaction R21 increases significantly. Christensen and Sehested suggest that the following reactions may occur:



Reactions R20 and R21 need to be investigated again. The simplest approach would be to develop the isotherms as a function of pH as shown in Figure 4-16 for temperatures above room temperature and then fit the rate constants to this data, with the knowledge of the  $\text{pK}_A$  of  $\text{HO}_2$  and the extinction coefficients of  $\text{O}_2^-$  and  $\text{HO}_2^-$ .

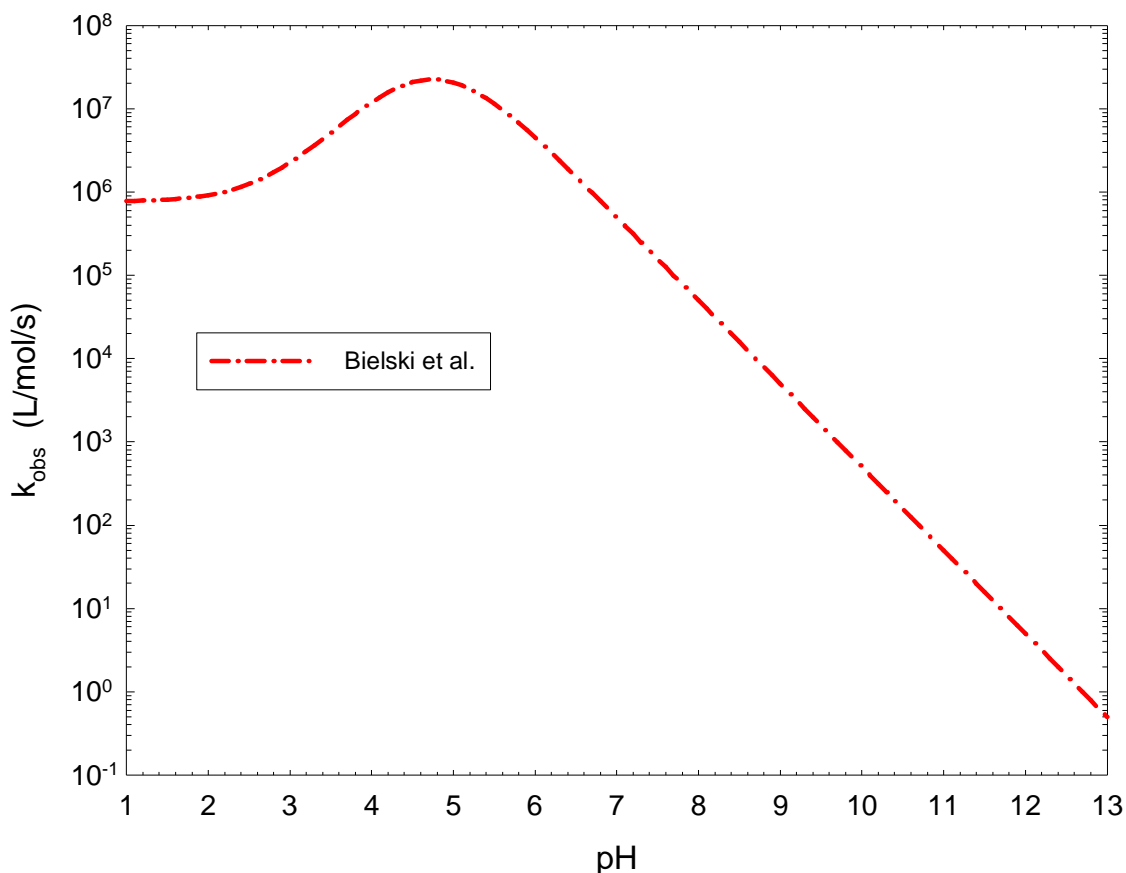


**Figure 4-16** The rate constant for the decay of  $\text{HO}_2/\text{O}_2^-$  as a function of pH at room temperature Bielski et al. [67].

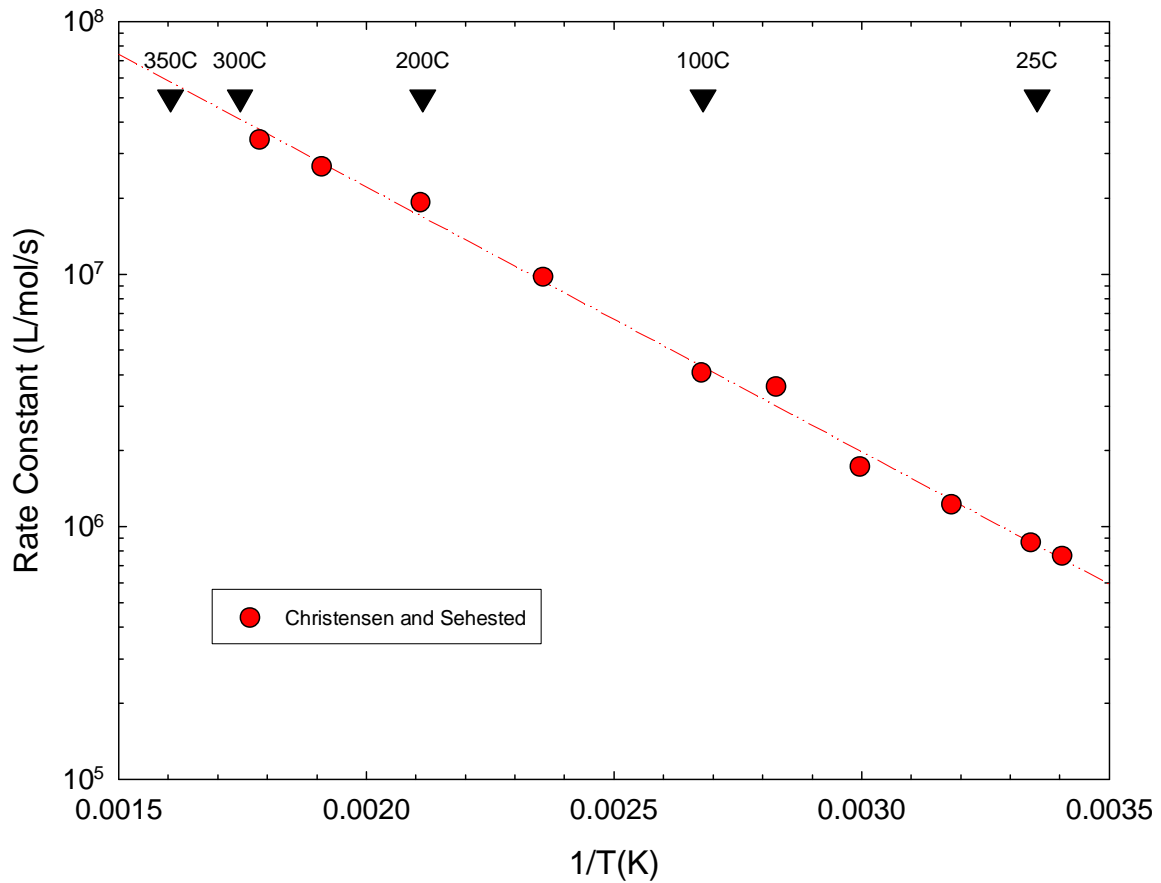


**Figure 4-17** The temperature dependence of the rate constant for the dismutation Reaction R19 of the perhydroxyl radical as calculated from the data of Christensen and Sehested [68].

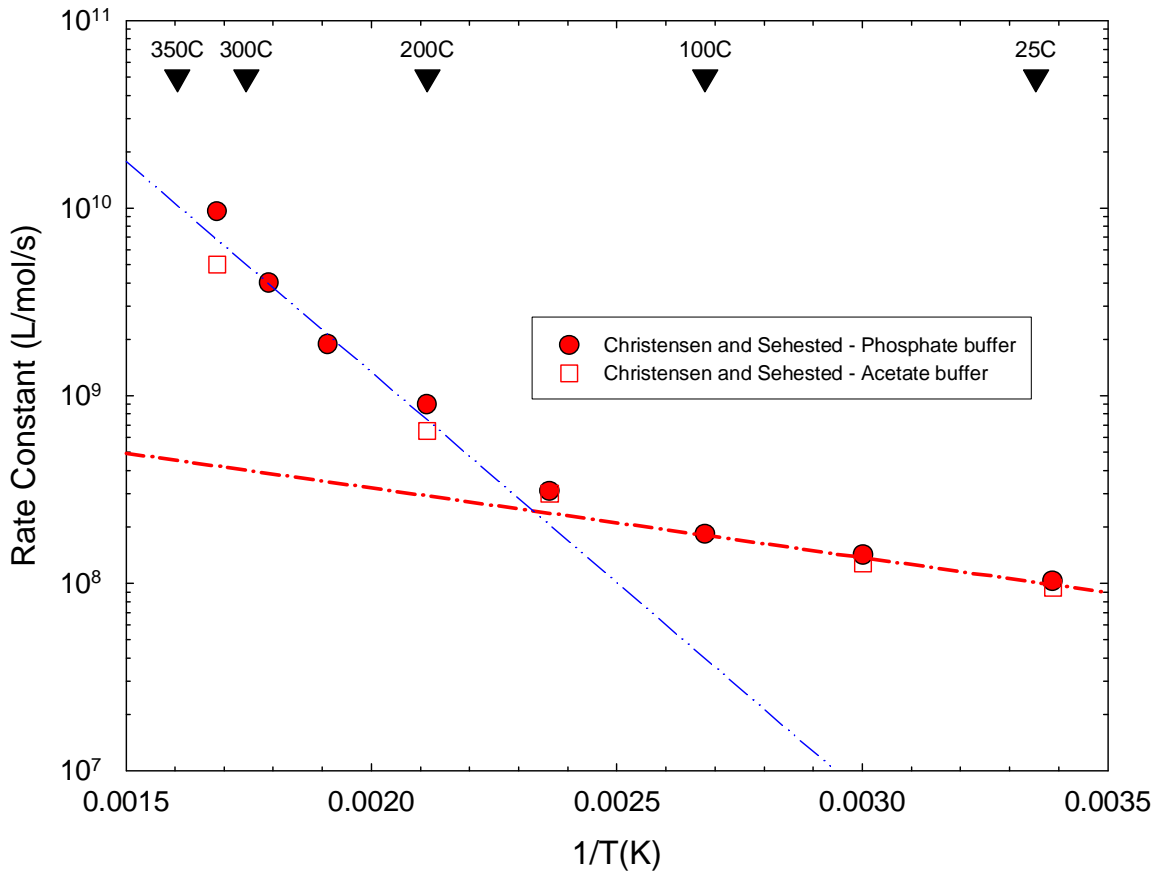
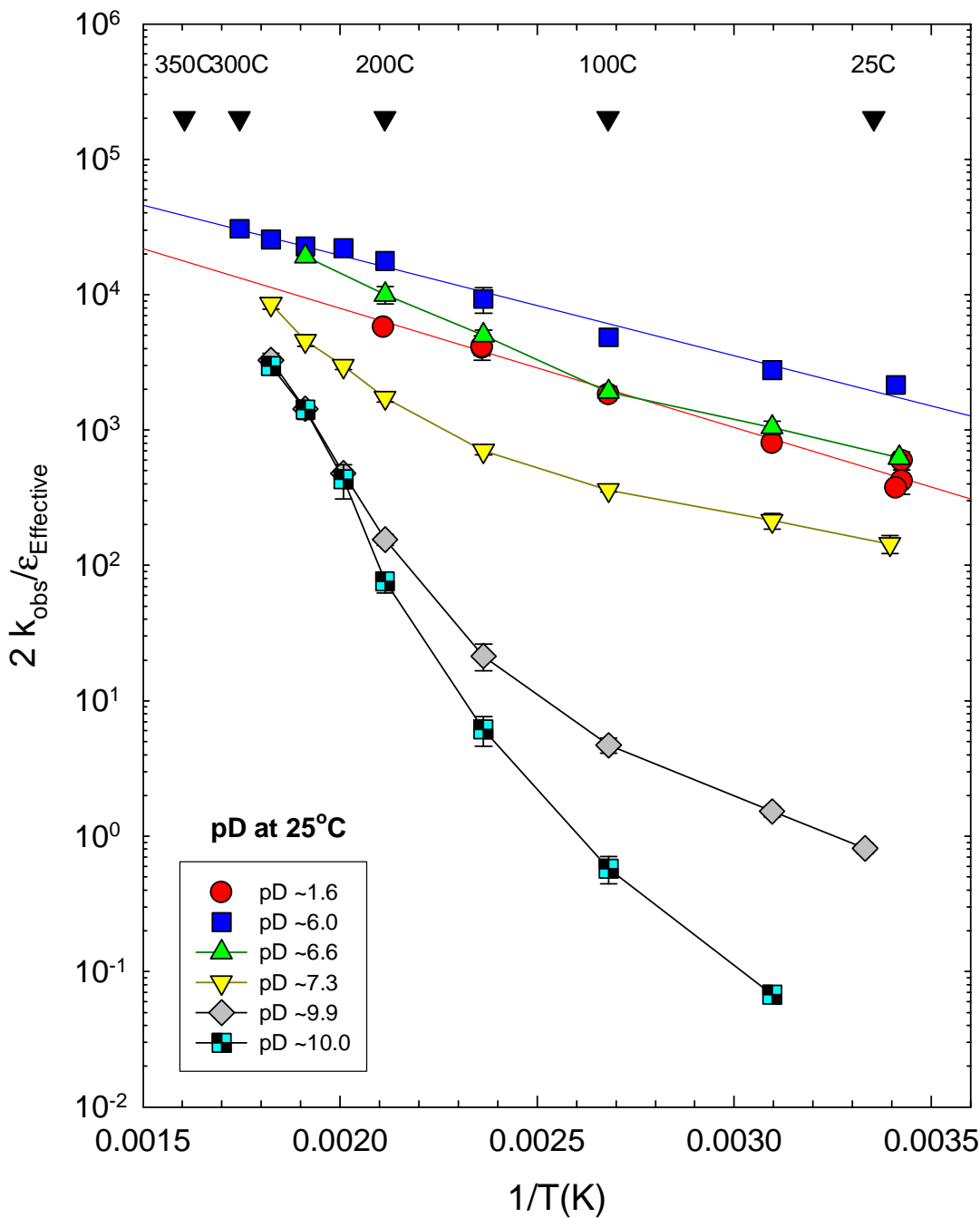


Figure 4-18 The rate constant for Reaction R20 between O<sub>2</sub><sup>-</sup> and HO<sub>2</sub> as a function of temperature [68] showing the two distinct temperature dependencies above and below 100°C.



**Figure 4-19** The observed bimolecular decay constant, expressed as  $2k_{obs}/\epsilon$ , for the reactions of  $O_2^-$  and  $DO_2$  in heavy water at different pD values. Unpublished work by Stuart and Chenier (AECL-CRL).



**4.1.19 Reaction R22:  $\text{H}_2\text{O}_2 \rightarrow \frac{1}{2}\text{O}_2 + \text{H}_2\text{O}$** 

In high temperature aqueous systems, the thermal decomposition of hydrogen peroxide has been shown to form oxygen as shown in the *overall* Reaction R22:



As will be discussed later in this section, it is not clear whether the initial step of the thermal decomposition is dissociation to form two hydroxyl radicals:



or is some mechanism which forms oxygen without the hydroxyl radical as an intermediate as could possibly happen on a metal surface.

Since the 1980's, the thermal decomposition of hydrogen peroxide has been studied extensively in high temperature loops or autoclaves as detailed in [69], [70], [71], [72], [73], [74] and references therein. It is well established that the decomposition follows first order kinetics. The results from a number of laboratories, from experiments where hydrogen peroxide was flowed through similar sized tubes although prepared from different materials, are remarkably similar in shape (Figure 4-20) if the data from Croiset [74] measured at 5 and 10 MPa above  $\sim 280^\circ\text{C}$  are not considered. It appears that there could be two regimes where an activation energy near 65 kJ/mole is observed up to  $\sim 200^\circ\text{C}$  and then a lower value near 43 kJ/mole is observed above  $200^\circ\text{C}$ . As will be discussed below, this apparent change of activation energy is considered to be a consequence of the reaction becoming mass transport limited for the transfer of hydrogen peroxide from the bulk solution to the walls. The decomposition reaction is considered to occur principally on the wall surface.

It has been demonstrated in decomposition experiments using small bore tubing that a significant proportion of the peroxide decomposition occurred on the system surfaces. This has been established in the experiments performed in flowing tubes by comparing the reaction rate as a function of the surface material for the tube and on diameter of the reaction tubes where the surface-to-volume ratio is varied [69], [70], [72], [73], [74].

The effect of using PTFE coated tubing compared to metal tubing can be seen in Figure 4-21 and Figure 4-22. The impact of the diameter of the tubing can be seen in Figure 4-21 where the decomposition rate increased as the bore of the tubing decreased. Rebensdorff and Widmark [69] have also demonstrated that hydrogen peroxide decayed more rapidly as the thickness of the iron oxide on the tubing surface increased.

The decomposition of hydrogen peroxide does follow an Arrhenius relationship as can be seen in Figure 4-21, Figure 4-22 and Figure 4-23. However, in some of the tests using the thin tubes, at the highest temperatures the rate constants fell below the Arrhenius line as measured on data obtained at the lower end of the temperature ranges studied (Figure 4-20, Figure 4-22 and Figure 2 in Reference [69]). This decrease in the rate of increase of the decay constant has been ascribed to the rate of mass transport of hydrogen peroxide in the bulk solution to the walls beginning to influence the overall rate of the decomposition reaction [69], [72], [73].

The thermal decomposition of hydrogen peroxide also depends on the alkalinity of the solution. In a study of the decomposition of hydrogen peroxide in a stainless steel lined autoclave, Haines and McCracken found that the rate in a lithium hydroxide solution (room temperature pH 10.3) was 4-5 times that in neutral pH water (Figure 4-23).

It is assumed that the decrease in the activation energy observed above 200°C in Figure 4-20 can be explained in terms of the surface reaction being mass transport limited. The activation energy for the thermal decomposition of hydrogen peroxide in metal systems appropriate for modelling falls in the range 65±10 kJ/mole. The choice of the appropriate pre-exponential factor should be made on a case-by-case basis, depending on the (sub-) system being modelled but will likely be the range 10<sup>5</sup> to 10<sup>6</sup> s<sup>-1</sup>.

As to the actual mechanism of the thermal decomposition, it is not clear whether the initial step is dissociation to form two hydroxyl radicals [72], [73], [75].



or by some mechanism which forms oxygen without the hydroxyl radical as an intermediate as could possible happen on a metal surface:



Lin et al. [72], [73] has studied the thermal decomposition of ~6.5×10<sup>-5</sup> mol/kg hydrogen peroxide in the presence of ~8×10<sup>-5</sup> mol/kg hydrogen in both titanium tubing (Figure 4-22) and stainless steel [72], [73]. No difference was found in the decomposition rate from tests when no hydrogen was present. If hydroxyl radicals were formed, an enhanced rate of loss of peroxide might have been expected from the chain reaction:



In competition with:



Chenier and Elliot (unpublished AECL-CRL data from 1991) studied the thermal decomposition at 110°C of 2×10<sup>-4</sup> mol/kg hydrogen peroxide solutions containing 10<sup>-6</sup> mol/kg EDTA<sup>28</sup> in Pyrex glass ampoules. The presence of 2.6×10<sup>-4</sup> mol/kg dissolved hydrogen did not increase the rate of decomposition of the peroxide as can be seen in Figure 4-24. This seems to support the observation that formation of hydroxyl radicals is not a significant pathway in the aqueous decomposition of the peroxide.

However, some caution needs to be applied when assessing these experiments with added hydrogen. In particular, the rate of Reaction R32b has to be significantly faster than Reaction R16 to sustain a chain reaction.<sup>29</sup> At a nominal 200°C, at the concentrations

<sup>28</sup> The EDTA was added to complex any transition metal ions that may catalyze the peroxide decomposition. The first order decay constant was ~6×10<sup>-6</sup> s<sup>-1</sup>.

<sup>29</sup> Rate (s<sup>-1</sup>) is given by k (L/mol/s)×concentration (mol/L).

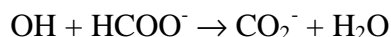
used by Lin et al. [72], [73], the rate of Reaction R32b will be about 3.9 times higher than the rate of Reaction R16. For the AECL-CRL experiment at 110°C the rate of Reaction R32b will be about 5.8 times higher than the rate of Reaction R16. Presumably these relatively small excess rates are sufficient to sustain a short chain reaction.

Lin et al. [72], [73] also added  $\sim 2 \times 10^{-3}$  mol/kg ethanol as a hydroxyl radical scavenger. For reasons not stated, only the product oxygen was monitored and its yield was unaffected by the ethanol. This was taken as evidence that no hydroxyl radicals were formed during the thermal decomposition. In this case, the concentration of ethanol should have been sufficient to scavenge any hydroxyl radicals formed.

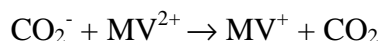
However, there is some evidence to suggest that hydroxyl radicals may be formed. Ashmore et al. [76] show a figure in a report (replicated in Figure 4-25 below) where they note: “In a separate test it can be seen that when H<sub>2</sub>O<sub>2</sub> was added in a thermal experiment it reacted with sodium formate to give CO<sub>2</sub> ...”. They do not discuss the test further in the report. The test was performed in an all stainless steel system where the solution was flowed through a reaction vessel in front of a Van de Graaff accelerator, which was not operating at the time. At face value, it appears that hydrogen peroxide is decomposing to form hydroxyl radicals:



The hydroxyl radicals formed then react with the formate present:



The CO<sub>2</sub><sup>-</sup> radical anion then reacted with methyl viologen:



The overall stoichiometry of this reaction set is that for every hydrogen peroxide molecule decomposed, two carbon dioxide molecules are formed.

It can be seen in Figure 4-25, that the carbon dioxide concentration increases with the solution temperature above 150°C. The concentration of carbon dioxide measured at  $\sim 200^\circ\text{C}$  is  $\sim 1.1 \times 10^{-5}$  mol/kg which is similar to the starting hydrogen peroxide concentration. Although the remaining hydrogen peroxide concentration was not reported and a material balance can not be undertaken, the results are consistent with Reaction R22a being the initiating step in their system.<sup>30</sup>

At the present time, based on the information to hand, no recommendation can be given as to which is the appropriate mechanism for the thermal decomposition of hydrogen peroxide, Reaction R22 or Reaction R22a. In any radiolysis model, it would be prudent to try both mechanisms to see if they have any significant effect on the overall result.

---

<sup>30</sup> One possible mechanism that may contribute to the decomposition of hydrogen peroxide to form hydroxyl radicals is Fenton's reaction. The source of the ferrous ion is oxide dissolution from, or corrosion of, the stainless steel surfaces of the experimental apparatus as the temperature increases. Repeating this test with PTFE covered tubing would help resolve this issue.

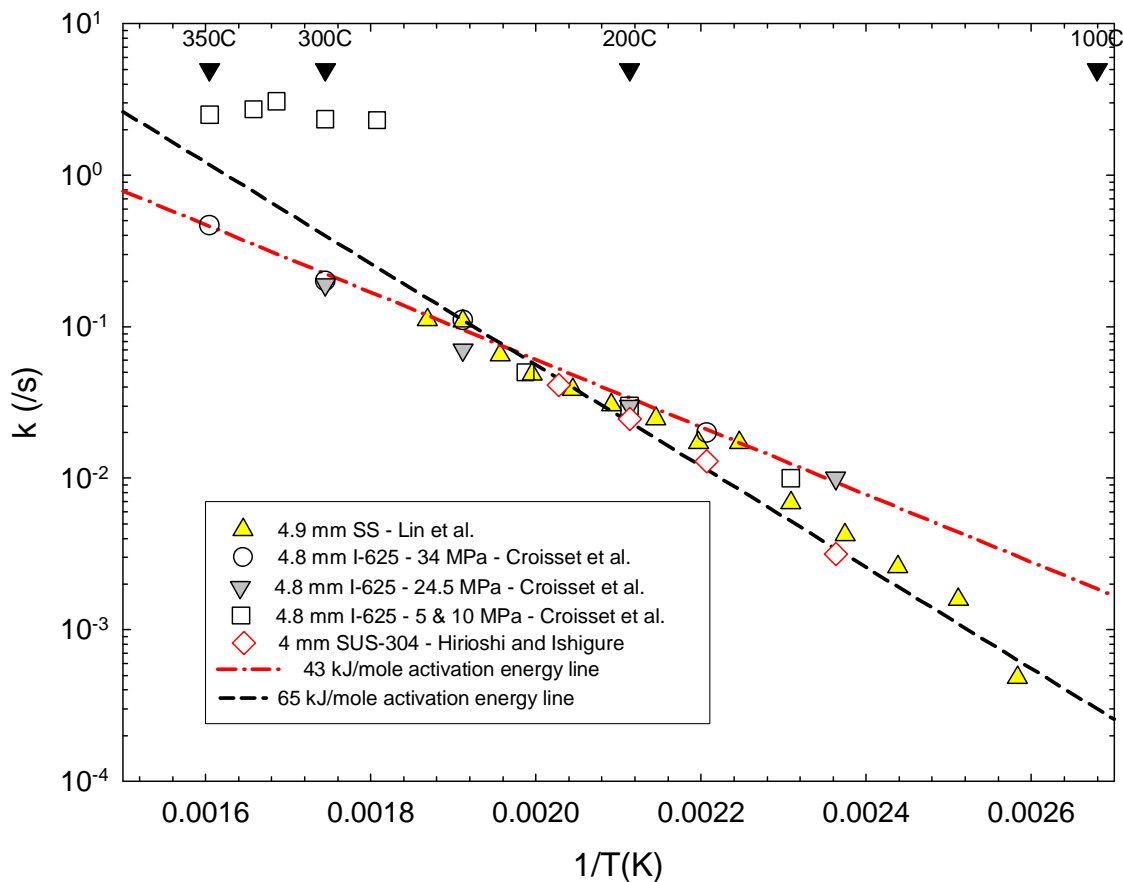


Figure 4-20 Arrhenius plot of the thermal decomposition of hydrogen peroxide in ~4-5 mm tubing [70], [72], [74] showing a possible activation energies.

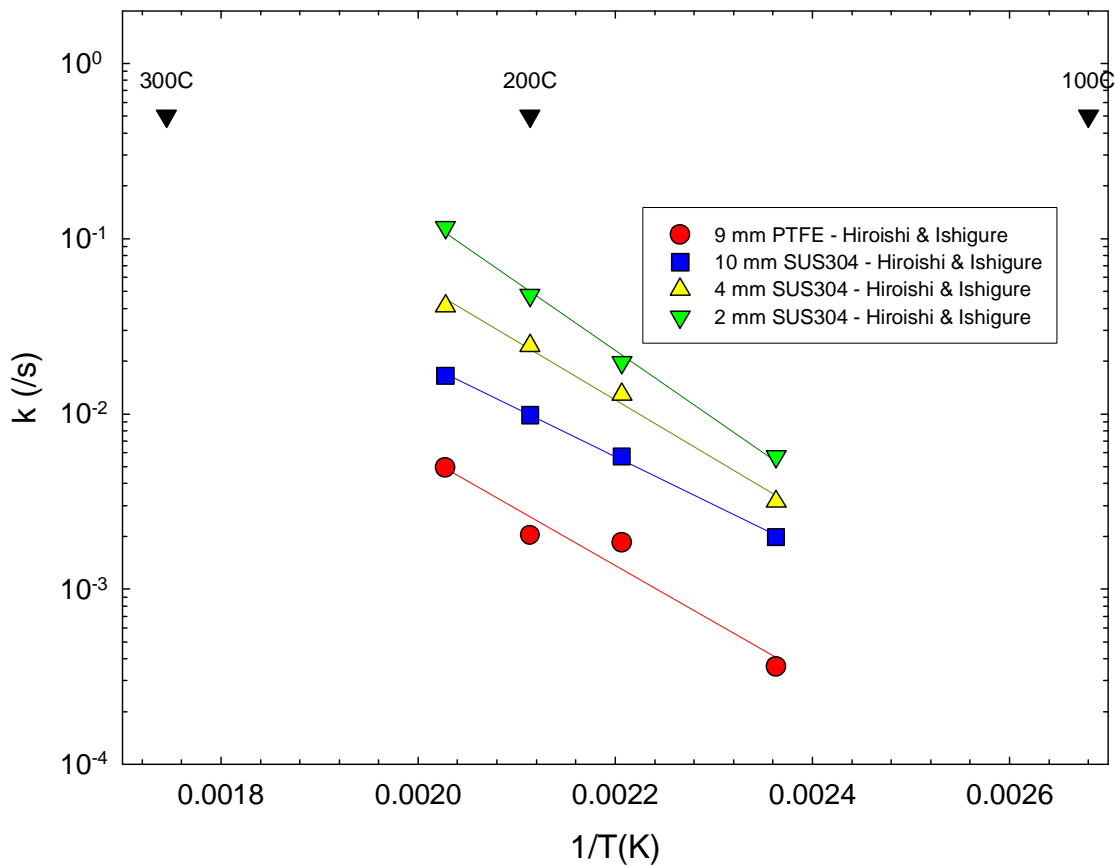


Figure 4-21 Arrhenius plot of the thermal decomposition of hydrogen peroxide in neutral water showing the effect of tube diameter and of stainless steel and PTFE tube material [70].

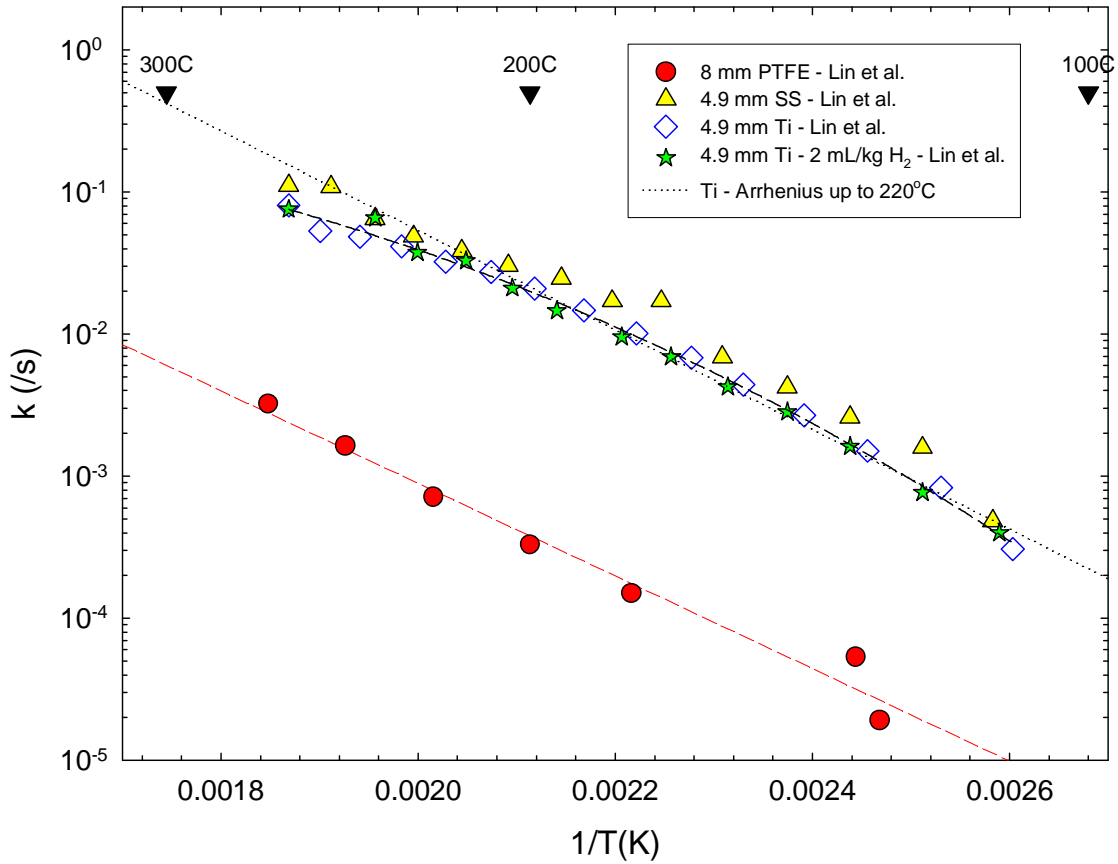


Figure 4-22 Arrhenius plot of the thermal decomposition of hydrogen peroxide in neutral water showing the effect of tube material (PTFE, stainless steel and titanium) and of hydrogen [72], [73].

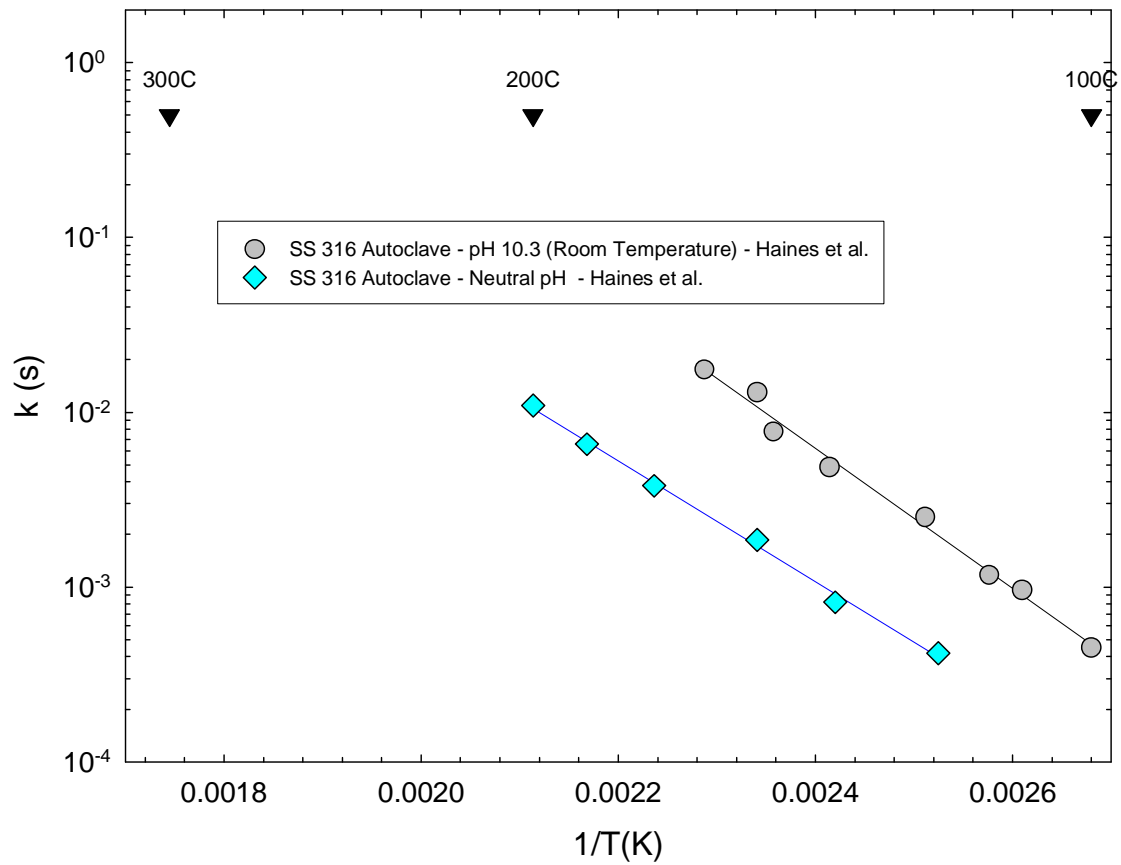
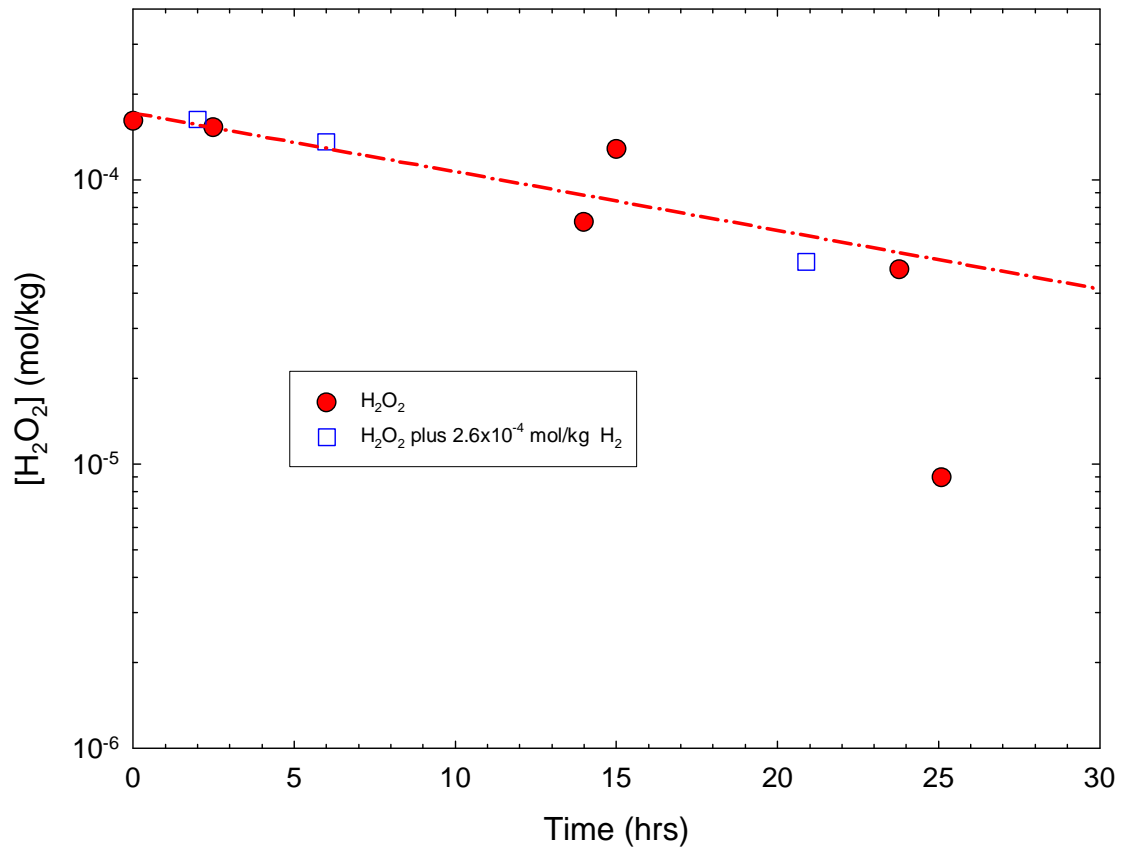
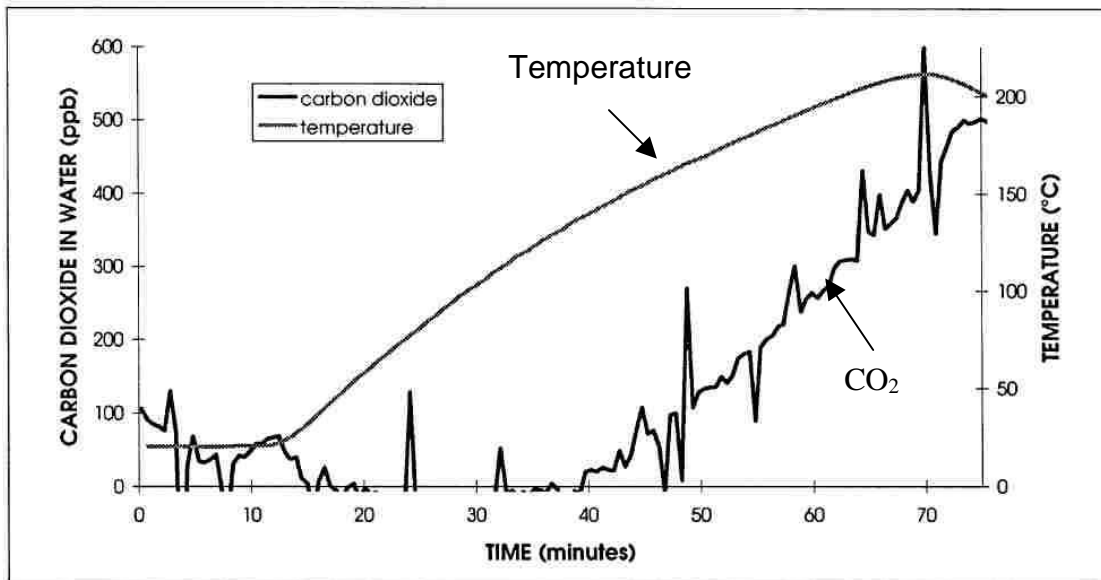


Figure 4-23 Arrhenius plot of the thermal decomposition of hydrogen peroxide in an SS 316 lined autoclave showing the effect of pH as reported by Haines et al. [71].



**Figure 4-24 The thermal decomposition of hydrogen peroxide in Pyrex glass ampoules at  $110^\circ\text{C}$ , with and without  $2 \times 10^{-4}$  mol/kg hydrogen (Chenier and Elliot - unpublished data).**





**Figure 4-25 The effect of temperature on the yield of CO<sub>2</sub> from the reaction of hydrogen peroxide and sodium formate in a solution containing  $5 \times 10^{-3}$  mol/kg HCOONa,  $2 \times 10^{-4}$  mol/kg methyl viologen and  $1.2 \times 10^{-5}$  mol/kg H<sub>2</sub>O<sub>2</sub>. Figure copied from Reference [76]. 500 µg/kg carbon dioxide in water is equivalent  $\sim 1.1 \times 10^{-5}$  mol/kg.**

## 4.2 Equilibria and Associated Rate Constants

There are a number of acid/base equilibria associated with the water radiolysis data set and these are defined in Table 4-2 and Table 4-3. In dealing with the participation of water in these equilibria, the approach taken is to use the following definition of the equilibrium constant for the dissociation of water:

$$K_{\text{H}_2\text{O}} = [\text{H}^+][\text{OH}^-]/[\text{H}_2\text{O}]$$

$$K_{\text{H}_2\text{O}} = K_w/[\text{H}_2\text{O}]$$

where  $K_w$  is the ionic product for water given by  $K_w = [\text{H}^+][\text{OH}^-]$ . It should be noted that the mechanism of the rate-controlling step of the approach to equilibrium could differ depending on the pH of the water. This has to be accounted for in the modelling reaction set as shown for the pairing Equilibria  $K_{\text{H}_2\text{O}_2}$  and  $K_{\text{H}_2\text{O}_2}^{\text{B}}$  and Equilibria  $K_{\text{OH}}$  and  $K_{\text{OH}}^{\text{B}}$ , etc. (see Table 4-2 for equilibria reactions). Rate constants have to be estimated for both the forward and back reactions involved in the equilibria.

### 4.2.1 Acid/Base Equilibrium Constants

Figure 4-26 shows the  $\text{pK}_A$  values for:  $\text{H}_2\text{O}$  [77];  $\text{H}_2\text{O}_2$  [78];  $\text{OH}$  [79], [80], [81];  $\text{HO}_2$  [68], [79], [82]; and  $\text{H}$  [83], as a function of temperature where  $K$  is expressed in ‘molar’ units. The molar units are used in kinetic calculations where rate constants are measured in units involving volume. In the case of water [77] and hydrogen peroxide [78], the  $\text{pK}$  values in the literature were reported in ‘molal’ units. These were converted to the appropriate ‘molar’ units using the density ( $\rho$ ) of water along the liquid-vapour coexistence curve as given in the equation below [84] where  $t$  is the temperature in  $^\circ\text{C}$ :

$$\rho \text{ (g/mL)} = 0.999 + 1.094 \times 10^{-4} t - 7.397 \times 10^{-6} t^2 + 2.693 \times 10^{-8} t^3 - 4.714 \times 10^{-11} t^4$$

(Note that the reaction rates reported in this review are measured at a range of pressures between 1 and 250 bar. Because water is not very compressible, the pressure has little effect on the density or reaction rates below about  $350^\circ\text{C}$ . As a worst case, at  $350^\circ\text{C}$  the density is 10% greater at 250 bar than on the coexistence curve at 165 bar. Above this temperature, pressure becomes a major variable.)

To calculate the value of  $\text{pK}_{\text{H}_2\text{O}}$ , the concentration of water (in units of mole/L) as a function of temperature,  $t$  ( $^\circ\text{C}$ ), is required. This is given by the function:

$$[\text{H}_2\text{O}] = 55.50 + 6.075 \times 10^{-3} t - 4.110 \times 10^{-4} t^2 + 1.496 \times 10^{-6} t^3 - 2.619 \times 10^{-9} t^4$$

The  $\text{pK}_{\text{OH}}$  for the hydroxyl radical has only been measured up to  $200^\circ\text{C}$ ; above this temperature it was assumed that the  $\text{pK}_{\text{OH}}$  could be approximated as being parallel to the  $\text{pK}_w$  of water. As the  $\text{pK}_{\text{H}_2\text{O}_2}$  has only been reported up to  $50^\circ\text{C}$  and, as it is essentially the same value as  $\text{pK}_{\text{OH}}$  (Figure 4-26) over that temperature range, it has been assumed that it has the same temperature dependence as  $\text{pK}_{\text{OH}}$  up to  $350^\circ\text{C}$ .

The values for  $\text{pK}_\text{H}$  have only been reported up to  $250^\circ\text{C}$ . The extrapolation of the value of  $\text{pK}_\text{H}$  up to  $350^\circ\text{C}$  has assumed that  $\text{pK}_\text{H}$  approximately parallels the  $\text{pK}_w$  of water. For the  $\text{pK}_{\text{HO}_2}$ , the extrapolation from the last data point at  $285^\circ\text{C}$  to  $350^\circ\text{C}$  was done as the simple extension of the polynomial fit to the available results.

The polynomial fits to the pK data in Figure 4-26 are given in Table 4-5.

**Table 4-5 Polynomials describing the pKs (in ‘Molar’ units) of H<sub>2</sub>O, H<sub>2</sub>O<sub>2</sub>, OH, HO<sub>2</sub> and H\***

<b>pK</b>	<b>Function</b>
pK <sub>w</sub>	$14.947 - 4.273 \times 10^{-2} t + 2.115 \times 10^{-4} t^2 - 5.786 \times 10^{-7} t^3 + 7.529 \times 10^{-10} t^4$
pK <sub>H<sub>2</sub>O</sub>	$16.690 - 4.262 \times 10^{-2} t + 2.071 \times 10^{-4} t^2 - 5.594 \times 10^{-7} t^3 + 7.161 \times 10^{-10} t^4$
pK <sub>H<sub>2</sub>O<sub>2</sub></sub>	$12.383 - 3.020 \times 10^{-2} t + 1.700 \times 10^{-4} t^2 - 5.151 \times 10^{-7} t^3 + 6.960 \times 10^{-10} t^4$
pK <sub>OH</sub>	$12.383 - 3.020 \times 10^{-2} t + 1.700 \times 10^{-4} t^2 - 5.151 \times 10^{-7} t^3 + 6.960 \times 10^{-10} t^4$
pK <sub>HO<sub>2</sub></sub>	$4.943 - 6.230 \times 10^{-3} t + 4.125 \times 10^{-5} t^2 - 8.182 \times 10^{-9} t^3$
pK <sub>H</sub>	$10.551 - 4.430 \times 10^{-2} t + 1.902 \times 10^{-4} t^2 - 4.661 \times 10^{-7} t^3 + 5.980 \times 10^{-10} t^4$

\* Temperature, t, in °C

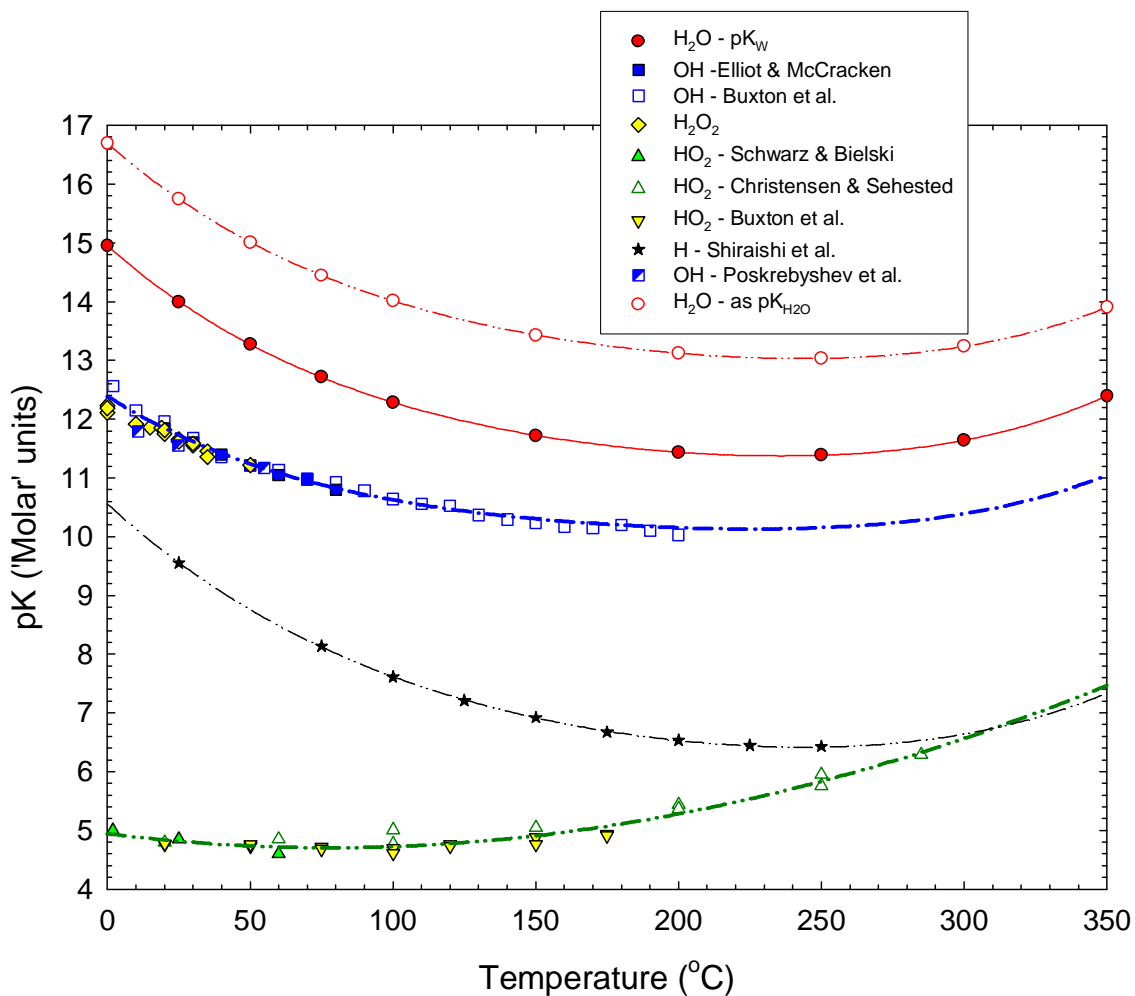


Figure 4-26 The measured and extrapolated values for the pK (in 'Molar' units) of  $\text{H}_2\text{O}$  as  $\text{pK}_w$  [77],  $\text{H}_2\text{O}_2$  [78], OH [79], [80], [81],  $\text{HO}_2$  [79], [82], [68] and H [83] as a function of temperature. The pK (in 'Molar' units) of  $\text{H}_2\text{O}$  as  $\text{pK}_{\text{H}_2\text{O}}$  (see text) is also shown.

#### 4.2.2 Rate Constants Associated with Acid/Base Equilibria (Table 4-2)

There is only limited information on the rate constants associated with the equilibria shown in Table 4-2. For neutralization reactions involving the proton, it will be assumed that these are diffusion-controlled reactions and the temperature dependence for the rate constants are given by the Smoluchowski equation with the Debye factor for reaction between two charged species 'A' & 'B' [85].

$$k_{\text{diff}} = 4 \pi (D_A + D_B) d_{\text{AD}} \times (\delta / (e^\delta - 1))$$

$$\delta = Z_A Z_B e^2 / 4 \pi \epsilon_0 \epsilon d_{\text{AD}} k T$$

For species 'A' and 'B':  $D_A$  and  $D_B$  are the diffusion coefficients;  $d_{\text{AD}}$  is the reaction distance;  $Z_A$  and  $Z_B$  are the charges on the ions;  $e$  is the charge on an electron,  $\epsilon_0$  is permittivity of free space,  $\epsilon$  is the relative permittivity of the water (i.e., the dielectric constant);  $k$  is Boltzmann's constants; and  $T$  is the temperature in Kelvin.

The diffusion coefficients for the proton and hydroxide ion used in this compilation are shown in Figure 4-27. As can be seen, both species diffuse faster than water at 'low' temperatures but approach the rates of water near 350°C. For other species, such as  $\text{HO}_2^-$  and  $\text{O}_2^-$ , the temperature dependence for self-diffusion in water will be used. The lines in Figure 4-27 are the polynomials describing the diffusion coefficients for the proton, hydroxide ion and water and these are given in Table 4-6.

The relative permittivity of water,  $\epsilon$ , used was:

$$\epsilon = 87.717 - 3.809 \times 10^{-1} t + 5.443 \times 10^{-4} t^2 + 6.752 \times 10^{-7} t^3 - 2.515 \times 10^{-9} t^4$$

**Table 4-6 Polynomials describing the diffusion coefficients for  $\text{H}^+$ ,  $\text{OH}^-$  and  $\text{H}_2\text{O}$**

Species	Polynomials (D in units of $10^{-9} \text{ m}^2/\text{s}$ )
$\text{H}^+$	$\text{Log } D = 2.672 - 9.847 \times 10^2/T + 3.306 \times 10^5/T^2 - 5.621 \times 10^7/T^3$
$\text{OH}^-$	$\text{Log } D = 3.324 - 1.719 \times 10^3/T + 5.890 \times 10^5/T^2 - 9.188 \times 10^7/T^3$
$\text{H}_2\text{O}$	$\text{Log } D = 4.311 - 2.722 \times 10^3/T + 8.565 \times 10^5/T^2 - 1.181 \times 10^8/T^3$

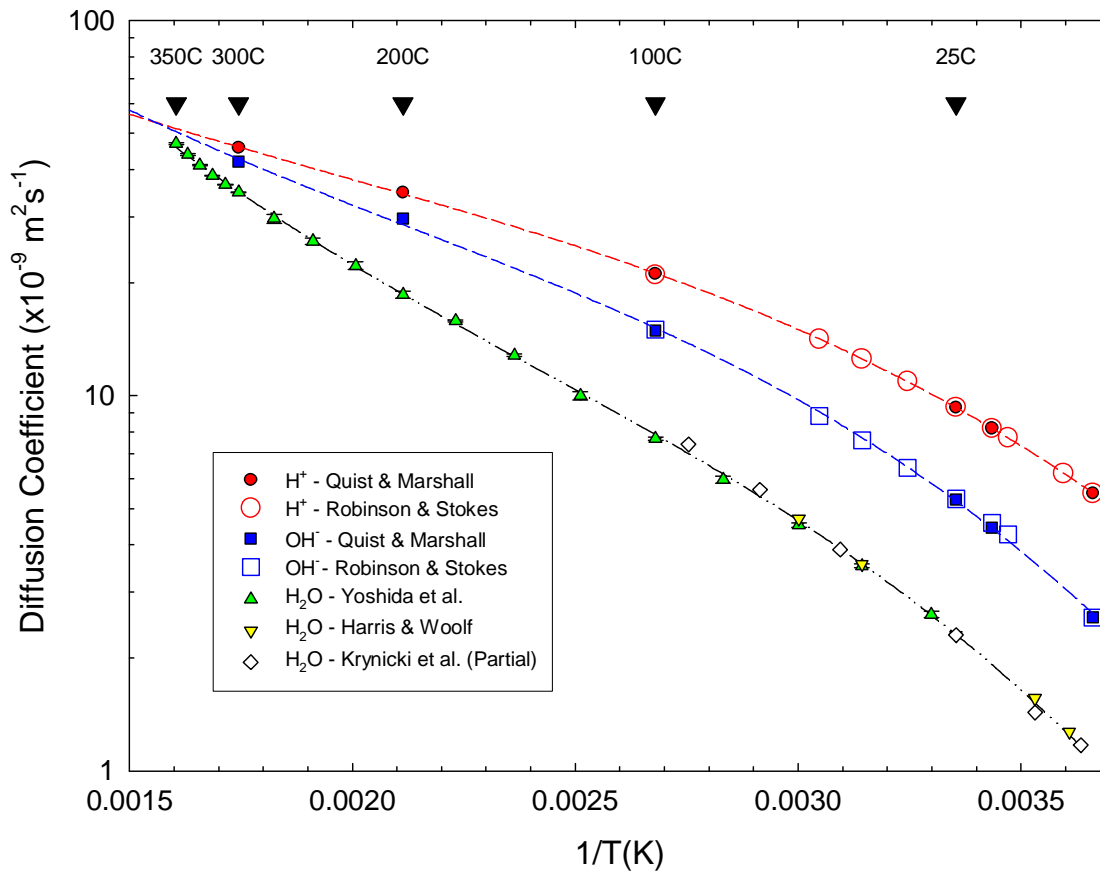


**Figure 4-27** The temperature dependence of the self-diffusion coefficient for water (Yosida et al. [86], Harris and Woolf [87] and by Krynicki et al. [88] and the diffusion coefficient for the proton and the hydroxide ion (Quist and Marshall [89] and Robinson and Stokes [90]).

#### 4.2.2.1 Equilibrium R23: $\text{H}_2\text{O} \rightleftharpoons \text{H}^+ + \text{OH}^-$

The rate constant for the recombination of the proton and the hydroxide ion has been studied at temperatures up to 80°C. The results of some of these studies are shown in Figure 4-28. To provide a temperature dependence up to 350°C, the Smoluchowski equation has been used with the reaction distance adjusted to a constant 0.7 nm to fit the observed experimental results (Figure 4-28).

The fitted line in Figure 4-28 can be described by the polynomial:

$$\text{Log } k_{\text{R23b}} = 20.934 - 1.236 \times 10^4 / T + 6.364 \times 10^6 / T^2 - 1.475 \times 10^9 / T^3 + 1.237 \times 10^{11} / T^4$$

where T is in Kelvin and where  $k_{\text{R23b}}$  has units of L/mol/s.

The forward rate constant,  $k_{\text{R23f}}$ , for the dissociation of water:



can now be calculated from the relationship:

$$k_{\text{R23f}} = k_{\text{R23b}} \times K_{\text{H}_2\text{O}}$$

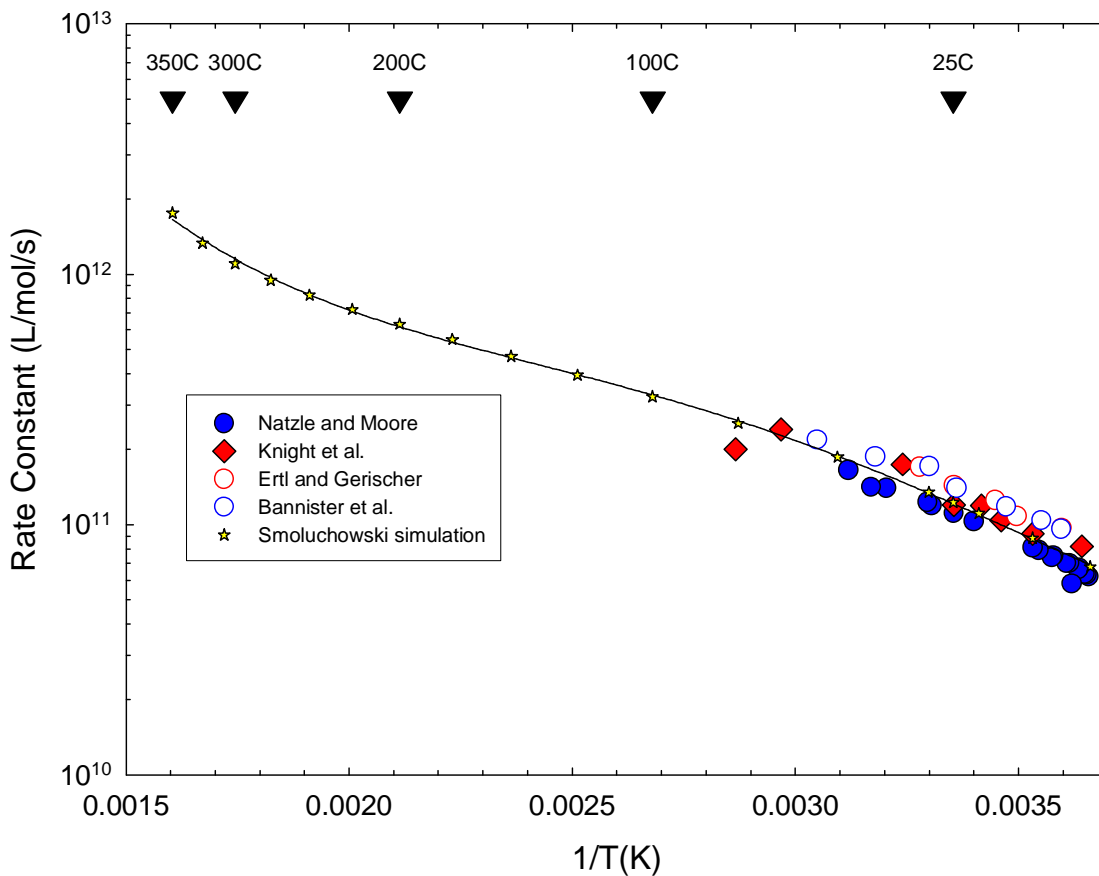


Figure 4-28 The rate constants for the recombination of H<sup>+</sup> and OH<sup>-</sup> (Natzle and Moore [91], Knight et al. [92], Ertl and Gerischer [93] and Bannister et al. [94]) and the Smoluchowski extrapolation to 350°C.

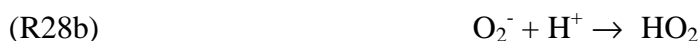


#### 4.2.2.2 Rate Constants for Acid-Base Equilibria R24 through R29

There are very little data for the rate constants of the reactions involved in the Equilibria R24 through R29 listed in Table 4-2. Buxton [95] and Zahavi and Rabani [96] have both measured a rate constant of  $1.3 \times 10^{10}$  L/mol/s at room temperature for  $k_{R27f}$ .



Ilan and Rabani [97] have measured a rate constant of  $5.0 \times 10^{10}$  L/mol/s at room temperature for  $k_{R28b}$ .



A pragmatic approach to estimating the temperature dependence up to 350°C for Reaction R27f and Reaction R28b has been taken. It was assumed the temperature dependence as given by the Smoluchowski equation is appropriate. This temperature dependence was used to generate higher temperature rate constants by normalizing the 25°C value to the measured room temperature rate constant value for both reactions. These normalizations are shown in Figure 4-29.

In the case of the Equilibrium R27:



the temperature dependence shown in Figure 4-29 for the forward reaction rate constant,  $k_{R27f}$ , is described by the polynomial:

$$\text{Log } k_{R27f} = 13.339 - 2.220 \times 10^3/T + 7.333 \times 10^5/T^2 - 1.065 \times 10^8/T^3$$

where T is the temperature in Kelvin and where k has units of L/mol/s. The second order rate constant for the back reaction,  $k_{R27b}$ , is then calculated as:

$$k_{R27b} = k_{R27f} / K_{OH}^B$$

where the equilibrium constant,  $K_{OH}^B$ , is calculated from the relationship:

$$K_{OH}^B = K_{OH} / K_{H_2O}$$

$$k_{R27b} = k_{R27f} \times K_{H_2O} / K_{OH}$$

In the case of the Equilibrium R28:



the fitted line in Figure 4-29 for the temperature dependence for the back reaction,  $k_{R28b}$ , is described by the polynomial:

$$\text{Log } k_{R28b} = 16.410 - 4.888 \times 10^3/T + 1.622 \times 10^6/T^2 - 2.004 \times 10^8/T^3$$

where T is the temperature in Kelvin and where k has units of L/mol/s. The forward first order reaction,  $k_{R28f}$ , is then calculated as:

$$k_{R28f} = k_{R28b} \times K_{HO_2}$$

In the absence of any other information, it has been assumed that the back rate constant,  $k_{R24b}$ , for Equilibrium R24:



and the back rate constant,  $k_{R26b}$ , for Equilibrium R26 :



have be set equal to the rate constant,  $k_{R28b}$ , for Reaction R28b:

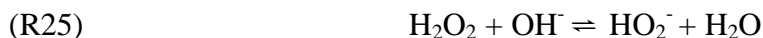


Based on this, the forward rate constants for Equilibria R24 and R26 can then be calculated from the following relationships:

$$k_{R24f} = k_{R24b} \times K_{H_2O_2}$$

$$k_{R26f} = k_{R26b} \times K_{OH}$$

Likewise the forward rate constants,  $k_{R25f}$ , for Equilibrium R25:



and  $k_{R29f}$  for Equilibrium R29:



have be set equal to the rate constant,  $k_{R27f}$ , for Reaction R27f:



Based on this, the values of the back rate constants for Equilibria R25 and R29 can then be calculated from the following relationships:

$$k_{R25b} = k_{R25f} \times K_{H_2O} / K_{H_2O_2}$$

$$k_{R29b} = k_{R29f} \times K_{H_2O} / K_{HO_2}$$

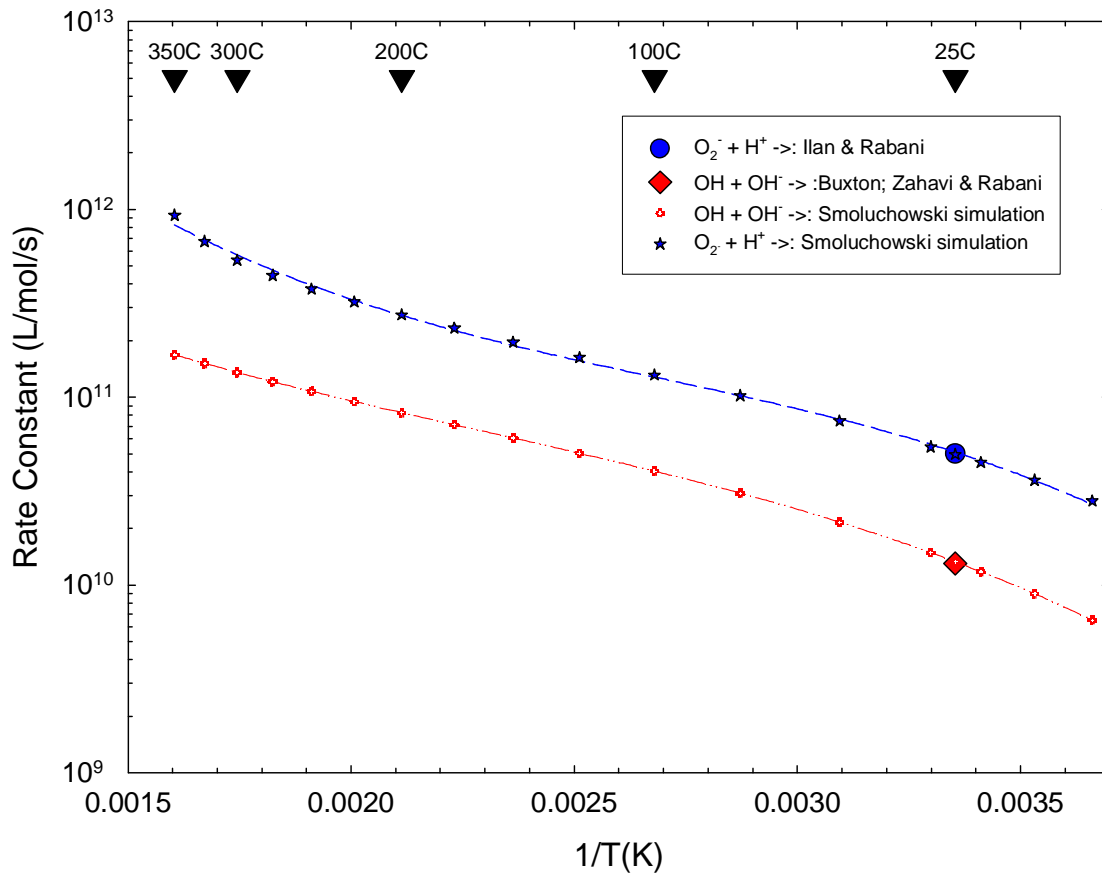


**Figure 4-29** The rate constants for the recombination of  $\text{H}^+$  and  $\text{O}_2^-$  (Ilan and Rabani [97]) and reaction  $\text{OH}$  with  $\text{OH}^-$  (Buxton [95]; Zahavi and Rabani [96]) and the Smoluchowski extrapolations to  $350^\circ\text{C}$ .

### 4.2.3 Rate constants associated with equilibria involving the hydrogen atom (Table 4-3)

#### 4.2.3.1 Equilibrium R30: $\text{H} \rightleftharpoons \text{H}^+ + \text{e}_{\text{aq}}^-$

The temperature dependence up to 350°C for the reaction of the hydrated electron reacting with the proton is shown in Figure 4-30. There is good agreement between the four laboratories that have studied Reaction R30b: Elliot [18], Shiraishi et al. [83], Takahashi et al. [20], and Stanisky, Bartels and Takahashi [98].<sup>31</sup>

The temperature dependence for  $k_{\text{R30b}}$  is described by the polynomial:

$$\text{Log } k_{\text{R30b}} = 39.127 - 3.888 \times 10^4/T + 2.054 \times 10^7/T^2 - 4.899 \times 10^9/T^3 + 4.376 \times 10^{11}/T^4$$

where T is in Kelvin and where k has units of L/mol/s. The rate constant,  $k_{\text{R30b}}$ , for the reaction at 25°C is  $2.1 \times 10^{10}$  L/mol/s.

The rate constant for the forward Reaction R30f can be calculated from the expression:

$$k_{\text{R30f}} = k_{\text{R30b}} \times K_{\text{H}}$$

---

<sup>31</sup> The Stanisky, Bartels and Takahashi [98] data revises the rate constants for Reaction  $k_{\text{R30b}}$  above 250°C reported in Reference [20].

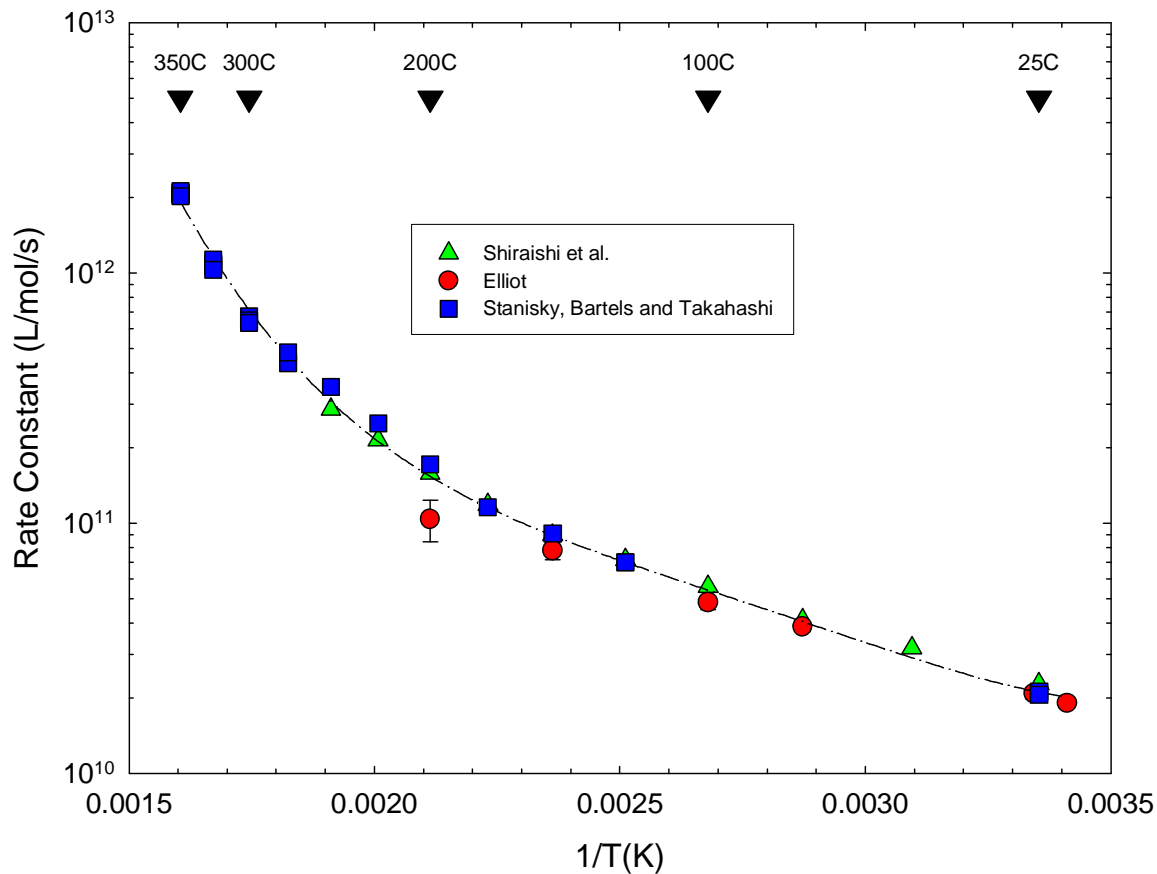


**Figure 4-30 The temperature dependence of the reaction on the hydrated electron with the proton as measured by Elliot [18], Shiraishi et al. [83] and Stanisky, Bartels and Takahashi [98].**

#### 4.2.3.2 Equilibrium R31: $\text{H} + \text{OH}^- \rightleftharpoons \text{e}_{\text{aq}}^- + \text{H}_2\text{O}$

The temperature dependence of the rate constant for the reaction of the hydrogen atom with the hydroxide ion is shown in Figure 4-31. All the data shown has been measured by Bartels and co-workers [21], [23], [99], [100]. In the 2005 publication [23], it was recommended that only the 2002 data measured above 300°C [21] be used in kinetic evaluations. This is what is shown in Figure 4-31.

Also shown in Figure 4-31 is a polynomial fit through the data for the temperature dependence. The temperature dependence of the rate constant,  $k_{\text{R31f}}$ , for Reaction R31f is given by:

$$\text{Log } k_{\text{R31f}} = 22.970 - 1.971 \times 10^4/T + 1.137 \times 10^7/T^2 - 2.991 \times 10^9/T^3 + 2.803 \times 10^{11}/T^4$$

where T is temperature in Kelvin and where  $k_{\text{R31f}}$  has units of L/mol/s. The value of  $k_{\text{R31f}}$  at 25°C is estimated to be  $2.5 \times 10^7$  L/mol/s.

As the equilibrium constant,  $K_{\text{H}}^{\text{B}}$ , can be written as:

$$K_{\text{H}}^{\text{B}} = K_{\text{H}} / K_{\text{H}_2\text{O}}$$

The reverse reaction rate constant for this equilibrium can be calculated from:

$$k_{\text{R31b}} = k_{\text{R31f}} \times K_{\text{H}_2\text{O}} / K_{\text{H}}$$

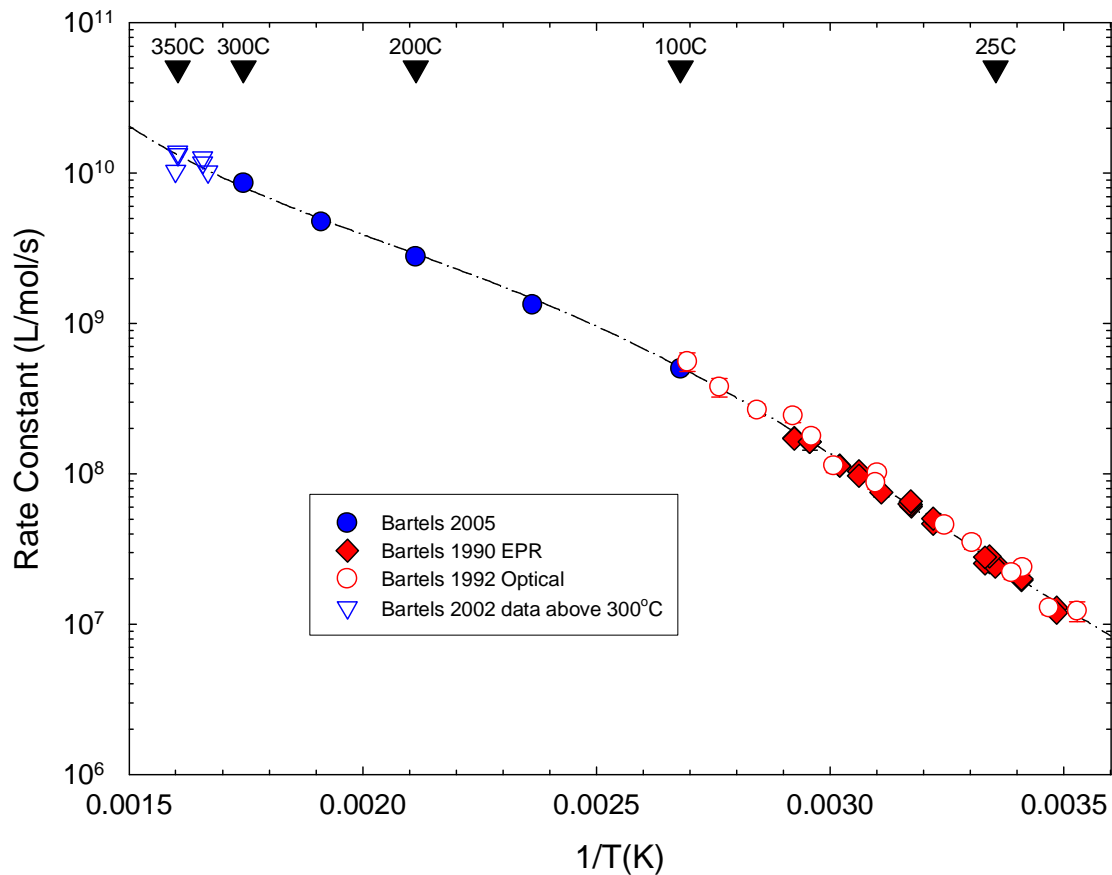


**Figure 4-31** The temperature dependence of the rate constant for the reaction of hydrogen atoms with the hydroxide ion as measured by Bartels and co-workers [21], [23], [99], [100].

### 4.2.3.3 Equilibrium R32: $\text{H} + \text{H}_2\text{O} \rightleftharpoons \text{H}_2 + \text{OH}$

At room temperature, the reaction rate of hydrogen atoms with water is considered to be very slow. Shiraishi et al. [83] estimated a pseudo-first order rate constant of  $10^{-3} \text{ s}^{-1}$ , which translates to a bimolecular rate constant of  $3.6 \times 10^{-5} \text{ L/mol/s}$ . Bartels [101] has determined the value of the rate constant,  $k_{\text{R32f}}$ , up to  $350^\circ\text{C}$  based on the calculation of the equilibrium constant from thermodynamics, and the measured rate constant for Reaction R32b. This is shown in Figure 4-32. The value for  $k_{\text{R32f}}$  increased eight orders of magnitude as the temperature increased from  $25^\circ\text{C}$  to  $350^\circ\text{C}$ . The only unknown in the calculation is the exact value of free energy of hydration for the OH radical. At  $300^\circ\text{C}$ , the uncertainty in rate constant amounts to a factor of two, though slightly larger extreme limits are shown in Figure 4-32. The temperature dependence is given by:

$$\text{Log } k_{\text{R32f}} = 9.408 - 2.827 \times 10^3 / T - 3.792 \times 10^5 / T^2$$

where T is the temperature in Kelvin and where  $k_{\text{R32f}}$  has units of L/mol/s.

The back Reaction R32b is the key reaction in controlling water radiolysis via 'hydrogen-water chemistry', as it converts the oxidizing hydroxyl radical to the reducing hydrogen atom and is the only reaction which removes molecular hydrogen.



The temperature dependence of the reaction of the hydroxyl radical has been measured in three laboratories: Riso ( $20^\circ\text{-}230^\circ\text{C}$ ) [102], AECL-CRL ( $20^\circ\text{-}200^\circ\text{C}$ ) [50], [57] and Argonne ( $200^\circ\text{-}350^\circ\text{C}$ ) [16]. The rate constants reported in References [50], [57], [102] were measured by pulse radiolysis techniques by following the pseudo-first order growth of the optical absorption of  $\text{O}_2^-$  in  $\text{N}_2\text{O}/\text{H}_2/\text{O}_2$  solutions. The results reported by Marin et al. [16] were measured by competition kinetics using nitrobenzene as competitive scavenger.<sup>32</sup> The competition kinetic method, using cuprous ions as the reference solute, was also used by Christensen and Sehested [102]. The collected results are shown in Figure 4-33 along with a polynomial fit through all the data. There is good agreement between the data from the three laboratories.

The temperature dependence of the rate constant,  $k_{\text{R32b}}$ , for Reaction R32b is given by:

$$\text{Log } k_{\text{R32b}} = -11.556 + 3.2546 \times 10^4 / T - 1.8623 \times 10^7 / T^2 + 4.5543 \times 10^9 / T^3 - 4.1364 \times 10^{11} / T^4$$

where T is in Kelvin and where  $k_{\text{R32b}}$  has units of L/mol/s. The value of  $k_{\text{R32b}}$  at  $25^\circ\text{C}$  is estimated to be  $3.9 \times 10^7 \text{ L/mol/s}$ .

<sup>32</sup> The rate constant originally measured by Marin et al. [16] at  $350^\circ\text{C}$  has been replaced by the revised value of  $6 \times 10^8 \text{ L/mol/s}$  measured by Janik et al. [24] from fitting the decay of the OH optical absorption in solutions containing  $\text{N}_2\text{O}$  and hydrogen.



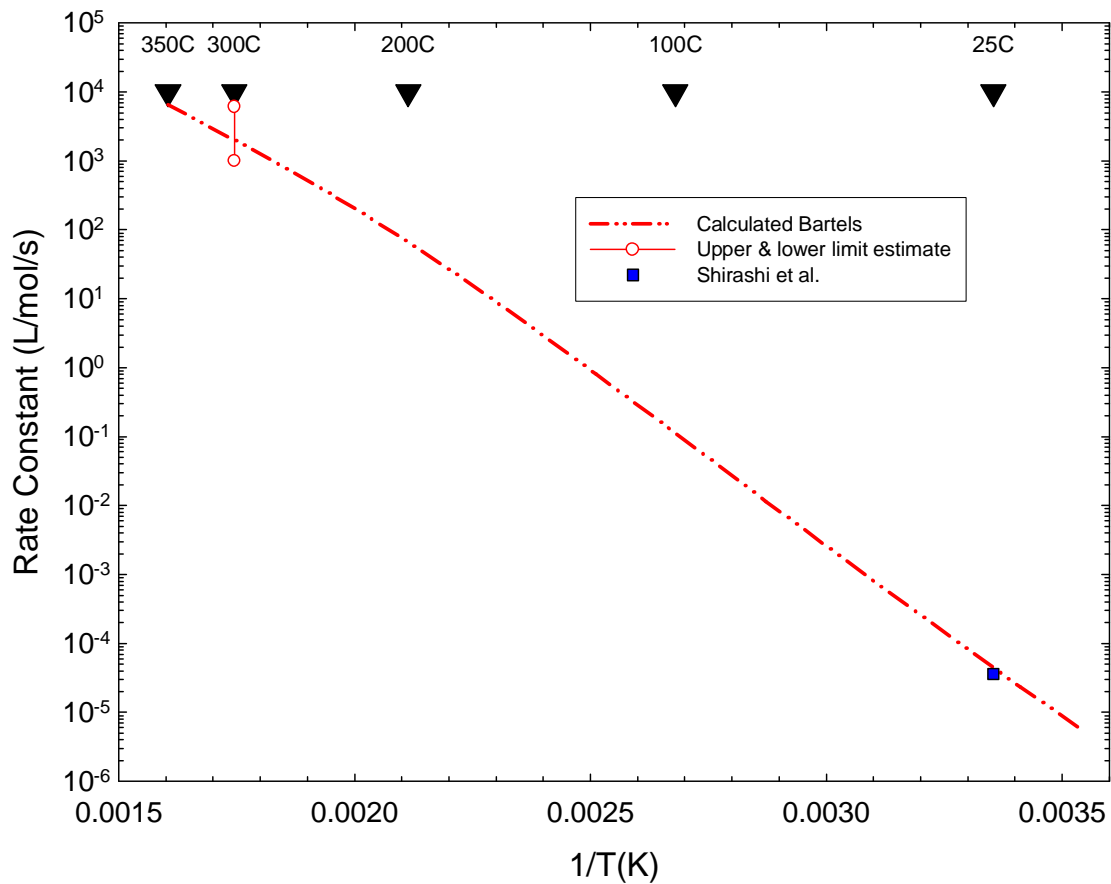


**Figure 4-32** The calculated rate constant,  $k_{R32f}$ , as a function of temperature for the reaction of the hydrogen atom with water as calculated by Bartels [101]. Also shown is the value reported by Shirashi et al. [83] estimated from experimental data at 25°C.

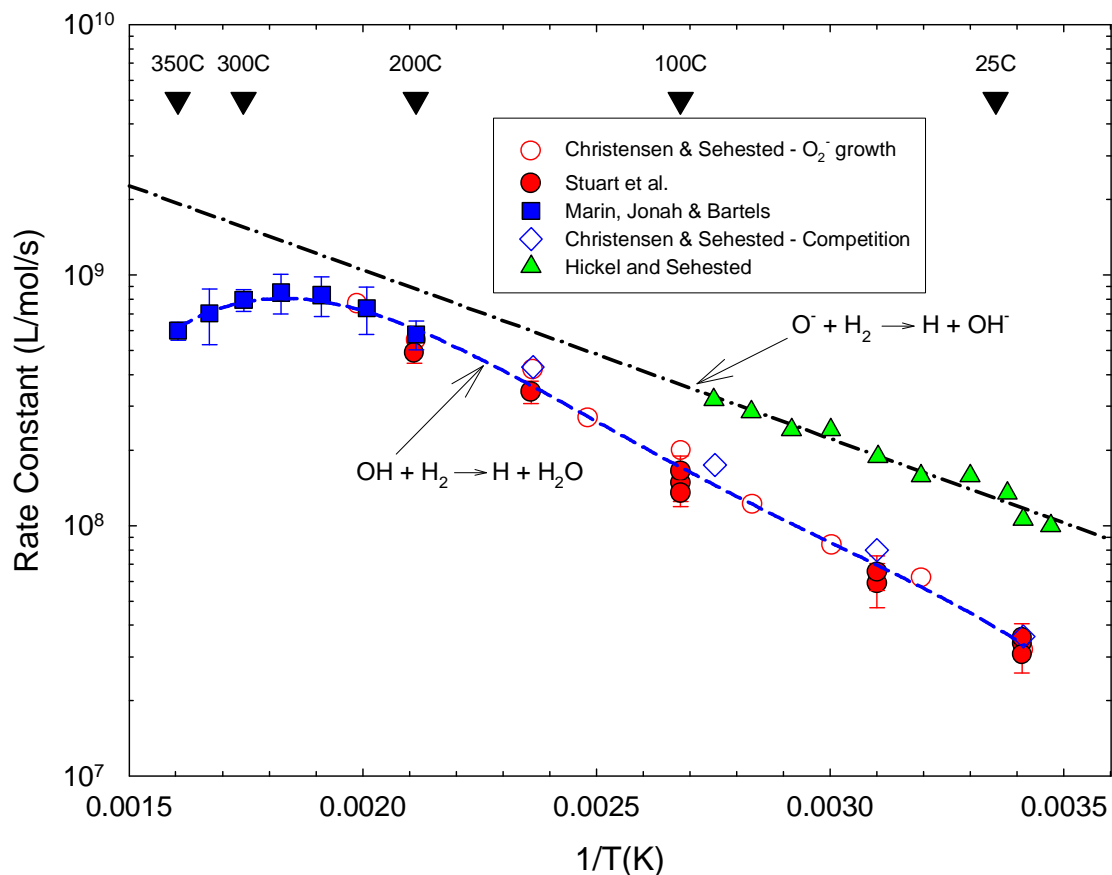


**Figure 4-33** The temperature dependence for the reaction of hydroxyl radicals with hydrogen as reported by Christensen and Sehested [102], by Stuart and co-workers [50], [57] and by Marin et al. [16]. The temperature dependence for the reaction of the oxide radical anion with hydrogen is also shown [103].

### 4.3 Reactions of Oxide Radical Anion Relevant to High Temperature Reactor Coolant Radiolysis

The radiolysis reaction set and g-values drawn together in this report are focused on slightly acid and slightly alkaline solutions. In using the radiolysis reaction set described in this current report, consideration of the pH of the solution to be modelled in regard to the  $pK_A$  of the reacting species has to be undertaken to see if reactions involving the oxide radical anion,  $O^-$ , or the base form of hydrogen peroxide,  $HO_2^-$ , beyond their acid-base equilibria reactions, could have an impact on the results. This will occur when the rate constant of a reaction involving  $O^-$  is significantly larger than the corresponding hydroxyl radical reaction rate constant. Likewise with reactions involving the  $H_2O_2/HO_2^-$  equilibrium couple. A limited number of reactions have been identified and will be discussed in this report:



As far as the other reactions important in alkaline solution, while an exhaustive literature search was not undertaken, there does not appear to have been many temperature studies of reactions occurring in alkaline solutions involving the oxide radical anion beyond what was reviewed in Reference [18].

#### 4.3.1 Reactions R16, R33, R34, R35: $OH/O^- + H_2O_2 \rightarrow H_2O/OH^- + HO_2/O_2^-$

The observed rate constant for reaction of the 'hydroxyl radical' with 'hydrogen peroxide' vs. the pH is shown in Figure 4-34. The room temperature  $pK_A$  for both hydroxyl radical and hydrogen peroxide is near pH 12. It is obvious from Figure 4-34 that the observed rate constant at room temperature for the overall reaction:



begins to increase above a pH of 9, about three pH units below the  $pK_A$  of the reacting species. As both PWR and CANDU reactors operate water systems with added lithium hydroxide, this increase in reaction rate has to be incorporated into the water radiolysis reaction set.

Stuart and Ouellette have studied Reactions R16, R33, R34 and R35 up to 100°C as a function of pH (Figure 4-34). The rate constant,  $k_{obs}$ , is given by the expression:

$$k_{obs} = (k_{R16} + A \times k_{R33} + B \times k_{R34} + A \times B \times k_{R35}) / ((1+A) \times (1+B))$$

and where  $A = 10^{(pH-pK_{OH})}$  and  $B = 10^{(pH-pK_{H_2O_2})}$ . As  $pK_{OH} = pK_{H_2O_2}$  over the 20° to 350°C temperature range (Figure 4-26), i.e.,  $A=B$ , the above expression reduces to:

$$k_{\text{obs}} = (k_{\text{R16}} + A \times (k_{\text{R33}} + k_{\text{R34}}) + A^2 \times k_{\text{R35}}) / (1 + 2A + A^2)$$

Stuart has fitted this expression to the experimental result as shown in Figure 4-34. The values of  $k_{\text{R16}}$  (Section 4.1.15) and  $k_{\text{R35}}$  are uniquely defined, however, only the sum of the ‘cross’ rate constants,  $k_{\text{R33}}$  and  $k_{\text{R34}}$ , can be defined by fitting the curves because of the near equality between  $K_{\text{OH}}$  and  $K_{\text{H2O2}}$ .<sup>33</sup>

The rate constants extracted from this fit are shown in the Arrhenius plot in Figure 4-35. The value of the rate constant,  $k_{\text{R16}}$ , at 25°C is  $2.9 \times 10^7$  L/mol/s and the activation energy is 13.8 kJ/mole, the same as reported in Section 4.1.15. The temperature dependence of the rate constant,  $k_{\text{R16}}$ , for Reaction R16 is given by:

$$k_{\text{R16}} = 7.68 \times 10^9 e^{-1661.4/T} \text{ L/mol/s}$$

where T is the temperature in Kelvin.

The value of the rate constants,  $(k_{\text{R33}} + k_{\text{R34}})$ , at 25°C is  $8.1 \times 10^9$  L/mol/s and the activation energy is 11.9 kJ/mole. The temperature dependence of the rate constant,  $(k_{\text{R33}} + k_{\text{R34}})$ , for Reactions R33 and R34 is given by:

$$(k_{\text{R33}} + k_{\text{R34}}) = 1.00 \times 10^{12} e^{-1434.6/T} \text{ L/mol/s}$$

where T is the temperature in Kelvin.

The value of the rate constant,  $k_{\text{R35}}$ , at 25°C is  $7.8 \times 10^8$  L/mol/s and the activation energy is 24.3 kJ/mole. The temperature dependence of the rate constant,  $k_{\text{R35}}$ , for Reaction R35 is given by:

$$k_{\text{R35}} = 1.45 \times 10^{13} e^{-2928.5/T} \text{ L/mol/s}$$

where T is the temperature in Kelvin.

An estimate of  $k_{\text{obs}}$  at 300°C based on the assumption that the Arrhenius temperature dependencies shown in Figure 4-35 hold up to this temperature is shown in Figure 4-34. Also shown in Figure 4-34 are the estimated  $k_{\text{obs}}$  for a light water solution with a pH of 10.3 at 20°C at 50°, 75°, 100°C and 300°C.<sup>34</sup> As the temperature increases, the contribution of Reactions R33 and R34 to the overall reaction of hydroxyl radicals with hydrogen peroxide decreases in this solution.

From a computer modelling stand point, the impact of only knowing the sum of  $k_{\text{R33}}$  and  $k_{\text{R34}}$  and not the rate constants individually is minimal. The value for  $(k_{\text{R33}} + k_{\text{R34}})$  can all be assigned to just one of the rate constants. This is because, at the concentrations of hydroxyl radicals and hydrogen peroxide involved, the rates of the forward and back reactions for Equilibria R25 and R27 are rapid enough to maintain the equilibrium mathematically.

<sup>33</sup> Christensen et al. [63] have made an upper estimate of  $k_{\text{R34}}$  of  $5 \times 10^8$  L/mol/s at room temperature based on  $\text{O}_2^-$  yields at different times after the pulse using a solution saturated with 4 MPa  $\text{N}_2\text{O}$ . Using the 20°C estimate for  $(k_{\text{R33}} + k_{\text{R34}})$  of  $8 \times 10^9$  L/mol/s obtained from the fittings in Figure 4-34, a value for  $k_{\text{R33}}$  of  $\sim 7.5 \times 10^9$  L/mol/s is obtained.

<sup>34</sup> The experimental studies in U-2 loop, NRU were performed with light water with a room temperature pH~10.3 [14].

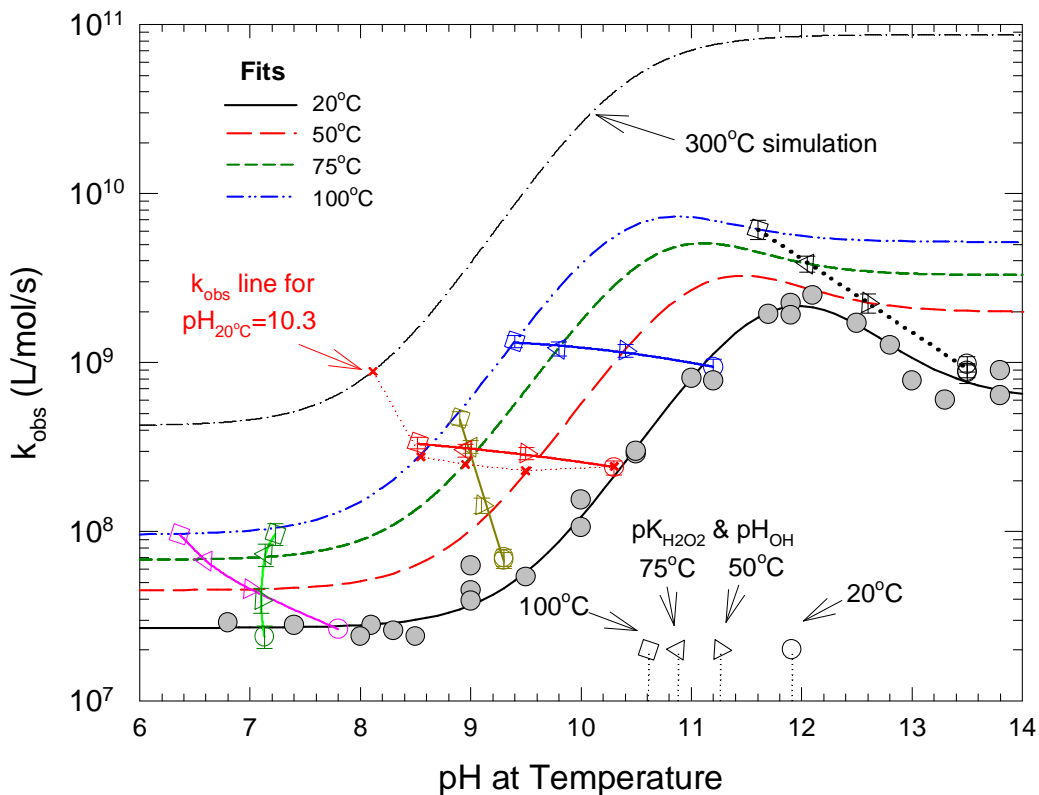


**Figure 4-34** The observed rate constant for the reaction of  $\text{OH}/\text{O}^-$  with  $\text{H}_2\text{O}_2/\text{HO}_2^-$  as a function of pH at the measurement temperature in  $\text{N}_2\text{O}$ -saturated solutions [57]. The coloured symbols are data from AECL-CRL with lines joining experimental sets. Some experiments used buffer solutions while others set the pH by adding LiOH. The grey circles are data of Christensen et al. [63] measured at room temperature. The simulation for  $k_{\text{obs}}$  as a function of pH at 300°C is shown (see text). Also shown is the simulation of  $k_{\text{obs}}$  at 20°, 50°, 75°, 100° and 300°C for an unbuffered solution that had a pH of 10.3 at 20°C (red x and red dotted line).

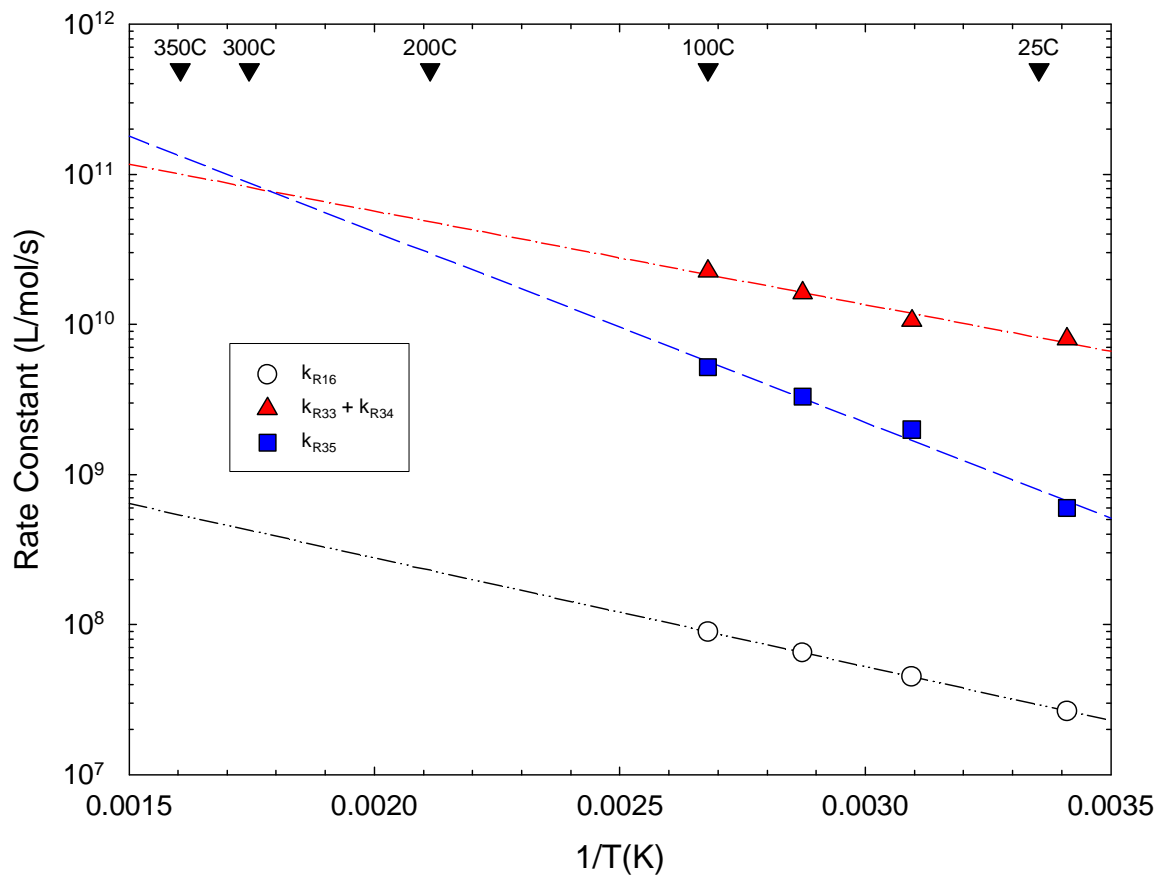


Figure 4-35 The temperature dependence for the rate constants  $k_{R16}$ ,  $(k_{R33} + k_{R34})$  and  $k_{R35}$  based on the fits in Figure 4-34.

### 4.3.2 Reaction R36: $\text{O}^- + \text{H}_2 \rightarrow \text{H} + \text{OH}^-$

Hickel and Sehested [103] have measured the rate constant,  $k_{\text{R36}}$ , for the reaction of the oxide radical anion with hydrogen (Figure 4-33). At room temperature, their measured value of  $k_{\text{R36}}$  is about three times greater than the corresponding rate constant,  $k_{\text{R32b}}$ , for the hydroxyl radical with hydrogen.

Assuming an Arrhenius temperature dependence, the value of the rate constant,  $k_{\text{R36}}$ , at 25°C is  $1.3 \times 10^8$  L/mol/s and the activation energy is 12.9 kJ/mole. The temperature dependence of the rate constant,  $k_{\text{R36}}$ , for Reaction R36 is given by:

$$k_{\text{R36}} = 2.32 \times 10^{10} e^{-1550.5/T} \text{ L/mol/s}$$

where T is the temperature in Kelvin.

### 4.3.3 Equilibrium R37: $\text{O}^- + \text{O}_2 \rightleftharpoons \text{O}_3^-$

The oxide radical anion is very different from the hydroxyl radical in that it reacts with oxygen to form the ozonide radical anion. Elliot and McCracken have measured the forward and back rate constants up to 90°C [80] as shown in Figure 4-36.

Assuming an Arrhenius temperature dependence, the value of the rate constant,  $k_{\text{R37f}}$ , at 25°C is  $3.7 \times 10^9$  L/mol/s and the activation energy is 11.2 kJ/mole. The temperature dependence of the rate constant,  $k_{\text{R37f}}$ , for Reaction R37f is given by:

$$k_{\text{R37f}} = 3.41 \times 10^{11} e^{-1344.9/T} \text{ L/mol/s}$$

where T is the temperature in Kelvin.

The value of the first order back rate constant,  $k_{\text{R37b}}$ , at 25°C is  $2.6 \times 10^3$  /s and the activation energy is 46.2 kJ/mole. The temperature dependence of the rate constant,  $k_{\text{R37b}}$ , for Reaction R37b is given by:

$$k_{\text{R37b}} = 3.20 \times 10^{11} e^{-5552.1/T} \text{ /s}$$

where T is the temperature in Kelvin.

This equilibrium has been included in this compilation because the formation of the ozonide radical anion,  $\text{O}_3^-$ , provides a 'gateway' to many other reactions in the radiolysis of alkaline water. If radiolysis modelling indicates the ozonide radical is formed, consideration should be given to including/developing a more complete alkaline radiolysis reaction set [104], [105].

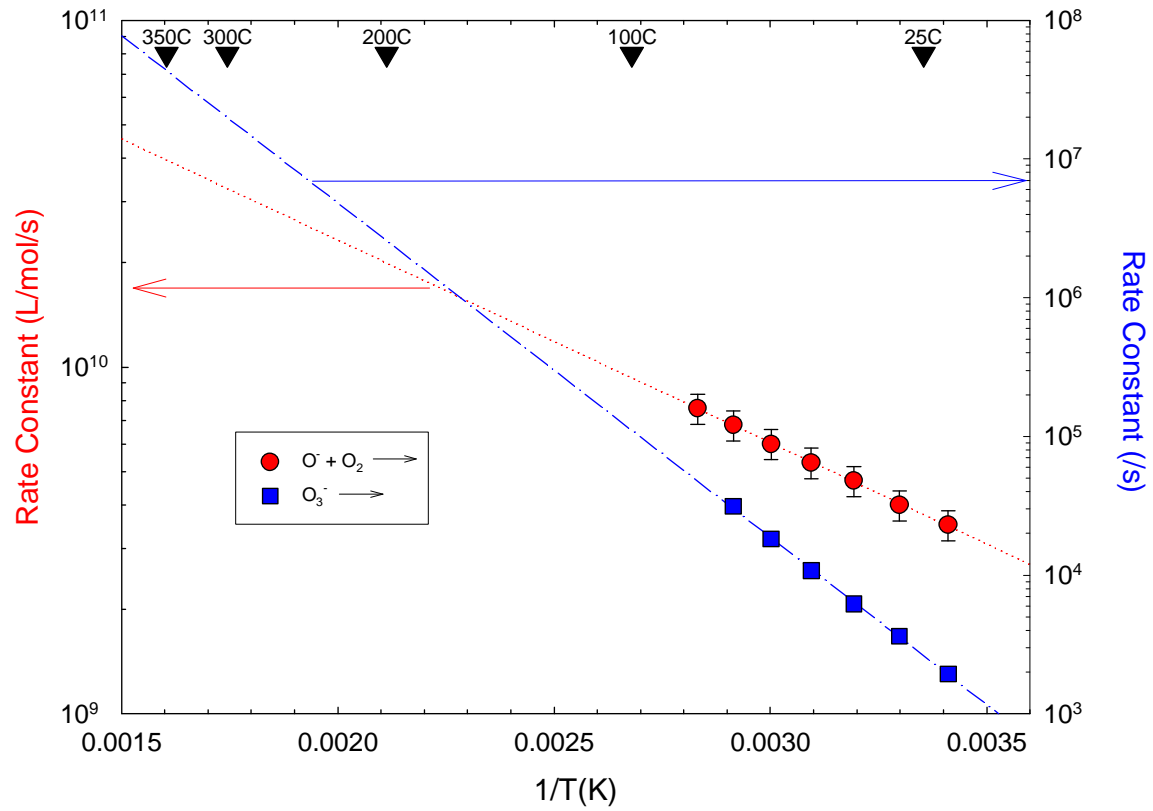


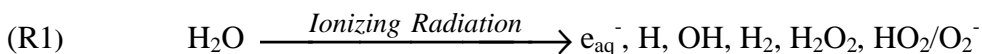
Figure 4-36 The temperature dependence for the reaction involved with Equilibrium R37 as reported by Elliot and McCracken [80].



## 5. HIGH LET G-VALUES

Fast neutrons deposit their energy in water by ion recoils of protons, although there is a small contribution from recoil oxygen ions also [106], [107]. Unlike low LET radiation, such as gamma and fast electrons, which deposit their energy in isolated spurs, the recoil ions deposit their energy in tracks. The consequence of this is that there are no reasonably defined 'escape' yields for the primary species formed in Reaction (R1) for high LET radiolysis. This is because of the 'tubular' nature of the track formed from high LET radiation (Figure 5-1) where primary radical species diffusing in an axial direction continue to react with other species while in the direction perpendicular to the track 'escape' of radicals is largely from the penumbra region around the track [108].

Consequently there is no 'well-defined' time when the species have escaped the track to form a homogeneous distribution in the solutions as there is for low LET radiation.



In this report, in order to define g-values for fast neutron radiolysis, the pragmatic approach is to use yields that were measured when  $k[\text{Scavenger}]$  is of the order of  $10^6$ - $10^7$   $s^{-1}$  or less. This corresponds to times  $\sim 0.1$ - $1$   $\mu s$  after the ionizing event; ideally times around  $\sim 10$   $\mu s$  or longer would be preferable but the data is not generally available. The effect of this is, in general, to provide free radical g-values that are slightly higher than would be expected under 'homogeneously distributed' conditions. Solute concentrations required to achieve  $\sim 10$   $\mu s$  are often so low that depletion of solute can occur. The effect of scavenging power on g-value measurements in high LET radiolysis experiments is discussed in Reference [106].

The measured yield of a primary species depends on the LET of the recoil ion [109]. The higher the LET of the recoil ion, the proportionately higher are the yields of the molecular products hydrogen and hydrogen peroxide, compared to the free radical species. This is because the free radical species have more time to react to form the molecular products in the dense track before a pseudo-homogeneous concentration of primary species is measured.

The approach to estimating the g-values for fast neutrons is to estimate the yields of the primary species for the recoil ions formed as the neutron is moderated. Depending on the nuclear reactor involved, there will be a particular flux profile of fast neutron energies produced and this, in turn, will produce protons and oxygen ions with a range of energies. The g-values for these recoil protons and oxygen ions can be estimated from experimental radiolysis data where high-energy ions have been used. There is an abundance of consistent g-value information for the primary species measured at room temperature [109]; however, there appear to be only two published reports where the temperature dependent g-values have been assessed for high LET radiation [76], [110].

The proton recoils from fast neutrons are totally absorbed/stopped in the water. As such, the appropriate yield for deterministic modelling is the track-averaged yield. It is track-averaged g-values that are generally measured in laboratory experiments as the ion beam is stopped in the solution under investigation [109]. In laboratory experiments, a

wide range of ion beams and particle energies have been used. While definitely not perfect, it is assumed that the track-averaged LET provides an adequate unification between these different ion beam experiments. Track-averaged LET is defined as:

$$\text{Track Averaged LET} = \left( \int_0^{E_0} (-dE/dx) dE \right) / E_0$$

and can be calculated from electronic stopping power tables where  $-dE/dx$  is the electronic stopping power (often called initial LET) and  $E_0$  is the incident energy of the ion beam. The correlation between stopping power (initial LET) and track-averaged LET is illustrated in Figure 5-2 along with the distribution of energy from recoil protons generated by a fast neutron flux from a light water cooled, natural uranium fuel bundle. As can be seen in Figure 5-2, it is recoil protons in the 1 to 6 MeV range that deposit most of the energy into the water. This means that the track-averaged LET range of interest does not exceed  $\sim 72$  eV/nm. Based on this observation, for the experimental results discussed below, the focus will be on results that have been obtained with track-averaged LET below about  $\sim 100$  eV/nm.

When comparing the results from two different ion beams that have the same track-averaged LET, it should be remembered that LET is a measure of the linear energy deposition rate and that the heavier ion will have a larger diameter track (i.e., less dense) than the lighter ion. This tends to lead to higher free radical yields for the heavier ion.

### Illustration LET Effect on Track Structure

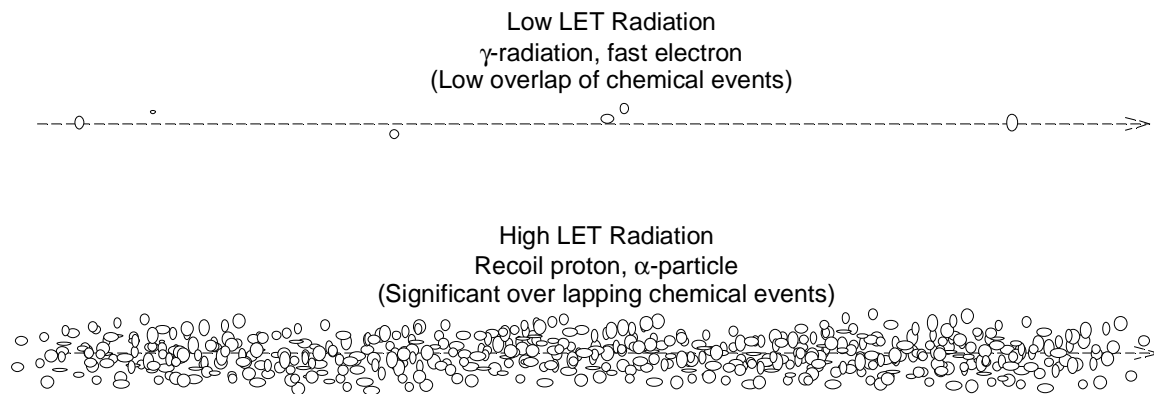


**Figure 5-1 Illustration of the effect of LET on distribution of chemical events initiated by the passage of ionizing radiation.**

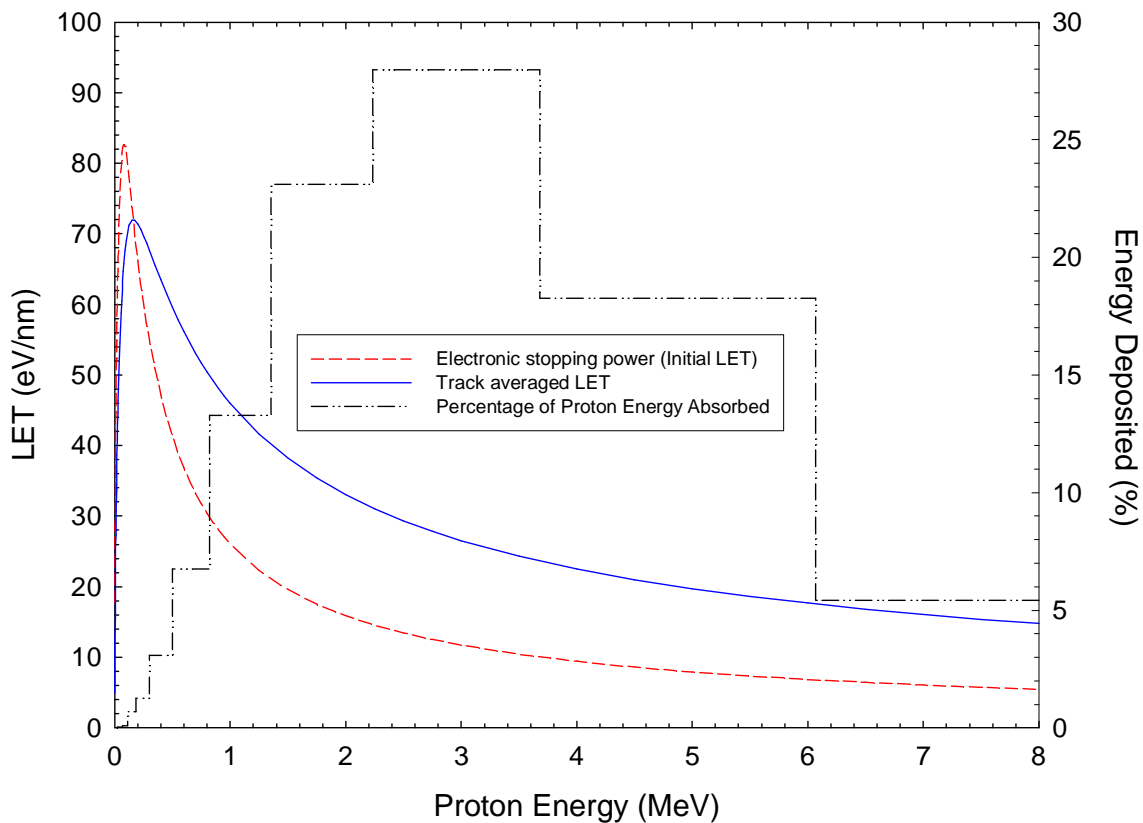


**Figure 5-2 The electronic stopping power [111] and the calculated track-averaged LET for protons as a function of incident proton energy. Also shown is the relative energy deposited by the recoil protons, in binned energy ranges, that were formed by a fast neutron flux from natural uranium fuel in light water.**

## 5.1 g-Value: Hydrated Electron

The g-values for the hydrated electron in light water reported by a number of laboratories as a function of LET are shown in Figure 5-3. These results were obtained at room temperature. The temperature dependence up to 180°C for the g-value of the hydrated electron is given in Figure 5-4 and Figure 5-5. Both figures demonstrate that a smaller temperature derivative for the g-value is observed as the LET increases.<sup>35</sup>

In Figure 5-5, the temperature dependence is broken out by radiation type. The results by Elliot et al. [38], [110] were all based on the same chemical system to simplify the comparison: nitrite ion yields from degassed solutions containing  $10^{-3}$  mol/kg  $\text{NO}_3^-$  and  $5 \times 10^{-3}$  mol/kg  $\text{HPO}_3^-$  [38], [110]. It should be noted that for gamma-radiation, this chemical system gave slightly lower g-values than that recommended in Section 3.1 as can be seen in Figure 5-5.

For 26 MeV  $^2\text{H}$  beam with a track-averaged LET of 12 eV/nm, the temperature dependence (t in °C) was:

$$g(e_{\text{aq}}^-) = 1.524 + 1.597 \times 10^{-3} t$$

For 157 MeV  $^7\text{Li}$  beam with a track-averaged LET of 62 eV/nm, the temperature dependence (t in °C) was:

$$g(e_{\text{aq}}^-) = 0.812 + 3.112 \times 10^{-4} t$$

Also shown in Figure 5-5 are the results reported by Ashmore et al. [76] where a solution (pH 8.1) containing  $\text{N}_2\text{O}$ , iodide ion and cyclohexane were irradiated with a 5.9 MeV proton beam for the lowest beam currents reported.<sup>36</sup> When this data (LET = 17.5 eV/nm) is compared to the data of Elliot et al. at an LET of 12 eV/nm, the temperature dependence is quite different. The fact that  $g(e_{\text{aq}}^-)$  at room temperature in the Ashmore et al. tests [76] falls below the trend line in Figure 5-3 suggests that scavenging of all the hydrated electrons by the  $\text{N}_2\text{O}$  may not be occurring. However, at higher temperatures (see Figure 5-5) the temperature trend of  $g(e_{\text{aq}}^-)$  does approach that reported of Elliot et al. [110]. Ashmore et al. [76] noted that better mixing in the radiation zone of their experimental arrangement occurred at higher temperatures due to more turbulence. Better mixing will reduce solute depletion in the radiation zone.

<sup>35</sup> The track-averaged LET as calculated at room temperature has been used. At 95°C and 180°C, the density correction would decrease the LET by ~4% and ~10%, respectively.

<sup>36</sup> Only the lowest beam energy has been plotted as the measured  $g(e_{\text{aq}}^-)$  decreases with increased beam current, i.e., dose rate, suggesting solute depletion is occurring in the radiation zone (Figure 5-3).

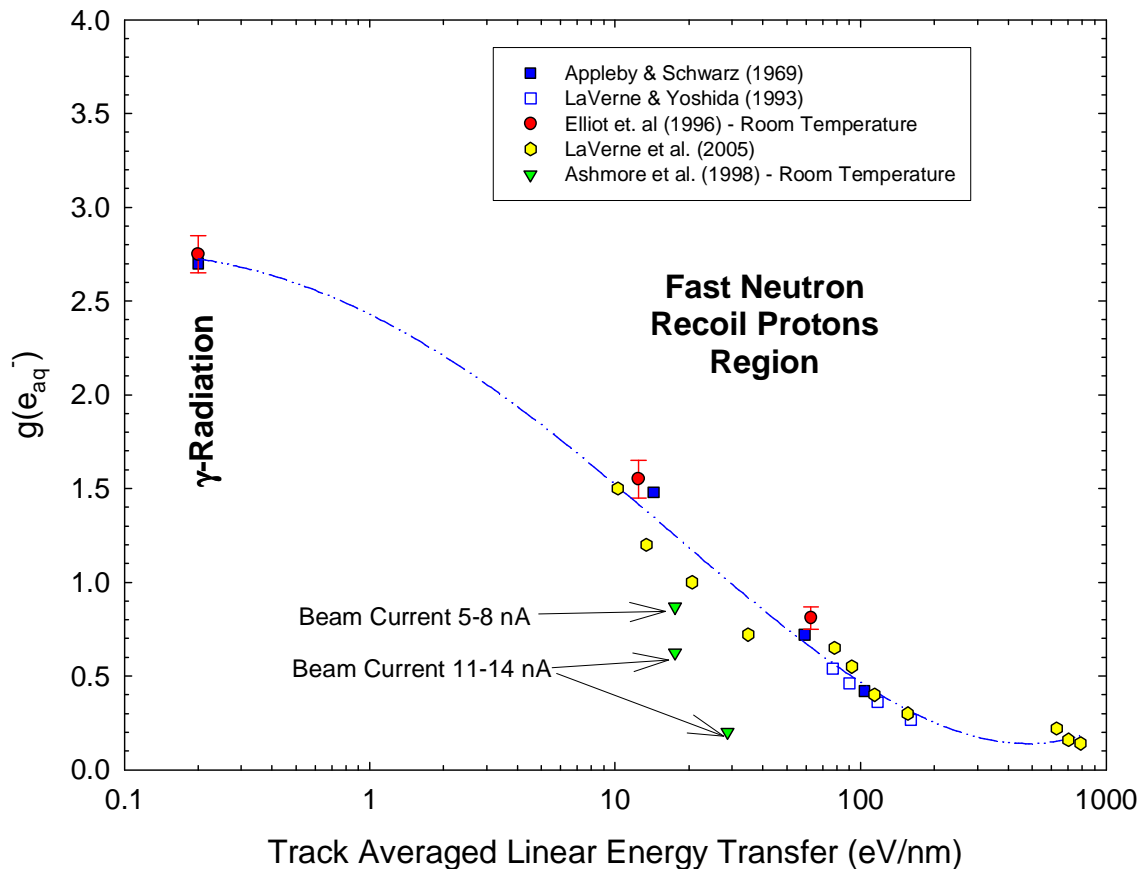


**Figure 5-3 The g-value of the hydrated electron as a function of track-averaged LET at room temperature as measured by Appleby and Schwarz [112], LaVerne and Yoshida [113], Elliot et al. [110], LaVerne et al. [114] and Ashmore et al. [76]. The line is the fit to the data given by the polynomial equation in Table 6-1.**

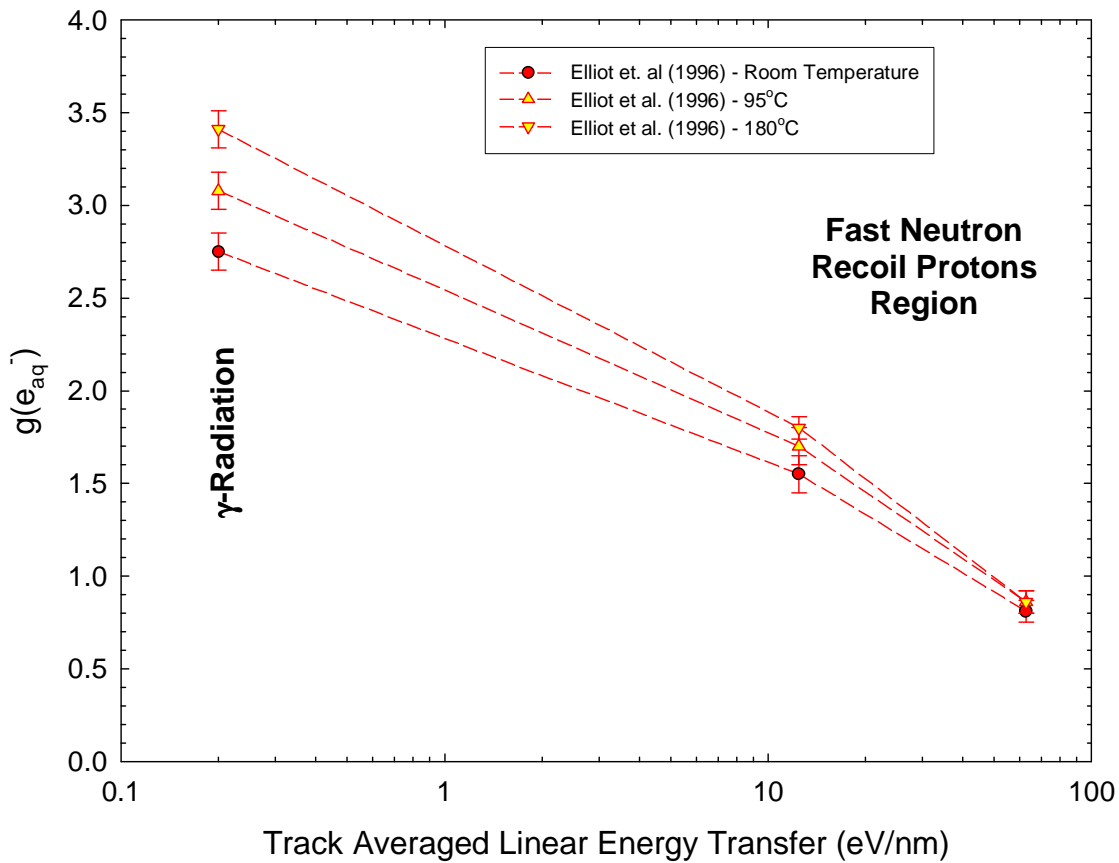
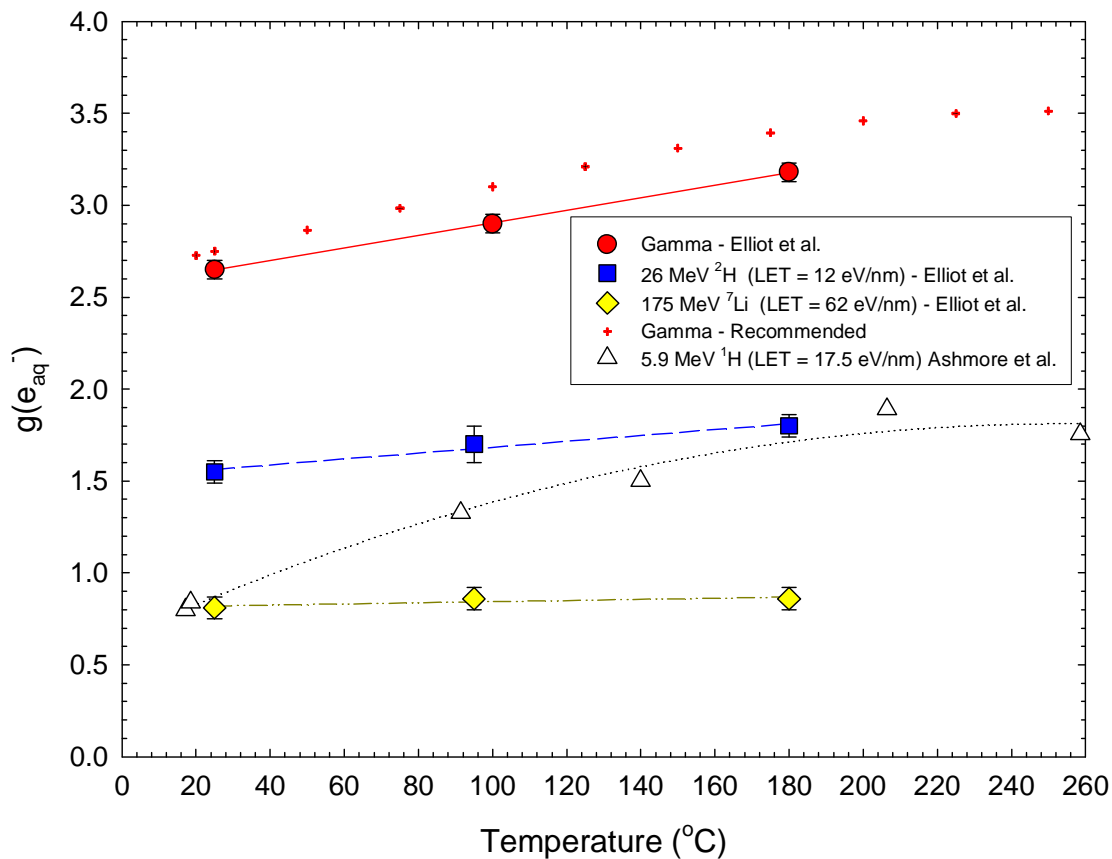


Figure 5-4 The  $g$ -value for the hydrated electron at different temperatures as a function of room temperature track-averaged LET [110].



**Figure 5-5 The temperature dependence of the g-value for the hydrated electron for gamma-radiation, 26 MeV <sup>2</sup>H and 157 MeV <sup>7</sup>Li ion beams measured by Elliot and co-workers [38], [110]. The results reported by Ashmore et al. [76] are for solutions at pH 8.1 (room temperature). Also shown is g-value for the hydrated electron recommended in Section 3.1 for gamma-radiation.**

## 5.2 g-Value: Molecular Hydrogen

The g-values for molecular hydrogen in light water as reported by a number of laboratories as a function of LET are shown in Figure 5-6. These results were obtained at room temperature. The temperature dependence obtained by Elliot et al. [110] up to 180°C for the g-value of the molecular hydrogen is given in Figure 5-7 and Figure 5-8. Ashmore et al. [76] have also measured the temperature dependence for g(H<sub>2</sub>) by measuring the hydrogen yield from solutions containing nitrite ions or iodine. The data obtained 2.6 and 5.9 MeV proton beams can be seen in Figure 5-8.<sup>37</sup>

In Figure 5-8, the temperature dependence is broken out by radiation type. In this case for gamma-radiation, the g-values are similar to the recommended dependence given in Section 3.4.

For 26 MeV <sup>2</sup>H beam with a track-averaged LET of 12 eV/nm, the temperature dependence (t in °C) was:

$$g(\text{H}_2) = 0.529 + 7.759 \times 10^{-4} t$$

For 157 MeV <sup>7</sup>Li beam with a track-averaged LET of 62 eV/nm, the temperature dependence (t in °C) was:

$$g(\text{H}_2) = 0.796 + 8.423 \times 10^{-4} t$$

For 5.9 MeV <sup>2</sup>H beam with a track-averaged LET of 17.5 eV/nm, the temperature dependence (t in °C) was:

$$g(\text{H}_2) = 0.722 + 1.288 \times 10^{-3} t$$

For 2.6 MeV <sup>1</sup>H beam with a track-averaged LET of 29 eV/nm, the temperature dependence (t in °C) was:

$$g(\text{H}_2) = 0.740 + 1.167 \times 10^{-3} t$$

The results of Ashmore et al. [76], while quite scattered, appear to show a ~50% higher temperature dependence than the results of Elliot et al. [110]. However, for the 2.6 MeV proton data, this difference disappears if the one low point at 25°C is ignored. Because of the large uncertainty in the results by Ashmore et al. [76], only the temperature dependence measured from the results of Elliot et al. [110] has been used in estimation of fast neutron g-values in Section 6.

---

<sup>37</sup> In their report, Ashmore et al. [76], also reported results for g(H<sub>2</sub>) using a 1.2 MeV proton beam (LET of 42 eV/nm). Judging by the low g-values obtained (Figure 5-6), it is apparent that depletion of scavenger in the radiation zone was occurring. For this reason the data has not been used for this report.



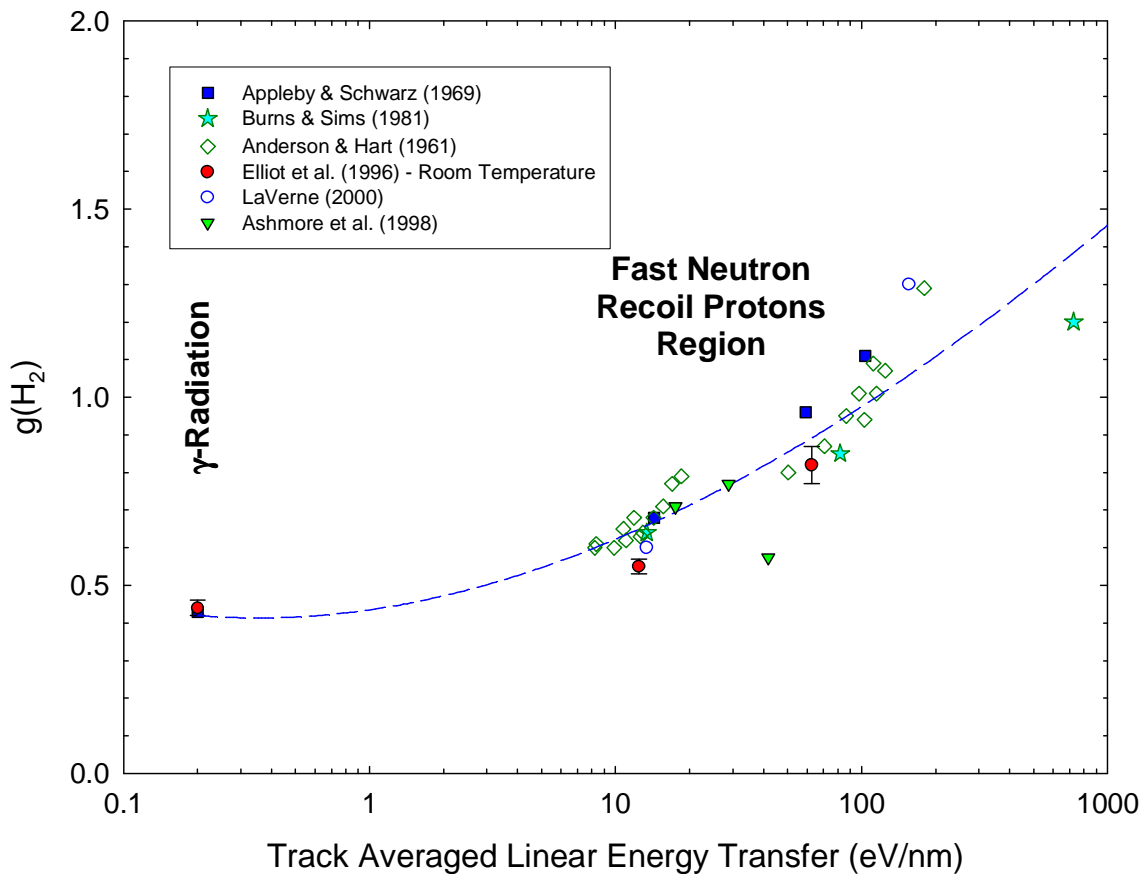


**Figure 5-6 The g-value of molecular hydrogen as a function of track-averaged LET at room temperature as measured by Appleby and Schwarz [112], Burns and Sims [115], Anderson and Hart [116], Elliot et al. [110], LaVerne [117] and Ashmore et al. [76]. The line is the fit to the data given by the polynomial equation in Table 6-1.**

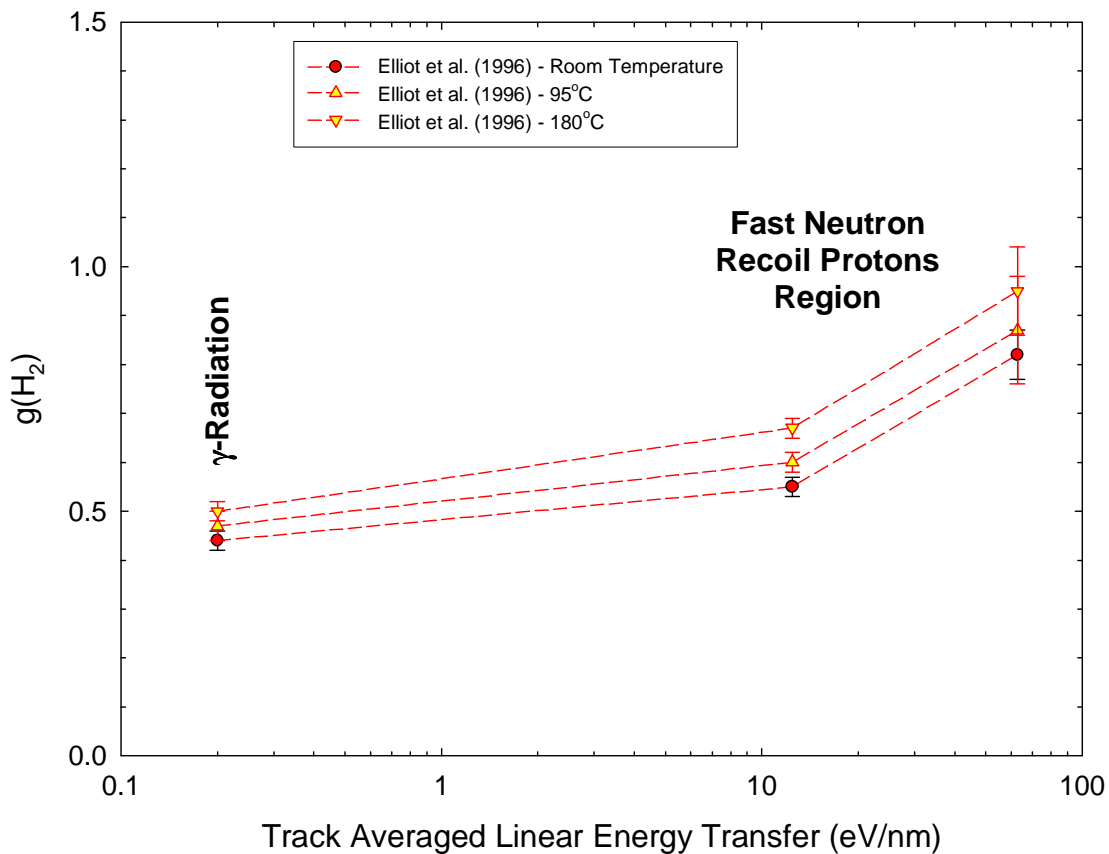
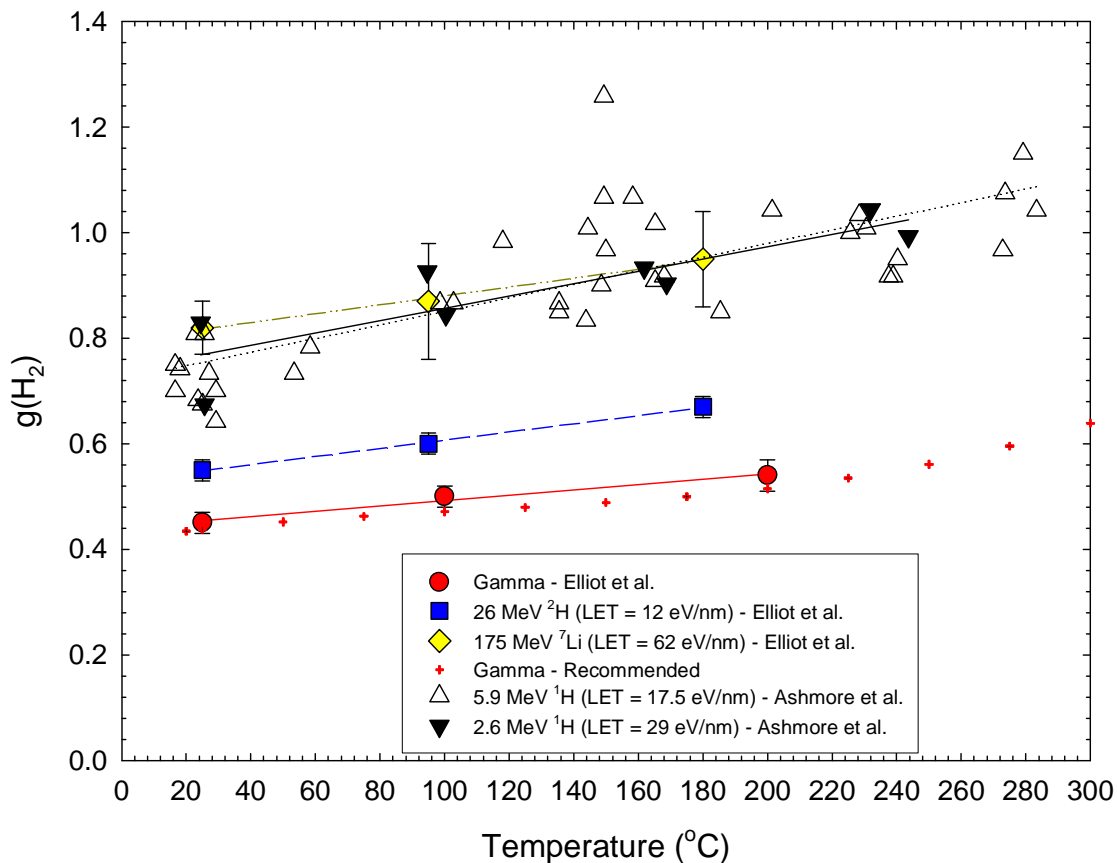


Figure 5-7 The g-value for molecular hydrogen at different temperatures as a function of room temperature track-averaged LET [110].



**Figure 5-8** The temperature dependence of the g-value for molecular hydrogen for gamma-radiation, 26 MeV  $^2\text{H}$  and 157 MeV  $^7\text{Li}$  ion beams measured by Elliot and co-workers using material balance [38], [110]. The results reported by Ashmore et al. [76] for a 2.6 and 5.9 MeV  $^1\text{H}$  ion beam are shown. Also shown is g-value for molecular hydrogen recommended in Section 3.4 for gamma-radiation.

### 5.3 g-Value: Hydrogen Atom

The g-values for atomic hydrogen in light water as reported by Appleby and Schwarz [112], Elliot et al. [38], [110] and Parajon et al. [118] as a function of LET are shown in Figure 5-9. The g-values for hydrogen atoms reported by Appleby and Schwarz [112] and by Elliot et al. [38], [110] are in reasonable agreement.<sup>38</sup> The g-values of Parajon et al. [118] are slightly lower than the other two sets of data<sup>39</sup> but show the same general dependence on track-averaged LET as the earlier reports [110], [112]. This trend is important, as the dependence of the g-value for atomic hydrogen on LET is different from that observed for the other primary species. For the purpose of this report, it is recommended that the g-value dependence given by the dashed line in Figure 5-9 be used.

The temperature dependence up to 180°C for the g-value of atomic hydrogen is given in Figure 5-10 and Figure 5-11. In Figure 5-11, the temperature dependence is broken out by radiation type. There appears to be a decrease in the temperature dependence as the temperature increases. In the case of gamma-radiation, the g-values are lower than the values derived by material balance in Section 3.6, as can be seen in Figure 5-11.

For 26 MeV <sup>2</sup>H beam with a track-averaged LET of 12 eV/nm, the temperature dependence (t in °C) was:

$$g(\text{H}) = 0.490 + 5.353 \times 10^{-4} t$$

For 157 MeV <sup>7</sup>Li beam with a track-averaged LET of 62 eV/nm, the temperature dependence (t in °C) was:

$$g(\text{H}) = 0.337 - 8.298 \times 10^{-6} t$$

---

<sup>38</sup> Different chemistry systems were used in each laboratory, with the end result in agreement.

<sup>39</sup> The g-value for atomic hydrogen was measured in two ways by Parajon et al. [118]: by the HD yield where formate-D ion was used as a scavenger and by the difference between total hydrogen yield and g(H<sub>2</sub>) in the same solution. The g-value for atomic hydrogen of 0.45 given by Parajon et al. [118] for gamma radiolysis is lower than the accepted value of 0.50-0.61 given in Table 3-1. Further work is continuing to resolve this mismatch at the University of Notre Dame. It may be related to the NO<sub>2</sub>, formed from the electron scavenger NO<sub>3</sub><sup>-</sup>, scavenging H atoms in the spur before they can react with formate-D ions.

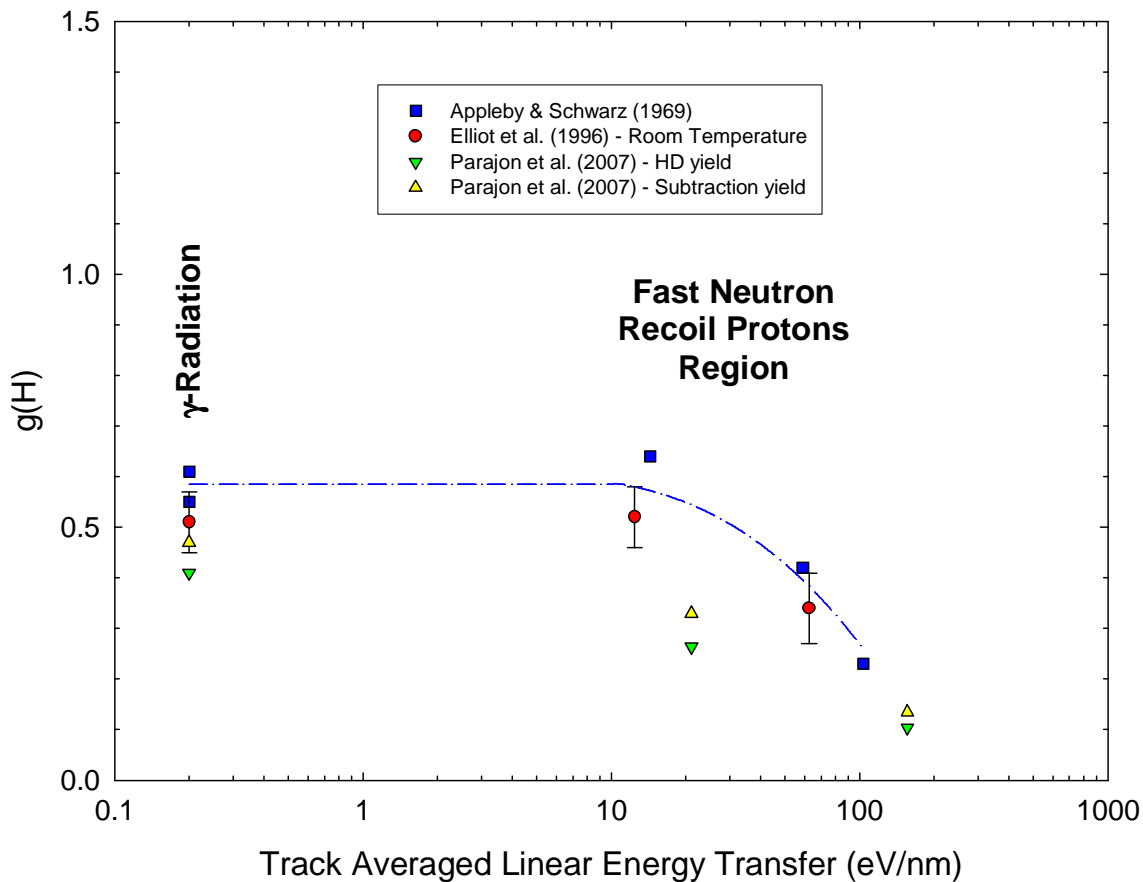


**Figure 5-9 The g-value of atomic hydrogen as a function of track-averaged LET at room temperature as measured by Appleby and Schwarz [112], Elliot et al. [38], [110] and Parajon et al. [118]. The line is the fit to the data given by the polynomial equation in Table 6-1.**

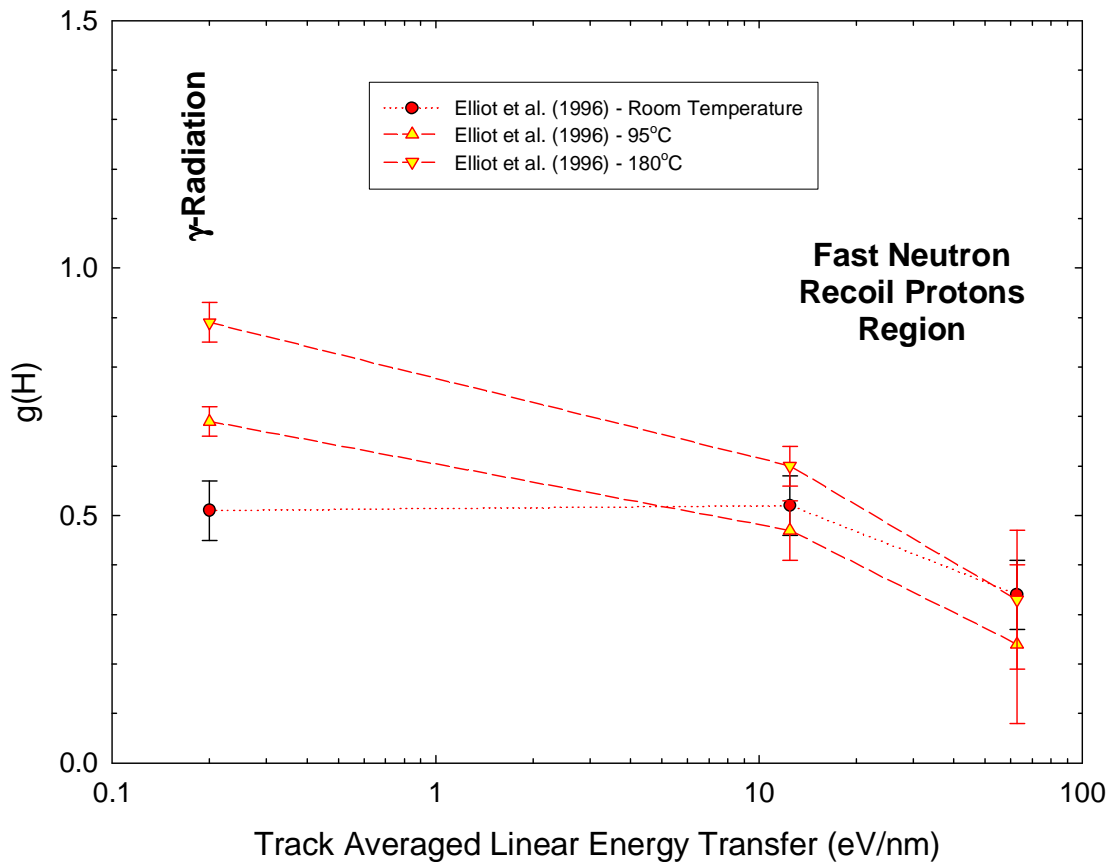
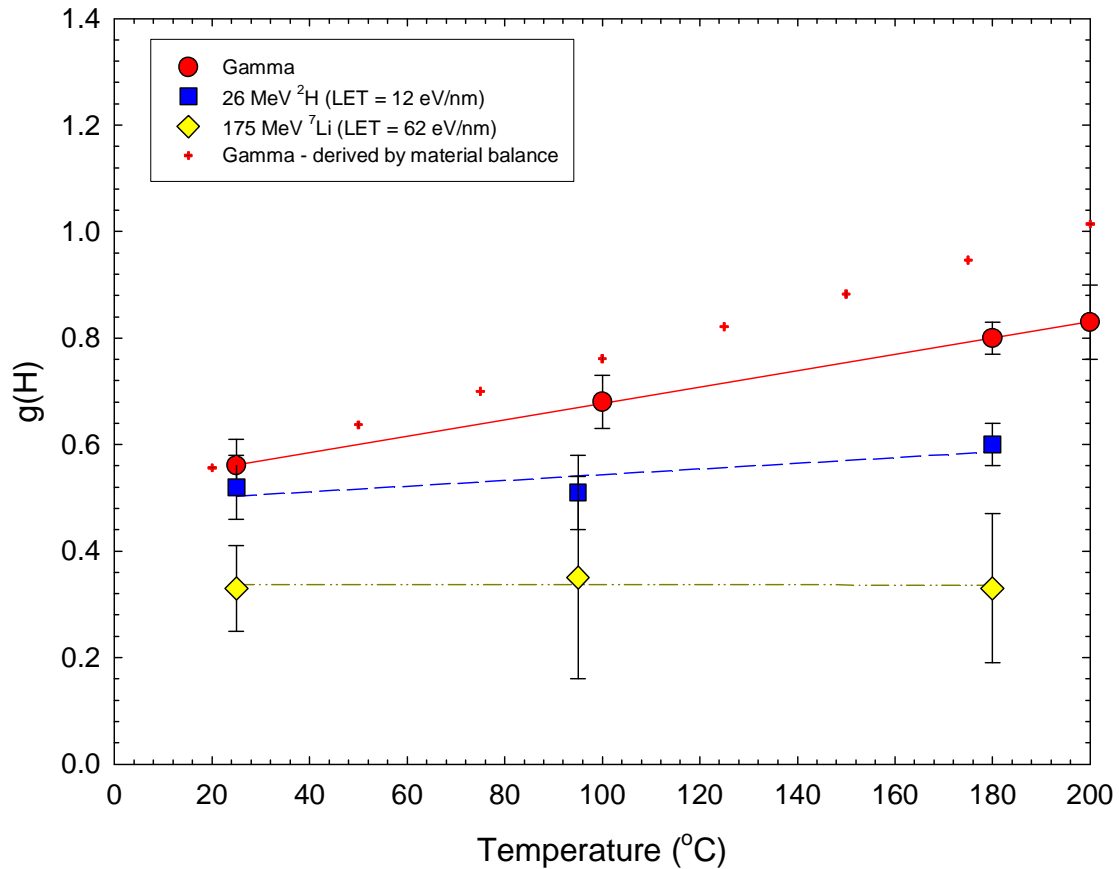


Figure 5-10 The g-value for atomic hydrogen at different temperatures as a function of room temperature track-averaged LET [38], [110].



**Figure 5-11** The temperature dependence of the g-value for atomic hydrogen for gamma-radiation, 26 MeV  $^2\text{H}$  and 157 MeV  $^7\text{Li}$  ion beams measured by Elliot and co-workers [38], [110]. Also shown is g-value for atomic hydrogen derived in Section 3.6 for gamma-radiation.

#### 5.4 g-Value: $\text{HO}_2/\text{O}_2^-$

Figure 5-12 summarises the room temperature yield of  $\text{HO}_2/\text{O}_2^-$  measured by Appleby and Schwarz [112], LaVerne and co-workers [109] and Burns and Sims [115] as a function of track-averaged LET. As all workers have used the ferrous sulphate-cuprous sulphate aqueous system to estimate the yields of  $\text{HO}_2/\text{O}_2^-$  by conversion of  $\text{HO}_2/\text{O}_2^-$  to oxygen, any oxygen produced in the track will also be measured in this  $\text{HO}_2/\text{O}_2^-$  yield [109].

There does not appear to be any reports on the temperature dependence of the yield of  $\text{HO}_2/\text{O}_2^-$ . The mechanism for the formation of  $\text{HO}_2/\text{O}_2^-$  in the track is unclear, it has been suggested that it may be formed through the reaction of O atoms reacting with hydroxyl radicals in the track [119]. The yield of O atoms could be expected to have a minimal temperature dependence. As the yield of  $\text{HO}_2/\text{O}_2^-$  is small over the track-average LET range of interest, it is assumed that the yield does not have a strong temperature dependence.



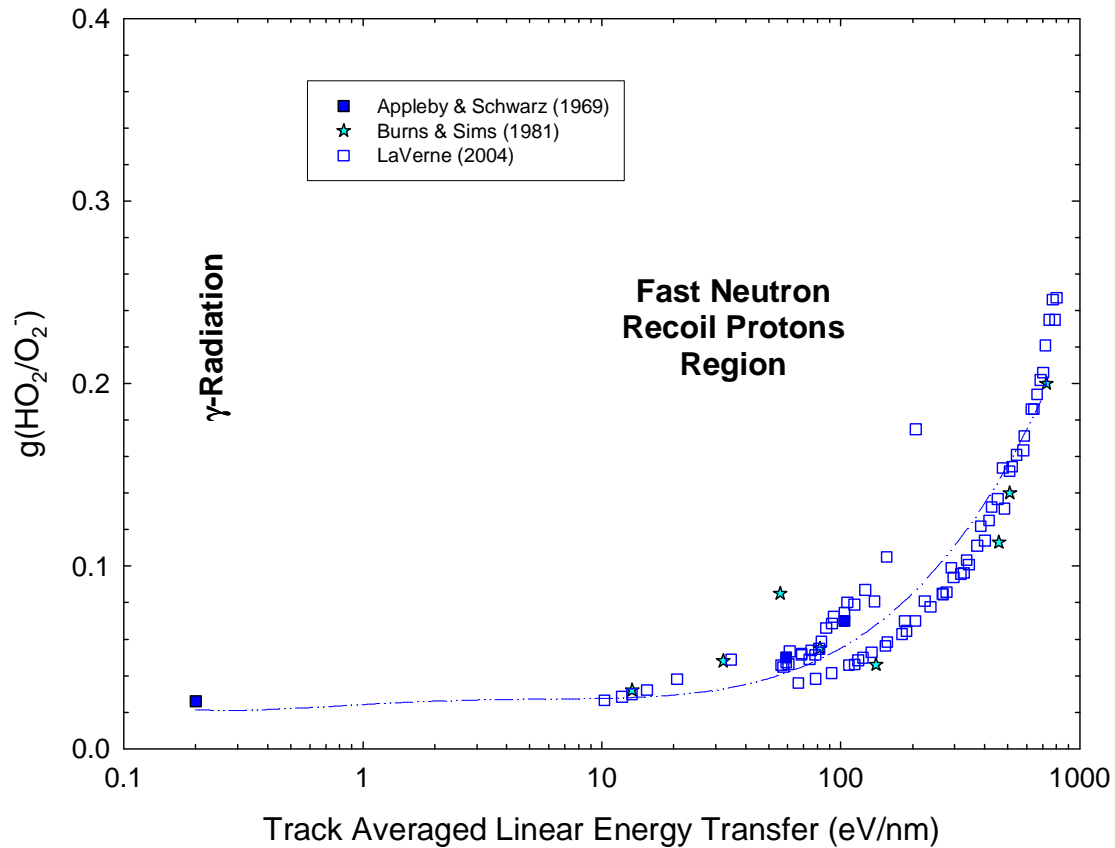


**Figure 5-12 The g-value for the yield of  $\text{HO}_2/\text{O}_2^-$  (and possibly  $\text{O}_2$ ) as a function of track-averaged LET at room temperature as measured by Appleby and Schwarz [112], LaVerne [109] and Burns and Sims [115]. The line is the fit to the data given by the polynomial equation in Table 6-1.**

## 5.5 g-Value: Hydrogen Peroxide

The g-values for hydrogen peroxide in light water as reported by a number of laboratories as a function of LET are shown in Figure 5-13. These results were obtained at room temperature. The temperature dependence for the g-value of the hydrogen peroxide is given in Figure 5-14. Ashmore et al. [76] have measured the temperature dependence for  $g(\text{H}_2\text{O}_2)$  by measuring the oxygen yield from solutions containing  $1\text{-}10 \times 10^{-4}$  mol/kg  $\text{I}_2$  using a 5.9 MeV proton beam (track-averaged LET of 17.5 eV/nm). Their results, using the oxygen yield as measured by mass spectrometer, for the lowest beam currents they studied, are shown in Figure 5-14.<sup>40</sup> Their results, while scattered, do tend to parallel the results of Elliot et al. [110].<sup>41</sup>

Ashmore et al. [76] cover a much wider temperature range than did Elliot et al. [110] who only measured data at room temperature and 95°C. In Figure 5-14, the temperature dependence is separated by radiation type. A simple extrapolation to higher temperatures of  $g(\text{H}_2\text{O}_2)$  based on the two temperature points for the 26 MeV  $^2\text{H}$  and 157 MeV  $^7\text{Li}$  ion beams (Elliot et al. [110]) indicates that  $g(\text{H}_2\text{O}_2)$  would be zero near 325°C (see Figure 5-14). Clearly this situation is unlikely and is probably a consequence of the long extrapolation and the experimental uncertainty in the data as shown in Figure 5-14. The data of Ashmore et al. [76] suggests a lower temperature dependence for  $g(\text{H}_2\text{O}_2)$ .

For the purpose of calculating the g-values associated with fast neutron in Section 6, the temperature dependence for  $g(\text{H}_2\text{O}_2)$  measured in the gamma-radiolysis (Section 3.3) has been assumed to apply to the LET range of interest as shown in Figure 5-14. The y-axis intercept in the equations has been adjusted to fit LET.

For 26 MeV  $^2\text{H}$  beam with a track-averaged LET of 12 eV/nm, the temperature dependence (t in °C) assumed is:

$$g(\text{H}_2\text{O}_2) = 0.750 - 1.620 \times 10^{-3} t$$

For 157 MeV  $^7\text{Li}$  beam with a track-averaged LET of 62 eV/nm, the temperature dependence (t in °C) assumed is:

$$g(\text{H}_2\text{O}_2) = 0.810 - 1.620 \times 10^{-3} t$$

For 5.9 MeV  $^1\text{H}$  beam of Ashmore et al. [76] with a track-averaged LET of 17.5 eV/nm, if the two low data points near room temperature are omitted (Figure 5-14), the temperature dependence for  $g(\text{H}_2\text{O}_2)$  (t in °C) is:

$$g(\text{H}_2\text{O}_2) = 0.951 - 1.509 \times 10^{-3} t$$

The temperature dependence from the data of Ashmore et al. [76] is very similar to the dependence assumed above.

<sup>40</sup> The experimental arrangement used by Ashmore et al. [76] coupled with the low energy proton beams used appeared to be prone to depletion of scavenger solutes in the small radiation zone. This is exacerbated by higher dose rates (i.e. beam current) and lower beam energy.

<sup>41</sup> In their report, Ashmore et al. [76], considered these measurements to indicate no temperature dependence for  $g(\text{H}_2\text{O}_2)$ .

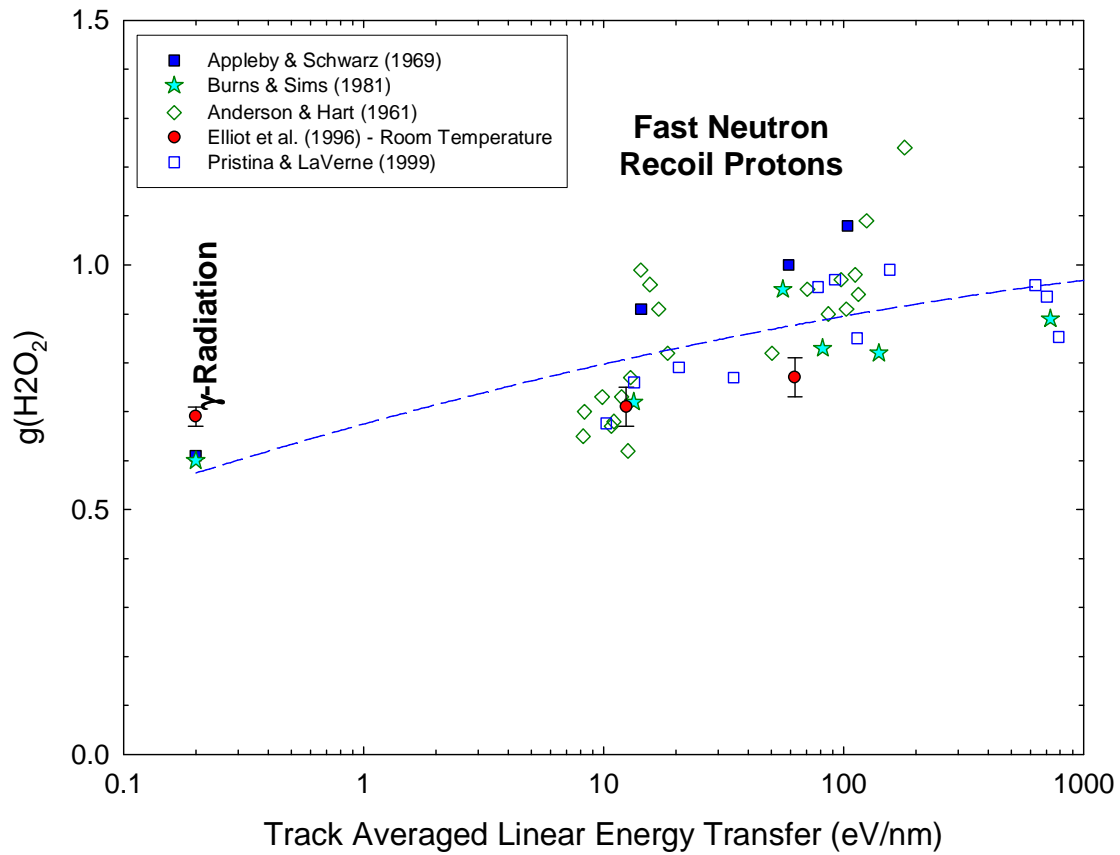


**Figure 5-13 The g-value of hydrogen peroxide as a function of track-averaged LET at room temperature as measured by Appleby and Schwarz [112], Burns and Sims [115], Anderson and Hart [116], Elliot et al. [110] and Pastina and LaVerne [120]. The line is the fit to the data given by the polynomial equation in Table 6-1.**

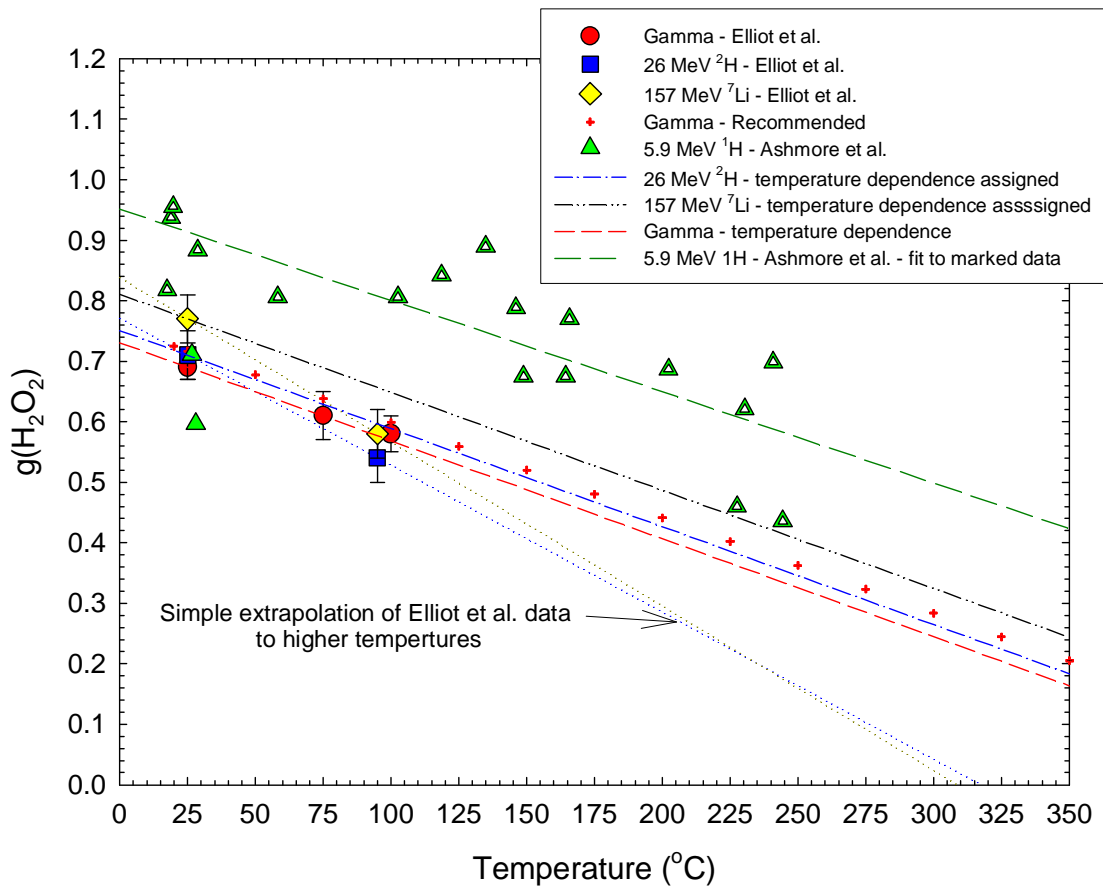


**Figure 5-14 The temperature dependence of the g-value for hydrogen peroxide for gamma-radiation, 26 MeV  $^2\text{H}$  and 157 MeV  $^7\text{Li}$  ion beams measured by Elliot and co-workers [38], [110]. The results reported by Ashmore et al. [76] for a 5.9 MeV  $^1\text{H}$  ion beam are shown. Also shown is g-value for hydrogen peroxide recommended in Section 3.3 for gamma-radiation.**

## 5.6 g-Value: Hydroxyl Radical

The g-values for the hydroxyl radical in light water as reported by a number of laboratories as a function of LET are shown in Figure 5-15. These results were obtained at room temperature. The temperature dependence up to 180°C for the g-value of the hydroxyl radical is given in Figure 5-16 and Figure 5-17. Both figures demonstrate that the temperature dependence is similar for the g-value as the LET increases.

In Figure 5-17, the temperature dependence is separated by radiation type. These hydroxyl radical results are all based on material balance calculated using the g-values for hydrogen peroxide estimated in the previous Section 5.5. It should be noted that for gamma-radiation, this material balance estimate gave slightly lower g-values than that recommended in Section 3.2 as can be seen in Figure 5-17.

For 26 MeV  $^2\text{H}$  beam with a track-averaged LET of 12 eV/nm, the temperature dependence (t in °C) was:

$$g(\text{OH}) = 1.450 + 6.925 \times 10^{-3} t$$

For 157 MeV  $^7\text{Li}$  beam with a track-averaged LET of 62 eV/nm, the temperature dependence (t in °C) was:

$$g(\text{OH}) = 0.940 + 5.228 \times 10^{-3} t$$

Ashmore et al. [76] have attempted to measure the temperature dependence for g(OH) by measuring the carbon dioxide yield from solutions containing formate and methyl viologen. We have chosen not to incorporate these data into the current evaluations as not all the chemistry issues have been resolved as to what corrections should be applied to carbon dioxide yields to calculate the hydroxyl radical yield. In particular, the role of the thermal decomposition of hydrogen peroxide in the formation of carbon dioxide remains to be established in this system.

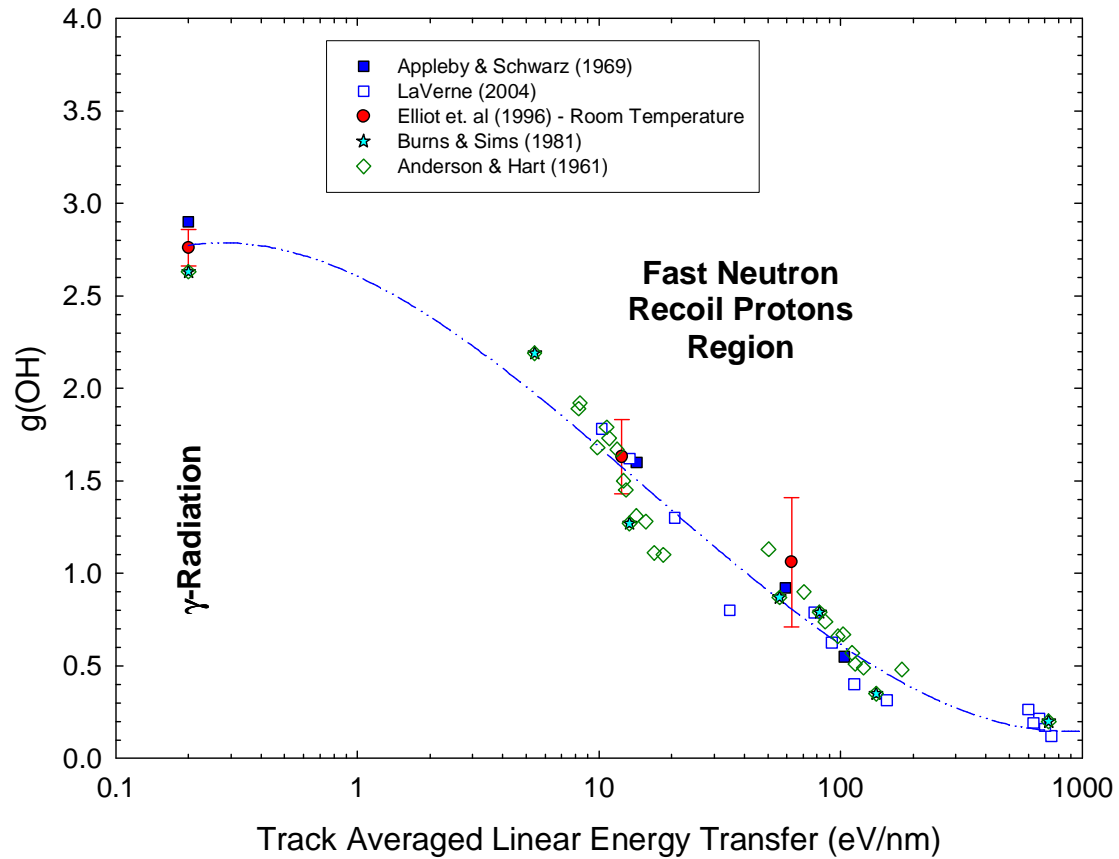


**Figure 5-15** The g-value of the hydroxyl radical as a function of track-averaged LET at room temperature as measured by Appleby and Schwarz [112] (material balance), LaVerne [109], Elliot et al. [110] (material balance), Burns and Sims [115], Anderson and Hart [116]. The line is the fit to the data given by the polynomial equation in Table 6-1.

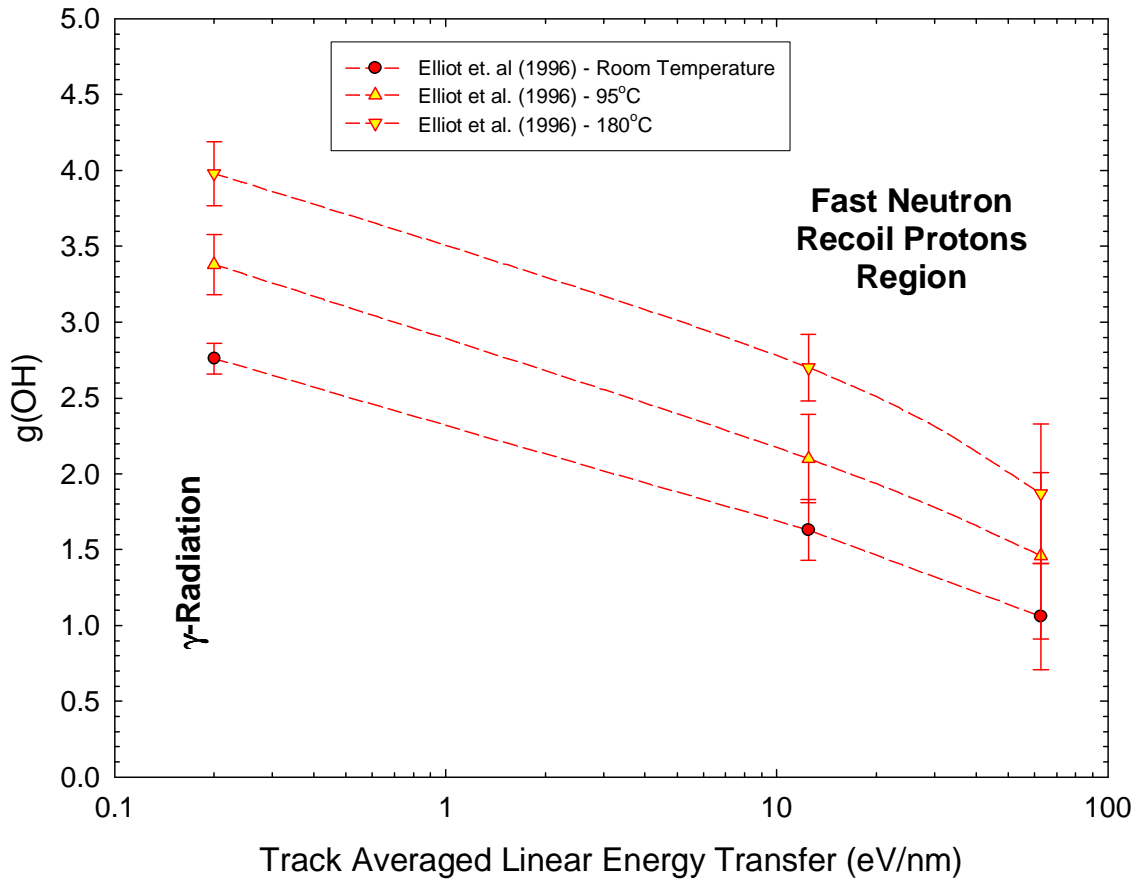
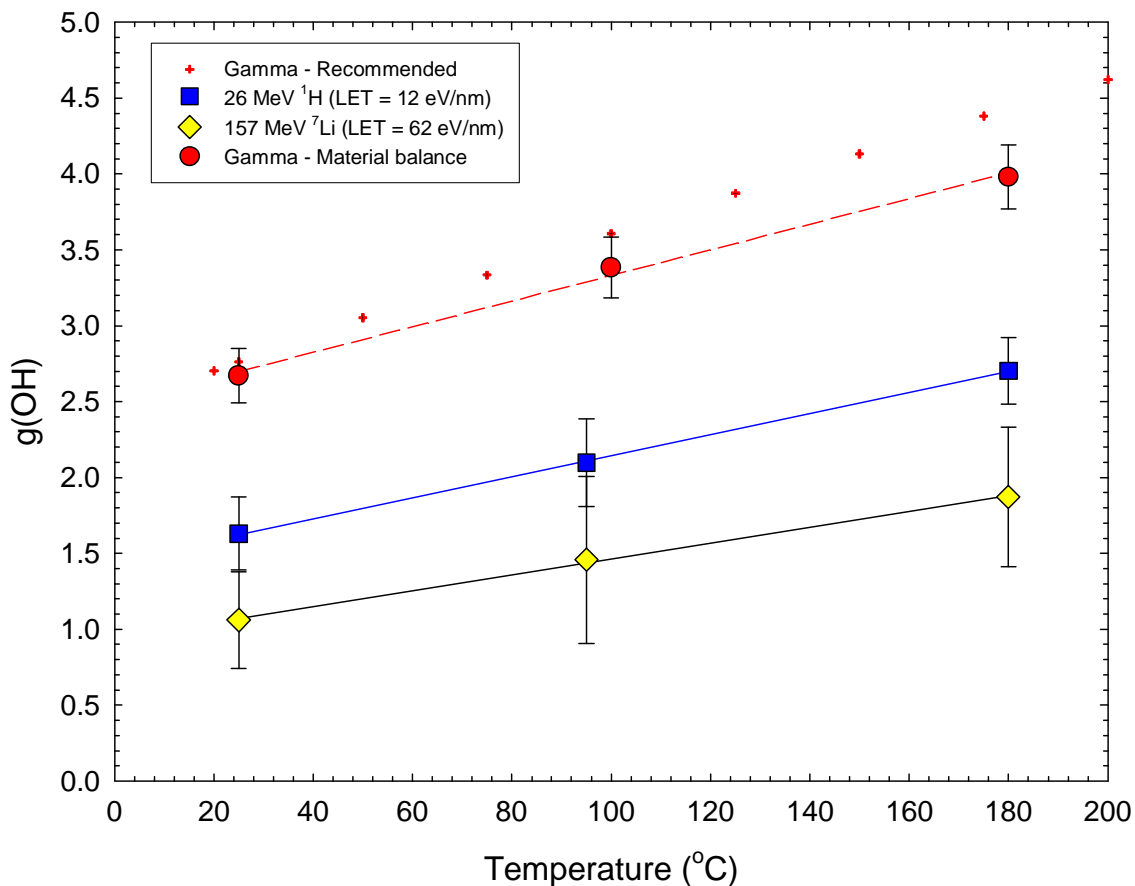


Figure 5-16 The g-value for the hydroxyl radical at different temperatures as a function of room temperature track-averaged LET [110].



**Figure 5-17** The temperature dependence of the g-value for the hydroxyl radical for gamma-radiation, 26 MeV  $^2\text{H}$  and 157 MeV  $^7\text{Li}$  ion beams measured by Elliot and co-workers [38], [110] using material balance with the revised  $g(\text{H}_2\text{O}_2)$  in Section 5.2. Also shown is g-value for the hydroxyl radical recommended in Section 3.2 for gamma-radiation.



## 6. ESTIMATION OF FAST NEUTRON G-VALUES AS A FUNCTION OF TEMPERATURE

(with R.E. Donders, Reactor and Radiation Physics Branch, AECL-CRL)

In this section, the methodology to estimate the fast neutron g-values will be outlined. The example will be based on the fast neutron spectrum from the natural uranium fuel used in the light water-cooled, high temperature U-2 loop in the NRU reactor at Chalk River for the radiolysis tests in 1995 [14].<sup>42</sup> A very similar, more detailed simulation was carried out by Edwards et al. [107] for the fast neutron hydrated electron yield from N<sub>2</sub>O scavenging in the TRIGA test reactor at University of Wisconsin which operates on 70% U-235 enriched fuel.

Fast neutrons deposit their energy in the water through ion recoils; in light water about 93% of the energy is deposited by proton recoils while the remainder is deposited through oxygen atom recoils [106]. For this report, only the proton recoil component will be considered for estimating fast neutron g-values. The oxygen recoil ions are characterized by much higher LET, giving very smaller g-values for free radicals and larger g-values for molecular products. Neglect of the oxygen recoils will, overall, give slightly higher g-values for radical primary species and slightly lower g-values for molecular primary species for fast neutron radiolysis. These errors are probably minor compared to the other approximations made in this estimate.

The overall approach to estimating the fast neutron g-values can be broken down into four steps:

1. Obtain the fast neutron flux spectrum distribution;<sup>43</sup>
2. Determine the recoil proton spectrum distribution;
3. Determine the g-values of the primary species (see Reaction (R1)) for each proton energy bin (based on the g-value dependence with LET); and
4. Summing the individual g-values determined in the previous Step 3, weighted by their fraction of total energy absorbed in that energy bin.

In the present example, the room temperature g-value of a primary specie is first calculated in Step 3. If the g-value at a higher temperature is required, the temperature dependence associated with the g-value and the LET of the proton is applied to this room temperature value.

---

<sup>42</sup> The g-values depend on the spectrum of the fast neutron flux in question. In general, the spectrum is expected to only vary slightly from reactor-to-reactor using uranium as a fuel. This does not take into consideration the ion recoils as a consequence of the use of boron as a neutron flux control agent in PWRs.

<sup>43</sup> As will be seen below, the flux spectrum is generally 'binned' in energy groups. Hence mathematical operations are done on an individual 'bin'.

## 6.1 Determination of the recoil proton spectrum

The fast neutron group-flux distribution in the light water from the natural uranium fuel in the U-2 loop, NRU, is shown in Figure 6-1. This spectrum was calculated using an AECL in-house multi-group neutron transport code WIMS-AECL. The spectrum is calculated in energy groupings or 'bins'. As can be seen, most of the fast neutron flux falls into the 0.5 to 6 MeV energy range.

When fast neutrons of a given energy scatter off the protons in the water, the recoil protons that are formed will have a range of energies. The distribution of protons in the different energy bins has been calculated using the Energy Transfer Factors as described and tabulated by McCracken et al. [106]. The proton recoil spectrum is given in Figure 6-1 along with the percentage of the total energy deposited by the protons from each 'bin'.

## 6.2 Estimation of the g-values for fast neutron at room temperature

The track-averaged LET for the protons in each of the seven energy bins spanning the region of interest (0.2 to 11 MeV) can now be estimated from the information in Figure 5-2. The mid-point of each bin was used for the proton energy (P) to calculate the track-averaged LET. The polynomial function given in Table 6-1 was used to calculate the track-averaged LET.

The next step is to calculate the g-values for the primary species associated with each of the energy bins. To do this, the dependences of the g-values on track-averaged LET given in Figure 5-3, Figure 5-6, Figure 5-9, Figure 5-12, Figure 5-13 and Figure 5-15 have to be used. The fit lines in these figures have been used and the polynomial equations to the fits are given in Table 6-1.<sup>44</sup> The g-value for each proton energy bin is given in Table 6-2. Each g-value was calculated with no consideration of overall material balance for the decomposition of water, i.e., they were calculated from independently. To check the material balance, g(H) was also estimated separately based on material balance with the other g-values. This material balance g(H) is given in the last column in Table 6-2. As can be seen, the material balance g(H) agrees acceptably with the measured g(H) to within 0.13 #/100 eV indicating that the g-values are self-consistent within experimental uncertainty.

The fast neutron g-values are then calculated by summing the g-value for each energy bin weighted to its fraction of the total fast neutron energy absorbed; the g-values are given in the bottom line of Table 6-2. These room temperature fast neutron g-values are similar to those estimated by Ruiz et al. [121] by McCracken [106] and Edwards, et al. [107].

The fast neutron g-values in Table 6-2 tend to have higher free radical yields and low molecular yields than those typically used in the past [13]. One reason for this is that often a mono-energetic 2 MeV neutron was taken as representative of a fast neutron flux in a reactor. The proton recoil energies calculated from a 2 MeV neutron were 1.3 MeV or less, biasing the energy spectrum to higher LET particles, which have lower free

---

<sup>44</sup> Note the polynomial fits use  $\text{Log}_{10}(\text{LET})$ , not LET as the fit parameter.

radical yields. This is illustrated in Table 6-2 where the effect of LET on radiolysis yields covers the LET range of interest.

### 6.3 Estimation of the g-values for fast neutron at reactor operating temperatures

As can be seen in Figure 5-5, Figure 5-8, Figure 5-11, Figure 5-14 and Figure 5-17, the g-value for a given radiation type changes linearly with temperature over the temperature range studied from room temperature up to 180°C. This linear dependence has been used to estimate the g-values for the primary species for the different proton energies at higher temperatures. It has been assumed that the linear dependence extends up to reactor operating temperatures, although based on the gamma-radiolysis g-values yields (Figure 3-10) it would be expected that there is likely some curvature in the dependences above 180°C. It is beyond the scope of this report to estimate what this curvature would be.

The rate of change of the g-values with temperature, i.e.,  $d(\text{g-value})/d(\text{temperature})$ , as a function of the track-averaged LET is shown in Figure 6-2. The value of  $d(\text{g-value})/d(\text{temperature})$  at the LET associated with the proton energy bins has been interpolated from the data in Figure 6-2 assuming a linear relationship between the available LET data points of 12 and 73 eV/nm. This dependence is summarized in Table 6-3. These temperature dependences have been applied to the room temperature g-values for the different proton energy bins in Table 6-2. The fast neutron g-values were then calculated as before for each temperature and are shown in Figure 6-3. The g-values (units #/100 eV) in Figure 6-3 can be described by the following equations where  $t$  is the temperature in °C.

$$g(e_{aq}^-) = 0.96 + 1.09 \times 10^{-3} t$$

$$g(H_2) = 0.75 + 8.02 \times 10^{-4} t$$

$$g(H) = 0.49 + 3.22 \times 10^{-4} t$$

$$g(OH) = 0.99 + 6.26 \times 10^{-3} t$$

$$g(H_2O_2) = 0.89 - 1.62 \times 10^{-3} t$$

$$g(HO_2/O_2^-) = 0.03$$

These equations do not amount to a material balance for the decomposition of water. If they are to be used in computer modelling of the radiolysis of water, one of the g-values should be calculated from the material balance equation. At the present time, it is recommended that  $g(H)$  be that g-value.

$$g(H) = g(OH) + 2 g(H_2O_2) - g(e_{aq}^-) - 2 g(H_2) + 3 g(HO_2).$$

For the data in Figure 6-3, the difference was within 0.1 #/100 eV between  $g(H)$  estimated by material balance and the calculated  $g(H)$ . This indicates there is internal consistency within the calculations.

Table 6-4 summarizes the fast neutron g-values for temperatures between 25° and 350°C. These g-values at reactor temperatures (~280°-300°C) tend to have higher radical yields

than have been typically estimated [13] with the exception of the g-values estimated by McCracken et al. [106], whose more complete methodology to g-value estimation has been followed in this report but using re-assessed experimental data.

It should be remembered that these g-values for fast neutrons reported here will be higher than the true 'escape' yield because of the solute scavenging powers used in most of the experiments.

**Table 6-1**  
**Polynomial functions describing track-averaged LET as function of proton energy and**  
**g-values as a function of LET at room temperature**

<b>Parameter</b>	<b>Function</b>
Track-Averaged LET (eV/nm) (Proton Energy = P in MeV)	$82.018 - 56.022 P + 26.053 P^2 - 7.026 P^3 + 1.090 P^4 - 9.548 \times 10^{-2} P^5 + 4.372 \times 10^{-3} P^6 - 8.103 \times 10^{-5} P^7$ (for proton energy = 0.2-11 MeV in Figure 5-2)
$g(e_{aq}^-)$ (L = Log <sub>10</sub> (LET))	$2.429 - 0.647 L - 0.311 L^2 + 2.726 \times 10^{-2} L^3 + 2.241 \times 10^{-2} L^4$ (Figure 5-3)
$g(H_2)$ (L = Log <sub>10</sub> (LET))	$0.435 + 9.401 \times 10^{-2} L + 9.962 \times 10^{-2} L^2 - 5.794 \times 10^{-3} L^3$ (Figure 5-6)
$g(H)^*$ (L = Log <sub>10</sub> (LET))	$0.583 + 3.924 \times 10^{-3} L + 1.959 \times 10^{-2} L^2 - 3.773 \times 10^{-3} L^3 - 2.351 \times 10^{-2} L^4$ (Figure 5-9)
$g(OH)$ (L = Log <sub>10</sub> (LET))	$2.605 - 0.608 L - 0.440 L^2 + 0.123 L^3$ (Figure 5-15)
$g(H_2O_2)$ (L = Log <sub>10</sub> (LET))	$0.675 + 0.135 L - 1.221 \times 10^{-2} L^2$ (Figure 5-13)
$g(HO_2/O_2^-)$ (L = Log <sub>10</sub> (LET))	$2.415 \times 10^{-2} + 7.237 \times 10^{-3} L - 2.246 \times 10^{-3} L^2 - 6.382 \times 10^{-3} L^3 + 4.778 \times 10^{-3} L^4$ (Figure 5-12))

\* Function not valid above a track-averaged LET of 100 eV/nm.

**Table 6-2**  
**The g-Values for the different energy recoil protons and for fast neutrons at room temperature**

Mid-point Energy (MeV)	Track-Averaged LET (eV/nm)	% Energy Deposited (Figure 6-1)	$g(e_{aq}^-)$	$g(H_2)$	$g(H)$	$g(OH)$	$g(H_2O_2)$	$g(HO_2)$	$g(H)^*$
8.6	14.5	5.5	1.34	0.67	0.57	1.50	0.81	0.03	0.53
4.9	20.1	18.7	1.18	0.71	0.55	1.34	0.83	0.03	0.48
3.0	27.0	28.6	1.04	0.76	0.52	1.20	0.84	0.03	0.42
1.8	34.5	23.6	0.92	0.79	0.49	1.08	0.85	0.03	0.38
1.1	44.3	13.6	0.81	0.83	0.45	0.96	0.86	0.04	0.33
0.7	54.6	6.9	0.71	0.87	0.42	0.87	0.87	0.04	0.28
0.4	63.4	3.1	0.65	0.89	0.38	0.80	0.88	0.04	0.25
<b>Fast Neutrons g-values =</b>			<b>0.99</b>	<b>0.78</b>	<b>0.50</b>	<b>1.15</b>	<b>0.85</b>	<b>0.03</b>	<b>0.40</b>

\* Calculated by material balance:  $g(H) = g(OH) + 2 g(H_2O_2) + 3 g(HO_2) - g(e_{aq}^-) - 2 g(H_2)$

**Table 6-3**  
**Polynomial functions describing the rate of change of d(g-value)/d(temperature)**  
**with track-averaged LET**

Parameter	Function
$d(g(e_{aq}^-))/d(\text{temperature})$	$1.92 \times 10^{-3} - 2.56 \times 10^{-5} \text{ LET}$
$d(g(H_2))/d(\text{temperature})$	$7.59 \times 10^{-4} + 1.32 \times 10^{-6} \text{ LET}$
$d(g(H))/d(\text{temperature})$	$6.70 \times 10^{-4} - 1.08 \times 10^{-5} \text{ LET}$
$d(g(OH))/d(\text{temperature})$	$7.34 \times 10^{-3} - 3.37 \times 10^{-5} \text{ LET}$
$d(g(H_2O_2))/d(\text{temperature})$	$-1.62 \times 10^{-3}$
$d(g(HO_2/O_2^-))/d(\text{temperature})$	No temperature dependence

**Table 6-4**  
**The g-Values for fast neutrons deposited in light water at temperatures between 25°**  
**and 350°C for natural uranium**

Temperature (°C)	g(e)	g(H <sub>2</sub> )	g(H)	g(OH)	g(H <sub>2</sub> O <sub>2</sub> )	g(HO <sub>2</sub> )
25	0.99	0.78	0.50	1.15	0.85	0.03
50	1.02	0.80	0.51	1.30	0.81	0.03
100	1.07	0.84	0.52	1.61	0.73	0.03
150	1.13	0.88	0.54	1.93	0.64	0.03
200	1.18	0.92	0.56	2.24	0.56	0.03
250	1.23	0.96	0.57	2.55	0.48	0.03
300	1.29	1.00	0.59	2.87	0.40	0.03
350	1.34	1.04	0.60	3.18	0.32	0.03

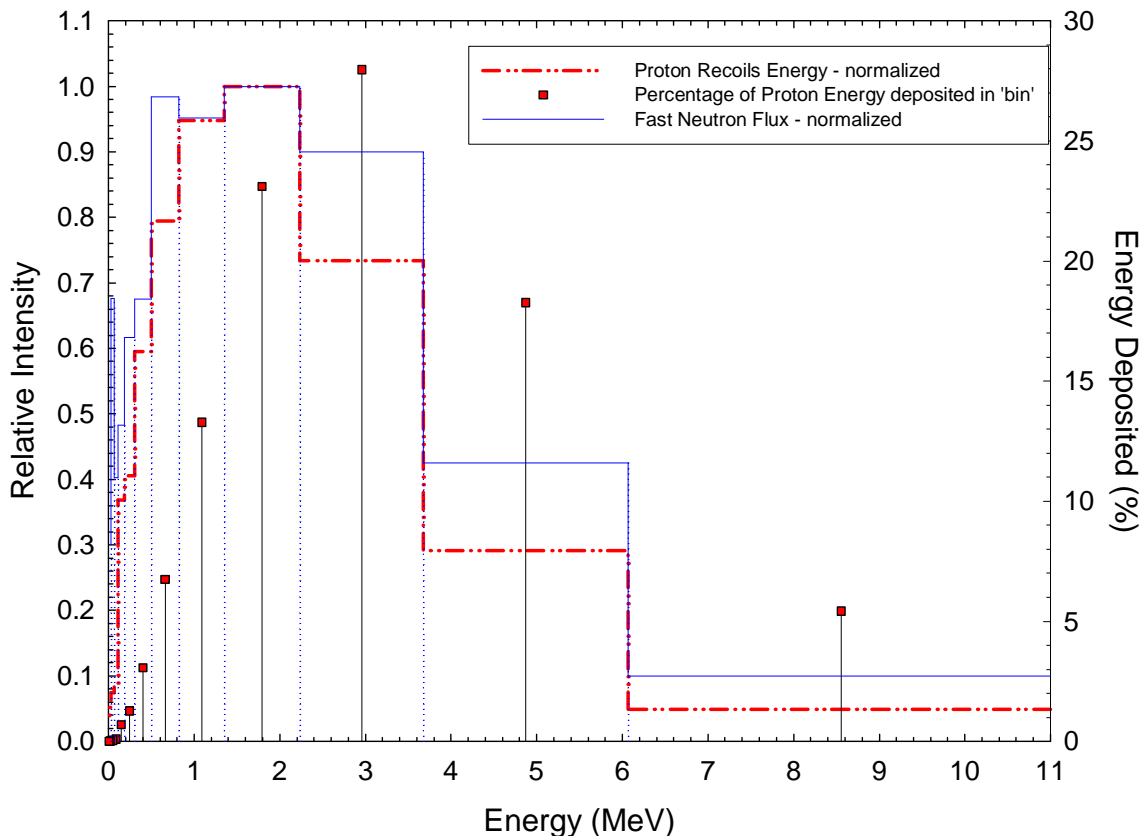


**Figure 6-1 The relative ‘energy binned’ fast neutron group-fluxes and proton recoil spectrum for the light water-cooled, high temperature U-2 loop, NRU reactor. The fuel was natural uranium after 250 MWh/kg uranium burn-up. Also shown are the percent of the total energy deposited by protons within each energy bin.<sup>45</sup>**

<sup>45</sup> Neutron group fluxes were calculated at a finer group structure, which were then collapsed to the indicated group structure to be consistent with the Energy Transfer Factors in Reference [106].



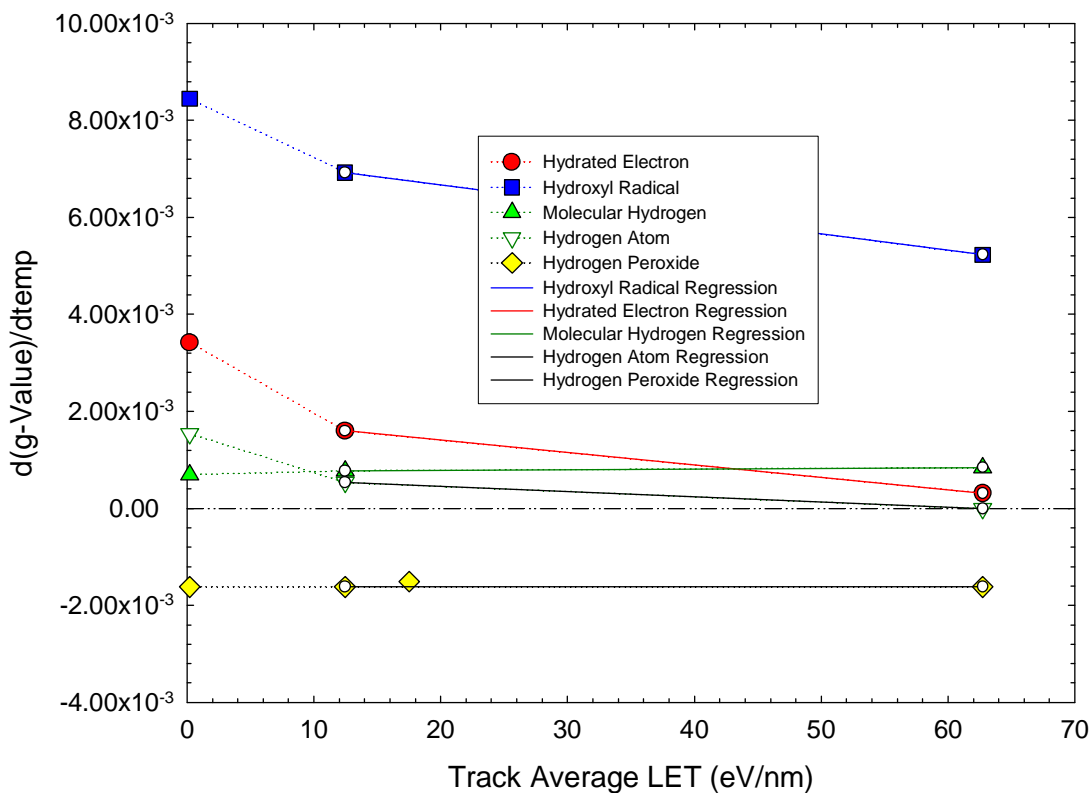


**Figure 6-2 The rate of change of the g-values with temperature as a function of track-averaged LET. The solid lines are dependences used to calculate the fast neutron g-values at reactor operating temperatures.**

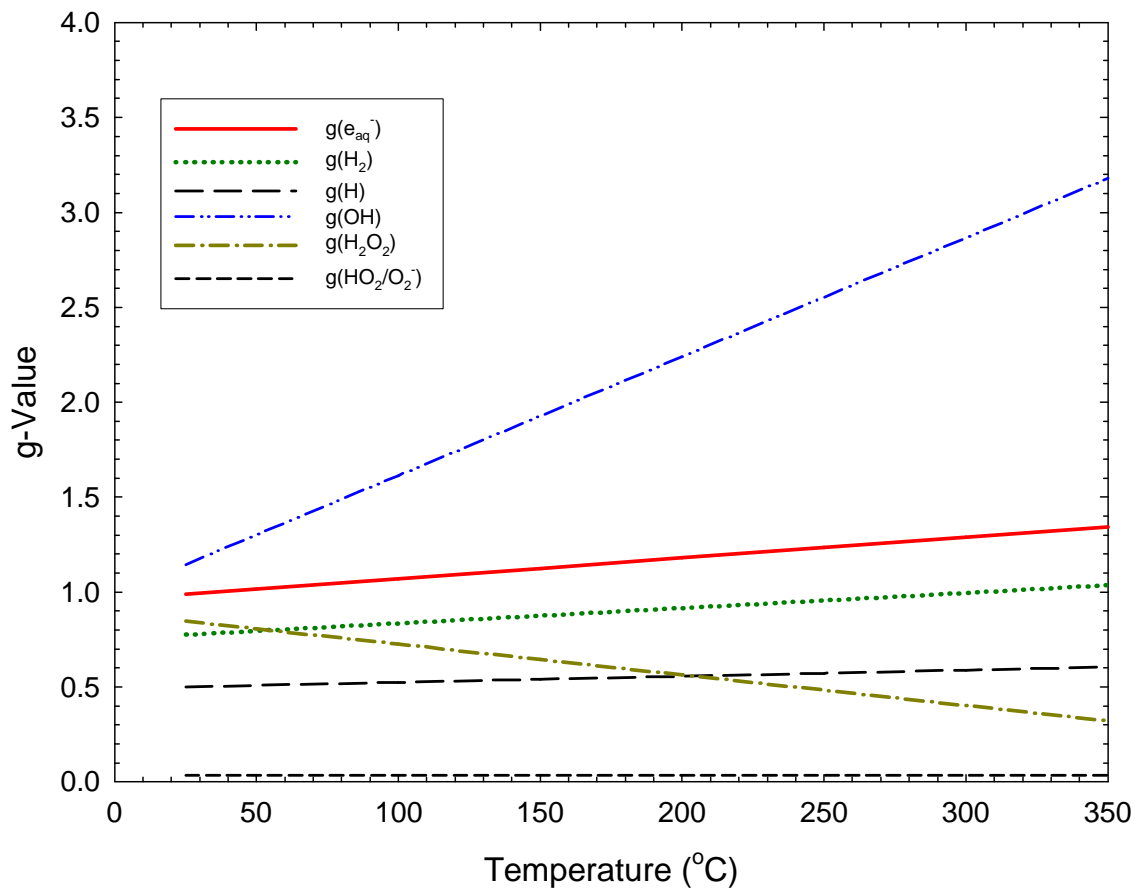


Figure 6-3 The g-values for fast neutrons as a function of temperature for natural uranium fuel.

## 7. CONCLUSIONS

The information contained in this report is based on data available up to the year 2008. The development of an improved radiolysis database is an iterative process. Many of the reaction rate constants catalogued in this report had been estimated by fitting data using some form of computer modelling. Often, since these rate constant estimates were made, there have been improved measurements to the rate constants and extinction coefficients that were incorporated into the original computer model. Ideally, many rate constants should be re-investigated using the revised/updated rate constants and extinction coefficients to generate a self-consistent radiolysis database.

One of the difficulties encountered in compiling this report has been the inconsistency in dosimetry and extinction coefficients used in different laboratories.<sup>46</sup> It is recommended that all laboratories standardize their pulse radiolysis dosimetry to that recommended by Buxton and Stuart [32].<sup>47</sup> Experimenters should, where possible, determine the extinction coefficient of a transient species independently to avoid situations where the extinction coefficient used does not match the dosimetry as has been found with the hydrated electron recently [51] and with the superoxide radical anion [24], [65].

One research area that requires some further assessment is the estimation of both gamma- and fast neutron g-values that represent the true 'escape' yield for use in deterministic radiolysis modelling over the 20°-350°C temperature range. The g-values estimated in this report are slightly elevated as a consequence of the solute scavenging powers used in many of the experiments. At this point in time, considering all the other uncertainties in the radiolysis database, in reactor dose rates, etc., the g-values given in this report should be satisfactory for radiolysis modelling purposes.

To summarize the overall conclusions of this report, the g-values for gamma- and fast neutron radiolysis at a number of temperatures between 25° and 350°C are given in Table 3-4 and Table 6-4. The rate constants and associated equilibria for the radiolysis of high temperature water have been calculated from the mathematical functions given in this report for a number of temperatures from 20°C to 350°C and are listed in Table A-1, Table A-2, Table A-3 and Table A-4 in Appendix A.

---

<sup>46</sup> Both authors of this report have been guilty of this infraction.

<sup>47</sup> The  $G \times \epsilon$  of  $2.51 \times 10^4$  ( $G$  in #/100 eV and  $\epsilon$  in L/mol/cm) recommended by Buxton and Stuart [32] for the oxygen saturated  $10^{-2}$  mol/L thiocyanate dosimeter at 475 nm has been confirmed by Bartels and co-workers (to be published), using the absorption extinction coefficient of the hydrated electron. This was determined independent of any dose or yield calibrations from the simultaneous measurements of the fluoride ion product in sulphur hexafluoride solutions,  $N_2$  product in  $N_2O$  solutions, or  $MV^+$  absorbance at 605 nm in methyl viologen solutions.

**8. ACKNOWLEDGEMENTS**

The authors would like to thank many who have provided data and comments during the development of this compilation: Bob Donders, Glenn Glowa, Patrick Hare, Irek Janik, Yasuke Katsumura, Jay LaVerne, Mingzhang Lin, Tim Marin, Howard Sims, Chris Stanisky, Craig Stuart and Kenji Takahashi.

John Elliot would like to acknowledge the collaboration and mentoring provided by George Buxton in the late 1980's and early 1990's when John Elliot was involved in high temperature water radiolysis studies. He would also like to acknowledge the contributions of the chemical technologists Denis Ouellette and Monique Chenier who performed many of the experimental studies at the Chalk River Laboratories and to Craig Stuart who continued the high temperature radiolysis studies through to the early 2000's.

## 9. REFERENCES

- [1] Uchida, S., Ibe, E. and Katsumura, R. (1985) "Effects of Irradiation on Corrosion Circumstances in Boiling Water." *Radiat. Phys. Chem.*, Vol. 22, pp. 515-526.
- [2] ASM International (1987) "Metals Handbook, Volume 13 Corrosion." 9<sup>th</sup> Edition.
- [3] Wood, C.J. (1994) "Recent Developments in BWR Water Chemistry." Proceedings of the International Conference on Chemistry in Water Reactors: Operating Experience and New Developments, SFEN, Nice.
- [4] Cowan, R.L. (1996) "The Mitigation of IGSCC of BWR Internals With Hydrogen Water Chemistry." Proceedings of the Water Chemistry of Nuclear Reactor Systems 7, BNES, pp. 196-206.
- [5] Macdonald, D.D. and Urquidi-Macdonald, M. (1995) "On the Interpretation of ECP Data from Boiling Water Reactors." Proceedings of 7<sup>th</sup> International Symposium on Environmental Degradation of Materials in Nuclear Power Systems – Water Reactors, NACE, 711.
- [6] Kruger, R.M., Romeo, G., Henshaw, J. and Burns, W.G. (1996) "Model Calculation of Water Radiolysis and Electrochemical Potentials in BWR Primary Coolant III." Proceedings of the Water Chemistry of Nuclear Reactor Systems 7, BNES, pp. 207-213.
- [7] Garbett, K., Henshaw, J., and Sims, H.E. (2000) "Hydrogen and Oxygen Behaviour in PWR Primary Coolant." Proceedings of the Water Chemistry of Nuclear Reactor Systems 8, BNES, pp. 85-92.
- [8] Dickinson, S., Henshaw, J., Tuson, A. and Sims, H.E. (2002) "Radiolysis Effects in Sub-Cooled Nucleate Boiling." Proceedings of the International Conference on Water Chemistry in Nuclear Reactor Systems: Operation, Optimization and New Developments, Avignon.
- [9] Henshaw, J., McGuire, J.C., Sims, H.E., Tuson, A., Dickenson, S. and Deshon, J. (2006) "The Fuel Crud Deposits and Its Effect on AOA in PWR Plants." Proceedings of the International Conference on Water Chemistry of Reactor Systems, Jeju Island, Korea.
- [10] Umehara, R. and Miukai, S. (2006) "Low Hydrogen Control for Suppression of PWSCC and Radiation Reduction." Proceedings of the 6<sup>th</sup> International Workshop on LWR Coolant Water Radiolysis and Electrochemistry, Jeju Is., Korea.
- [11] Slade, J.P. and Gendron, T.S., (2005) "Flow Accelerated Corrosion and Cracking of Carbon Steel Piping in Primary Water - Operating Experience at the Point Lepreau Generating Station." Proceedings of the 12<sup>th</sup> International Conference on Environmental Degradation of Materials in Nuclear Power Systems-Water Reactors, TMS, Salt Lake City, UT.
- [12] Wren, J.C. and Ball, J.M. (2001) "LIRIC-3.2: an Updated Model for Iodine Behaviour in the Presence of Organic Impurities." *Radiat. Phys. Chem.* Vol. 60, pp. 577-596.

- [13] Christensen, H. (2006) "Fundamentals Aspects of Water Coolant Radiolysis." SKI Report 2006:16.
- [14] Elliot, A.J. and Stuart, C.R. (2008) "Coolant Radiolysis Studies in the High Temperature U-2 Loop in the NRU Reactor." Atomic Energy of Canada Limited Report [153-127160-440-003](#).
- [15] Elliot, A.J. and Stuart, C.R. (2006) "Radiation Chemistry in Nuclear Reactor Systems: Does Modelling Provide Answers or Only Insights?" Proceedings of the 6<sup>th</sup> International Workshop on LWR Coolant Radiolysis and Electrochemistry, Jeju Island, Korea.
- [16] Marin, T.W., Jonah, C.D. and Bartels, D.M. (2003) "Reaction of OH Radicals with H<sub>2</sub> in Sub-Critical Water." Chem. Phys. Letters Vol. 371, pp. 144-149.
- [17] Henshaw, J. and Sims, H.E. (2008) "Modelling the AECL Minimum Hydrogen Concentration Data." Nexia Solutions Report BE00728/06/10/23-Draft.
- [18] Elliot, A.J. (1994) "Rate Constants and G-Values for the Simulation of the Radiolysis of Light water over the Range 0-300°C." Atomic Energy of Canada Limited Report AECL-11073.
- [19] Takahashi, K., Cline, J.A., Bartels, D.M. and Jonah, C.D. (2000) "Design of an Optical Cell for Pulse Radiolysis of Supercritical Water." Rev. Sci. Instr. Vol. 71, pp. 3345-3350.
- [20] Takahashi, K., Bartels, D.M., Cline, J.A. and Jonah, C.D. (2002) "Reaction Rates of the Hydrated Electron with NO<sub>2</sub><sup>-</sup>, NO<sub>3</sub><sup>-</sup> and the Hydronium Ion as a Function of Temperature from 125 to 380°." Chem. Phys. Letters Vol. 357, pp. 358-364.
- [21] Cline, J., Takahashi, K., Marin, T.W., Jonah, C.D. and Bartels, D.M. (2002) "Pulse Radiolysis of Supercritical Water. 1. Reactions between Hydrophobic and Anionic Species." J. Phys. Chem. A Vol. 106, pp. 12260-12269.
- [22] Marin, T.W., Cline, J.A., Takahashi, K., Bartels, D.M. and Jonah, C.D. (2002) "Pulse Radiolysis of Supercritical Water. 2. Reactions of Nitrobenzene with Hydrated Electrons and Hydroxyl Radicals." J. Phys. Chem. A Vol. 106, pp. 12270-12279.
- [23] Marin, T.W., Jonah, C.D. and Bartels, D.M. (2005) "Reaction of Hydrogen Atoms with Hydroxide Ions in High-Temperature and High-Pressure water." J. Phys. Chem. A Vol. 109, pp. 1843-1848.
- [24] Janik, I., Bartels, D.M., Marin, T.W., and Jonah, C.D. (2007) "Reaction of O<sub>2</sub> with the Hydrogen Atom in Water up to 350°C" J. Phys. Chem. A Vol. 111, pp. 79-88.
- [25] Janik, I., Bartels, D.M., and Jonah, C.D. (2007) "Hydroxyl Radical Self-Recombination and Absorption Spectrum in Water up to 350°C" J. Phys. Chem. A Vol. 111, pp. 1835-1843.
- [26] Janik, D., Janik, I., and Bartels, D.M. (2007) "Neutron and  $\beta/\gamma$  Radiolysis of Water up to Supercritical Conditions. 1.  $\beta/\gamma$  Yields for H<sub>2</sub>, H<sup>+</sup> Atom, and Hydrated Electron." J. Phys. Chem. A Vol. 111, pp. 7777-7786.

- [27] Marin, T.W., Takahashi, K., Jonah, C.D., Chemerisov, S.D. and Bartels, D.M. (2007) "Recombination of the Hydrated Electron at High Temperature and Pressure in Hydrogenated Alkaline Water." *J. Phys. Chem. A* Vol. 111, pp. 111540-111551.
- [28] Lin, M, Katsumura, Y., Muroya, Y, He, H., Wu, G., Han, Z., Miyazaki, T. and Kudo, H. (2004) "Pulse Radiolysis Study on the Estimation of Radiolytic Yields of Water Decomposition Products in High-Temperature and Supercritical Water: Use of Methyl Viologen as a Scavenger." *J. Phys. Chem. A* Vol. 108, pp. 8287-8295.
- [29] Lundström, T., Christensen, H. and Sehested, K. (2001) "The Reaction of Hydrogen Atoms with Hydrogen Peroxide as a Function of Temperature." *Radiat. Phys. Chem.* Vol. 61, pp.109-113.
- [30] Lundström, T., Christensen, H. and Sehested, K. (2002) "The Reaction of OH and H at Elevated Temperatures." *Radiat. Phys. Chem.* Vol. 64, pp. 29-33.
- [31] Lundström, T., Christensen, H. and Sehested, K. (2004) "Reactions of the HO<sub>2</sub> Radical with OH, H, Fe<sup>2+</sup> and Cu<sup>2+</sup> at Elevated Temperatures." *Radiat. Phys. Chem.* Vol. 69, pp. 211-216.
- [32] Buxton, G.V. and Stuart, C.R. (1995) "Re-Evaluation of the Thiocyanate Dosimeter for Pulse Radiolysis." *J. Chem. Soc. Faraday Trans.* Vol. 91, pp. 279-281.
- [33] Draganic, Z.D. and Draganic, I.G. (1973) "Studies on the Formation of Primary Yields of Hydroxyl Radical and Hydrated Electron in the  $\gamma$ -Radiolysis of Water." *J. Phys. Chem.* Vol. 77, pp. 765-772.
- [34] Spinks, J.W.T. and Woods, R.J. (1990) "An Introduction to Radiation Chemistry." Publisher: John Wiley & Sons, Inc., Third Edition.
- [35] Klassen, N.V. (1987) "Primary Products in Radiation Chemistry" in "Radiation Chemistry: Principles and Applications." Editors Farhataziz and M.A.J. Rodgers. Publisher: VCH.
- [36] Draganic, I.G. and Draganic, Z.D. (1971) "The Radiation Chemistry of Water." Publisher: Academic Press.
- [37] Jha, K.N., Ryan, T.G. and Freeman, G.R. (1972) "Radiolysis of H<sub>2</sub>O and D<sub>2</sub>O between 0 and 300°." *J. Phys. Chem.* Vol. 79, pp. 868-870.
- [38] Elliot, A.J., Chenier, M.P. and Ouellette, D.C. (1993) "Temperature Dependence of g Values for H<sub>2</sub>O and D<sub>2</sub>O Irradiated with Low Linear Energy Transfer Radiation." *J. Chem. Soc. Faraday Trans.* Vol. 89, pp. 1193-1197.
- [39] Shiraishi, H., Buxton, G.V. and Wood, N.D. (1989) "Temperature dependence of the Absorption Spectrum of Methyl Viologen Cation Radical and the Use of Methyl Viologen as a Scavenger for Estimating Yields of the Primary Radicals in the Radiolysis of High-Temperature Water." *Radiat. Phys. Chem.* Vol. 33, pp. 519-522.
- [40] Kent, M.C. and Sims, H.E. (1992) "The Yield of  $\gamma$ -Radiolysis Products from Water at Temperatures up to 270°C." Harwell Report AEA-RS-2301.

- [41] Watanabe, T. and Honda, K. (1982) "Measurement of the Extinction Coefficient of the Methyl Viologen Cation Radical and the Efficiency of its Formation by Semiconductor Photocatalyst." *J. Phys. Chem.* Vol. 86, pp. 2617-2619.
- [42] Das, T.N., Ghanty, T.K. and Pal, H. (2003) "Reactions of Methyl Viologen Di-cation ( $MV^{2+}$ ) with H Atoms in Aqueous Solutions: Mechanism Derived from Pulse Radiolysis Measurements and Ab Initio MO Calculations." *J. Phys. Chem. A* Vol. 107, pp. 5998-6006.
- [43] Buxton, G.V. and Wood, N.D. (1989) "Effect of Temperature and Scavenging Power on the Sum of  $G(e_{aq}^-) + G(H) + G(OH)$  in the Range 20-200°C – A Pulse Radiolysis Study." *Radiat. Phys. Chem.* Vol. 34, pp. 699-704.
- [44] Wu, G., Katsumura, Y., Muroya, Y., Lin, M. and Morioka, T. (2002) "Temperature Dependence of Carbonate Radical in  $NaHCO_3$  and  $Na_2CO_3$  Solutions: Is the Radical a Single Anion." *J. Phys. Chem.* Vol. 106, pp. 2430-2437.
- [45] Zuo, Z., Cai, Z., Katsumura, Y., Chitose, N. and Muroya, Y. (1999) "Reinvestigation of the Acid-Base Equilibrium of the (Bi)carbonate radical and pH Dependence of its Reactivity with Organic Reactants." *Radiat. Phys. Chem.* Vol. 55, pp. 15-23.
- [46] Lyman, S.V., Schwarz, H.A. and Czapski, G. (2000) "Medium Effects on Reactions of the Carbonate Radical with Thiocyanate, Iodide and Ferrocyanide Ions." *Radiat. Phys. Chem.* Vol. 59, pp. 387-392.
- [47] Stefanic, I. and LaVerne, J.A. (2002) "Temperature Dependence of the Hydrogen Peroxide Production in the  $\gamma$ -Radiolysis of Water." *J. Phys. Chem. A* Vol. 106, pp. 447-452.
- [48] Elliot, A.J., Chenier, M.P. and Ouellette, D.C. (1990) "g-Values for  $\gamma$ -irradiated water as a Function of Temperature Dependence." *Can. J. Chem.* Vol. 68, pp. 712-719.
- [49] Christensen, H. and Sehested, K. (1986) "The Hydrated Electron and its Reactions at High temperature." *J. Phys. Chem.* Vol. 90, pp. 186-190.
- [50] Elliot, A.J., Ouellette, D.C. and Stuart, C.R. (1996) "The Temperature Dependence of the Rate Constants and Yields for the Simulation of the Radiolysis of Heavy Water." Atomic Energy of Canada Limited Report AECL-11658.
- [51] Hare, P.M., Price, E.A. and Bartels, D.M. (2008) "Hydrated Electron Extinction Coefficient Revisited." *J. Phys. Chem. A* Vol. 112, pp. 6800-6802.
- [52] Sehested, K. and Christensen, H. (1990) "The Rate Constant of Bimolecular Reaction of Hydrogen Atoms at Elevated Temperatures." *Radiat. Phys. Chem.* Vol. 36, pp. 499-500.
- [53] Christensen, H. and Sehested, K. (1980) "Pulse Radiolysis at High Temperatures and High Pressures." *Radiat. Phys. Chem.* Vol. 16, pp. 183-186.
- [54] Elliot, A.J., McCracken, D.R., Buxton, G.V. and Wood, N.D. (1990) "Estimation of Rate Constants for Near-Diffusion-Controlled Reactions in Water at High Temperatures" *J. Chem. Soc. Faraday.* Vol. 86, pp. 1539-1547.



- [55] Christensen, H., Sehested, K. and Logager, T. (1994) "Temperature Dependence of the Rate Constant for Reactions of Hydrated Electrons with H, OH and H<sub>2</sub>O<sub>2</sub>." *Radiat. Phys. Chem.* Vol. 43, pp. 527-531.
- [56] Schwarz, H.A. (1992) "Reaction of the Hydrated Electron with Water." *J. Phys. Chem.* Vol. 96, pp. 8937-8941.
- [57] Stuart, C.R., Ouellette, D.C. and Elliot, A.J. (2002) "Pulse Radiolysis Studies of Heavy Water at Temperatures up to 250°C." Atomic Energy of Canada Limited Report AECL-12107.
- [58] Elliot, A.J. and Ouellette, D.C. (1994) "Temperature Dependence of the Rate Constant for the Reaction of e<sub>aq</sub><sup>-</sup> + OH in water up to 150°C." *J. Chem. Soc. Faraday Trans.* Vol. 90, pp. 837-841.
- [59] Buxton, G.V. and Elliot, A.J. (1993) "Temperature Dependence of the Rate Constant for Reaction of H + OH in Liquid Water up to 200°C." *J. Chem. Soc. Faraday.* Vol. 89, pp. 485-488.
- [60] Gruenbein, W., Henglein, A., Stevens, G. and Beck, G. (1971) "Vielfachpuls-Radiolyse: Sukzessive Anlagerung zweier hydratisierter Elektronen an Sauerstoff, Nitrobenzol und Nitromethan." *Ber. Bunsenges. Phys. Chem.* Vol. 75, pp. 126-134.
- [61] Elliot, A.J. (1989) "A Pulse Radiolysis Study of the Temperature Dependence of Reactions Involving H, OH and e<sub>aq</sub><sup>-</sup> in Aqueous Solution." *Radiat. Phys. Chem.* Vol. 34, pp. 753-758.
- [62] Mezyk, S.P. and Bartels, D.M. (1995) "Direct EPR Measurement of Arrhenius Parameters for the Reaction of H Atoms with H<sub>2</sub>O<sub>2</sub> and D Atoms with D<sub>2</sub>O<sub>2</sub> in Aqueous Solution." *J. Chem. Soc. Faraday.* Vol. 91, pp. 3127-3132.
- [63] Christensen, H., Sehested, K. and Corfitzen, H. (1982) "Reaction of Hydroxyl Radicals with Hydrogen Peroxide at Ambient and Elevated Temperatures." *J. Phys. Chem.* Vol. 86, pp. 1588-1590.
- [64] Christensen, H., Sehested, K. and Bjergakke, E. (1989) "Radiolysis of Reactor Water: Reaction of OH Radicals with O<sub>2</sub><sup>-</sup>." *Proceedings of the Water Chemistry of Nuclear Reactor Systems 5.* BNES, pp. 141-144.
- [65] Elliot, A.J. and Buxton, G.V. (1992) "Temperature Dependence of the Reaction of OH + O<sub>2</sub><sup>-</sup> and OH + HO<sub>2</sub> in Water up to 200°C." *J. Chem. Soc. Faraday Trans.* Vol. 88, pp. 2465-2570.
- [66] Bielski, B.H.J. and Gebicki, J.M. (1970) "Species in Oxygenated Water." *Advances in Radiation Chemistry* Vol. 2, pp. 177-272. Editors M. Burton and J.L. Magee.
- [67] Bielski, B.H., Cobeilli, D.E. and Arudi, L. (1985) "Reactivity of HO<sub>2</sub>/O<sub>2</sub><sup>-</sup> Radicals in Aqueous Solution." *J. Phys. Chem. Ref. Data* Vol. 14, pp. 1041-1100.
- [68] Christensen, H and Sehested, K. (1988) "HO<sub>2</sub> and O<sub>2</sub><sup>-</sup> Radicals at High Temperature." *J. Phys Chem.* Vol. 92, pp. 3007-3011.

- [69] Rebensdorff, B. and Wikmark, G. (1989) "Decomposition of Hydrogen Peroxide in High Temperature Water: a Laboratory Study." Proceedings of the Water Chemistry of Nuclear Reactor Systems 5. BNES, pp. 153-157.
- [70] Hiroishi, D. and Ishigure, K. (1989) "Homogeneous and Heterogeneous Decomposition of Hydrogen Peroxide in High-Temperature Water." Proceedings of the Water Chemistry of Nuclear Reactor Systems 5. BNES, pp. 311-312.
- [71] Haines, R.I., McCracken, D.R. (1989) "Decomposition of Hydrogen Peroxide under Coolant Chemistry Conditions." Proceedings of the Water Chemistry of Nuclear Reactor Systems 5. BNES, pp. 309-310 and unpublished AECL data.
- [72] Lin, C.C., Smith, F.R., Ichikawa, N., Baba, T. and Itow, M. (1991) "Inter. J. of Chem. Kinetics, Vol. 23, pp. 971-987.
- [73] Lin, C.C. and Smith, F.R. (1990) "Decomposition of Hydrogen Peroxide at Elevated Temperatures." Electric Power Research Institute Report NP-6733.
- [74] Croiset, E., Rice, S.F. and Hunush, R.G. (1997) "Hydrogen Peroxide Decomposition in Supercritical Water." AIChE Journal Vol. 43, pp. 2343-2352.
- [75] Hiroki, A. LaVerne, J.A. (2005) "Decomposition of Hydrogen Peroxide at Water-Ceramic Oxide Interfaces." J. Phys. Chem. B. Vol. 109, pp. 3364-3370.
- [76] Ashmore, C.B., Sims, H.E., Tait, P.K. and Walters, W.S. (1998) "The Measurement of Water Radiolysis Product Yields at High Temperature and Pressure. Final Report." AEA Technology Report AEAT-2223.
- [77] Bandura, A.V. and Lvov, S.N. (2006) "The Ionization Constant of Water over Wide Ranges of Temperature and Density." J. Phys. Ref. Data Vol. 35, pp. 15-29.
- [78] Perrin, D.D. (1982) "Ionization Constants of Inorganic Acid and Bases in Aqueous Solution." IUPAC Chemical Data Series, No. 29. Pergamon Press, 2<sup>nd</sup> Edition.
- [79] Buxton, G.V., Wood, N.D. and Dyster, S. (1988) "Ionisation Constants of OH and HO<sub>2</sub> in Aqueous Solutions up to 200°C." J. Chem. Soc. Faraday I Vol. 84, pp. 1113-1121.
- [80] Elliot, A.J. and McCracken, D.R. (1989) "Effect of Temperature on O<sup>-</sup> Reactions and Equilibria: A Pulse Radiolysis Study." Radiat. Phys. Chem. Vol. 34, pp. 69-74.
- [81] Poskrebyshev, G.A., Neta, P. and Huie, R.E. (2005) "Temperature dependence of the Acid Dissociation Constant of the Hydroxyl Radical." J. Phys. Chem. A Vol. 106, pp. 11488-11491.
- [82] Schwarz, H.A. and Bielski, B.H.J. (1986) "Reactions of HO<sub>2</sub> and O<sub>2</sub><sup>-</sup> with Iodine and Bromine and the I<sub>2</sub><sup>-</sup> and I Reduction Potentials." J. Phys Chem. Vol. 90, pp. 1445-1448.
- [83] Shiraishi, H, Sunaryo, G.R. and Ishigure (1994) "Temperature Dependence of the Equilibrium and Rate Constants of Reactions Inducing the Conversion Between the Hydrated Electron and Atomic Hydrogen." J. Phys Chem. Vol. 98, pp. 5164-5173.
- [84] Irvine, T.F. and Hartnett, J.P. (1976) "Steam and Air Tables in SI Units." McGraw-Hill.
- [85] Laidler, K.J. (1970) "Electrolyte Solutions." Third Edition, Harper Collins.

- [86] Yoshida, K., Wakai, C., Matubayasi, N and Nakahara, M. (2005) "A New High-Temperature Multinuclear-Magnetic-Resonance Probe and the Self-Diffusion of Light and Heavy Water in sub- and Supercritical Conditions." *J. Chem. Phys.* Vol. 123, pp. 164506\_1-164506\_9 (Published on-line).
- [87] Harris, K.R. and Woolf, L.A. (1980) "Pressure and Temperature Dependence of the Self-Diffusion Coefficient of Water and Oxygen-18 Water." *J. Chem. Soc. Faraday I* Vol. 76, pp. 377-385.
- [88] Krynicki, K., Green, C.D. and Sawyer (1980) "Pressure and Temperature Dependence of the Self-Diffusion in Water." *Faraday Discussion* Vol. 66, pp. 198-208.
- [89] Quist, A.S. and Marshall, W.L. (1965) "Assignment of Limiting Conductance for Single Ions to 400°C." *J. Phys. Chem.* Vol. 69, pp. 2984-2987.
- [90] Robinson, R.A. and Stokes, R.H. (1987) "Chemical Kinetics." Second Edition, Butterworths.
- [91] Natzle, W.C. and Moore, C.B. (1985) "Recombination of  $H^+$  and  $OH^-$  in Pure Liquid Water." *J. Phys. Chem.* Vol. 89, pp. 2605-2612.
- [92] Knight, B., Goodall, D.M. and Greenhow, R.C. (1979) "Single-Photon Vibrational Photochemistry. Part 1: Wavelength and Temperature Dependence of the Quantum Yield for the Laser-Induced Ionization of Water." *J. Chem. Soc. Faraday 2* Vol. 75, pp. 841-856.
- [93] Ertl, V.G. and Gerischer (1962) "Ein Vergleich der Kinetik der Neutralisationsreaktionen des Leichten und Schweren Wassers." *Zeit. Elektrochem.* Vol. 66, pp. 560-563.
- [94] Bannister, J.J., Gormally, J., Holzwarth, J.F. and King, T.A. (1984) "The Iodine Laser and Fast Reactions." *Chem. Brit.* Vol. 20, pp. 227-229.
- [95] Buxton, G.V. (1970) "Pulse Radiolysis of Aqueous Solutions. Rates of Reaction of  $OH$  with  $OH^-$ ." *Trans. Faraday Soc.* Vol. 66, pp. 1656-1660.
- [96] Zahavi, D. and Rabani, J. (1971) "Pulse Radiolytic Investigations of  $O_{aq}^-$  Radical Ions." *J. Phys. Chem.* Vol. 75, pp. 1738-1744.
- [97] Ilan, Y. and Rabani, J. (1976) "On some Fundamental Reactions In Radiation Chemistry: Nanosecond Pulse Radiolysis." *Int. J. Radiat. Chem.* Vol. 8, pp. 609-611.
- [98] Stanisky, C.M., Bartels, D.M. and Takahashi, K. (2009) "Rate Constants for the Reaction of Hydronium Ions with Hydrated Electrons up to 350°C." *Radiat. Phys. Chem.* Submitted.
- [99] Han, P. and Bartels, D.M. (1990) "Re-evaluation of Arrhenius Parameters for  $H + OH^- \rightarrow (e^-)_{aq} + H_2O$  and the Enthalpy and Entropy of the Hydrated Electron." *J. Phys. Chem.* Vol. 94, pp. 7249-7299.
- [100] Han, P. and Bartels, D.M. (1992) "H/D Isotope Effects in Water Radiolysis. 4. The Mechanism of  $(H)_{aq} \rightleftharpoons (e^-)_{aq}$  Interconversion." *J. Phys. Chem.* Vol. 96, pp. 4899-4906.

- [101] Bartels, D.M. (2008) "Comment on the Possible Role of the Reaction  $\text{H} + \text{H}_2\text{O} \rightarrow \text{H}_2 + \text{OH}$  in the Radiolysis of Water at High Temperatures." *Radiat. Phys. Chem.* Vol. 78, pp. 191-194.
- [102] Christensen, H. and Sehested, K. (1983) "Reaction of Hydroxyl Radicals with Hydrogen at Elevated Temperatures. Determination of the Activation Energy." *J. Phys. Chem.* Vol. 87, pp. 118-120.
- [103] Hickel, B. and Sehested, K. (1991) "Activation Energies for the Reaction  $\text{O}^- + \text{H}_2$  and  $\text{O}^- + \text{D}_2$  in Aqueous Solution." *J. Phys. Chem.* Vol. 95, pp. 744-747.
- [104] Elliot, A.J. and McCracken, D.R. (1990) "Computer Modelling of the Radiolysis in an Aqueous Lithium Salt Blanket: Suppression of Radiolysis by Addition of Hydrogen." *Fusion Engineering and Design* Vol. 13, pp. 21-27.
- [105] Elliot, A.J. and Chenier, M.C. (1992) "Radiolysis of  $4.5 \text{ mol dm}^{-3}$  LiOH with  ${}^6\text{Li}(n,\alpha)$   ${}^3\text{H}$  ion Recoil." *J. Nuclear Mat.* Vol. 187, pp. 230-238.
- [106] McCracken, D.R., Tsang, K.T. and Laughton, P.J. (1998) "Aspects of the Physics and Chemistry of Water Radiolysis by Fast Neutrons and fast Electrons in Nuclear Reactors." Atomic Energy of Canada Report AECL-11895.
- [107] Edwards, E.J., Wilson, P.P.H., Anderson, M.H., Mezyk, S.P., Pimblott, S.M. and Bartels, D.M. (2007) "An Apparatus to Study the High Temperature Water Radiolysis in a Nuclear Reactor: Calibration of Dose in a Mixed Neutron/Gamma Radiation Field." *Rev. Sci. Instrum.* Vol. 78, pp. 124101\_1-124101\_11.
- [108] Magee, J.L. and Chatterjee, A. (1987) "Theoretical Aspects of Radiation Chemistry." in "Radiation Chemistry: Principles and Applications." Editors Farhataziz and M.A.J. Rodgers. Publisher: VCH.
- [109] LaVerne, J.A. (2004) "Radiation Chemical Effects of Heavy Ions." In "Charged Particle and Photon Interactions with Matter." Edited by A. Mozumder and Y. Hatano. Published by Marcel Dekker, Inc.
- [110] Elliot, A.J., Chenier, M.P., Ouellette, D.C. and Koslowsky, V.T. (1996) "Temperature Dependence of G-Values for Aqueous Solutions Irradiated with 23 MeV  ${}^2\text{H}^+$  and 173 MeV  ${}^7\text{Li}^+$  Ion Beams." *J. Phys. Chem.* Vol. 100, pp. 9014-9020.
- [111] Berger, M.J., Coursey, J.S., Zucker, M.A and Chang J. (2005) "Stopping-Power and Range Tables for Electrons, Protons, and Helium Ions." <http://physics.nist.gov/PhysRefData/Star/Text/contents.html>
- [112] Appleby, A and Schwarz, H.A. (1969) "Radical and Molecular Yields in Water Irradiated by  $\gamma$  Rays and Heavy Ions." *J. Phys. Chem.* Vol. 73, pp. 1937-1941.
- [113] LaVerne, J.A. and Yoshida, H. (1993) "Production of the Hydrated Electron Yields in Radiolysis of Water with Helium Ions." *J. Phys. Chem.* Vol. 97, pp. 10720-10724.
- [114] LaVerne, J.A., Stefanic, I. and Pimblott, S.M. (2005) "Hydrated Electron Yields in Heavy Ion Radiolysis of Water." *J. Phys. Chem. A* Vol. 109, pp. 9393-9401.

- [115] Burns, W.G. and Sims, H.E. (1981) "Effect of Radiation Type on Water Radiolysis." J. Chem. Soc. Faraday Trans. 1 Vol. 77, pp. 2803-2813.
- [116] Anderson, A.R. and Hart, E.J. (1961) "Molecular Product and Free Radical Yields in the Decomposition of Water by Protons, Deuterons, and Helium Ions." Radiation Research, Vol. 14, pp. 689-704.
- [117] LaVerne, J.A., (2000) "New Mechanism for H<sub>2</sub> Formation in Water." J. Phys. Chem. A Vol. 104, pp. 9820-9822.
- [118] Parajon, M.H., Rajesh, P., Mu, T., Pimblott, S.M. and LaVerne, J.A. (2008) "H Atom Yields in the Radiolysis of Water." Radiat. Phys. Chem. Vol. 77, pp. 1203-1207.
- [119] LaVerne, J.A. (1989) "Radical and Molecular Yields in the Radiolysis of Water with Carbon Ions." Radiat. Phys. Chem. Vol. 34, pp. 135-143.
- [120] Pistina, B. and LaVerne, J.A., (1999) "Hydrogen Peroxide Production in the Radiolysis of Water with Heavy Ions." J. Phys. Chem. A Vol. 103, pp. 1592-1597.
- [121] Ruiz, C.P., Lin, C., Robinson, R., Burns, W.G. and Curtis, A.R. (1987) "Model Calculations of Water Radiolysis in BWR Primary Coolant." Proceedings of Water Chemistry of Nuclear Reactor Systems 5. BNES, pp. 131-140.

**Appendix A**

**Tabulations of Rate Constants and pKs at Different Temperatures based on Mathematical Functions provided in this Report**

**Table A-1 Rate Constants Associated with Reactions in Table 4-1**

	Temp (°C)	20	50	100	150	200	250	300	350
Number	Reaction	Rate Constant (Units: L/mol/s for 2 <sup>nd</sup> order; /s for 1 <sup>st</sup> order)							
R2	$e_{aq}^- + e_{aq}^- + (2 H_2O) \rightarrow H_2 + 2 OH^-$	6.20E+09	1.44E+10	3.85E+10	7.52E+10	1.55E+10	4.71E+08	6.06E+06	
R3	$H + H \rightarrow H_2$	4.62E+09	8.35E+09	1.81E+10	3.27E+10	5.21E+10	7.60E+10	1.04E+11	1.35E+11
R4	$OH + OH \rightarrow H_2O_2$	4.54E+09	6.24E+09	8.77E+09	1.03E+10	1.08E+10	1.06E+10	9.87E+09	8.98E+09
R5	$e_{aq}^- + H (+ H_2O) \rightarrow H_2 + OH^-$	2.49E+10	4.40E+10	9.27E+10	1.64E+11	2.56E+11	3.68E+11	4.97E+11	6.39E+11
R6	$e_{aq}^- + OH \rightarrow OH^-$	3.34E+10	4.90E+10	8.53E+10	1.36E+11	2.01E+11	2.80E+11	3.73E+11	4.77E+11
R7	$H + OH \rightarrow H_2O$	1.03E+10	1.45E+10	2.28E+10	3.23E+10	4.24E+10	5.28E+10	6.34E+10	7.39E+10
R8	$e_{aq}^- + H_2O_2 \rightarrow OH + OH^-$	1.22E+10	2.22E+10	4.87E+10	8.85E+10	1.42E+11	2.08E+11	2.85E+11	3.71E+11
R9	$e_{aq}^- + O_2 \rightarrow O_2^-$	2.11E+10	3.30E+10	5.89E+10	9.18E+10	1.30E+11	1.73E+11	2.18E+11	2.66E+11
R10	$e_{aq}^- + O_2^- (+ H_2O) \rightarrow H_2O_2 + 2 OH^-$	1.19E+10	1.95E+10	3.73E+10	6.12E+10	9.04E+10	1.24E+11	1.61E+11	2.00E+11
R11	$e_{aq}^- + HO_2 \rightarrow HO_2^-$	1.19E+10	1.95E+10	3.73E+10	6.12E+10	9.04E+10	1.24E+11	1.61E+11	2.00E+11
R12	$H + H_2O_2 \rightarrow OH + H_2O$	3.16E+07	7.04E+07	2.01E+08	4.49E+08	8.46E+08	1.41E+09	2.15E+09	3.07E+09
R13	$H + O_2 \rightarrow HO_2$	1.20E+10	1.87E+10	3.03E+10	4.08E+10	4.93E+10	5.58E+10	6.06E+10	6.42E+10
R14	$H + HO_2 \rightarrow H_2O_2$	See Section 4.1.13							
R14a	$H + HO_2 \rightarrow 2 OH$	1.03E+10	1.83E+10	3.89E+10	6.94E+10	1.09E+11	1.58E+11	2.14E+11	2.77E+11
R15	$H + O_2^- \rightarrow HO_2^-$	1.03E+10	1.83E+10	3.89E+10	6.94E+10	1.09E+11	1.58E+11	2.14E+11	2.77E+11
R16	$OH + H_2O_2 \rightarrow HO_2 + H_2O$	2.65E+07	4.49E+07	8.95E+07	1.51E+08	2.29E+08	3.21E+08	4.23E+08	5.34E+08
R17	$OH + O_2^- \rightarrow (HO_3^-) \rightarrow O_2 + OH^-$	1.02E+10	1.54E+10	2.65E+10	4.00E+10	5.55E+10	7.22E+10	8.98E+10	1.08E+11
R18	$OH + HO_2 \rightarrow (H_2O_3) \rightarrow O_2 + H_2O$	8.44E+09	1.09E+10	1.52E+10	1.95E+10	2.38E+10	2.80E+10	3.20E+10	3.58E+10
R19	$HO_2 + HO_2 \rightarrow H_2O_2 + O_2$	7.31E+05	1.57E+06	4.28E+06	9.20E+06	1.68E+07	2.74E+07	4.10E+07	5.75E+07
R20	$O_2^- + HO_2 (+ H_2O) \rightarrow H_2O_2 + O_2 + OH^-$	9.47E+07	1.29E+08	1.93E+08	See Section 4.1.18				
R21	$O_2^- + O_2^- (+ 2 H_2O) \rightarrow H_2O_2 + O_2 + 2 OH^-$	See Section 4.1.18							
R22	$H_2O_2 \rightarrow \frac{1}{2} O_2 + H_2O$	8.29E-08	9.86E-07	2.52E-05	3.00E-04	2.11E-03	1.03E-02	3.78E-02	1.13E-01
R22a	$H_2O_2 \rightarrow 2 OH$								

Table A-2 Rate Constants Associated with the Equilibrium Reactions in Table 4-2 and Table 4-3

	Temp (°C)	20	50	100	150	200	250	300	350
Number	Equilibrium Reactions	Rate Constant (Units: L/mol/s for 2 <sup>nd</sup> order; /s for 1 <sup>st</sup> order)							
R23f	$\text{H}_2\text{O} \rightleftharpoons \text{H}^+ + \text{OH}^-$	1.29E-05	1.78E-04	3.13E-03	1.68E-02	4.58E-02	7.50E-02	6.52E-02	2.03E-02
R23b	$\text{H}_2\text{O} \rightleftharpoons \text{H}^+ + \text{OH}^-$	1.06E+11	1.83E+11	3.22E+11	4.54E+11	6.05E+11	8.14E+11	1.13E+12	1.63E+12
R24f	$\text{H}_2\text{O}_2 \rightleftharpoons \text{H}^+ + \text{HO}_2^-$	6.49E-02	4.36E-01	3.06E+00	9.56E+00	1.98E+01	2.92E+01	2.52E+01	8.27E+00
R24b	$\text{H}_2\text{O}_2 \rightleftharpoons \text{H}^+ + \text{HO}_2^-$	4.52E+10	7.55E+10	1.27E+11	1.87E+11	2.71E+11	3.92E+11	5.69E+11	8.22E+11
R25f	$\text{H}_2\text{O}_2 + \text{OH}^- \rightleftharpoons \text{HO}_2^- + \text{H}_2\text{O}$	1.18E+10	2.16E+10	4.04E+10	6.06E+10	8.26E+10	1.07E+11	1.36E+11	1.68E+11
R25b	$\text{H}_2\text{O}_2 + \text{OH}^- \rightleftharpoons \text{HO}_2^- + \text{H}_2\text{O}$	9.97E+05	3.65E+06	1.63E+07	4.40E+07	8.56E+07	1.33E+08	1.76E+08	2.08E+08
R26f	$\text{OH}^- \rightleftharpoons \text{H}^+ + \text{O}^-$	6.49E-02	4.36E-01	3.06E+00	9.56E+00	1.98E+01	2.92E+01	2.52E+01	8.27E+00
R26b	$\text{OH}^- \rightleftharpoons \text{H}^+ + \text{O}^-$	4.52E+10	7.55E+10	1.27E+11	1.87E+11	2.71E+11	3.92E+11	5.69E+11	8.22E+11
R27f	$\text{OH}^- + \text{OH}^- \rightleftharpoons \text{O}^- + \text{H}_2\text{O}$	1.18E+10	2.16E+10	4.04E+10	6.06E+10	8.26E+10	1.07E+11	1.36E+11	1.68E+11
R27b	$\text{OH}^- + \text{OH}^- \rightleftharpoons \text{O}^- + \text{H}_2\text{O}$	9.97E+05	3.65E+06	1.63E+07	4.40E+07	8.56E+07	1.33E+08	1.76E+08	2.08E+08
R28f	$\text{HO}_2 \rightleftharpoons \text{H}^+ + \text{O}_2^-$	6.62E+05	1.39E+06	2.39E+06	2.31E+06	1.42E+06	5.72E+05	1.55E+05	2.82E+04
R28b	$\text{HO}_2 \rightleftharpoons \text{H}^+ + \text{O}_2^-$	4.52E+10	7.55E+10	1.27E+11	1.87E+11	2.71E+11	3.92E+11	5.69E+11	8.22E+11
R29f	$\text{HO}_2 + \text{OH}^- \rightleftharpoons \text{O}_2^- + \text{H}_2\text{O}$	9.78E-02	1.14E+00	2.09E+01	1.82E+02	1.20E+03	6.78E+03	2.87E+04	6.10E+04
R29b	$\text{HO}_2 + \text{OH}^- \rightleftharpoons \text{O}_2^- + \text{H}_2\text{O}$	1.18E+10	2.16E+10	4.04E+10	6.06E+10	8.26E+10	1.07E+11	1.36E+11	1.68E+11
R30f	$\text{H} \rightleftharpoons \text{H}^+ + \text{e}_{\text{aq}}^-$	3.70E+00	5.08E+01	1.31E+03	1.08E+04	4.57E+04	1.17E+05	1.65E+05	8.95E+04
R30b	$\text{H} \rightleftharpoons \text{H}^+ + \text{e}_{\text{aq}}^-$	2.02E+10	2.90E+10	5.40E+10	8.92E+10	1.54E+11	3.06E+11	7.16E+11	1.94E+12
R31f	$\text{H} + \text{OH}^- \rightleftharpoons \text{e}_{\text{aq}}^- + \text{H}_2\text{O}$	1.86E+07	8.46E+07	4.99E+08	1.44E+09	2.86E+09	4.90E+09	8.03E+09	1.32E+10
R31b	$\text{H} + \text{OH}^- \rightleftharpoons \text{e}_{\text{aq}}^- + \text{H}_2\text{O}$	1.23E+01	4.71E+01	2.01E+02	4.38E+02	7.30E+02	1.18E+03	2.01E+03	3.55E+03
R32f	$\text{H} + \text{H}_2\text{O} \rightleftharpoons \text{H}_2 + \text{OH}^-$	2.26E-05	1.07E-03	1.29E-01	4.08E+00	5.50E+01	4.17E+02	2.10E+03	7.87E+03
R32b	$\text{H} + \text{H}_2\text{O} \rightleftharpoons \text{H}_2 + \text{OH}^-$	3.37E+07	7.04E+07	1.71E+08	3.60E+08	6.08E+08	7.85E+08	7.80E+08	6.17E+08



**Table A-3 pK Values for Equilibria in Table 4-2 and Table 4-3**

	Temp (°C)	20	50	100	150	200	250	300	350
PK	Equilibria	Molar Units							
pK <sub>w</sub>	$\text{H}_2\text{O} \rightleftharpoons \text{H}^+ + \text{OH}^-$	14.17	13.27	12.29	11.72	11.44	11.38	11.64	12.39
pK <sub>H2O2</sub>	$\text{H}_2\text{O}_2 \rightleftharpoons \text{H}^+ + \text{HO}_2^-$	11.84	11.24	10.62	10.29	10.14	10.13	10.35	11.00
pK <sub>OH</sub>	$\text{OH} \rightleftharpoons \text{H}^+ + \text{O}^-$	11.84	11.24	10.62	10.29	10.14	10.13	10.35	11.00
pK <sub>HO2</sub>	$\text{HO}_2 \rightleftharpoons \text{H}^+ + \text{O}_2^-$	4.83	4.73	4.72	4.91	5.28	5.84	6.57	7.46
pK <sub>H</sub>	$\text{H} \rightleftharpoons \text{H}^+ + \text{e}_{\text{aq}}^-$	9.74	8.76	7.62	6.92	6.53	6.42	6.64	7.34
pK <sub>H2O</sub>	$\text{H}_2\text{O} \rightleftharpoons \text{H}^+ + \text{OH}^-$	15.92	15.01	14.01	13.43	13.12	13.04	13.24	13.90
pK <sub>32</sub>	$\text{H} + \text{H}_2\text{O} \rightleftharpoons \text{H}_2 + \text{OH}$	12.17	10.82	9.12	7.95	7.04	6.28	5.57	4.89

Table A-4 Rate Constants Associated with the Alkaline Reactions in Discussed in Section 4.3

	Temp (°C)	20	50	100	150	200	250	300	350
Number	Reaction or Equilibria	Rate Constant (Units: L/mol/s for 2 <sup>nd</sup> order; /s for 1 <sup>st</sup> order)							
<b>R33 + R34</b>	OH + HO <sub>2</sub> <sup>-</sup> → H <sub>2</sub> O + O <sub>2</sub> <sup>-</sup> O <sup>-</sup> + H <sub>2</sub> O <sub>2</sub> → OH <sup>-</sup> + HO <sub>2</sub>	7.49E+09	1.18E+10	2.14E+10	3.37E+10	4.82E+10	6.44E+10	8.18E+10	1.00E+11
<b>R35</b>	O <sup>-</sup> + HO <sub>2</sub> <sup>-</sup> → OH <sup>-</sup> + O <sub>2</sub> <sup>-</sup>	6.65E+08	1.68E+09	5.66E+09	1.43E+10	2.97E+10	5.37E+10	8.76E+10	1.32E+11
<b>R36</b>	O <sup>-</sup> + H <sub>2</sub> → H + OH <sup>-</sup>	1.17E+08	1.91E+08	3.64E+08	5.95E+08	8.76E+08	1.20E+09	1.55E+09	1.93E+09
<b>R37f</b>	O <sup>-</sup> + O <sub>2</sub> ⇌ O <sub>3</sub> <sup>-</sup>	3.47E+09	5.31E+09	9.28E+09	1.42E+10	1.99E+10	2.61E+10	3.26E+10	3.94E+10
<b>R37b</b>	O <sup>-</sup> + O <sub>2</sub> ⇌ O <sub>3</sub> <sup>-</sup>	1.90E+03	1.11E+04	1.10E+05	6.41E+05	2.56E+06	7.87E+06	1.99E+07	4.32E+07